UNIVERSITY RESEARCH

1 DOT/RSPA/DPB-50/79/4

# DYNAMIC THEORIES AND EXPERIMENTS OF ALTERNATIVE GUIDEWAY-VEHICLE SYSTEMS

## PART II

ORIGINAL

**MARCH 1979**

**FINAL REPORT**

**UNDER CONTRACT: DOT-OS-60130**

Document is available to the U.S. public through
The National Technical Information Service,
Springfield, Virginia 22161

Prepared for

**U.S.DEPARTMENT OF TRANSPORTATION**
**Research and Special Programs Administration**
**Office of University Research**
**Washington, D.C.20590**

189

Technical Report Documentation Page

| 1. Report No. | 2. Government Accession No. | 3. Recipient's Catalog No. |
|---|---|---|
| DOT/RSPA/DPB-50/79/4 | | |

| 4. Title and Subtitle | 5. Report Date |
|---|---|
| Dynamic Theories and Experiments of Alternative Guideway-Vehicle Systems Part II | March 1979 |
| | 6. Performing Organization Code |
| 7. Author(s) James F. Wilson | 8. Performing Organization Report No. |
| 9. Performing Organization Name and Address<br>Civil Engineering Department<br>Duke University<br>Durham, North Carolina 27706 | 10. Work Unit No. (TRAIS)<br>11. Contract or Grant No. DOT-OS-60130 |
| 12. Sponsoring Agency Name and Address<br>Research and Special Programs Administration<br>Office Of University Research<br>U.S. Dept. of Transportation<br>Washington, D.C. 20590 | 13. Type of Report and Period Covered<br>Final Report<br>June 1977-March 1979<br>14. Sponsoring Agency Code DPB-50 |

15. Supplementary Notes

Technical Monitor: Robert J. Ravera, DPB-50

16. Abstract In both the companion report (Part I) and the present study, the broad purpose is to investigate theoretically and experimentally guideway-vehicle system dynamics. Four alternative systems are studied here in terms of nondimensional parameters. First, critical moment responses are predicted for simple, horizontally curved spans subjected to a variety of transit force distributions and torques. These results are validated with a series of laboratory-scale experiments. Second, measured moment responses are presented for curved, multiple spans with both even and uneven pier spacings and with several types of end constraints, all subjected to tandem vehicle loads. Results show that span dynamic responses may exceed 4 or 5 times those for vehicles at crawl speed. Third, dynamic responses are predicted for several three and six-span cable-stayed guideways subjected to a constant speed, vertical point force. These results are also validated with laboratory experiments. Finally, a statistical response analysis is presented for an AGT vehicle traversing a rigid, statistically rough, banked, curved guideway. With solutions of the covarient propagation equation, those design parameters are identified which strongly affect the lateral rms accelerations and mean suspension system strokes. The results obtained in all of these studies are directly applicable to the design of analogous intraurban and intercity transport systems.

| 17. Key Words | 18. Distribution Statement |
|---|---|
| guideways, experimental dynamics, beam vibrations, multiple spans, curved beams, cable-stayed bridges; mass transit vehicles | Document is available to the public through National Technical Information Services, Springfield, Va. 22161 |

| 19. Security Classif. (of this report) | 20. Security Classif. (of this page) | 21. No. of Pages | 22. Price |
|---|---|---|---|
| UNCLASSIFIED | UNCLASSIFIED | | |

Form DOT F 1700.7 (8-72) Reproduction of completed page authorized

# METRIC CONVERSION FACTORS

## Approximate Conversions to Metric Measures

| Symbol | When You Know | Multiply by | To Find | Symbol |
|---|---|---|---|---|
| | **LENGTH** | | | |
| in | inches | *2.5 | centimeters | cm |
| ft | feet | 30 | centimeters | cm |
| yd | yards | 0.9 | meters | m |
| mi | miles | 1.6 | kilometers | km |
| | **AREA** | | | |
| $in^2$ | square inches | 6.5 | square centimeters | $cm^2$ |
| $ft^2$ | square feet | 0.09 | square meters | $m^2$ |
| $yd^2$ | square yards | 0.8 | square meters | $m^2$ |
| $mi^2$ | square miles | 2.6 | square kilometers | $km^2$ |
| | acres | 0.4 | hectares | ha |
| | **MASS (weight)** | | | |
| oz | ounces | 28 | grams | g |
| lb | pounds | 0.45 | kilograms | kg |
| | short tons (2000 lb) | 0.9 | tonnes | t |
| | **VOLUME** | | | |
| tsp | teaspoons | 5 | milliliters | ml |
| Tbsp | tablespoons | 15 | milliliters | ml |
| fl oz | fluid ounces | 30 | milliliters | ml |
| c | cups | 0.24 | liters | l |
| pt | pints | 0.47 | liters | l |
| qt | quarts | 0.95 | liters | l |
| gal | gallons | 3.8 | liters | l |
| $ft^3$ | cubic feet | 0.03 | cubic meters | $m^3$ |
| $yd^3$ | cubic yards | 0.76 | cubic meters | $m^3$ |
| | **TEMPERATURE (exact)** | | | |
| °F | Fahrenheit temperature | 5/9 (after subtracting 32) | Celsius temperature | °C |

*1 in = 2.54 (exactly). For other exact conversions and more detailed tables, see NBS Misc. Publ. 286, Units of Weights and Measures, Price $2.25, SD Catalog No. C13.10:286.

## Approximate Conversions from Metric Measures

| Symbol | When You Know | Multiply by | To Find | Symbol |
|---|---|---|---|---|
| | **LENGTH** | | | |
| mm | millimeters | 0.04 | inches | in |
| cm | centimeters | 0.4 | inches | in |
| m | meters | 3.3 | feet | ft |
| m | meters | 1.1 | yards | yd |
| km | kilometers | 0.6 | miles | mi |
| | **AREA** | | | |
| $cm^2$ | square centimeters | 0.16 | square inches | $in^2$ |
| $m^2$ | square meters | 1.2 | square yards | $yd^2$ |
| $km^2$ | square kilometers | 0.4 | square miles | $mi^2$ |
| ha | hectares (10,000 $m^2$) | 2.5 | acres | |
| | **MASS (weight)** | | | |
| g | grams | 0.035 | ounces | oz |
| kg | kilograms | 2.2 | pounds | lb |
| t | tonnes (1000 kg) | 1.1 | short tons | |
| | **VOLUME** | | | |
| ml | milliliters | 0.03 | fluid ounces | fl oz |
| l | liters | 2.1 | pints | pt |
| l | liters | 1.06 | quarts | qt |
| l | liters | 0.26 | gallons | gal |
| $m^3$ | cubic meters | 35 | cubic feet | $ft^3$ |
| $m^3$ | cubic meters | 1.3 | cubic yards | $yd^3$ |
| | **TEMPERATURE (exact)** | | | |
| °C | Celsius temperature | 9/5 (then add 32) | Fahrenheit temperature | °F |

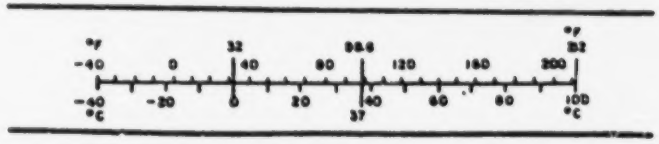


MICROFILMED FROM
BEST AVAILABLE COPY

## ACKNOWLEDGEMENTS

Three graduate students are acknowledged: Thomas P. Joseph for his meticulous experimental work on curved guideways; Serghios Barbas for his experimental and theoretical work on cable-stayed bridges; and Dennis J. Fromnes for his statistical calculations. Technicians John Carroll, Fred Avent helped construct the equipment, and Preston Lowrey aided in every aspect of the experimental program. Discussions with faculty associate Devendra P. Garg on vehicle dynamics were very helpful. This study was sponsored by the U. S. Department of Transportation's Office of University Research, in cooperation with Duke University, Departments of Civil and Mechanical Engineering. The enthusiastic support of Robert J. Ravera, the Government's technical monitor for this research, is greatly appreciated.

BLANK PAGE

BLANK PAGE

Dynamic Theories and Experiments for
Alternative Guideway-Vehicle Systems: Part II

CONTENTS


| Chapter | | Page |
|---|---|---|
| 1 | EXECUTIVE SUMMARY | 1 |
| 2 | THEORY FOR SIMPLE, CURVED GUIDEWAYS | 3 |
| | Introduction, 3 | |
| | Dynamic Theory, 3 | |
| | Tandem Vehicle Simulations , 10 | |
| | Parametric Studies and Conclusions, 11 | |
| 3 | LABORATORY STUDIES OF CURVED GUIDEWAY-VEHICLE DYNAMICS | 27 |
| | Introduction, 27 | |
| | Guideway Models and Response Measurements, 27 | |
| | Vehicle Models, 34 | |
| | Simple Span Experiments, 40 | |
| | Two-Span Experiments, 52 | |
| | Three-Span Experiments, 69 | |
| | End Constraint Effects, 78 | |
| | Summary and Conclusions, 82 | |
| 4 | CABLE-STAYED GUIDEWAY STUDIES | 86 |
| | Introduction, 86 | |
| | Frequencies and Mode Shapes, 86 | |
| | Responses to Transit Loads, 97 | |
| | Theory and Experiment: Comparisons and Conclusions, 100 | |

Chapter Page

5 LATERAL RESPONSES OF VEHICLES ON CURVES 118

Introduction, 118
Equations of Motion, 120
System Equations and Parameters, 120
Response Statistics, 124
Solutions for Covariance, 126
Range of Parameters, 127
Numerical Results and Conclusions, 131

APPENDIX I 136

Cable-Stayed Guideway Response Program, 136

APPENDIX II 150

Equations of Vehicle Motion, 150

APPENDIX III 156

Vehicle Response Program, 156

REFERENCES 176

# 1. EXECUTIVE SUMMARY

In Part I,which details the first year's effort,and the present study, the purpose is to investigate theoretically and experimentally guideway-vehicle system dynamics. The present study addresses three strong needs. The first is to evaluate and experimentally validate analyses of both curved and cable-stayed guideway responses to transit loads. Of the few such analyses done in the last ten years, many contain errors. The second need is to experimentally determine nondimensional responses of related guideway-vehicle configurations which have not yet received theoretical treatment. The third need is to analyze theoretically the lateral response statistics of typical automated guideway transit (AGT) vehicles negotiating stochastically rough, curved, at grade guideways and to identify the most important system parameters affecting ride quality.

The present investigations were divided into four main parts, described in Chapters 2 through 5. In Chapter 2, theoretical, nondimensional response studies are made for simple, elevated, horizontally curved beam guideways with several curvatures, subject to single and tandem vehicle transit loads. Included are both vertical loadings and companion guideway torques arising from vehicle centrifugal forces. The nondimensional system parameters derived here serve as the basis for the experimental designs of curved guideway-vehicle systems of Chapter 3. In this latter Chapter, measured, elevated guideway responses to tandem loads are correlated for single and multiple spans, for uneven pier spacing, and for several types of end constraints. Critical curved guideway responses to a sprung, lightly damped scale model of a typical AGT vehicle are measured also. In Chapter 4, the dynamic response theory for cable-stayed guideways subject to a constant speed, vertical point force is presented for the first time. To validate this theory, calculations of transient responses such as midspan moment time histories are compared to laboratory model test results. In Chapter 5, a mathematical model of an AGT vehicle-rigid, curved guideway system is formulated in terms of 27 dimensionless parameters. The effects of these parameters on the vehicle lateral dynamics and on the suspension system stroke are studied in a statistical sense through

solutions of the steady-state covarient propagation equation. In all of these Chapters, results are presented in nondimensional forms which are directly applicable to the design of analogous intraurban and intercity transport systems.

The important conclusions given at the end of each Chapter are summarized. Tandem vertical loads on simple, curved spans may result in dynamic amplifications of critical moment and rotation angle by a factor of 4 to 5 above the static values, for critical combinations of the vehicle spacing and transit speed parameters. Also transit torques always cause unbounded span responses, but only in a narrow range of the transit speed parameter. Finally, span torsional stiffness, arc angle and radius of curvature also affect responses. Next, the measured responses for simple, curved spans with vertical loadings agree quite well with these predictions. It is shown experimentally that the multiple spans are not always more dynamically efficient than equivalent simple spans, placed end-to-end. Above a critical transit speed parameter, multiple curved span responses become many times higher than those for simple spans. Experiments also show that sprung vehicle models generally cause lower span responses than their point force representations. Multiple span responses are lowered also by clamping the extreme ends. For cable-stayed guideways, the predicted critical responses agree very well with the experimental results. Finally, in the statistical response calculations of the AGT vehicle traversing a rigid, statistically rough, curved guideway, the importance of identifying nondimensional system parameters is demonstrated. Of these 27 parameters, the two parameters representing the height of the side guidance wheels and vehicle speed had the strongest influence on the lateral rms acceleration and mean suspension system strokes. Such analytical studies are especially valuable to designers in optimizing vehicle design for ride quality.

## 2. THEORY FOR SIMPLE, CURVED GUIDEWAYS

Introduction - In this chapter, the dynamic responses are calculated for a horizontally curved guideway to the passage of constant load, constant speed transit vehicles. The guideway is an elastic beam of constant radius of curvature, simply supported on each end. No damping is assumed in the formulation.

Although several general dynamic studies of vehicle-elevated guideway interactions have been made in recent years [1,2,3], no such systematic numerical studies directly applicable in dynamic design have been made for curved beam elements. This paper fills this lack by recasting previous studies [3] in dimensionless form and by correcting a conceptual error in the application of transit torques to curved beams [4]. Figure 1 shows this torque $T_0$ set up by a horizontal load. In a companion paper [5] to the present study where the limitations of curved beam theory are investigated, it was concluded that curved beam theory may adequately model a curved guideway provided that $\eta$, the ratio of guideway width to mean radius of curvature, remained less than 0.2. This restriction is assumed here. The following results, some of which are also in [6], will aid in the design of light-weight, dynamically stable elevated guideways for future urban transit vehicles.

Dynamic Theory - Figure 1 shows a typical guideway section and defines the coordinates of the curved beam. For the sake of clarity and completeness, the beam frequencies $p_{mn}$, derived previously [3,5] are repeated. The reference frequency is $\rho$, the fundamental frequency of a straight, simply supported beam of length $\ell$, for zero damping, is given by

$$p = \pi^2 (EI/m_0 \ell^4)^{1/2} \tag{1}$$

where EI is the stiffness and $m_0$ is the mass per unit length. The frequencies of the curved beam are given by

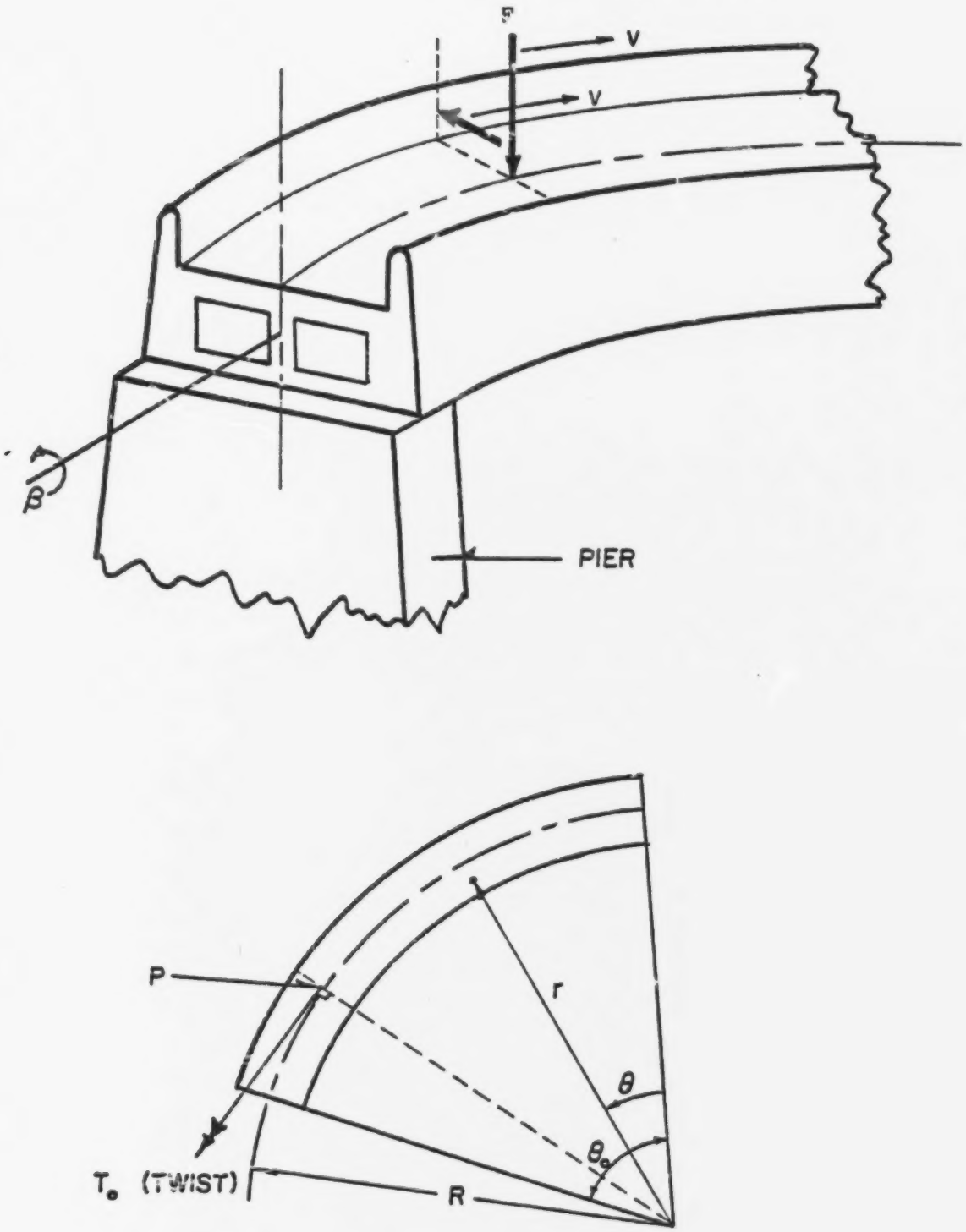


Figure 1. Loading and nomenclature for the curved beam guideway.

$$p_{mn} = n^2 \, p \, k_{mn}^{1/2} \qquad m = 1,2, \text{ only}$$
$$n = 1,2,3 \ldots \tag{2}$$

where

$$k_{mn} = \frac{1}{2}\left[\xi^2 \theta_n^4 \left(1 + \frac{A}{\theta_n^2}\right) + (1 + A\theta_n^2)\right]$$
$$+ \frac{(-1)^m}{2}\left\{\left[\xi^2 \theta_n^4 \left(1 + \frac{A}{\theta_n^2}\right) + (1 + A\theta_n^2)\right]^2\right.$$
$$\left. - 4A\xi^2 \theta_n^2 (1 - \theta_n^2)^2\right\}^{1/2} \tag{3}$$

$$\theta_n = \theta_0/n\pi; \qquad \xi = R/R_g; \qquad A = GJ/EI \tag{4}$$

where $R_g = (I_p/A_c)^{1/2}$, the radius of gyration based on $I_p$, the second moment of the cross section of area $A_c$ about its polar axis.* Thus, the three dimensionless parameters of Eqs. (4), or $\theta_0 = \ell/R$, $\xi$ and A (the rigidity ratio) define the curved beam counterpart of the straight beam.

The vertical deflection $w(\theta,t)$, the rotation angle $\beta(\theta,t)$ and the bending moment $M(\theta,t)$ are responses resulting from a constant speed vertical point load F and a transit twisting moment $T_0$ at the same location. Written in terms of dimensionless (barred) parameters, these responses are represented respectively by

$$\bar{w}(\theta,t) = \sum_{n=1}^{\infty} \bar{w}_n(\theta,t) = \frac{\pi^4 EI}{2F\ell^3} w(\theta,t) \tag{5a}$$

$$\bar{\beta}(\theta,t) = \sum_{n=1}^{\infty} \bar{\beta}_n(\theta,t) = \frac{1}{R\rho_1} \frac{\pi^4 EIR}{2F\ell^3} \beta(\theta,t) \tag{5b}$$

$$\bar{M}(\theta,t) = \sum_{n=1}^{\infty} \bar{M}_n(\theta,t) = \frac{\pi^4 R^2}{2F\ell^3} M(\theta,t) \tag{5c}$$

---

*The interpretation of subscripts mn is reversed in Ref. [3].

where

$$R\rho_{mn} = -\frac{1 + A}{\omega_n^2 + A - \frac{k_{mn}}{\omega_n^2 \xi^2}} \qquad (6)$$

$$R\rho_n = R\rho_{1n} \cdot R\rho_{2n}/(R\rho_{1n} - R\rho_{2n}) \qquad (7)$$

For the time period in which F and $T_0$ are on the beam, for $0 < t \leq \ell/v$, the displacement, rotation and moment responses are derived using techniques explained elsewhere. [3,4] In reference [3], the results for the transit load F, where $T_0 = 0$, are essentially correct, except for Eqs. (12); but this has been corrected in Eq. (6) above. The calculations of reference [4], Eq. (5.48), include the additional effect of the transit torque $T_0$; but those results are incorrect. In addition to several typographical errors, there was a conceptual error made there in the use of the matrix convolution integral to solve Eq. (5.33). The author [4] should have used the matrix impulse response function for impulsive torques rather than for impulsive <u>changes</u> in torques [6]. The properly rederived response functions which include effects of both F and $T_0$, and which are valid in the time interval $0 < t < \ell/v$, are

$$\bar{w}_n(\theta,t) = R\rho_n \left[ \frac{F_{2n}\sin(n\omega t)}{n^2 R\rho_{2n}(n^2 k_{2n} - \omega^2/p^2)} \right.$$

$$- \frac{F_{2n}(\omega/p)\sin(n^2\sqrt{k_{2n}}(p/\omega)\omega t)}{n^3 R\rho_{2n}\sqrt{k_{2n}}(n^2 k_{2n} - \omega^2/p^2}$$

$$- \frac{F_{1n}\sin(n\omega t)}{n^2 R\rho_{1n}(n^2 k_{1n} - \omega^2/p^2)}$$

$$\left. + \frac{F_{1n}(\omega/p)\sin(n^2\sqrt{k_{1n}}(p/\omega)\omega t)}{n^3 R\rho_{1n}\sqrt{k_{1n}}(n^2 k_{1n} - \omega^2/p^2)} \right] \sin(\theta/\theta_n) \qquad (8a)$$

$$\bar{\beta}_n(\theta,t) = \frac{R\rho_n}{R\rho_1}\left[\frac{F_{2n}\sin(n\omega t)}{n^2(n^2k_{2n}-\omega^2/p^2)}\right.$$

$$-\frac{F_{2n}(\omega/p)\sin(n^2\sqrt{k_{2n}}(p/\omega)\omega t)}{n^3\sqrt{k_{2n}}(n^2k_{2n}-\omega^2/p^2)}$$

$$-\frac{F_{1n}\sin(n\omega t)}{n^2(n^2k_{1n}-\omega^2/p^2)}$$

$$\left.+\frac{F_{1n}(\omega/p)\sin(n^2\sqrt{k_{1n}}(p/\omega)\omega t)}{n^2\sqrt{k_{1n}}(n^2k_{1n}-\omega^2/p^2)}\right]\sin(\theta/\theta_n) \qquad (8b)$$

$$\bar{M}_n(\theta,t) = R\rho_1\bar{\beta}_n(\theta,t) + \bar{w}_n(\theta,t)/\theta_n^2 \qquad (8c)$$

where

$$\omega = \pi v/\ell \qquad (9)$$

$$F_{1n} = 1 + \left[\frac{T_0}{k_g P}\right]\frac{\xi}{R\rho_{2n}} \qquad (10a)$$

$$F_{2n} = 1 + \left[\frac{T_0}{R_g P}\right]\frac{\xi}{R\rho_{1n}} \qquad (10b)$$

Equations (5a) and (5b), with Eqs. (8a) and (8b), reduce to Eqs. (30a) and (30b) of reference [3] when the transit torque term reduces to zero, or where $F_{1n} = F_{2n} = 1$.

It is seen by inspecting the above equations that the time history of the responses $\bar{w}$, $\bar{\beta}$ and $\bar{M}$ at a cross section $\theta$ can be expressed as a function of the dimensionless time variable $\omega t$ and the following five dimensionless system parameters:

$$\left.\begin{aligned}
\theta_0 &= \ell/R\ , && \text{total arc angle}\\
\xi &= R/R_G\ , && \text{radius ratio}\\
A &= GJ/EI\ , && \text{rigidity ratio}\\
\omega/p\ , &\quad \text{passage} && \text{frequency ratio}\\
\frac{T_0}{RF_g}\ , &\quad \text{transit} && \text{torque ratio}
\end{aligned}\right\} \qquad (11)$$

The above results are valid, of course, only when the point load and moment are on the beam, in the time range $0 < t \leq \ell/v$ or for $0 < \omega t \leq \pi$. For $\omega t > \pi$, the beam will undergo free vibrations, where the deflection $w_f(\theta,t)$, the rotation, $\beta_f(\theta,t)$, and the moment $M_f(\theta,t)$ have the form of Eqs. (5), or

$$\bar{w}_f(\theta,t) = \sum_{n=1}^{\infty} \bar{w}_{fn}(\theta,t) = \frac{\pi^4 EI}{2P\ell^3} w_f(\theta,t) \tag{12a}$$

$$\bar{\beta}_f(\theta,t) = \sum_{n=1}^{\infty} \bar{\beta}_{fn}(\theta,t) = R\rho_1 \frac{\pi^4 EI}{2P\ell^3 R} \beta_f(\theta,t) \tag{12b}$$

$$\bar{M}_f(\theta,t) = \sum_{n=1}^{\infty} \bar{M}_{fn}(\theta,t) = \frac{\pi^4 R^2}{2P\ell^3} M_f(\theta,t) \tag{12c}$$

As previously implied, [3], the forms for the free vibration responses are

$$\begin{aligned} \bar{w}_{fn}(\theta,t) = \Big[ & A_n \sin\left( n^2 \sqrt{k_{1n}}\, (p/\omega)(\omega t-\pi)\right) \\ & + B_n \cos\left( n^2 \sqrt{k_{1n}}\, (p/\omega)(\omega t-\pi)\right) \\ & + C_n \sin\left( n^2 \sqrt{k_{2n}}\, (p/\omega)(\omega t-\pi)\right) \\ & + D_n \cos\left( n^2 \sqrt{k_{2n}}\, (p/\omega)(\omega t-\pi)\right)\Big] \sin(\theta/\theta_n) \end{aligned} \tag{13a}$$

$$\begin{aligned} \bar{\beta}_{fn}(\theta,t) = \frac{1}{R\rho_1} \Big[ & R\rho_{1n} A_n \sin\left( n^2 \sqrt{k_{1n}}\, (p/\omega)(\omega t-\pi)\right) \\ & + R\rho_{1n} B_n \cos\left( n^2 \sqrt{k_{1n}}\, (p/\omega)(\omega t-\pi)\right) \\ & + R\rho_{2n} C_n \sin\left( n^2 \sqrt{k_{2n}}\, (p/\omega)(\omega t-\pi)\right) \\ & + R\rho_{2n} D_n \cos\left( n^2 \sqrt{k_{2n}}\, (p/\omega)(\omega t-\pi)\right) \Big] \sin(\theta/\theta_n) \end{aligned} \tag{13b}$$

$$\bar{M}_{fn}(\theta,t) = R\rho_1 \bar{\beta}_{fn}(\theta,t) + \bar{w}_{fn}(\theta,t)/\theta_n^2 \tag{13c}$$

The constants $A_n$, $B_n$, $C_n$ and $D_n$ of Eqs. (13) are calculated using the beam continuity conditions for the deflection, the rotation and their velocities just as the loads reach the beam exit. These conditions are:

$$w(\theta,\ell/v) = w_f(\theta,\ell/v) \tag{14a}$$

$$\dot{w}(\theta,\ell/v) = \dot{w}_f(\theta,\ell/v) \tag{14b}$$

$$\beta(\theta,\ell/v) = \beta_f(\theta,\ell/v) \tag{14c}$$

$$\dot{\beta}(\theta,\ell/v) = \dot{\beta}_f(\theta,\ell/v) \tag{14d}$$

When Eqs. (5), (8), (12), (13) and (14) are used, the results are

$$A_n = \frac{F_{1n}R\rho_n}{R\rho_{1n}} \left[ \frac{(\omega/p)\cos(n^2\pi\sqrt{k_{1n}}p/\omega)}{n^3\sqrt{k_{1n}}\,(n^2k_{1n}-\omega^2/p^2)} - \frac{(-1)^n(\omega/p)}{n^3\sqrt{k_{1n}}(n^2k_{1n}-\omega^2/p^2)} \right] \tag{15a}$$

$$B_n = \left[ \frac{F_{1n}R\rho_n}{R\rho_{1n}} \right] \frac{(\omega/p)\sin(n^2\pi\sqrt{k_{1n}}p/\omega)}{n^3\sqrt{k_{1n}}(n^2k_{1n}-\omega^2/p^2)} \tag{15b}$$

$$C_n = -\frac{F_{2n}R\rho_n}{R\rho_{2n}} \left[ \frac{(\omega/p)\cos(n^2\pi\sqrt{k_{2n}}p/\omega)}{n^3\sqrt{k_{2n}}(n^2k_{2n}-\omega^2/p^2)} - \frac{(-1)^n(\omega/p)}{n^3\sqrt{k_{2n}}(n^2k_{2n}-\omega^2/p^2)} \right] \tag{15c}$$

$$D_n = -\left[ \frac{F_{2n}R\rho_n}{R\rho_{2n}} \right] \frac{(\omega/p)\sin(n^2\pi^2\sqrt{k_{2n}}p/\omega)}{n^3\sqrt{k_{2n}}(n^2k_{2n}-\omega^2/p^2)} \tag{15d}$$

The procedure is now summarized for calculating the response histories to the transit point load P and its companion torque $T_0$. Specify the cross section location $\theta$ and fix each of the five system parameters of Eq. (11). Specify an upper limit for n. Calculate $k_{mn}$ from Eq. (3); $\theta_n$ from Eq. (4); $R\rho_{mn}$ and $R\rho_n$ from Eqs. (6) and (7); $F_{1n}$ and $F_{2n}$ from Eqs. (10). For specified values of $\omega t$ in the range $0 < \omega t \leq \pi$, calculate the responses from Eqs. (5) using Eqs. (8). For specified values of $\omega t > \pi$, calculate the responses from Eqs. (12) using Eqs. (13) and (15).

Tandem Vehicle Simulations - Consider a series of point loads $F_1, F_2, F_3 \ldots$ with invariant companion ratios $(T_0/R_gF)_1 = (T_0/R_gF)_2 = (T_0/R_gF)_3 = \ldots$, moving in tandem, each spaced $R\Delta\theta$ apart. Each $F_1, F_2, \ldots$ load may have a different magnitude (some may be zero); but they are time-invariant. Consider time $t=t_\alpha$ where

$$t_\alpha = \alpha R\Delta\theta/v \quad (\alpha = 1,2,\ldots) \tag{16}$$

and designate the deflection due to a unit load at position $\alpha R\Delta\theta$ as $w(\theta,t_\alpha)$. At time $t=t_1$, let $F=F_1$ be the first load of the tandem, located on the arc at position $R\theta = R\Delta\theta$. The span deflection at all $R\theta$ positions due to $F_1$ will then be $F_1w(\theta,t_1)$. At time $t_2$, load $F_2$ will be at position $2R\Delta\theta$ and its contribution to the span deflection will be $F_1w(\theta,t_2)$. Also, $F_2$ will be at position $R\theta=R\Delta\theta$ and will cause a deflection $F_2w(\theta,t_1)$. By superposition, the deflection due to both $F_1$ and $F_2$ at time $t=t_2$ are additive, and this sum is designated as $W(\theta,t_2)$ where

$$W(\theta,t_2) = F_1w(\theta,t_2) + F_2w(\theta,t_1) \tag{17}$$

It is easily deduced that the total span deflection at any time $t=t_\alpha$ is given by

$$W(\theta,t_\alpha) = \sum_{j=1}^{\infty} F_j w(\theta,t_{\alpha+1-j}) \tag{18}$$

where the value of $w(\theta,t_{\alpha+1-j})$ is the value derived for the unit point load in forced vibrations if $t_{\alpha+1-j} \leq \ell/v$. However, if $t_{\alpha+1-j} > \ell/v$, then the expression for deflection in Eq. (16) needs to be replaced by $w_f(\theta,t_{\alpha+1+j})$. Expressions similar to Eq. (18) follow for rotation and moment. In this way span responses can be calculated for multiple vertical loads of fixed magnitude, where each torque parameter is identical or zero. The numerical examples which follow illustrate these ideas.

Parameter Studies and Conclusions - A computer program was written to calculate the response histories in terms of $\omega t$ for the dimensionless amplitude ratios:

$$\frac{w(\theta,t)}{w_s(\theta,t)} \; ; \quad \frac{\beta(\theta,t)}{\beta_s(\theta,t)} \; ; \quad \frac{M(\theta,t)}{M_s(\theta,t)} \tag{19}$$

The normalizing quantities, subscripted s, correspond to the peak static responses for the chosen single or tandem load traveling at crawl speed, or $\omega/p=0$. For each chosen set of the system parameters defined by Eqs. (11), these response ratios at midspan ($\theta=\theta_0/2$) were calculated on an IBM 370/165 computer. The absolute value of the peak responses were observed in each case. The calculations were carried out well into the free vibration range to obtain these peak values.

The first series of responses, shown in Figs. 2 through 6, were calculated for laboratory test spans and several combinations of vertical point loads, meant to complement experiments discussed in Chapter 3. A steel plate was chosen with a of 1/8 x 5 in. cross-section and a mean radius of R=80.2 in. Thus, $\xi$=55.6 and A=1.57, corresponding to a Poisson's ratio of 0.3 [6]. In Figs. 2 through 6, the effects of transit torques * were omitted, or $T_0/R_gP = 0$.

Figure 2 shows these peak midspan responses as a function of the passage frequency ratio, $\omega/p$, for a single point force traversing a 15, 30, 45 and 60 deg. span. There are several

*It is shown presently, Figs. 12-15, that $T_0$ affects span dynamics only for $0.9<\omega/p<1.1$, for A>0.5. The experimental system could not achieve $\omega/p>0.9$.

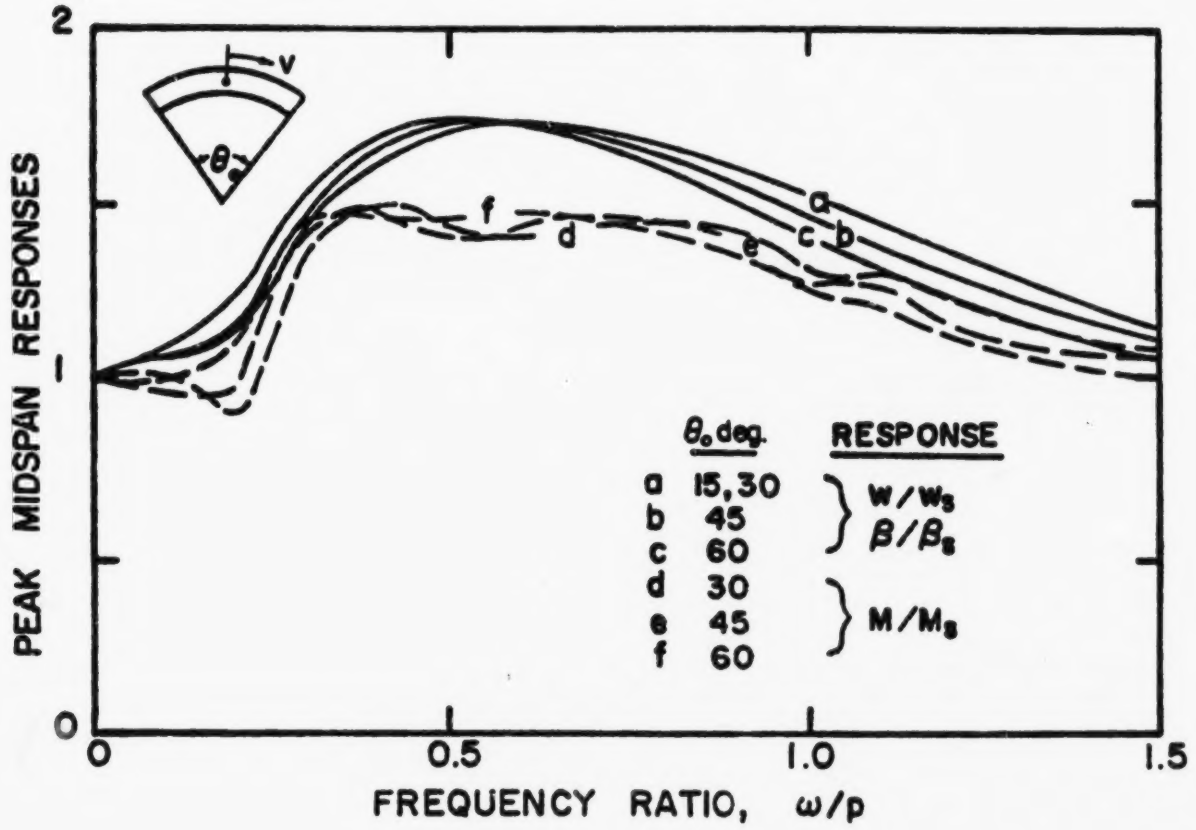


Figure 2. Peak midspan responses of laboratory model curved guideways with point loading; $\xi = 55.6$, $A = 1.57$.

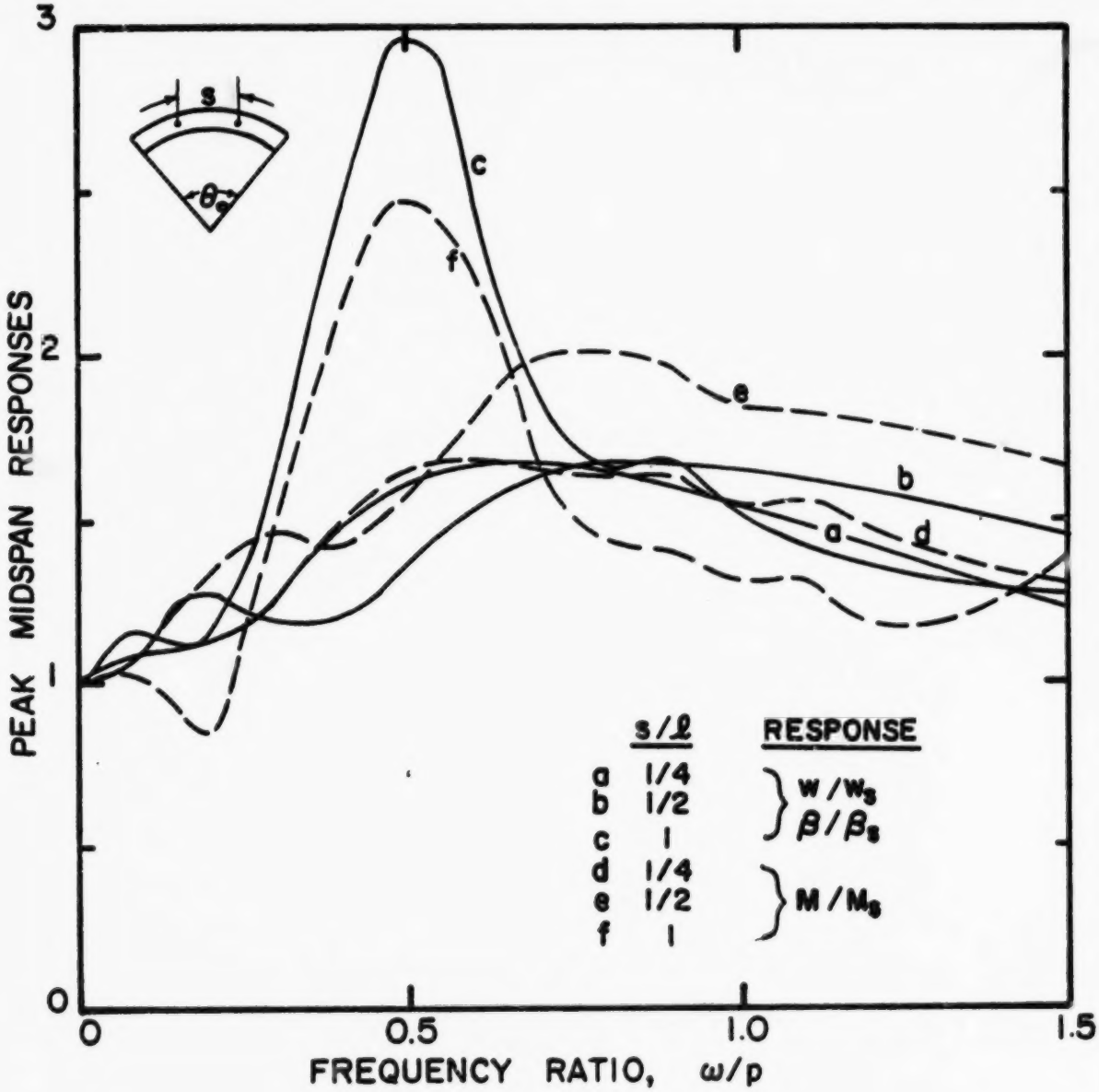


Figure 3. Guideway responses for two transit loads; $\theta_o$ = 30 deg., $\xi$ = 55.6, A = 1.57.

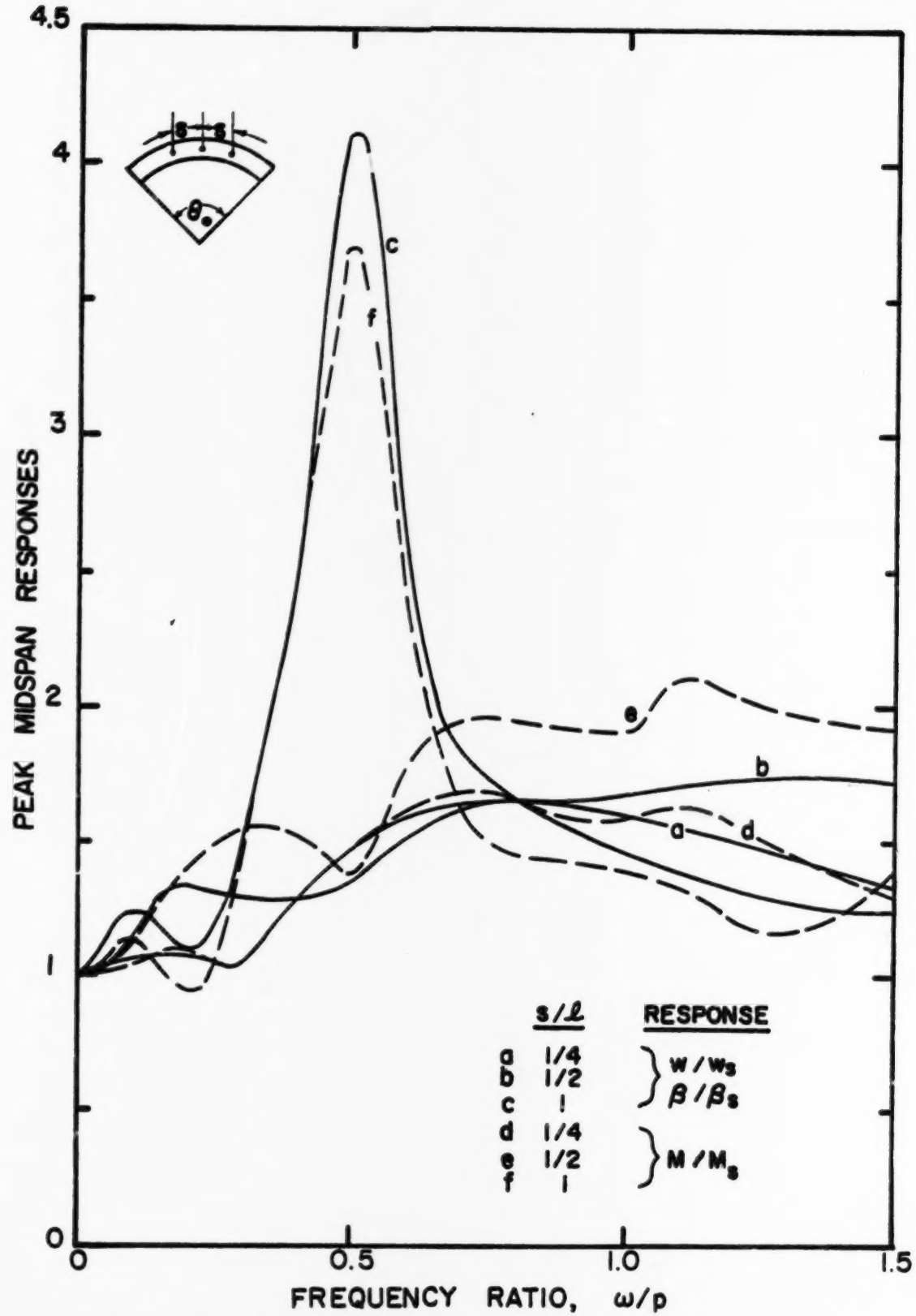


Figure 4. Guideway responses for three transit loads; $\theta_o$ = 45 deg., $\xi$ = 55.6, A= 1.57.

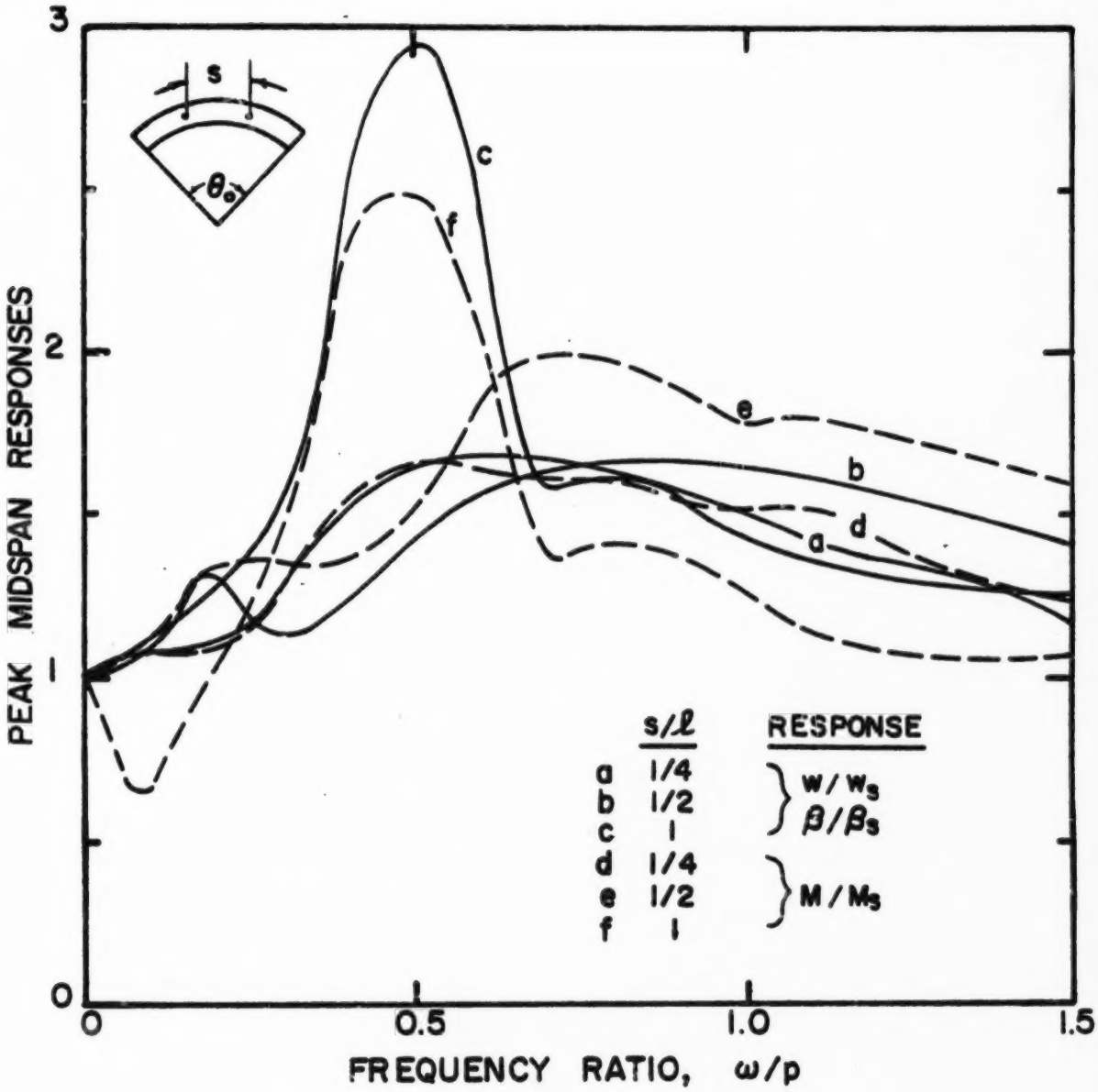


Figure 5. Guideway responses for two transit loads; $\theta_o$ = 45 deg., $\xi$ = 55.6, A = 1.57.

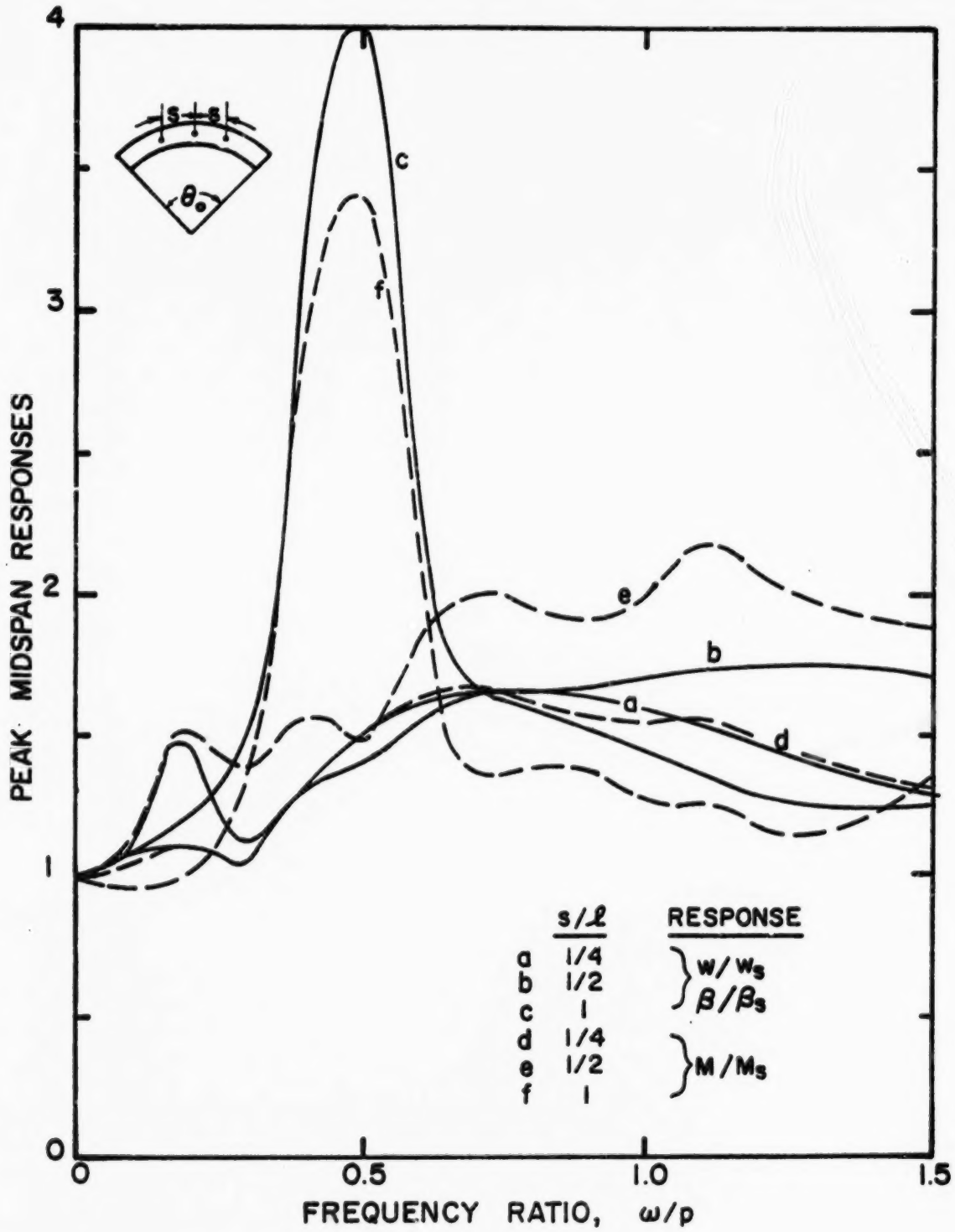


Figure 6. Guideway responses for three transit loads; $\theta_0$ = 45 deg., $\xi$ = 55.6, A = 1.57.

observations.* First, there are insignificant differences in response amplifications for the 15 and 30 deg. spans. Second, the deflection and rotation response amplifications are essentially identical, to within two significant figures. Third, the passage frequency ratio at which the absolute maximums of these two responses occur, shifts from 0.6 to 0.5 for increasing $\theta_0$. Fourth, the moment amplification is generally less than the other responses, reaching a peak value of about 1.5. Finally, peak responses (a,b,c) to the left of each respective absolute maximum occur while the load is on the span; but occur to the right after the load exits the span (during free vibration).

Figures 3 and 4 show the effects on responses of tandem transit point loads traversing a 30 deg. span. The effects of load separation distance s along the arc are apparent. Absolute maximum responses occur when the separation ratio $s/\ell=1$, for a frequency ratio of $\omega/p = 0.5$. For two loads in sequence, Fig. 3, the peak deflection ratio is 3.0; but for three loads in sequence, Fig. 4, this response peak is about 4.2. The respective moment amplifications for $s/\ell=1$ are less, or 2.5 and 3.7. It is noted from both figures however, that the moment amplifications exceed the deflection and rotation amplifications at a spacing ratio of 1/2.

Figures 5 and 6 are the counterparts to Figs. 3 and 4, with the single change that these results are for 45 deg. instead of 30 deg. spans. The data trends observed in the last paragraph apply here as well, where the respective absolute maximum response ratios are nearly the same.

In the next series of studies, shown in Figs. 7 through 11, responses were calculated for a single, transit vertical point force for zero transit torque, and for all combinations of the following parameters:

---

*The normalizing, simple span frequency, p, in the abscissa of all response curves introduces no "error". If $\omega/p_{mn}$, where m=n=1 for the curved span, were used instead of $\omega/p$, all abscissa scales would be shifted by less than 10% to the left.

$$\left.\begin{aligned} \theta_0 &= 30°;\ 45°;\ 60° \\ \xi &= 50;\ 100;\ 200 \\ A &= 0.05;\ 0.5;\ 1;\ 2 \end{aligned}\right\} \qquad (20)$$

These parameters cover the range of practical design, with the observation that span responses are negligibly different for $\theta_0$ in the 15 to 30 deg. range, other parameters remaining the same. For the radius ratio, for instance, a midrange value of $\xi = 105$ was calculated for a prestressed concrete box guideway of 700 ft. radius, a configuration considered the most economical [8]. For the rigidity ratio, $A = 1.14$ for this concrete box guideway; whereas for a steel plate of solid rectangular cross-section, $A = 1.57$. As discussed elsewhere [3], the practical range for existing structures today is for A between 0.5 and 1. However, for lightweight, flexible guideways, A may be smaller, so the lower value of 0.05 was chosen to accentuate the effects of loss of rigidity on the dynamic responses.

Figures 7 and 8 show the effects of rigidity ratio on peak responses at constant $\xi = 100$. For A in the range of 0.5 to 2, the deflection response curves (b,c) are very nearly coincident, as are the moment curves (e,f). The spread between (b,c) and also between (e,f) becomes greater, however, as $\theta_0$ increases from 30 deg. to 60 deg. At constant $\omega/p$, for $\theta_0 = 30$ deg. (Fig. 7), the respective responses are all within 2.6 percent; for $\theta_0 = 45$ deg. (not shown), they differ by at most 5 percent; and for $\theta_0 = 60$ deg. (Fig. 8), they differ by a maximum of 8.3 percent. As A decreases to 0.05, however, both responses (a,d) are shifted dramatically to the left; but their absolute peaks remain practically the same. Finally, at constant $\omega/p$, the deflection responses, $w/w_s$ and peak twist angle responses, $\beta/\beta_s$, (not shown) were found to be within 1 percent of each other for all values of A in the range of 0.5 to 2.0, for the range of $\theta_0$ between 15 and 60 deg., and $\xi = 100$.

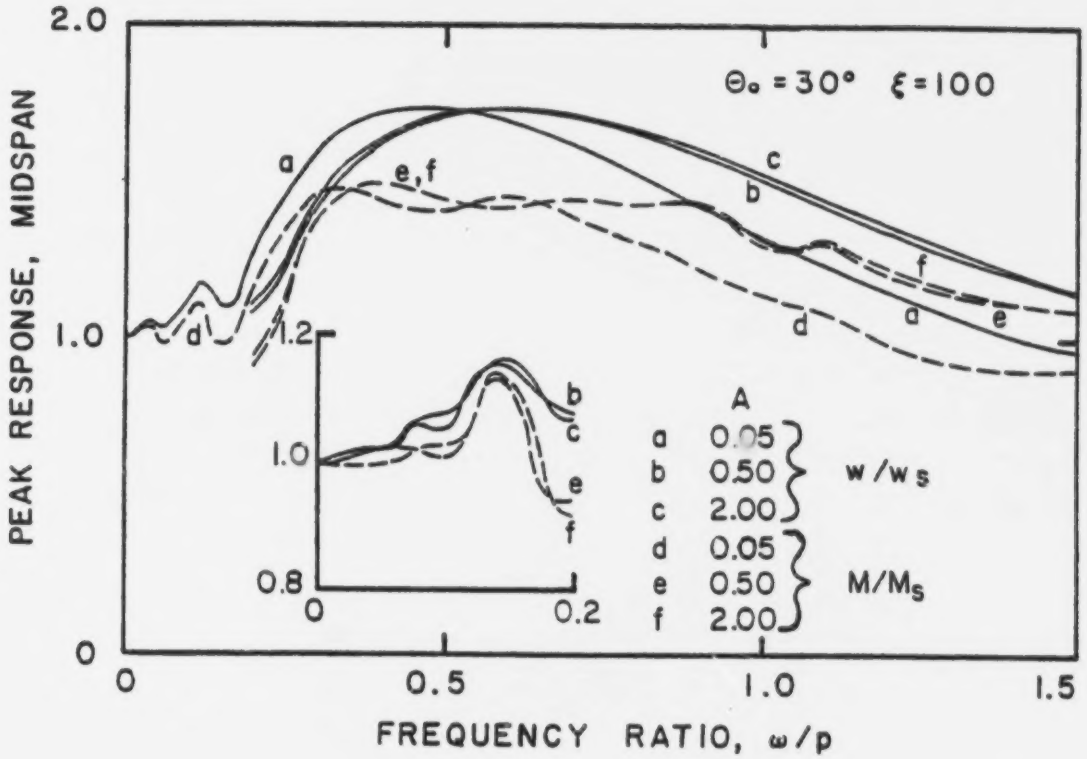


Figure 7. Rigidity effects for a 30° guideway.

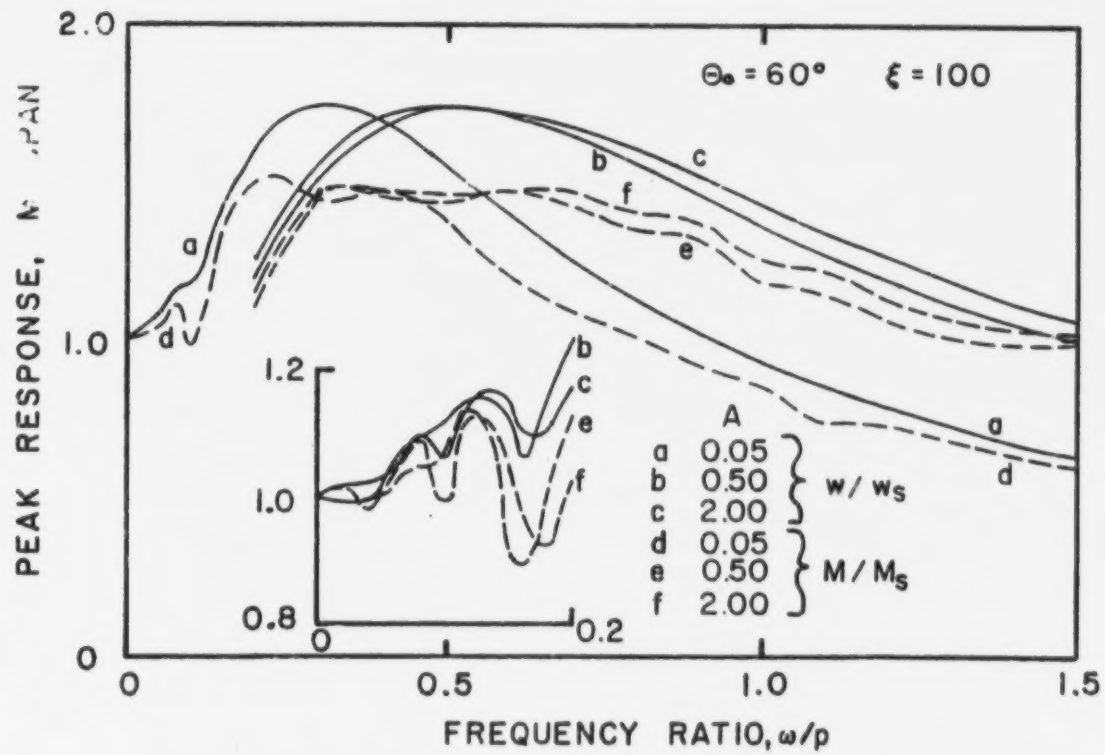


Figure 8. Rigidity effects for a 60° guideway.

Figures 9 through 11 show the responses are really not very sensitive to changes in radius ratio $\xi$ in the range of 50 to 200, other parameters remaining constant. In Fig. 9 for $\theta_0$ = 60 deg. and the values of A shown, the curves are essentially unchanged for $\xi$ varying in this range. Further calculations (not shown) revealed that if the only parameter change in Fig. 9 is $\theta_0$ = 30 deg., those response curves change by at most 3 percent. Again, the deflection and twist angle curves are coincident in Fig. 9 at $\theta_0$ = 30 and 60 deg. Figures 10 and 11, however, generally show a moderate increase in responses for an increase in $\xi$ for the extremely low value of A = 0.05. Also, all responses shift to the left as $\theta_0$ changes from 30 deg. (Fig. 10) to 60 deg. (Fig. 11).

The final series of studies show the effect on responses of a single transit torque together with its companion vertical load, traversing a 30, 45 and 60 deg. simple span. It is noted that a torque ratio of about 0.4 corresponds to a typical, 8 passenger urban transit vehicle traversing a 700 ft. radius curve at 55 mph. Thus, a practical range of study for $T_0/R_gP$ is between 0.25 and 1.0. The results, shown in Figs. 12 through 15, show that, except for a very narrow range of $\omega/p$, the midspan responses are practically identical to those for a torque ratio equal to zero. The resonance peaks are for a torque ratio of unity, where smaller values of $T_0/R_gP$ are contained within these envelopes. Figures 12 and 13 show that as A increases at constant $\theta_0$ and $\xi$, the resonance peaks become narrower and occur at a value of $\omega/p$ of unity. As $\theta_0$ increases from 30 to 60 deg., these peaks shift to the left, as shown in Fig. 14. It is noted again, Fig. 15, that the only effect of increasing the torque ratio is to make the width of the resonance peaks a little broader. Finally, a last series of studies, not shown in these Figures, indicates that the radius ratio $\xi$ has very little effect on these resonance peaks. The minor effect is that the resonance response peaks become somewhat narrower as $\xi$ is decreased, but those peaks still occur at the same value of $\omega/p$, other parameters remaining the same.

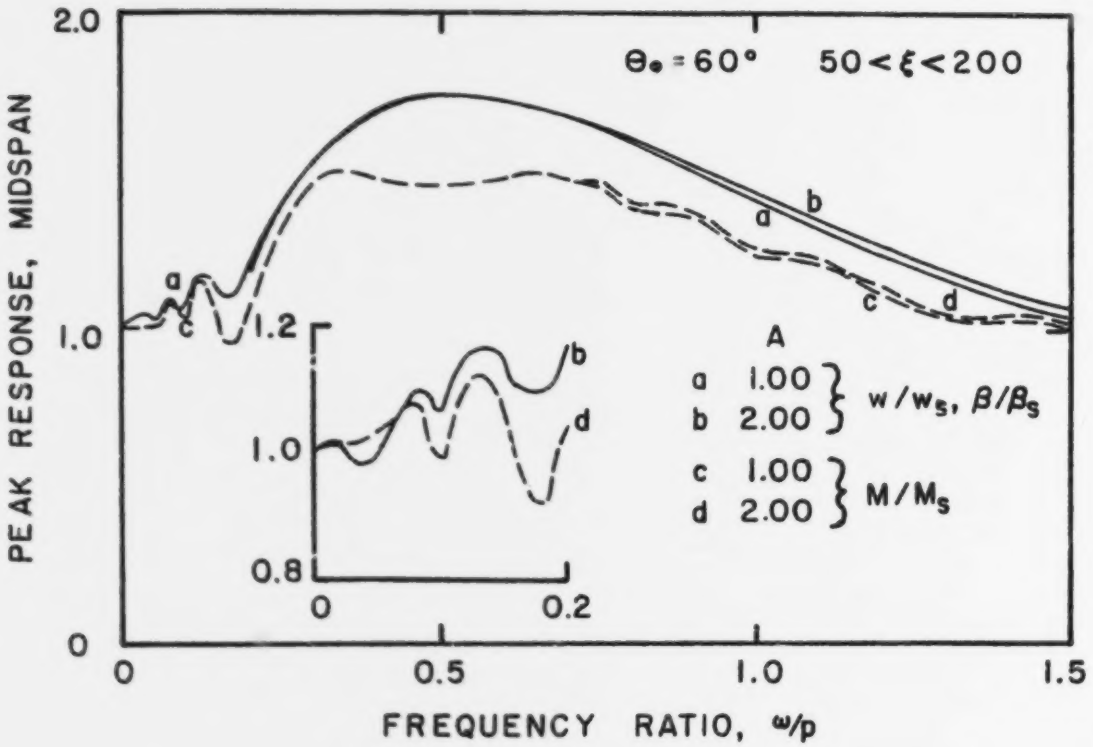


Figure 9. Curve radius effects for a 60° guideway.

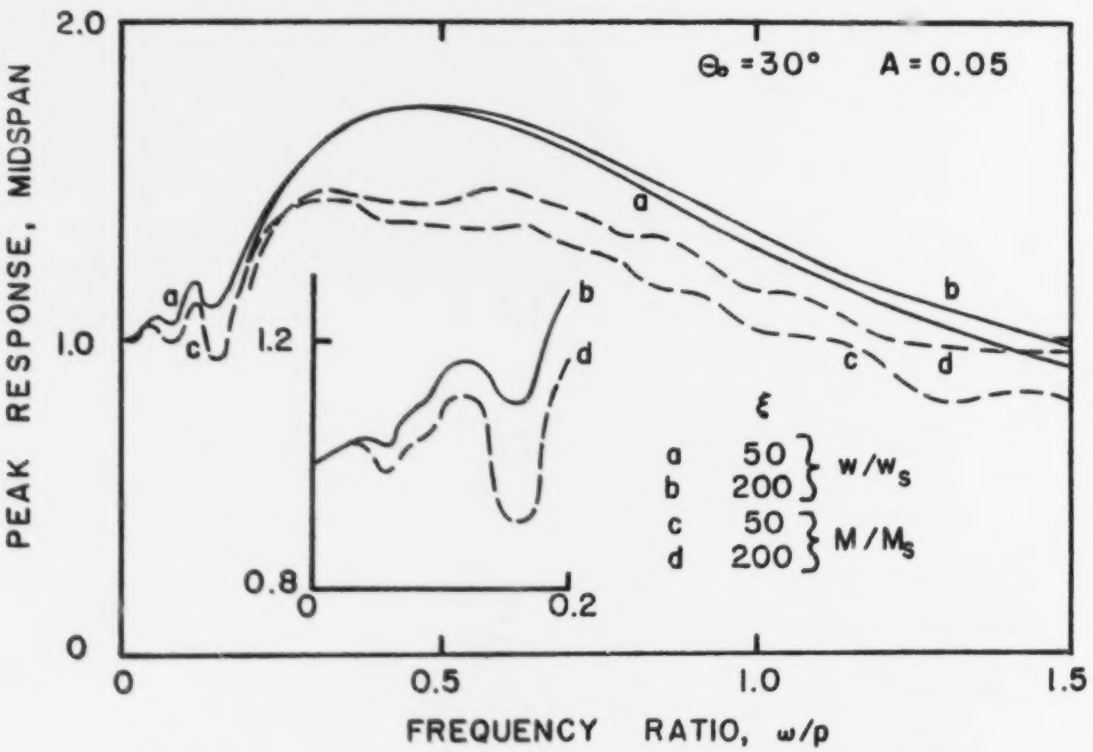


Figure 10. Curve radius effects for a 30° guideway.

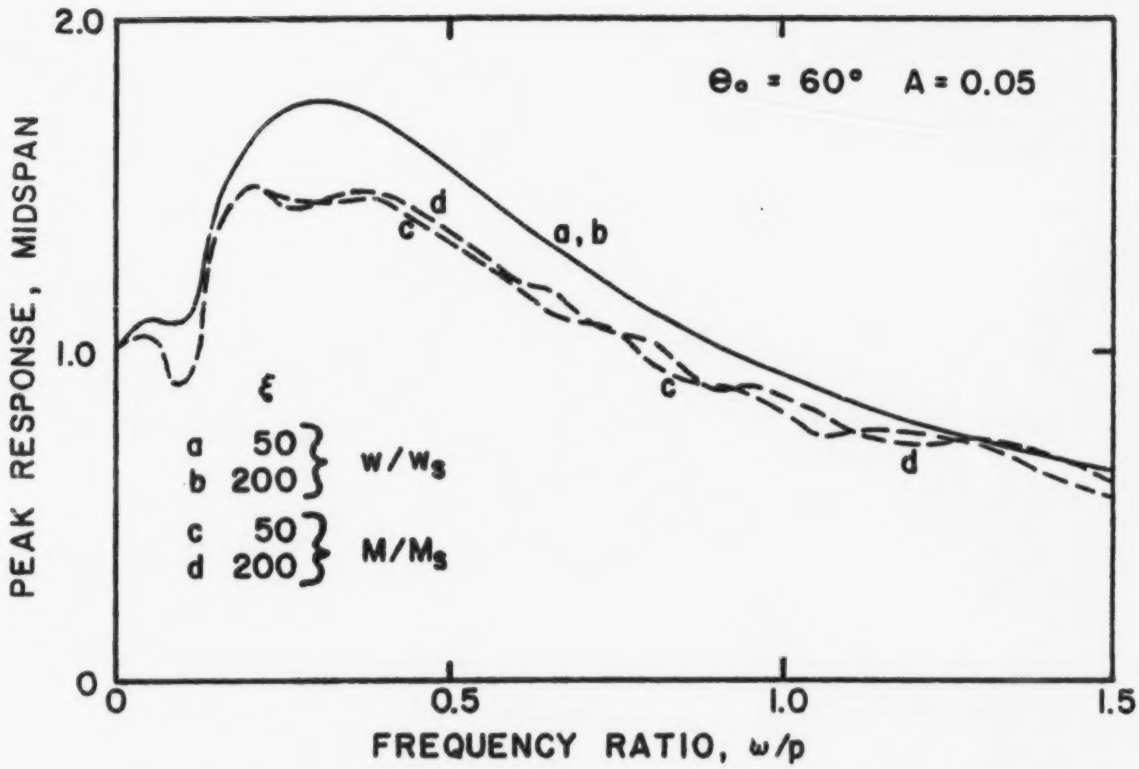


Figure 11. Curve radius effects for very low stiffness, 60° guideway.

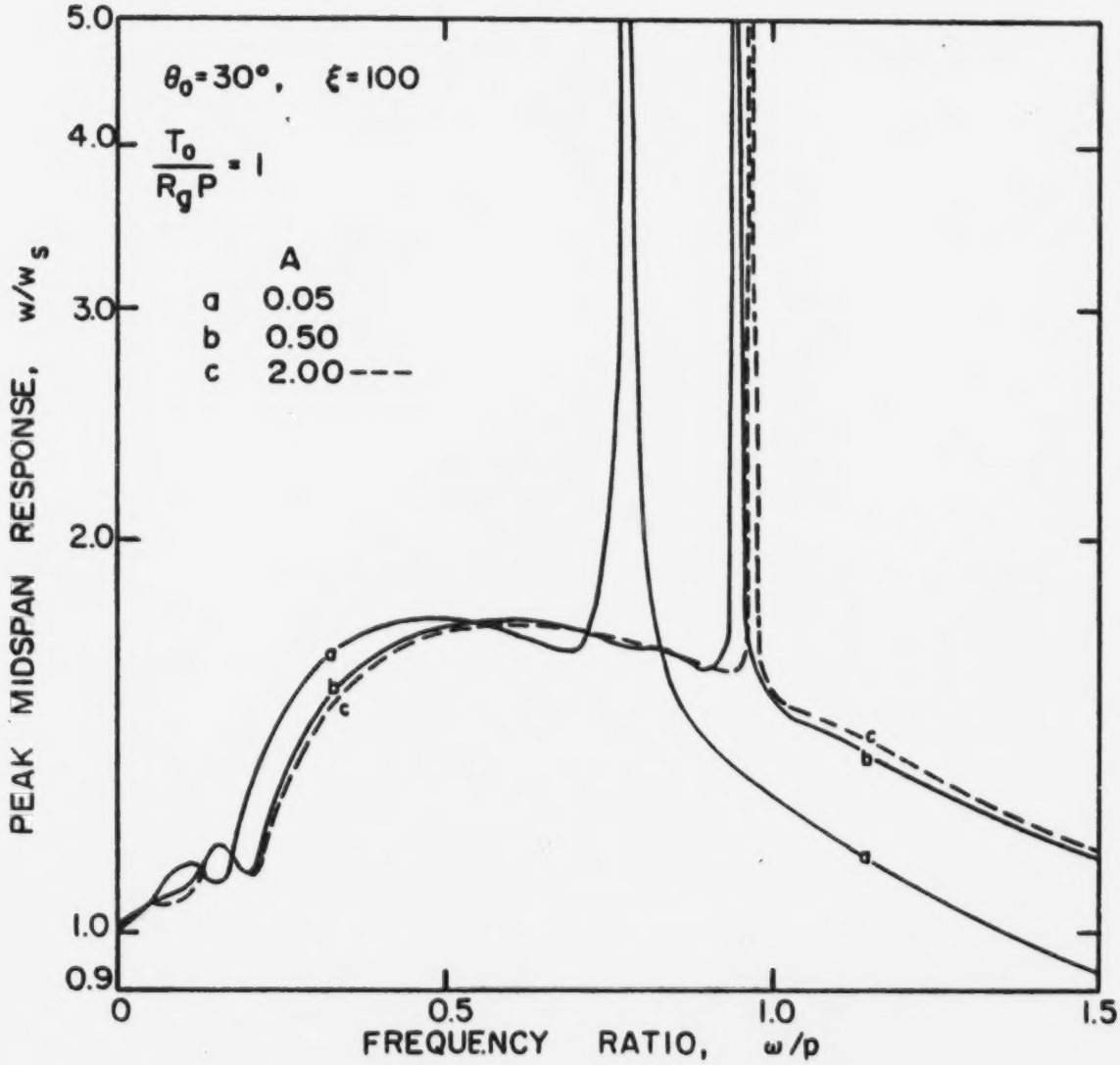


Figure 12. Transit torque-rigidity effects on deflection responses for a 30° , curved guideway with point loading.

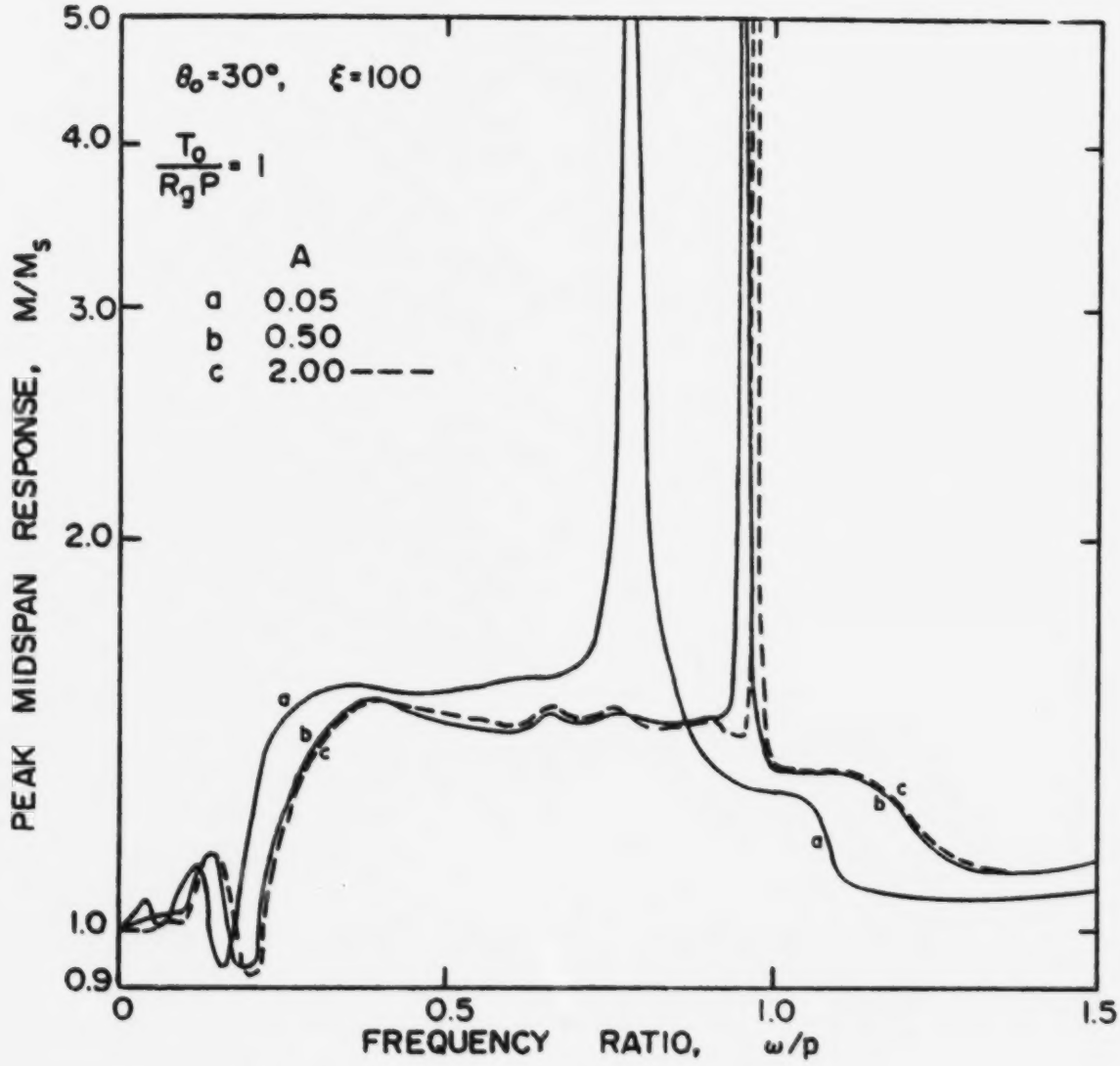


Figure 13. Transit torque-rigidity effects on moment responses for a 30° curved guideway with point loading.

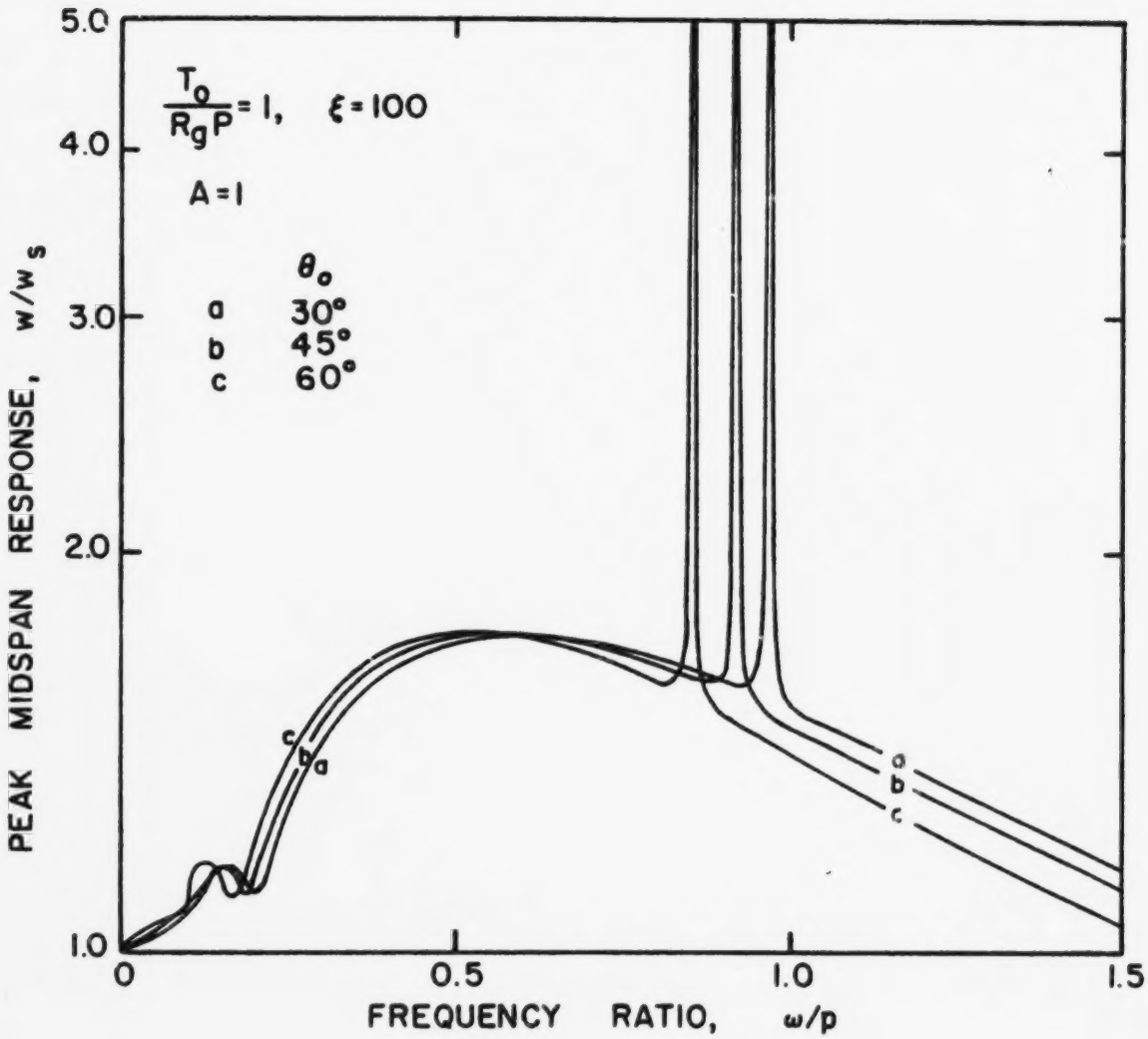


Figure 14. Curve angle effects on responses of guideways with transit torque and point loading.

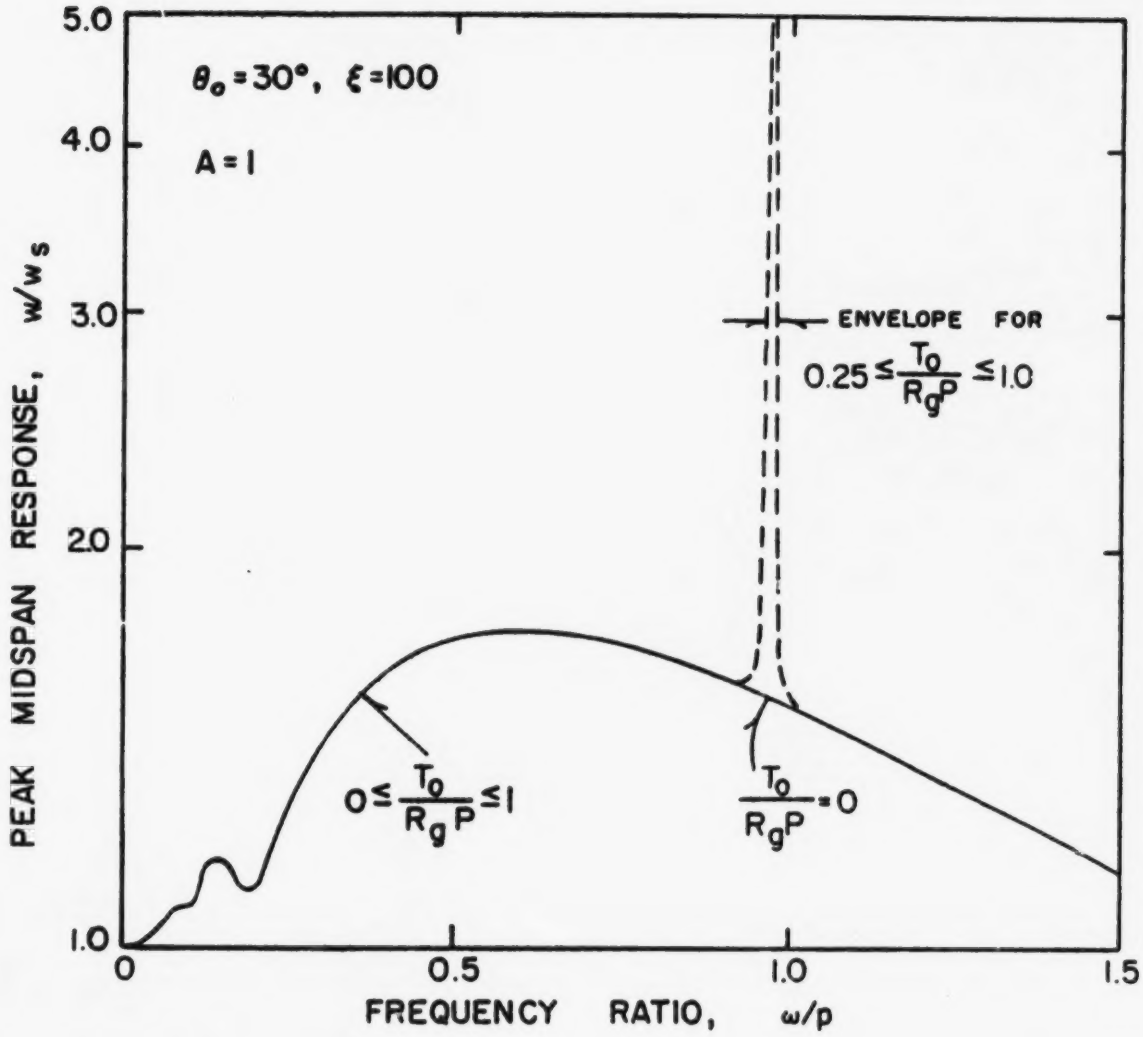


**Figure 15.** **Transit torque effects on responses for a 30° curved guideway with point loading.**

## 3. LABORATORY STUDIES OF CURVED GUIDEWAY - VEHICLE DYNAMICS

Introduction - The aims of this chapter are threefold: to describe the curved guideway test facility; to validate the simple, curved span response calculations of Chapter 2 with selected experiments; and to present the experimental responses of several multiple or continuous curved spans under a variety of transit loads and span end constraints. For these latter guideway spans, no corresponding analytic solutions are available.

Guideway Models and Response Measurements - The basic experimental designs of the curved guideways, the relatively short, light-weight vehicles represented as point loads, and the sprung Automated Guideway Transit (AGT) vehicle are outlined below. Further details are presented elsewhere (9,10,11).

Scale model guideway configurations were designed to be within the practical range of prototype designs. The five system parameters which need to be preserved from model to prototype, derived in Chapter 2 are:

$$\theta_0 = \ell/R \quad , \quad \text{total arc angle}$$
$$\xi = R/R_g \quad , \quad \text{radius ratio}$$
$$A = GJ/EI \quad , \quad \text{rigidity ratio}$$
$$\omega/p \quad , \quad \text{passage frequency ratio}$$
$$T_0/R_g F \quad , \quad \text{transit torque ratio}$$

where the $\ell$ is the arc length of curved beam centerline and R is its radius, shown in laboratory layout sketch of Figure 16. The reference frequency p is that of a straight simple beam of equal length $\ell$ and equal bending stiffness EI. The term $\omega = \pi v/\ell$ is the passage frequency of the vertical load F moving at constant speed v along the arc. The transit torque $T_0$, due to vehicle side loads, applies a twist to the beam which is resisted by its torsional rigidity GJ. Finally, $R_g = (I_p/A_c)^{1/2}$ is the radius of gyration based on $I_p$, the second moment of the cross-section $A_c$ about its polar axis.

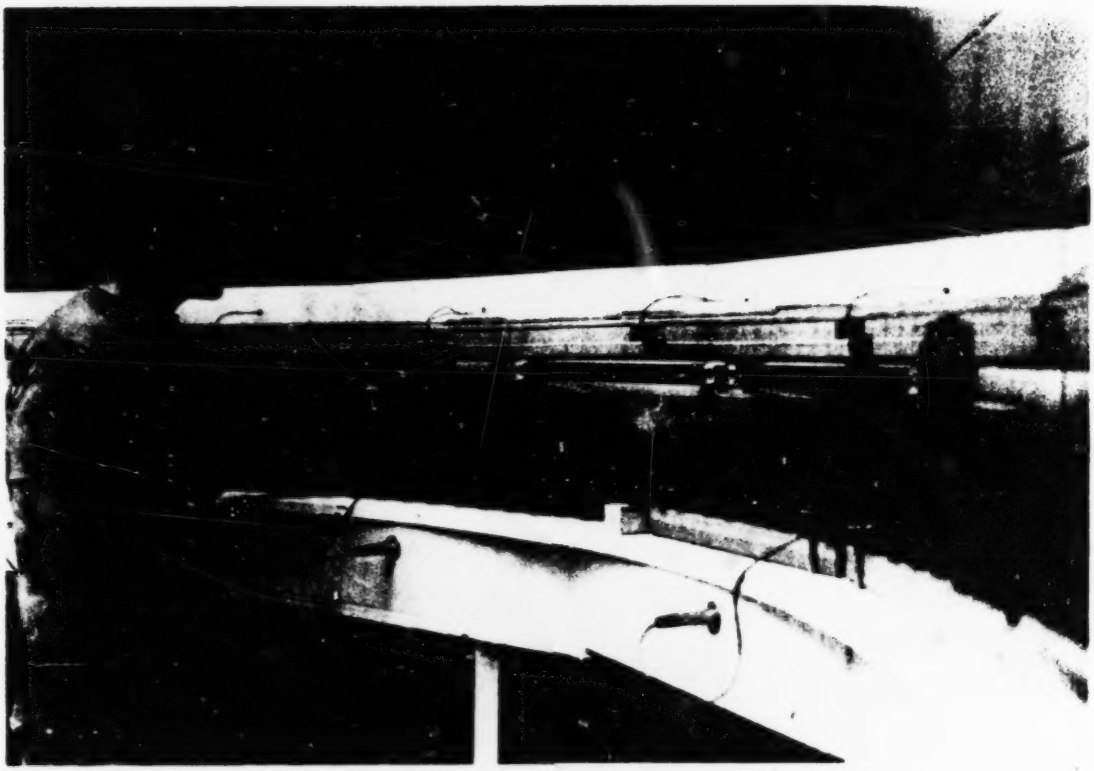

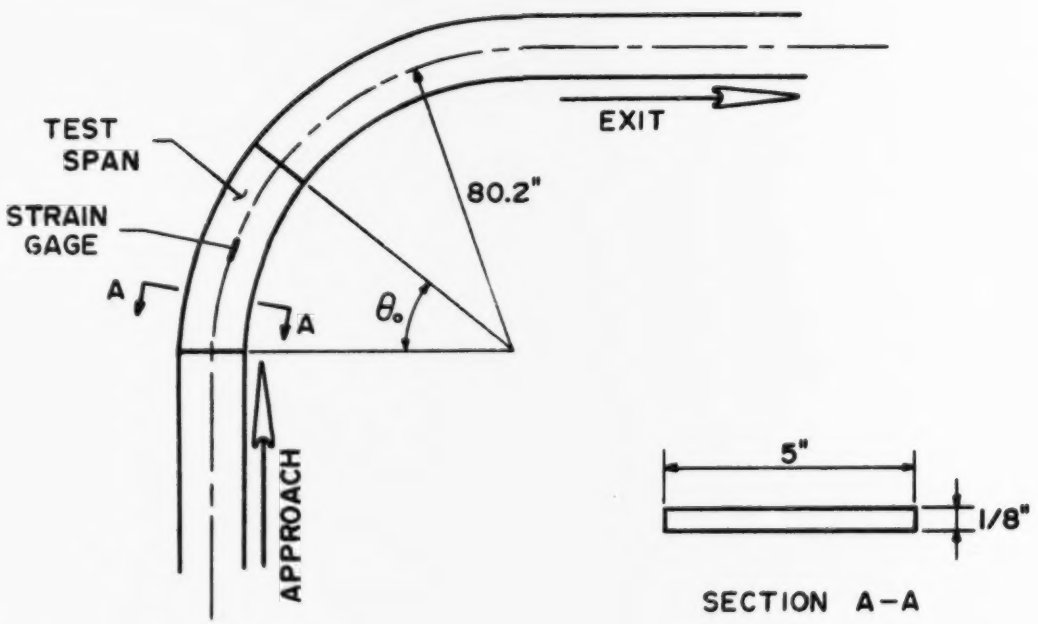


Figure 16. Curved guideway and vehicle models.

The dimensionless responses of the curved span model at a position x along its arc, subject to the same support conditions and the same relative load distribution (as a fraction of $\ell$) as the prototype, are given in the form

$$w/w_s \; ; \quad \beta/\beta_s \; ; \quad M/M_s$$

where w, $\beta$ and M, respectively, represent the deflection, angle of twist and circumferential bending moment as a function of the dimensionless dependent variables $x/\ell$ and $\omega t$, where t is time. The subscript s refers to the peak static responses at midspan for the load at crawl speed.

As shown in Chapter 2, prototype guideways for $\theta_0$ in the range of 30 to 60 deg. show that $0.5 \leq A \leq 2.0$ and $50 \leq \xi \leq 200$. Further, except in the narrow range $0.9 \leq \omega/p \leq 1.0$, the transit torque ratio has negligible effect on curved beam responses. Thus the model guideway was designed without side loading ($T_0 = 0$), for the realistic values $A = 1.54$ and $\xi = 55.6$. Calculations showed that response data for a simple, curved span were relatively insensitive to values of A in the range $0.5 \leq A \leq 2$ and to a factor of two variation in $\xi$ from the experimentally chosen one of 55.6.

The experimental setup shown in Fig. 16 was designed to accommodate all of the experimental spans and vehicle load configurations listed in Table 1. For each of the span configurations listed, the fundamental frequency p was calculated from Eq. (2). The corresponding frequency was determined experimentally also by plucking each span and measuring the midspan bending strain history during free vibration. As shown in Table 2, agreement between the predicted and measured values are within 2.9%, giving confidence in the experimental curved span designs.

Table 1. Curved Guideway-Vehicle Test Program

| Guideway Configurations | Load Configurations |
|---|---|
| 30° simple span | 1 point load<br>2 point loads @ ℓ/4 spacing<br>3 point loads @ ℓ/4 spacing<br>2 point loads @ ℓ/2 spacing<br>3 point loads @ ℓ/2 spacing<br>AGT vehicle |
| 45° simple span | 1 point load<br>2 point loads @ ℓ/4 spacing<br>3 point loads @ ℓ/4 spacing<br>2 point loads @ ℓ/2 spacing<br>3 point loads @ ℓ/2 spacing<br>AGT vehicle |
| 30°-30° 2-span continuous | 1 point load<br>2 point loads @ ℓ/4 spacing<br>3 point loads @ ℓ/4 spacing<br>2 point loads @ ℓ/2 spacing<br>3 point loads @ ℓ/2 spacing<br>AGT vehicle |
| 45°-45° 2-span continuous | 1 point load<br>2 point loads @ ℓ/4 spacing<br>3 point loads @ ℓ/4 spacing<br>2 point loads @ ℓ/2 spacing<br>AGT vehicle |
| 30°-30°-30° 3-span continuous | 1 point load<br>2 point loads @ ℓ/4 spacing<br>3 point loads @ ℓ/4 spacing<br>2 point loads @ ℓ/2 spacing<br>3 point loads @ ℓ/2 spacing<br>AGT vehicle |

Table 2. Experimental and Theoretical Fundamental Frequencies for the Curved Guideway Model.

| Guideway Configuration | Experimental Fundamental Frequency (hertz) | Theoretical Fundamental Frequency (hertz) | Difference % |
|---|---|---|---|
| 30° simple span | 3.68 | 3.75 | 1.9 |
| 30°-30° 2-span continuous | 3.68 | 3.75 | 1.9 |
| 30°-30°-30° 3-span continuous | 3.64 | 3.75 | 2.9 |
| 45° simple span | 2.58 | 2.59 | 0.4 |
| 45°-45° 2-span continuous | 2.55 | 2.59 | 1.5 |

In addition to the midspan strain gages used to obtain the dynamic bending moment during vehicle passage, a twistometer was developed to measure the time history of the twist angle $\beta$ at midspan. This device, shown in Fig. 17, consists of two spring steel cantilever beams, 0.03 x 0.25 x 9 in., which respectively sense the vertical midspan deflection on the inside and the outside of the curve. The active strain gages, one attached to the root of each cantilever, are wired to a standard bridge circuit in such a way as to measure only the difference in strain, or the relative vertical deflection. When calibrated with dial gages, the device proved to be linear, capable of measuring $\beta$ in the desired range of 0.2 to 2 deg. with an accuracy of 0.063 deg.

Table 1 lists the combinations of guideway and vehicle (load) configurations which were tested. A PRT vehicle is relatively short compared to a guideway span and is thus modeled as a point load. Due to stopping distance limitations, it was not possible to investigate the 45 deg. - 45 deg. 2-span guideway subjected to 3 point loads spaced at $\ell/2$. Other restrictions prevented the gathering of twist data for the 45 deg. simple span configuration with the AGT vehicle and with 3 point loads at $\ell/4$, and also limited twist data of multiple span configuration to the first span.*

Time histories of midspan bending strains and twist angles were measured simultaneously. Of interest in design are the peak dynamic bending moment (M) and twist angle ($\beta$) responses which occur for a given vehicle speed (v). By varying v one can obtain experimental results relating the peak dynamic responses of the guideway with the speed of the vehicle. Expressed in this form the experimental results would be applicable only to the model from which they came. The data must be

*The twistometer was designed to measure twist for downward but not upward beam deflections. The device was thus satisfactory for measuring twist during vehicle loading on the particular span; but free vibrations during the upward cycle were not measured since the feelers of Fig. 17 lost contact with the span.

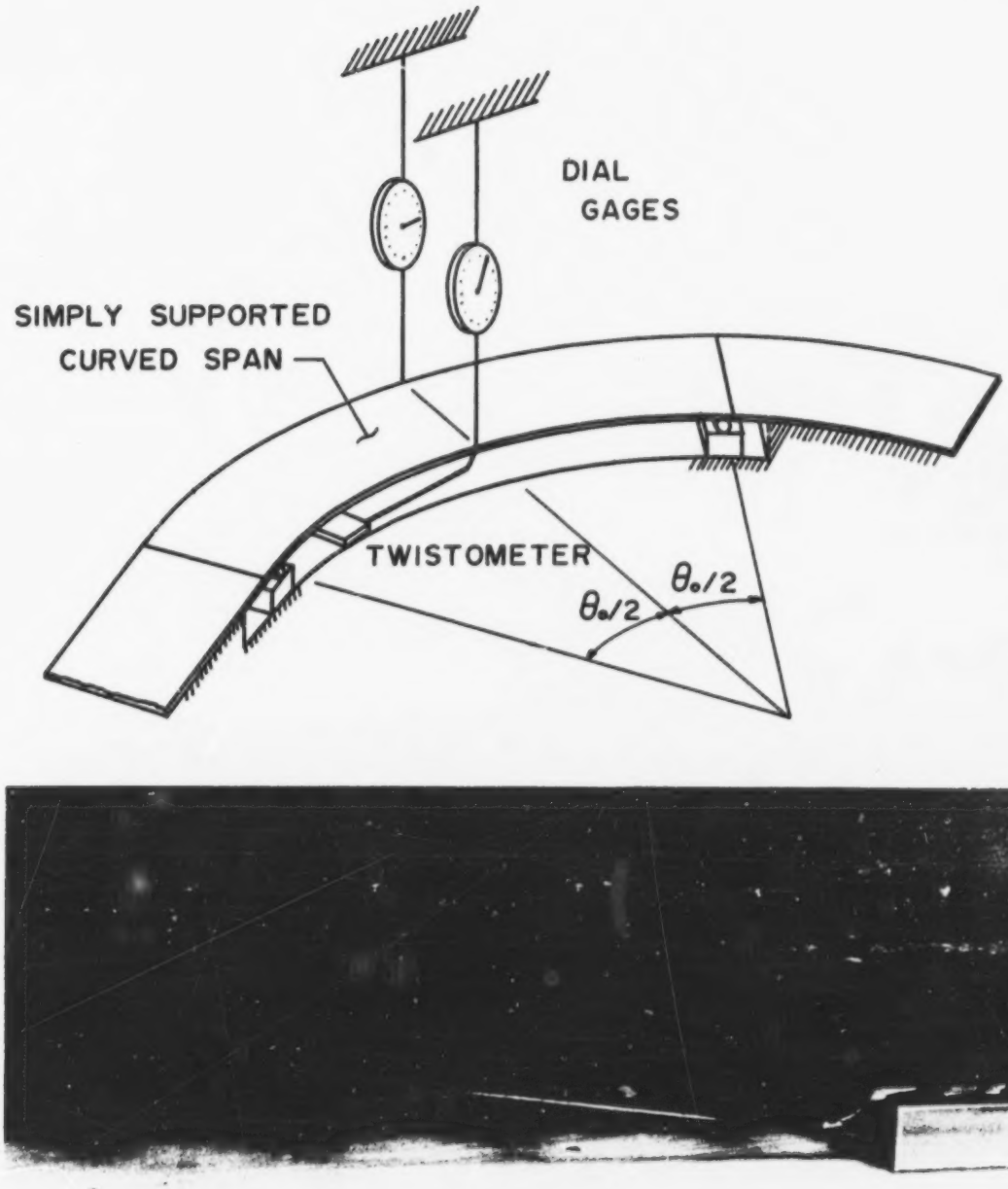


Figure 17. Twistometer, showing calibration setup and the in-place location at midspan.

non-dimensionalized so that they can be used in prototype design. Thus, the speed parameter is the frequency ratio $\omega/p$ defined previously. The response parameters are $M/M_s$ and $\beta/\beta_s$ where M and $\beta$ are the peak midspan dynamic responses obtained from the strain and twist angle histories, and $M_s$ and $\beta_s$ are the maximum midspan static responses for the vehicle (load) configuration under study. $M_s$ and $\beta_s$ were determined by moving the vehicle configuration at crawl speeds on the guideway thus creating static load conditions. The maximum static responses for bending and twist were recorded and later used in determining the ratios $M/M_s$ and $\beta/\beta_s$.

Hence, the experimental data is presented in the form of plots of the peak midspan response ($M/M_s$ or $\beta/\beta_s$) versus the frequency ratio ($\omega/p$). Approximately 10 runs, each at a different vehicle speed, were made for each of the guideway-vehicle combinations. Thus, each plot contains approximately 10 data points. In addition, the point given by $\omega/p = 0$ and $M/M_s = 1$ or $\beta/\beta_s = 1$ is common to all of the curves, since for $\omega/p = 0$, $v = 0$ and the resulting bending and twist responses are the static responses. In the remainder of this Chapter, the experimental results are presented and interpreted. For discussion purposes they are grouped according to guideway configurations. Finally, all moment data presented can be converted to dynamic responses relative to a simple span moment $M_{ss}$ by multiplying by the corresponding measured static ratio $M_s/M_{ss}$ of Table 3.

Vehicle Models - The vehicles designed to traverse these instrumented guideways are modified versions of the point load type (arbitrarily spaced tandem PRT vehicles) and the AGT vehicle, both previously described in detail [9]. Although these vehicles worked well on straight guideways, centrifugal force effects caused vehicle side sway during negotiation of curved guideways. This problem was solved by positioning a vertical guidewall along the curve. A ball-bearing caster was mounted in an adjustable length fixture, mounted low, centered on a vehicle model. Adjustments were made until this ball-bearing restraint abutted

Table 3. Peak Midspan Moments of a Curved Span Relative to a Straight, Simple Span, $M_s/M_{ss}$. (All point loads are equal.)

| SPAN TYPE | EXTREME ENDS | SPAN NO. | LOAD TYPE AND SPACING | | | | |
|---|---|---|---|---|---|---|---|
| | | | 1-POINT | 2-POINT @ ℓ/4 | 3-POINT @ ℓ/4 | 2-POINT @ ℓ/2 | 3-POINT @ ℓ/2 |
| straight (single) | simple | 1 | 1 | 1 | 1 | 1 | 1 |
| 30° (single) | simple | 1 | 1.000 | 0.968 | 0.988 | 0.955 | 0.955 |
| 30°-30° (double) | simple | 1 | 0.850 | 0.778 | 0.793 | 0.773 | 0.773 |
| | | 2 | 0.900 | 0.841 | 0.854 | 0.841 | 0.864 |
| 30°-30°-30° (triple) | simple | 1 | 0.800 | 0.762 | 0.768 | 0.750 | 0.705 |
| | | 2 | 0.775 | 0.698 | 0.707 | 0.705 | 0.727 |
| | | 3 | 0.875 | 0.825 | 0.854 | 0.818 | 0.818 |
| 30°-30°-30° | clamped | 1 | 0.675 | 0.556 | 0.549 | 0.636 | 0.659 |
| | | 2 | 0.800 | 0.667 | 0.659 | 0.727 | 0.750 |
| | | 3 | 0.650 | 0.587 | 0.585 | 0.614 | 0.614 |
| 30°-30°-30° | 1/3 clamped | 1 | 0.425 | 0.317 | 0.305 | 0.409 | 0.409 |
| | | 2 | 0.725 | 0.651 | 0.646 | 0.659 | 0.682 |
| | | 3 | 0.450 | 0.333 | 0.305 | 0.409 | 0.455 |
| 45° (single) | simple | 1 | 1.120 | 1.122 | 1.081 | 1.106 | 1.091 |
| 45°-45° (double) | simple | 1 | 0.959 | 0.899 | 0.845 | 0.879 | 0.883 |
| | | 2 | 0.934 | 0.889 | 0.853 | 0.863 | 0.863 |

the vertical guidewall while the vehicle model was maintained on the centerline of the guideway. This restraint eliminated side sway and smoothly engaged and disengaged with the guidewall. Photographs of restraints on both the PRT and AGT vehicles are shown in Figs. 18, 19 and 20.

The following additional modifications were made to improve negotiation of a typical curved test span. New, less constraining bolts for attaching the spacing bars between a series of PRT vehicles were installed and padded with foam rubber. This allowed the flexibility needed between bar and vehicle to negotiate the curve. This attachment presents no loose or noisy vibration. On the AGT vehicle, the pair of trolley carriages running below the motor channel and the pair of wheel units running on the test span were pivoted so that they track properly in the curve. See Fig. 20. The mounting on the trolley carriages is flexible and padded so that it is curved in the curve and straightens for the straight sections, yet is rigid for handling purposes. The whole system, including the AGT and PRT vehicles and their spacing bars were designed to be readily interchangeable between the curved and straight test facilities.

For proper interpretation of the experimental data which follow, it is important to preserve similitude between model and prototype [9]. In the point load-curved guideway response studies, two ratios need to be preserved for each tandem set:

$$m_0/m_g = 1/7 \; ; \quad d_0/\ell = 0,\ 1/4,\ 1/2 \tag{21}$$

where

$m_0$ = mass of one point load
$m_g$ = mass of guideway between consecutive supports
$d_0$ = spacing between point loads
$\ell$ = guideway arc length between consecutive supports.

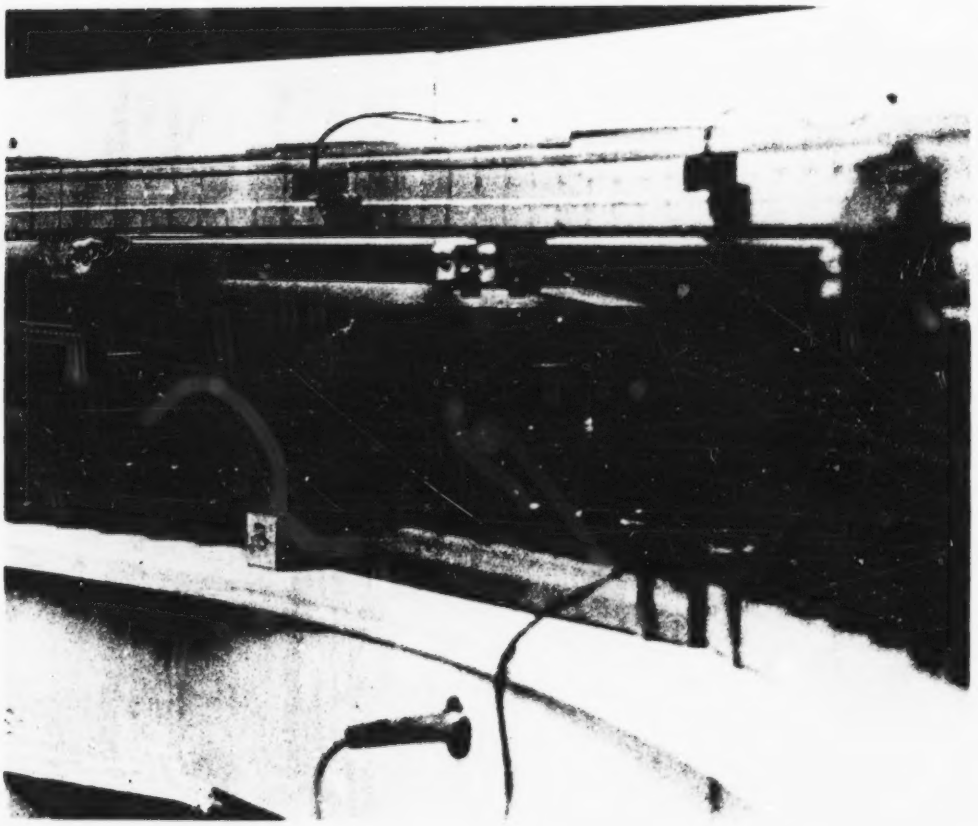

Figure 18. Tandem PRT vehicles with padded spacer bars, ball bearing casters and vertical guidance wall.

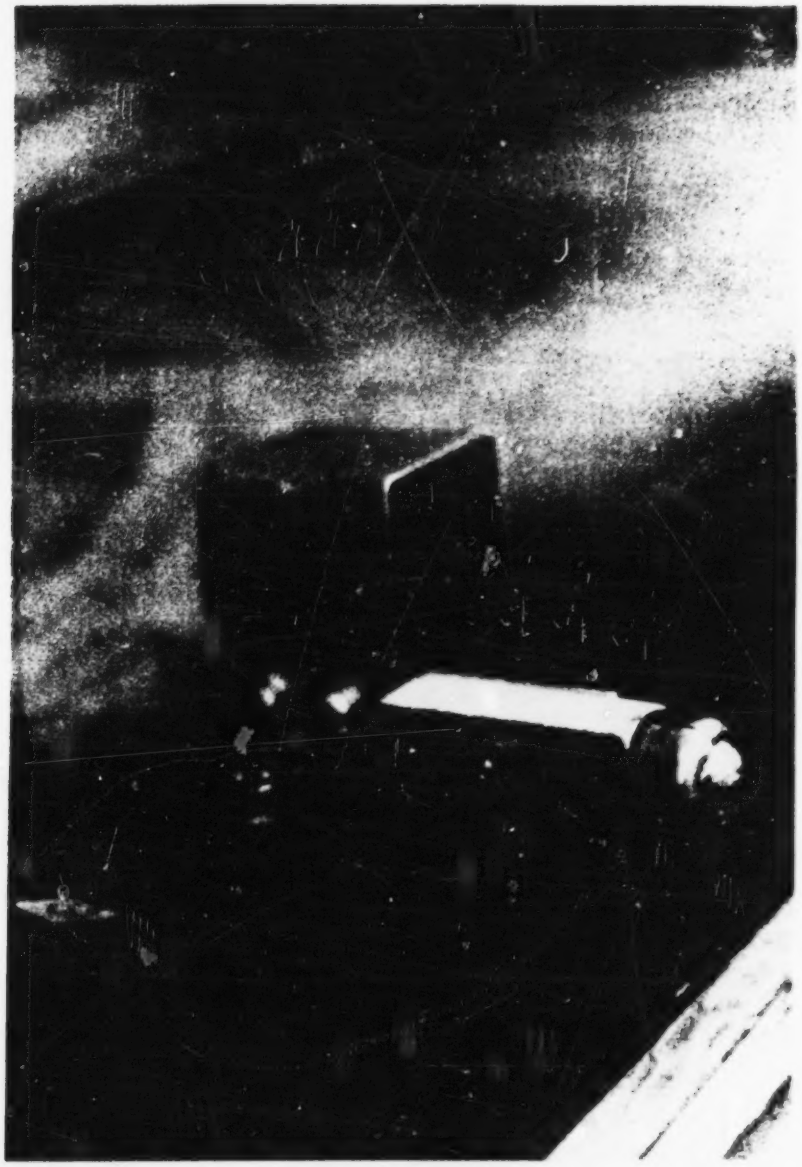

Figure 19. Detail of caster design on a PRT vehicle model.

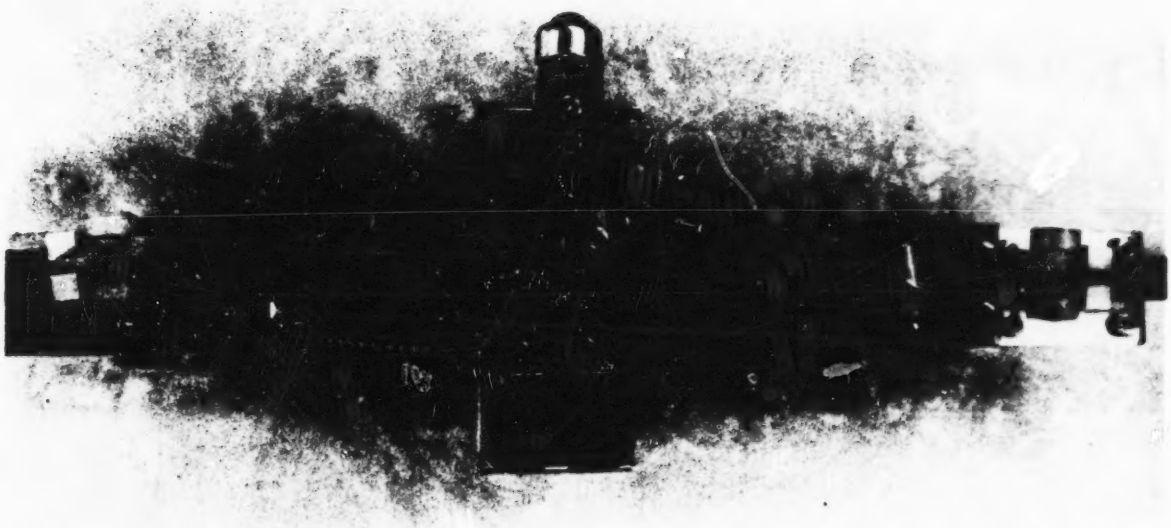

Figure 20. Underside view of AGT vehicle showing caster and pivoted wheel units.

Since the AGT vehicle allows for the pitch ($\phi$) and heave (y) degrees of freedom (see Fig. 21), the ratios of these respective vehicle frequencies $\Omega_\phi$ and $\Omega_y$ to the reference span frequency p (see Eq. 1) are design parameters also. Thus, for the dynamic responses which follow to be applicable to prototype design, the following dimensionless ratios need to be preserved.

For curved spans where $\theta_0 = 30$ deg.:

$$\frac{\Omega_y}{p} = 0.970, \quad \frac{\Omega_\phi}{p} = 1.467, \quad \frac{m_1}{m_g} = 0.152, \text{ and } \frac{d}{\ell} = 0.250 \qquad (22a)$$

For curved spans where $\theta_0 = 45$ deg.:

$$\frac{\Omega_y}{p} = 1.384, \quad \frac{\Omega_\phi}{p} = 2.085, \quad \frac{m_1}{m_g} = 0.271, \text{ and } \frac{d}{\ell} = 0.167. \qquad (22b)$$

where $m_1$ is the AGT vehicle mass and d is its wheel base.

Simple Span Experiments - Data from 30 deg. and 45 deg. simple span experiments with various load configurations are shown in Figs. 22 through 31. The dashed lines represent theoretical results as calculated in Chapter 2. The first observation is that theory and experiment are in good agreement for most load configurations. For 3 point loads spaced at $\ell/2$, however, the experimental results are lower than those predicted by theory for $\omega/p$ greater than about 0.5 as seen in Figs. 26 and 31. A possible reason for this is that the theory assumes the loads acting on the guideway are moving point forces of constant magnitude, and in the experiment these loads are actually moving masses. The inertial effects of these masses when they are subjected to the vibrating motion of the guideway may increase or decrease the load experienced by the guideway. Apparently for 3 point loads at $\ell/2$ traveling at the higher speeds ($\omega/p \geq 0.5$) the effective load on the guideway is less than the vehicle body weight of $m_0 g$. As a check on the first group of data points for this configuration a series of tests was run on another day, and both sets are plotted in Fig. 31. Because of their close agreement it may be concluded that the experimental results obtained from the model are reproducible.

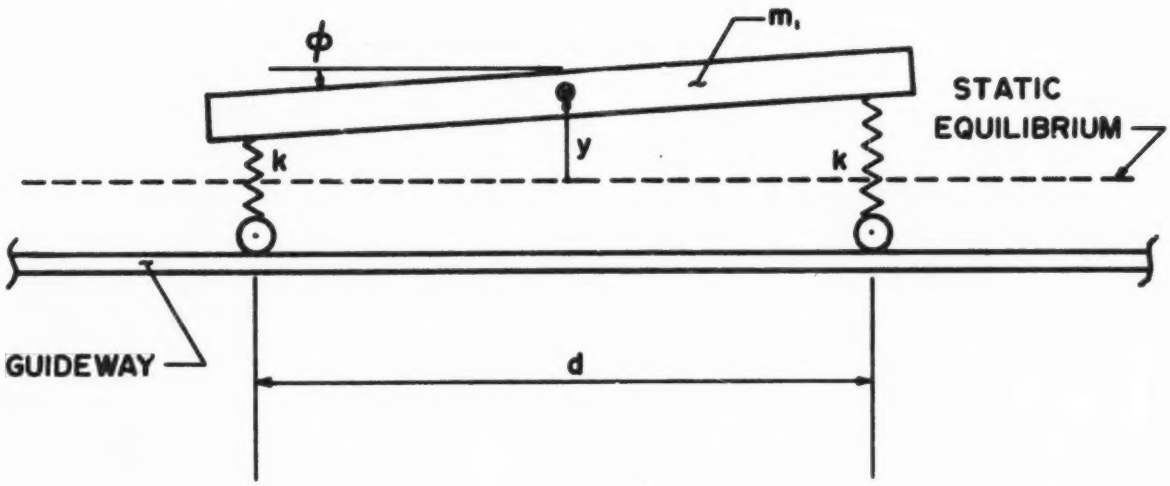


Figure 21. Analytical representation of the AGT vehicle model.

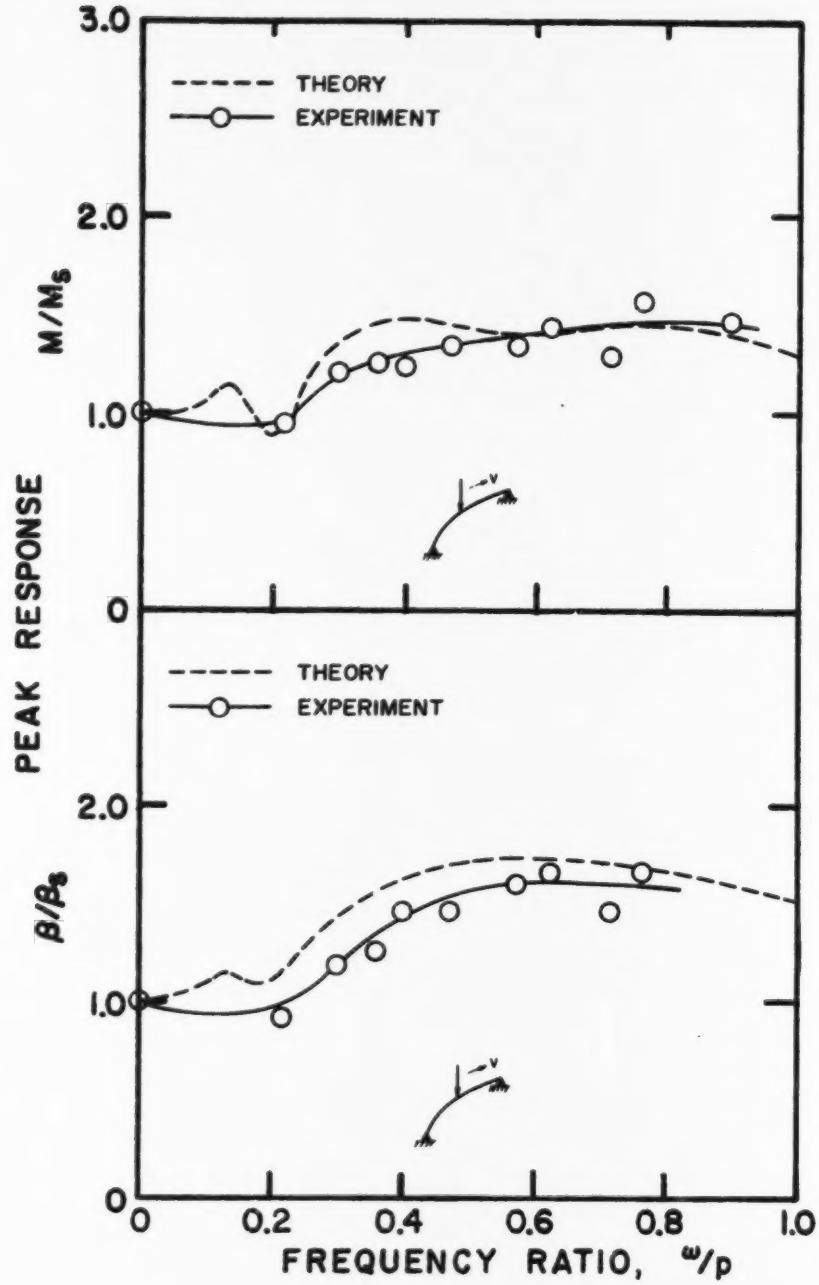


Figure 22. Response envelopes of a 30° simple span curved guideway for 1 point load.

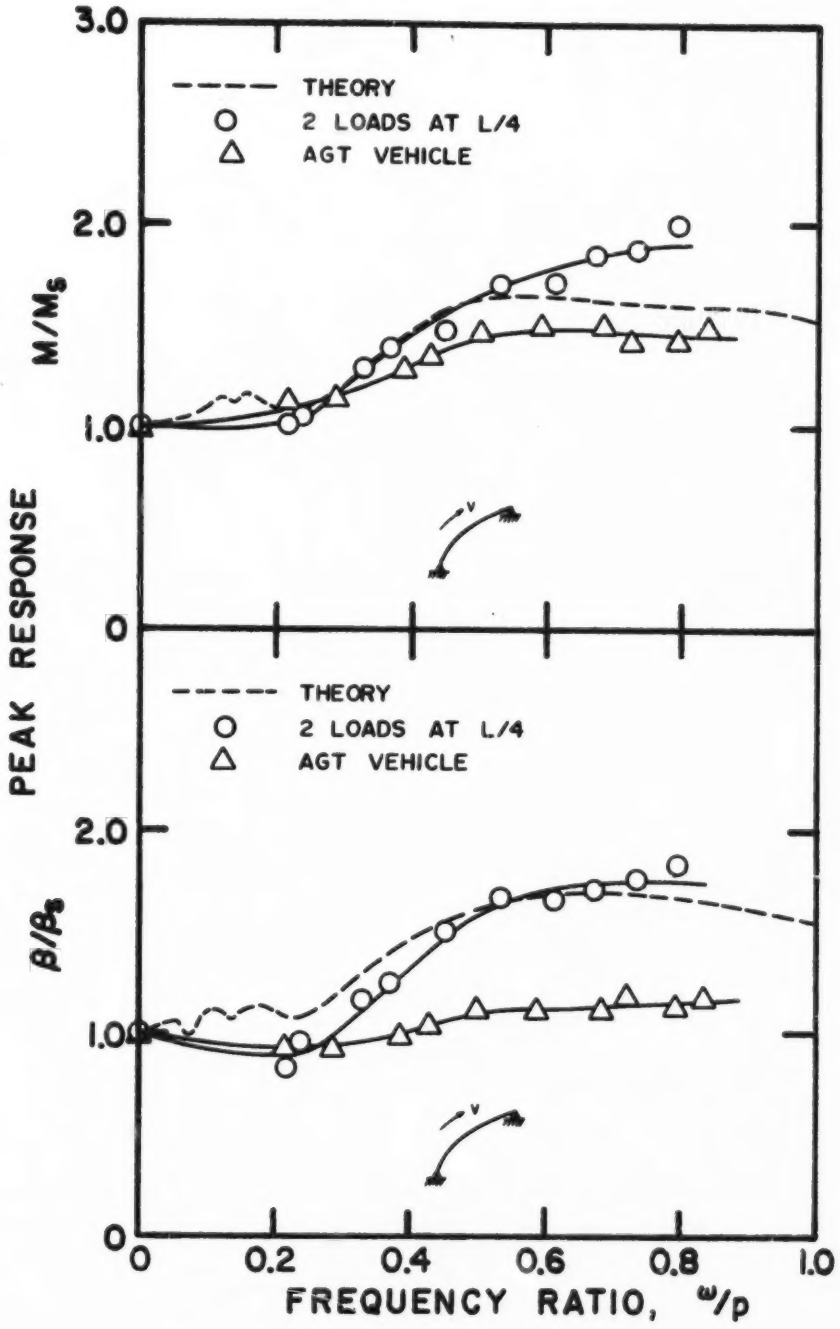


Figure 23. Response envelopes of a 30° simple span curved guideway for 2 point loads spaced at $\ell/4$ and the AGT vehicle.

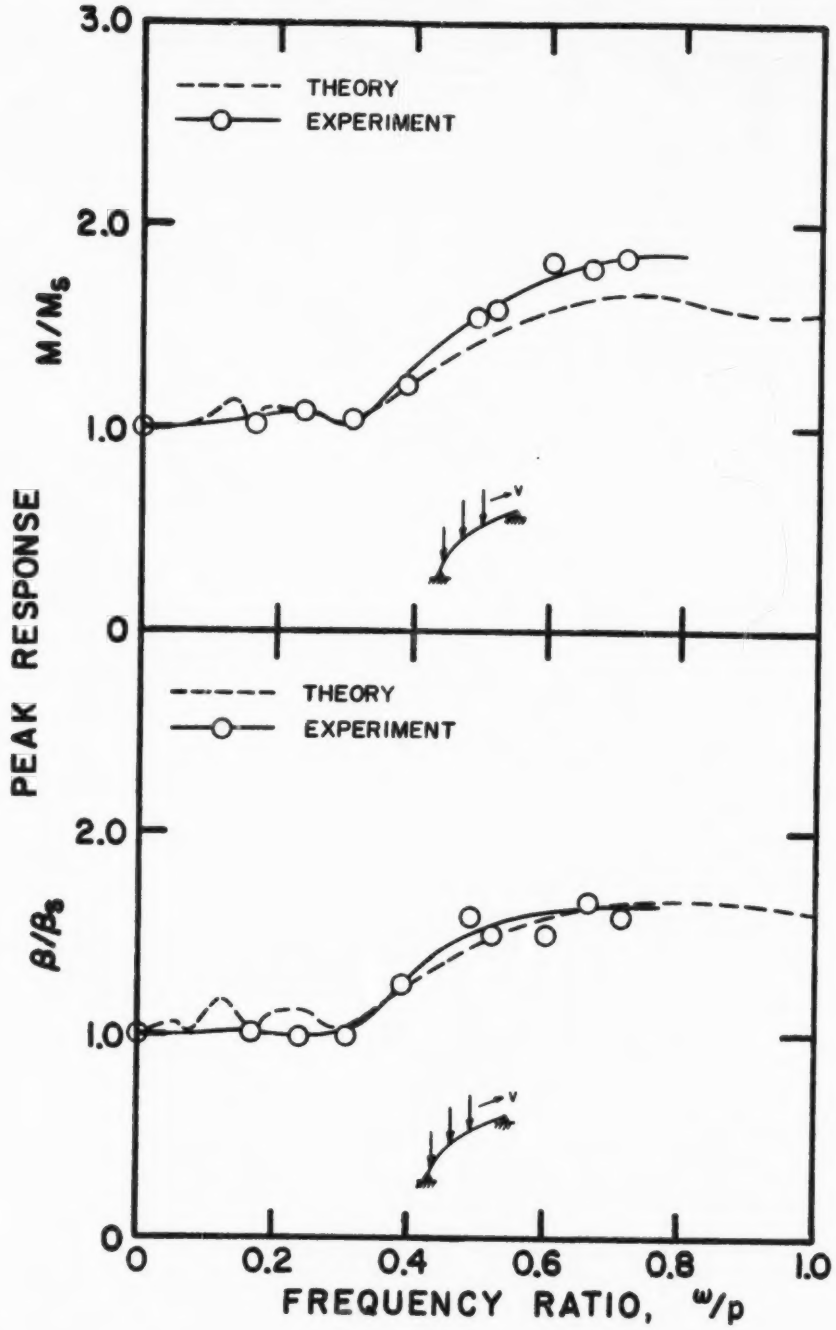


Figure 24. Response envelopes of a 30° simple span curved guideway for 3 point loads spaced at $\ell/4$.

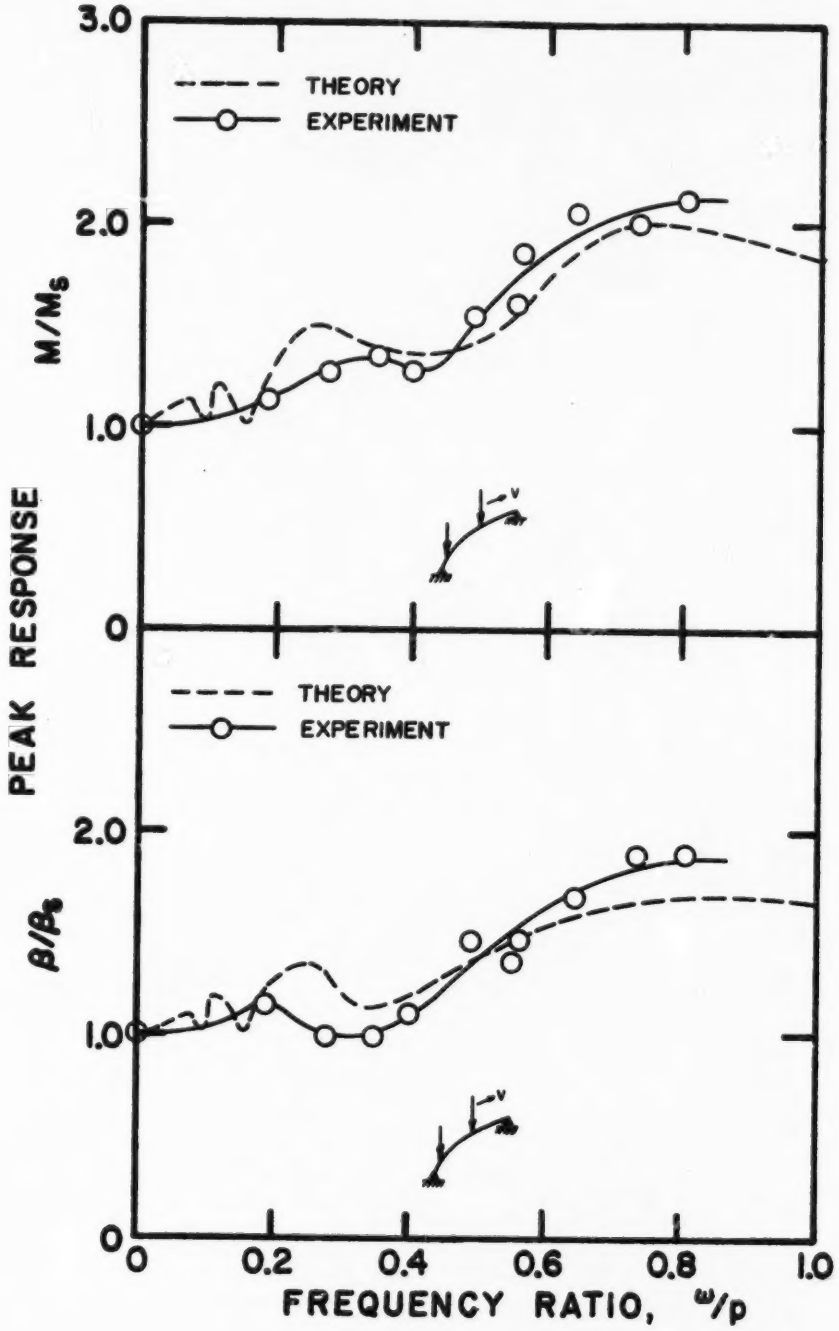


Figure 25. Response envelopes of a 30° simple span curved guideway for 2 point loads spaced at $\ell/2$.

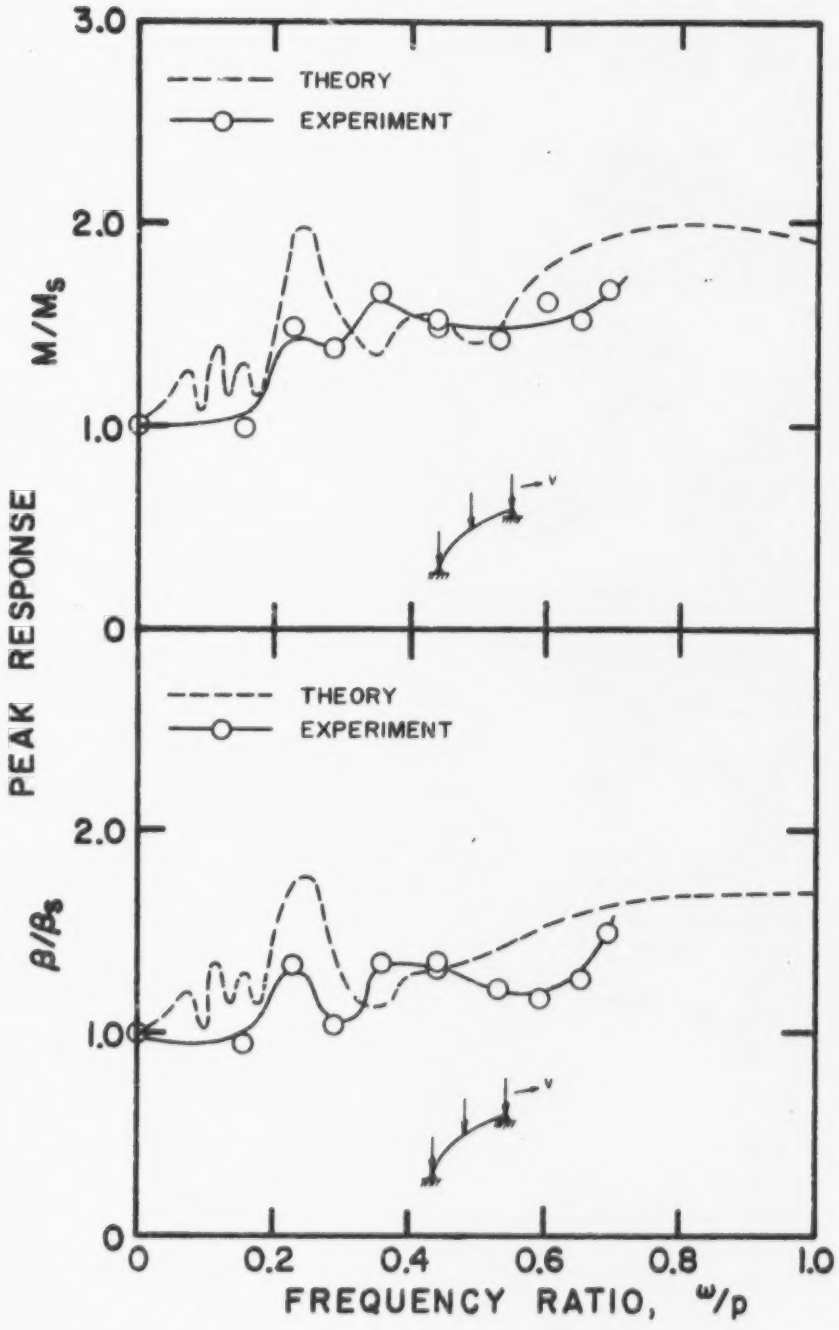


Figure 26. Response envelopes of a 30° simple span curved guideway for 3 point loads spaced at $\ell/2$.

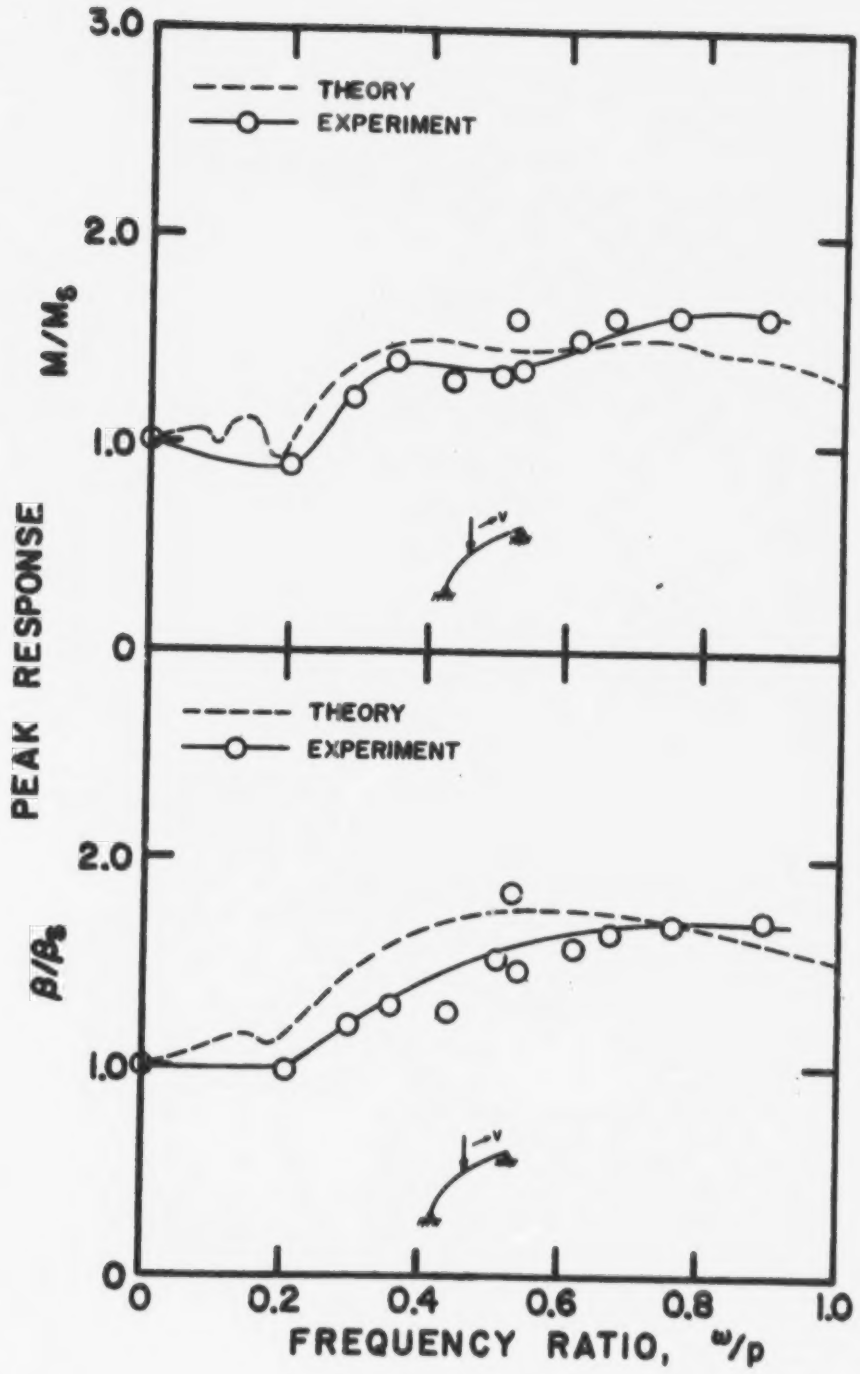


Figure 27. Response envelopes of a 45° simple span curved guideway for 1 point load.

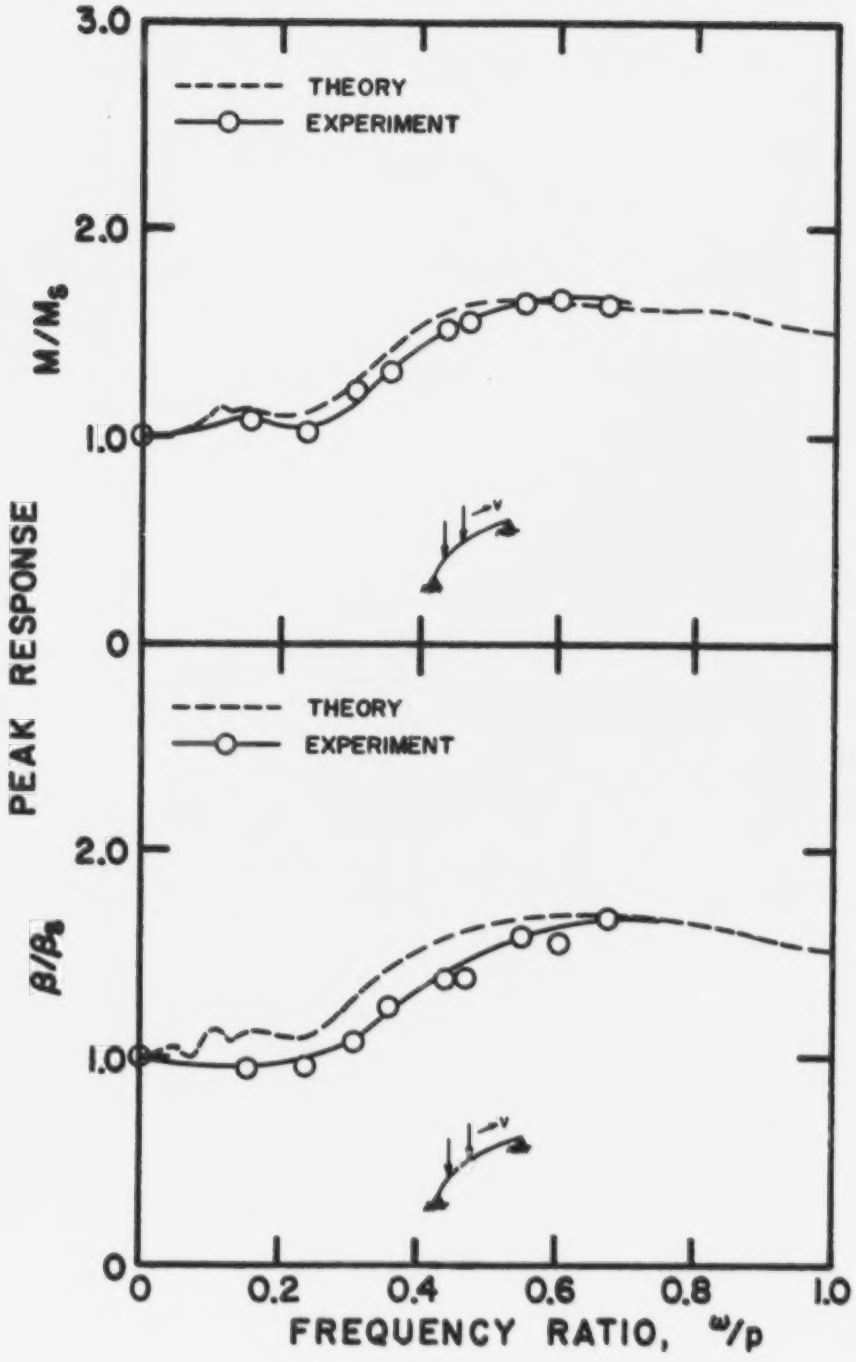


Figure 28. Response envolopes of a 45° simple span curved guideway for 2 point loads spaced at $\ell/4$.

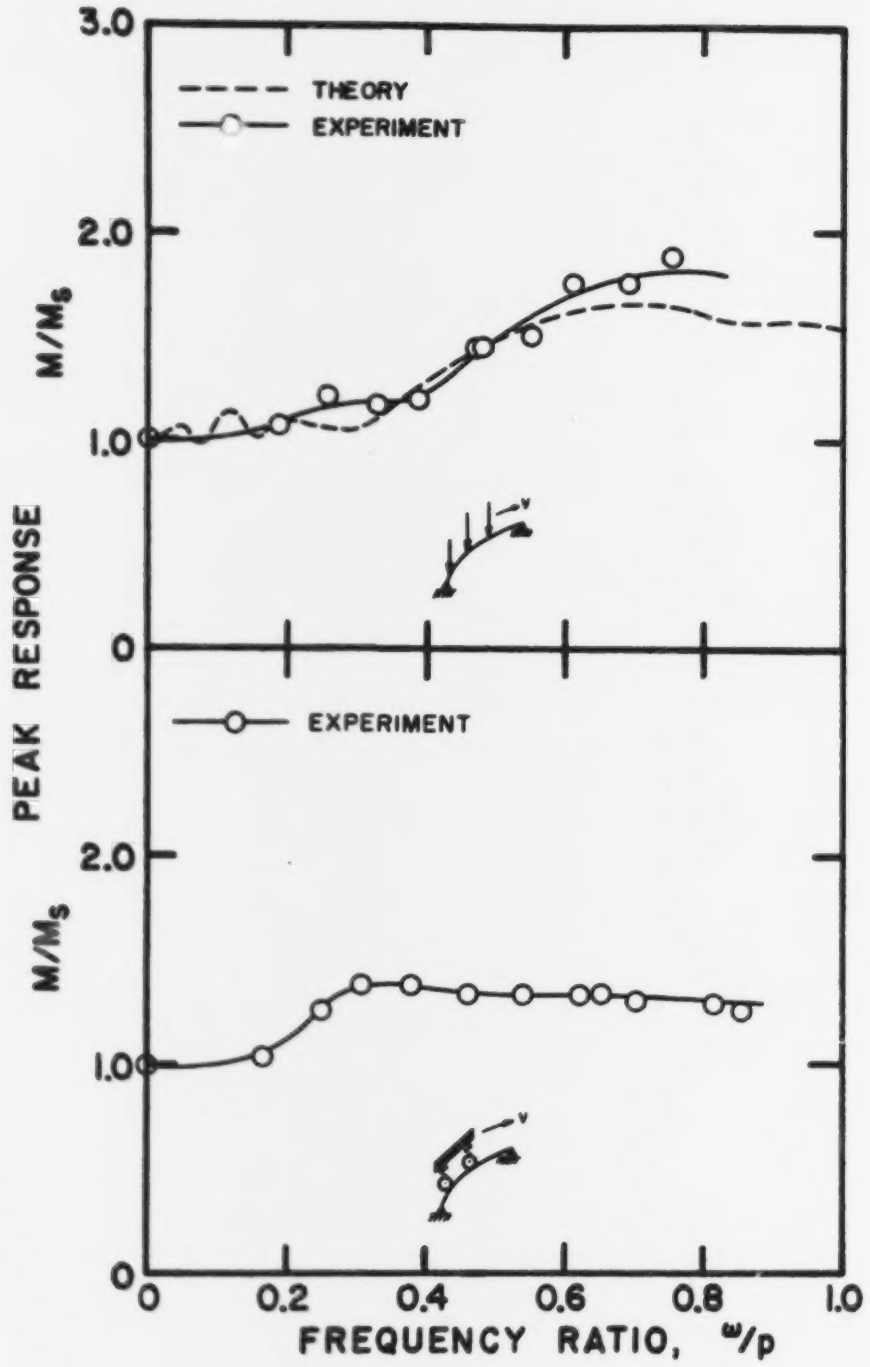


Figure 29. Response envelopes of a 45° simple span guideway for 3 point loads spaced at $\ell/4$ (top) and the AGT vehicle (bottom).

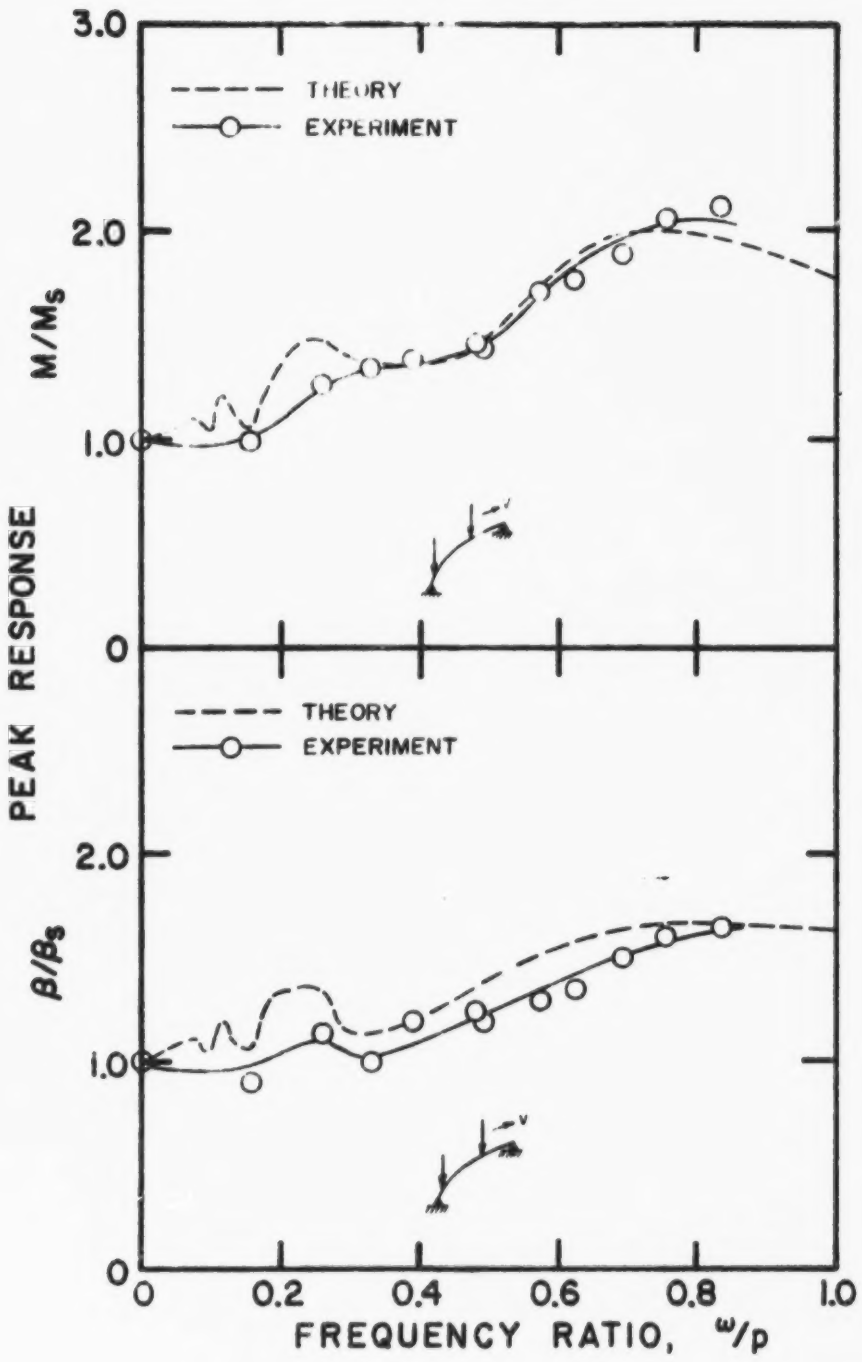


**Figure 30.** Response envelopes of a 45° simple span curved guideway for 2 point loads spaced at ℓ/2.

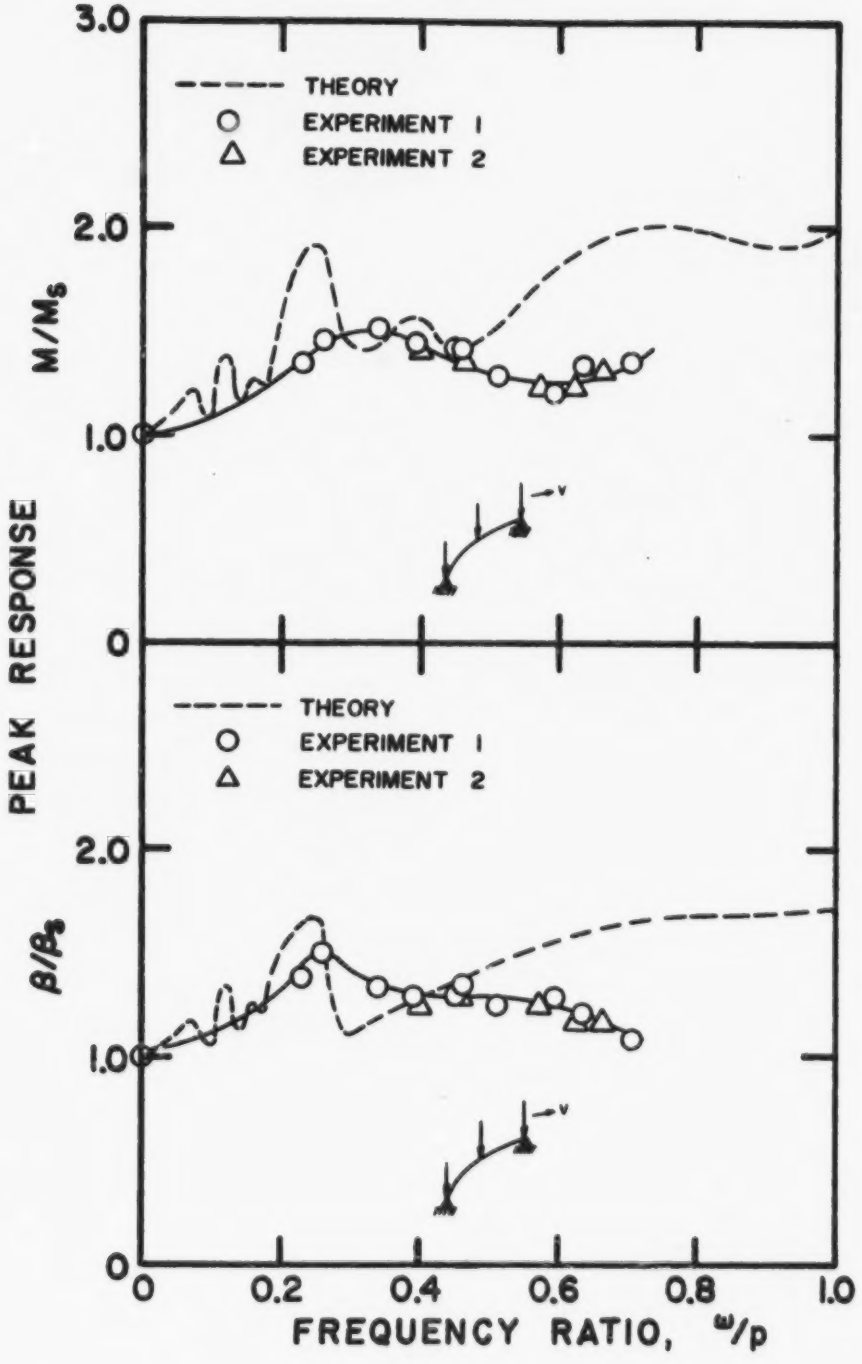


Figure 31. Response envelopes of a 45° simple span curved guideway for 3 point loads spaced at ℓ/2.

The effects of guideway-AGT vehicle interaction are illustrated in Figs. 23 and 29. The wheel spacing of the AGT vehicle is equal to $\ell/4$ for the 30 deg. span. One sees that the AGT vehicle response curve is lower than that of 2 point loads at $\ell/4$ for most values of $\omega/p$. Evidently, for the AGT vehicle some of the energy of the system is absorbed by its pitch motion while for the PRT vehicles this energy is available to excite the guideway. This form of guideway "damping" is also apparent for the AGT vehicle on the 45 deg. simple span where the maximum peak moment response is only about 1.4, as seen in Fig. 29.

In comparison the bending moment response curves with those of the twist angle response for the various simple span curved guideway-vehicle combinations, it can be seen that these curves are very similar in shape, with small differences in their maximum responses. Furthermore, the response curves for all point load configurations tested show some similarity in shape with maximum dynamic bending and twist magnifications of between 1.5 and 2.0 at frequency ratios between 0.3 and 0.8. Care must be taken in generalizing for design purposes, however, since load configurations not tested may produce different responses from these. In Chapter 2, for example, theoretical results for 2 and 3 point loads spaced at $\ell$ show peak dynamic response magnifications of around 4.0 at a frequency ratio of 0.5.

Two-Span Experiments - The response curves for the 30°-30° and 45°-45° 2-span continuous guideways are given in Figs. 32 through 45. In comparing spans 1 and 2 one sees that the bending moment response curves for span 2, the exit span, generally are higher than those for span 1, particularly at high values of $\omega/p$. This is consistent with findings for straight guideways that the exit span of a multiple span guideway receives the highest moment magnification [9].

As with the simple curved spans, the energy absorbing effect of the AGT vehicle is apparent with the 2-span curved guideways.

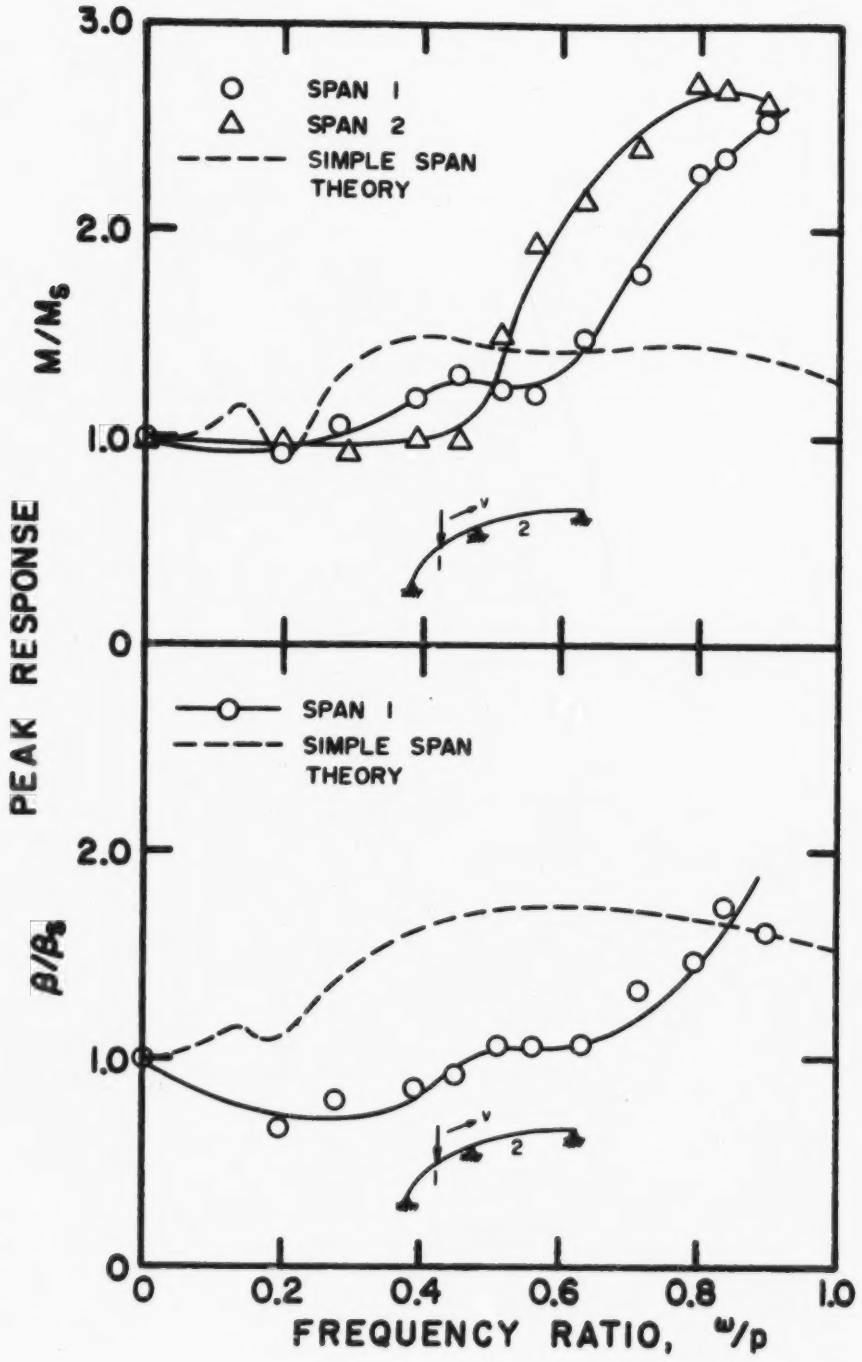


Figure 32. Response envelopes of a 30°-30° 2-span continuous curved guideway for 1 point load.

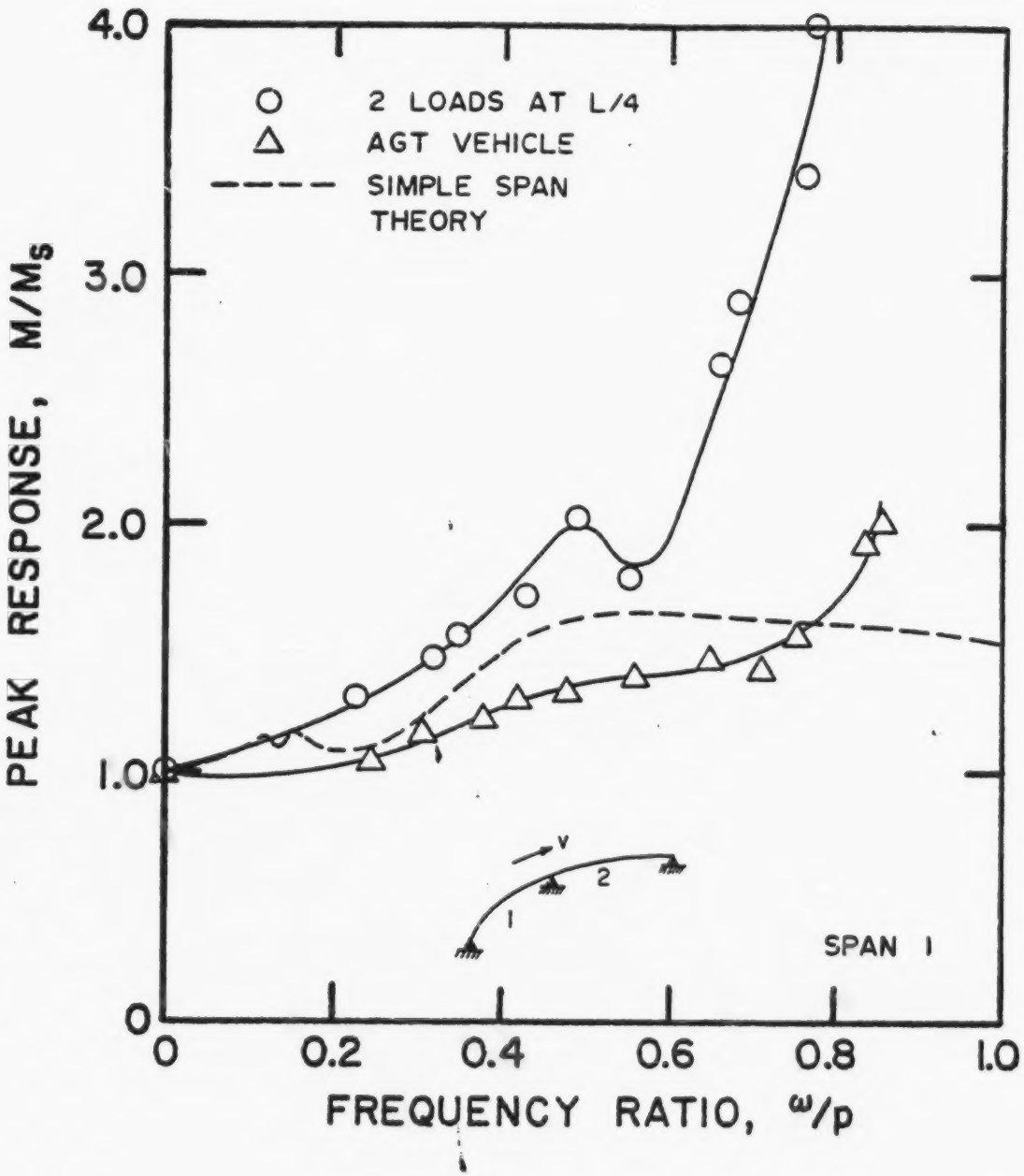


Figure 33. Response envelopes for span 1 of a 30°-30° 2-span continuous curved guideway for 2 point loads spaced at ℓ/4 and the AGT vehicle.

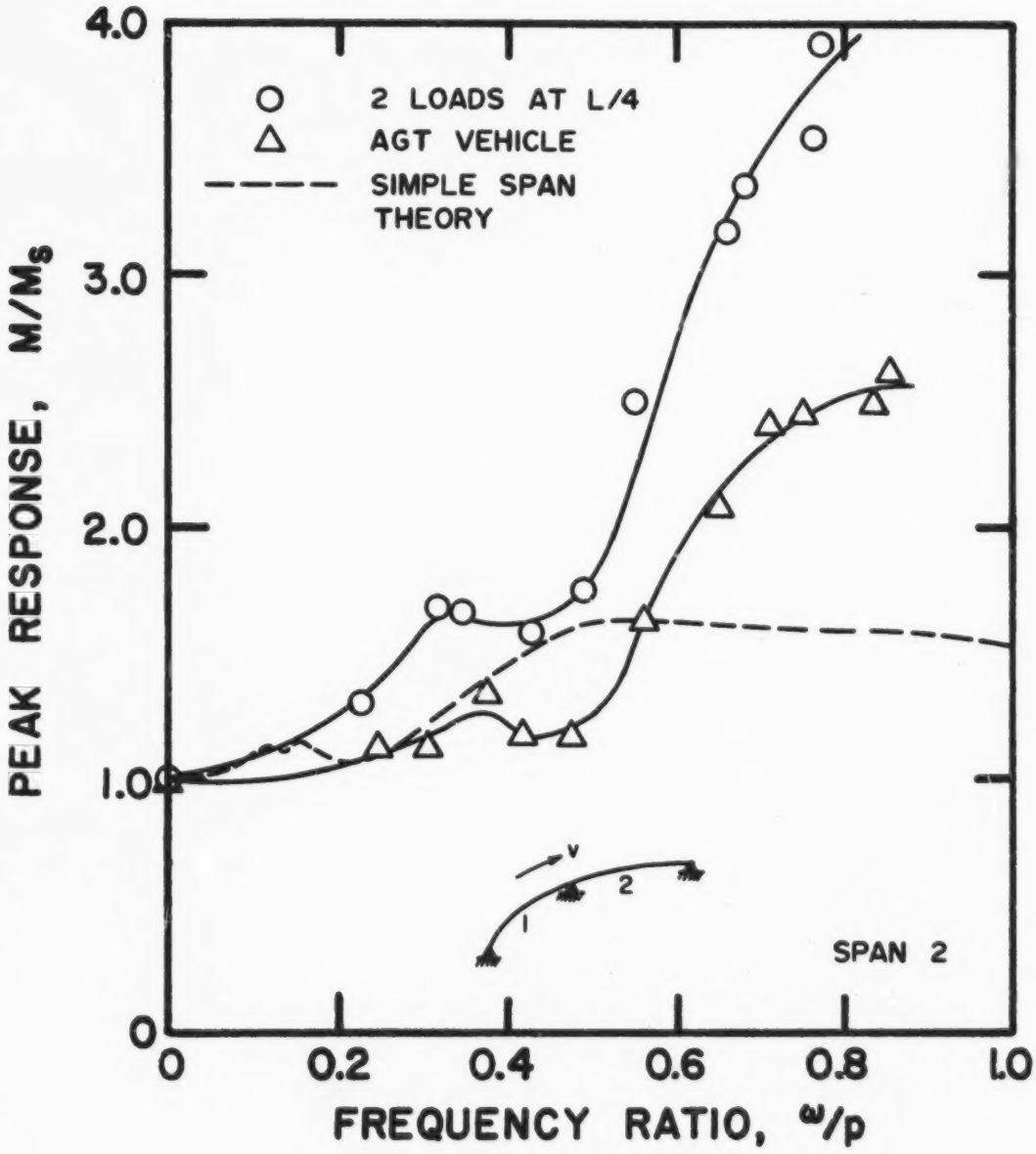


Figure 34. Response envelopes for span 2 of a 30°-30° 2-span continuous curved guideway for 2 point loads spaced at ℓ/4 and the AGT vehicle.

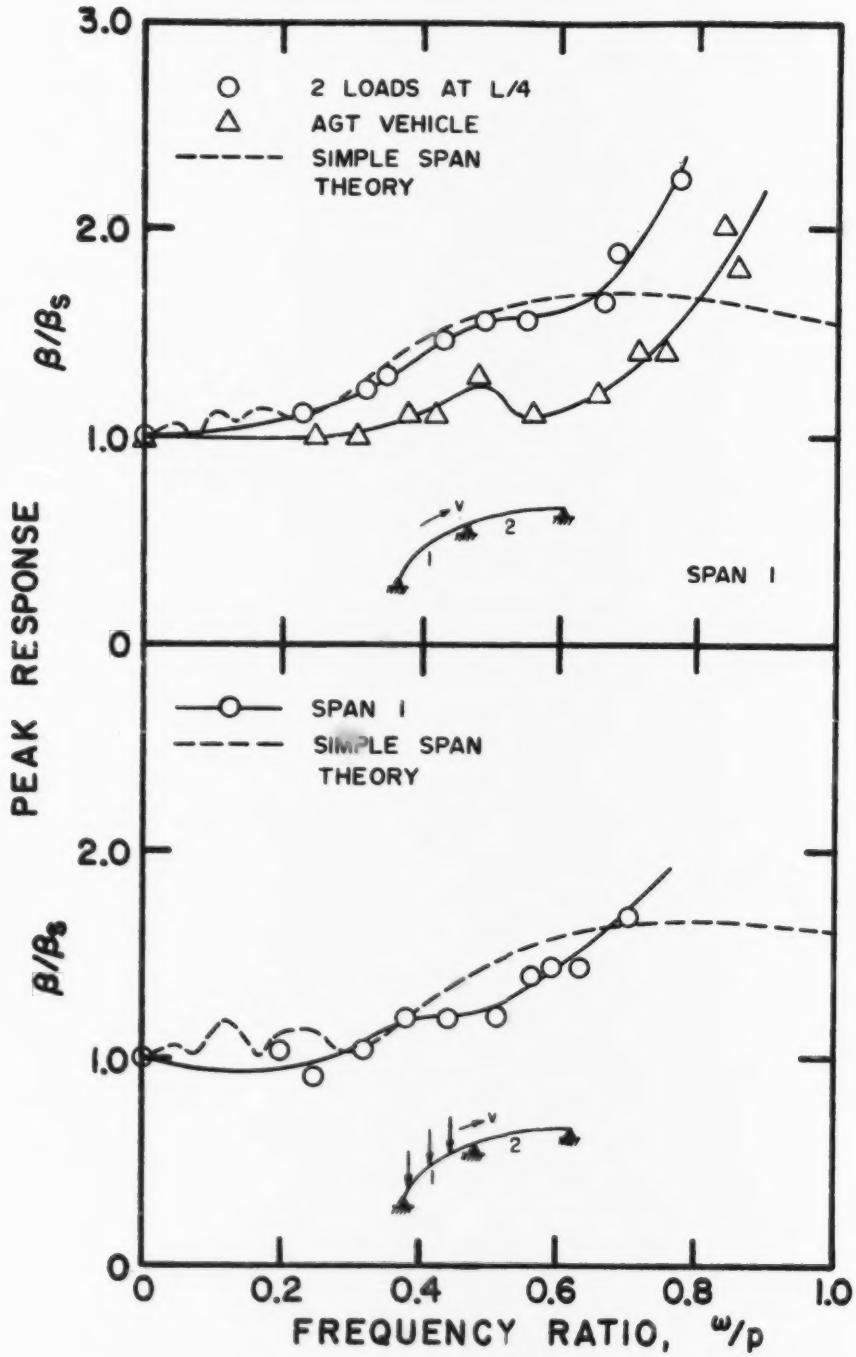


Figure 35. Twist angle response envelopes for span 1 of a 30°-30° 2-span continuous curved guideway for 2 point loads spaced at ℓ/4 and the AGT vehicle (top); and 3 point loads spaced at ℓ/4 (bottom).

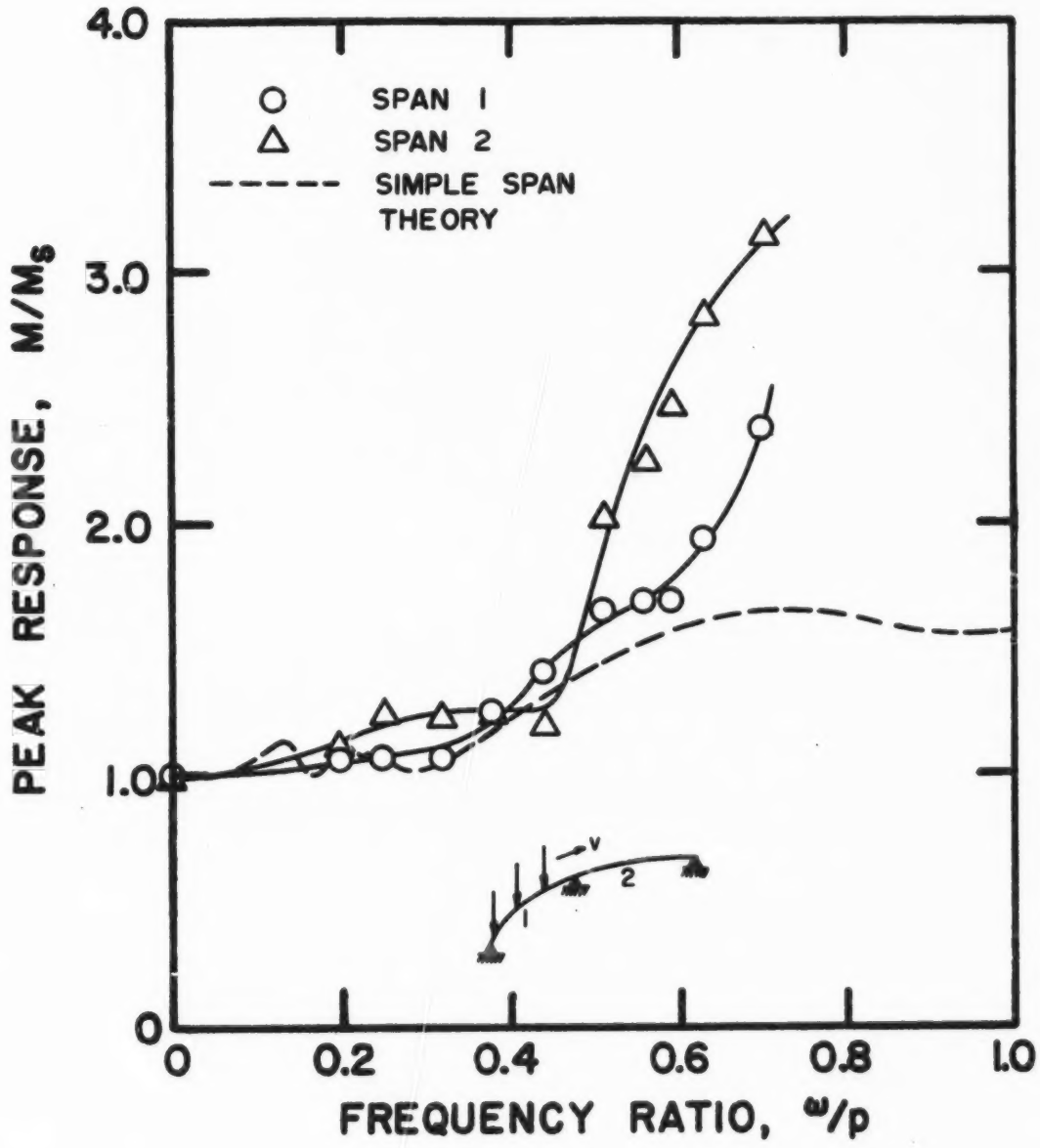


Figure 36. Response envelopes of a 30°-30° 2-span continuous curved guideway for 3 point loads spaced at ℓ/4.

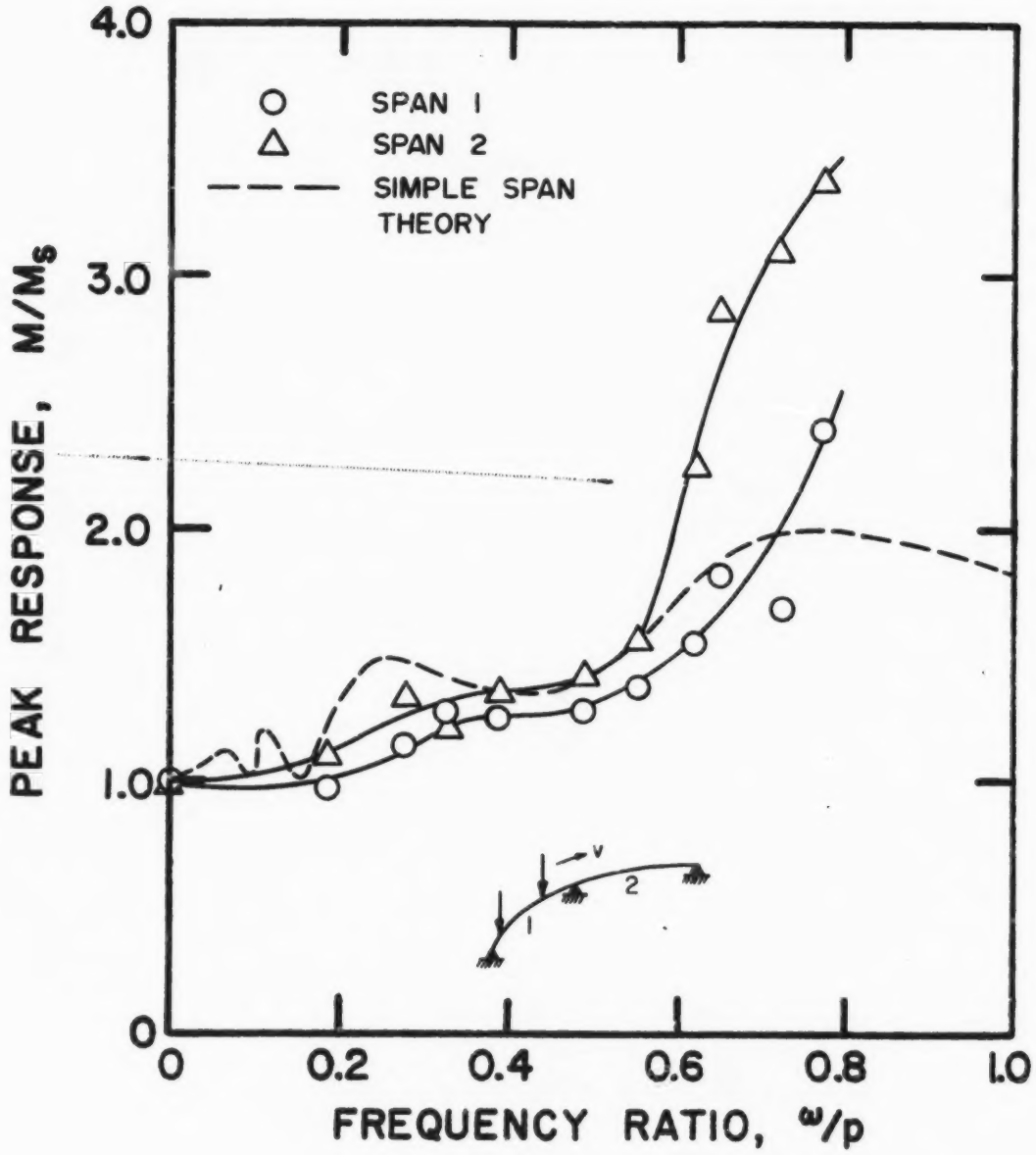


Figure 37. Moment response envelopes of a 30°-30° 2-span continuous curved guideway for 2 point loads spaced at ℓ/2.

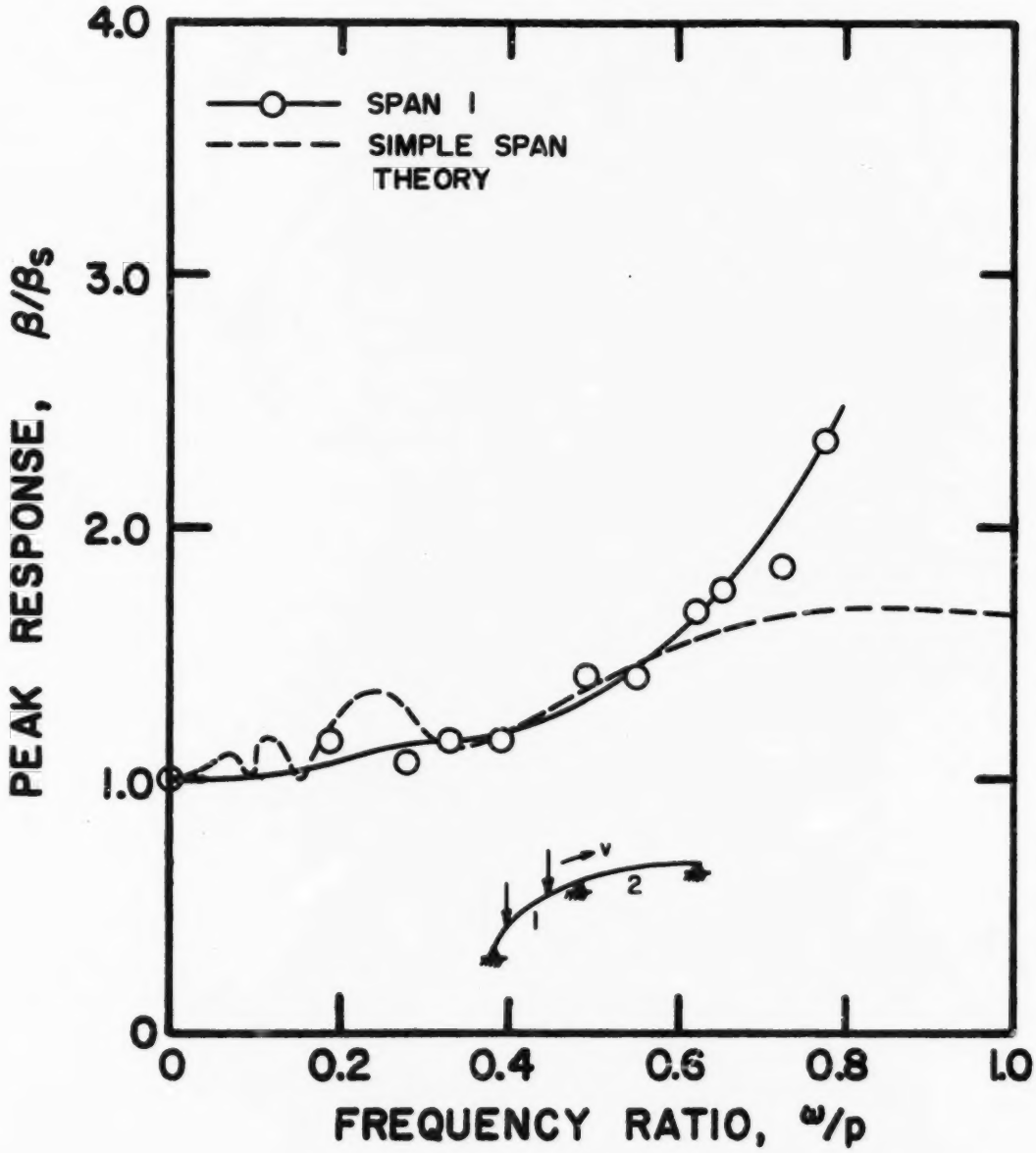


Figure 38. Twist angle response envelope of a 30°-30° 2-span continuous curved guideway for 2 point loads spaced at $\ell/2$.

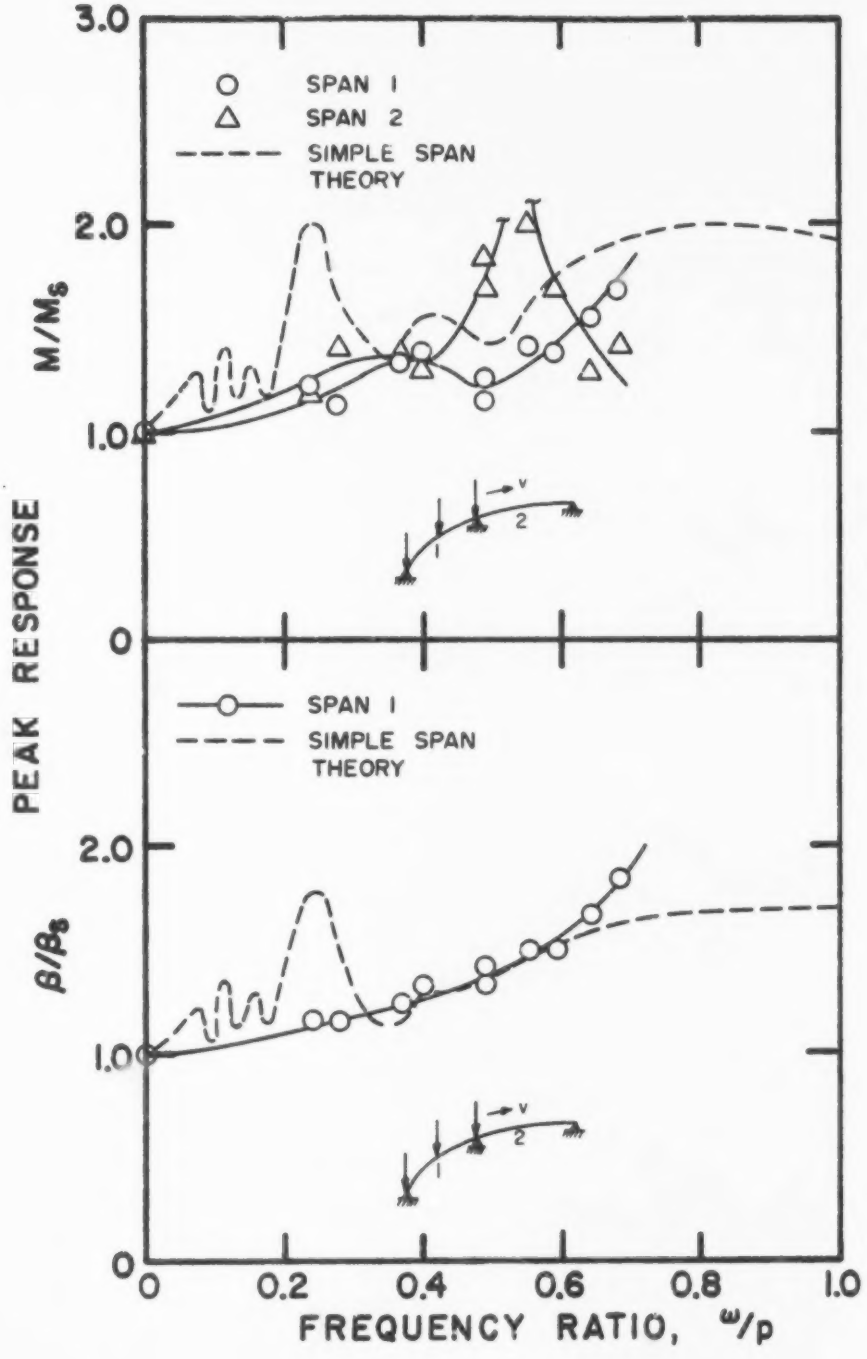


Figure 39. Response envelopes of a 30°-30° 2-span continuous curved guideway for 3 point loads s paced at ℓ/2.

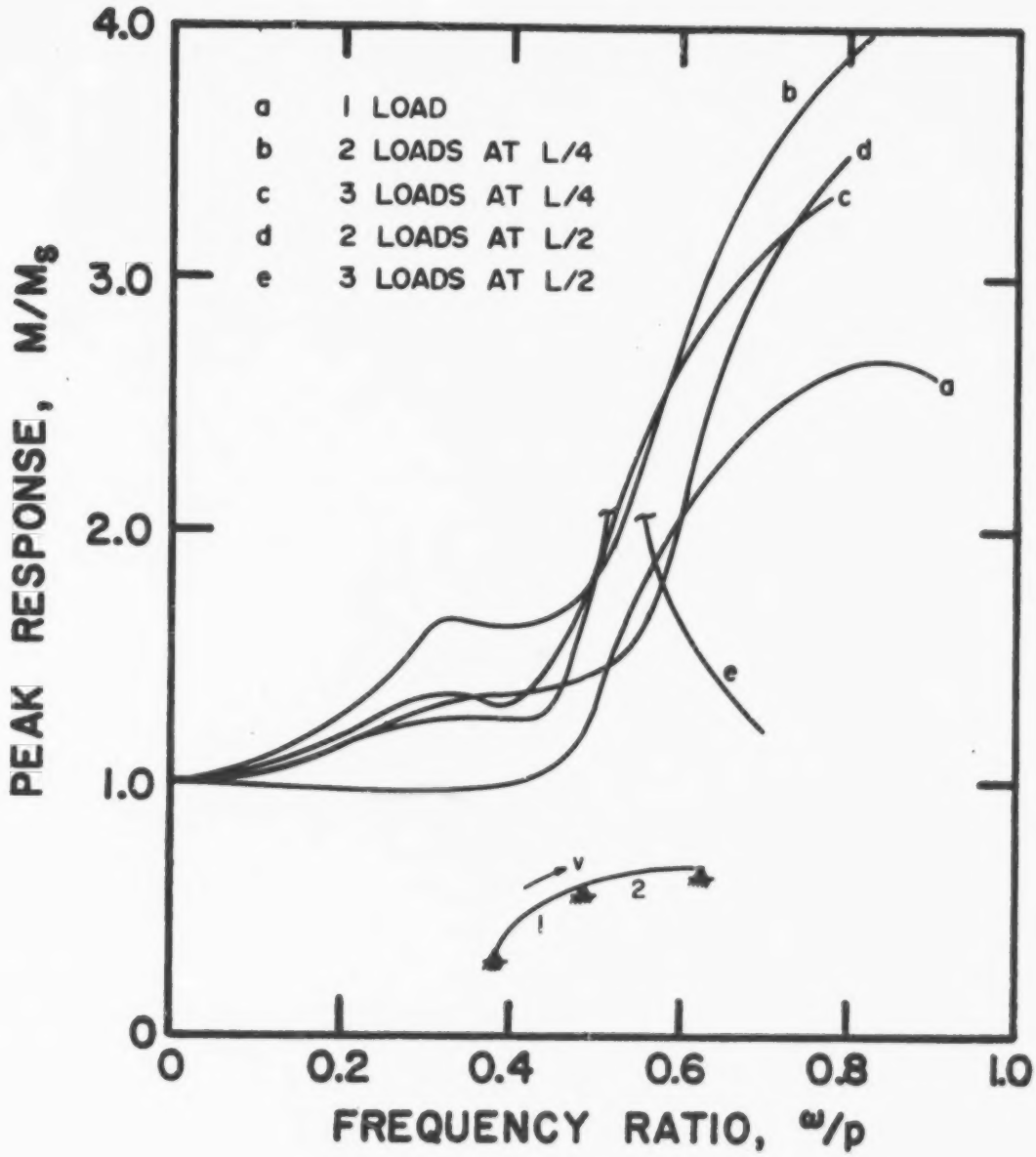


Figure 40. Response envelopes for span 2 of a 30°-30° 2-span continuous curved guideway for various point load configurations.

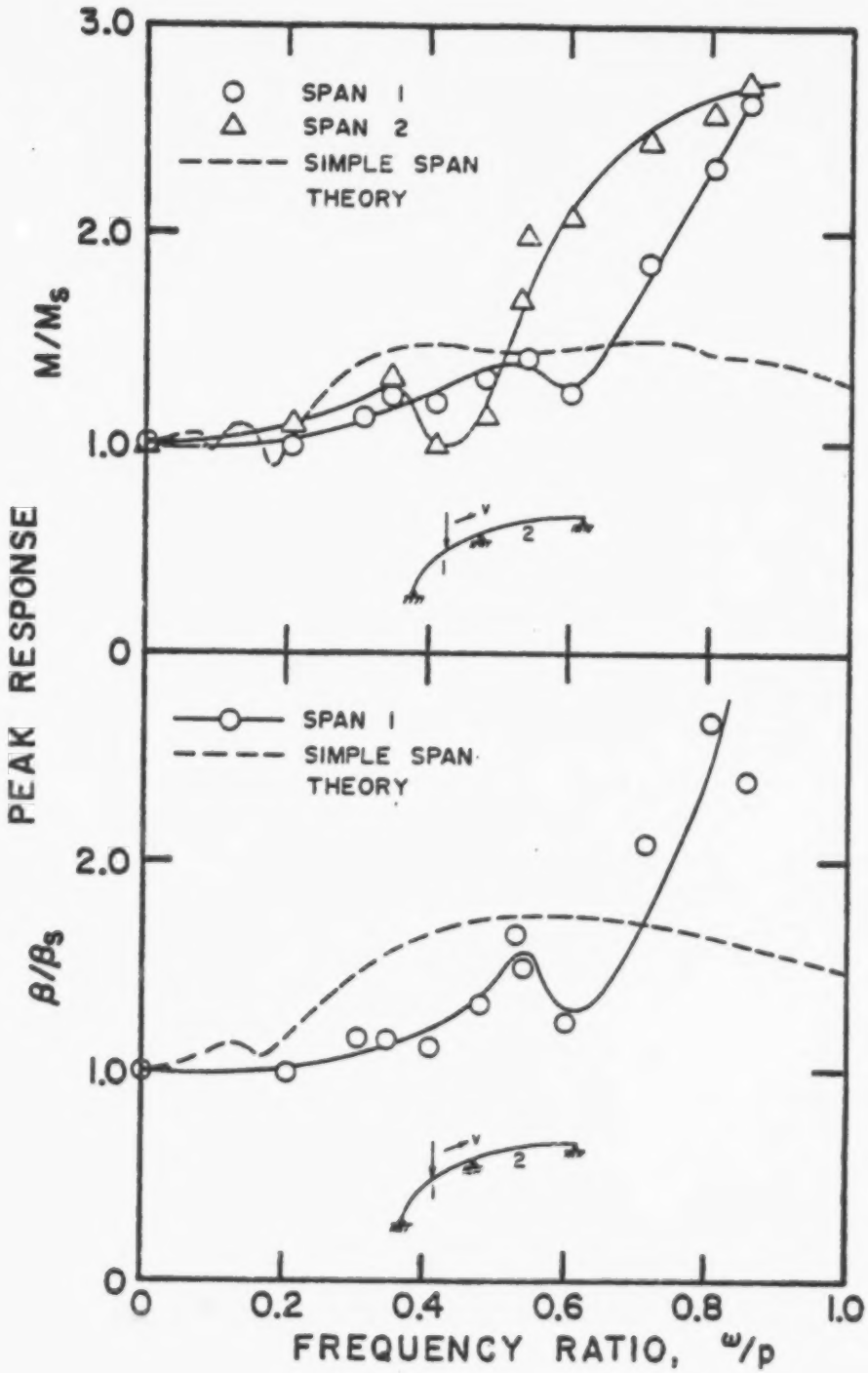


Figure 41. Response envelopes for a 45°-45° 2-span continuous curved guideway for 1 point load.

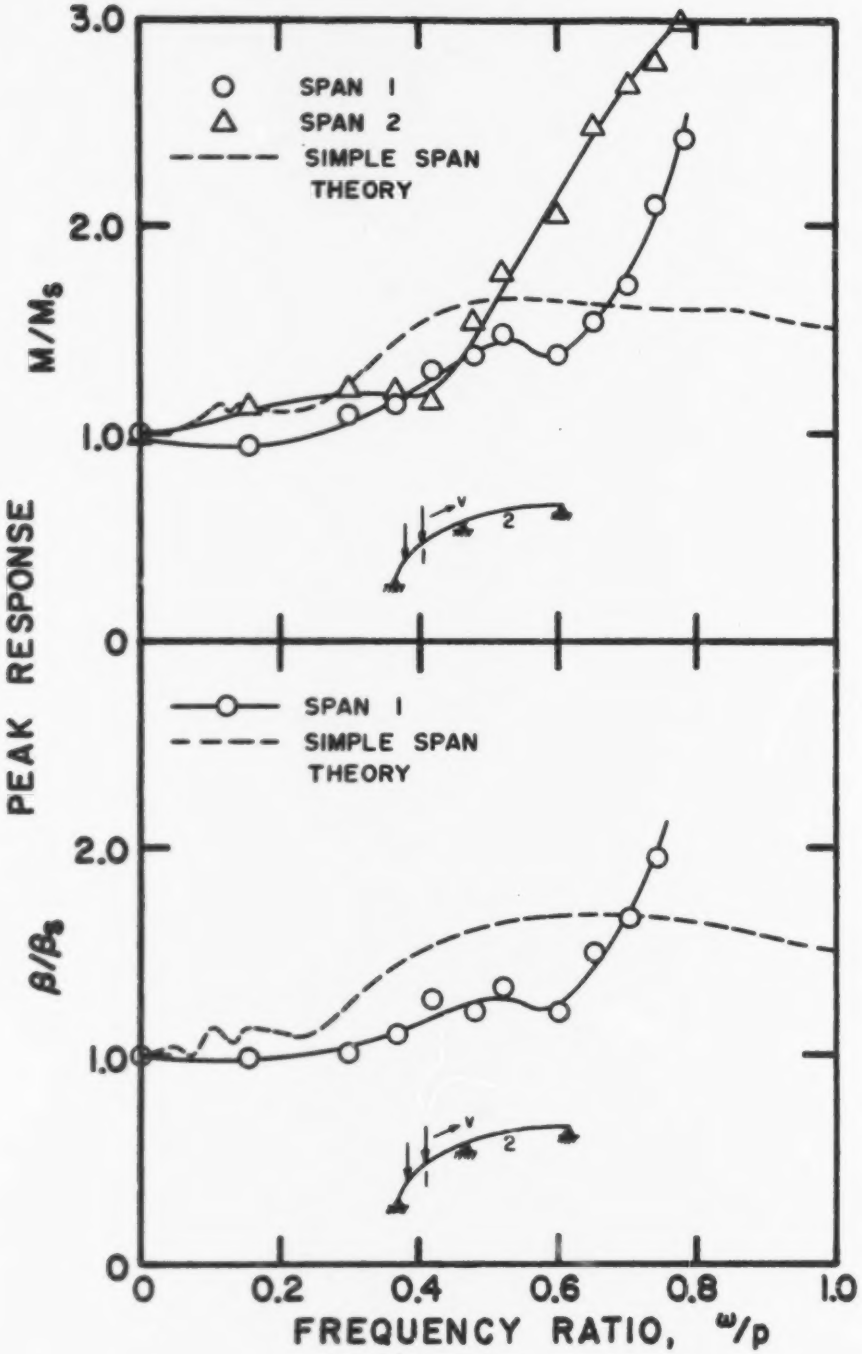


Figure 42. Response evvelopes of a 45°-45° 2-span continuous guideway for 2 point loads spaced at ℓ/4.

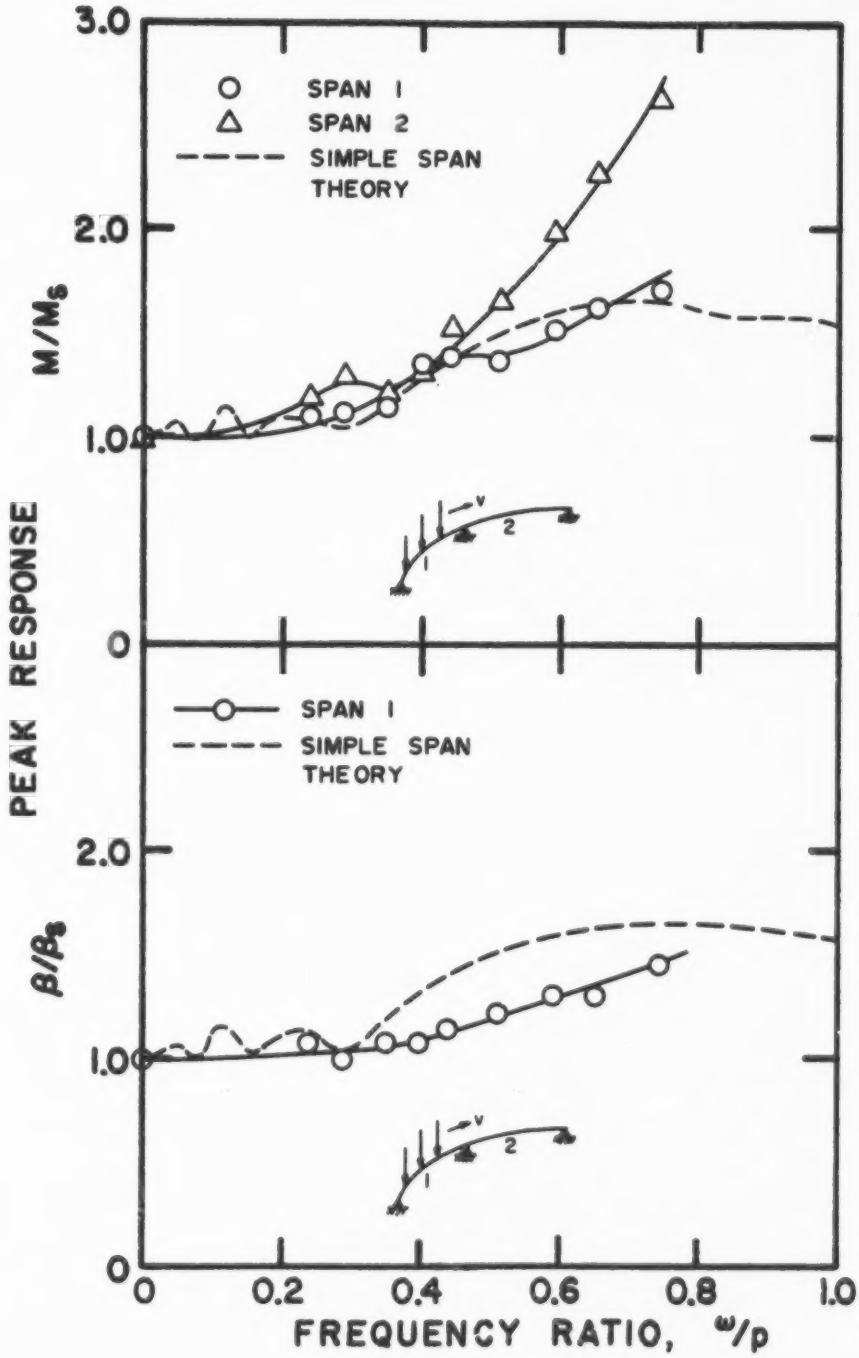


Figure 43. Response envelopes of a 45°-45° 2-span continuous curved guideway for 3 point loads spaced at ℓ/4.

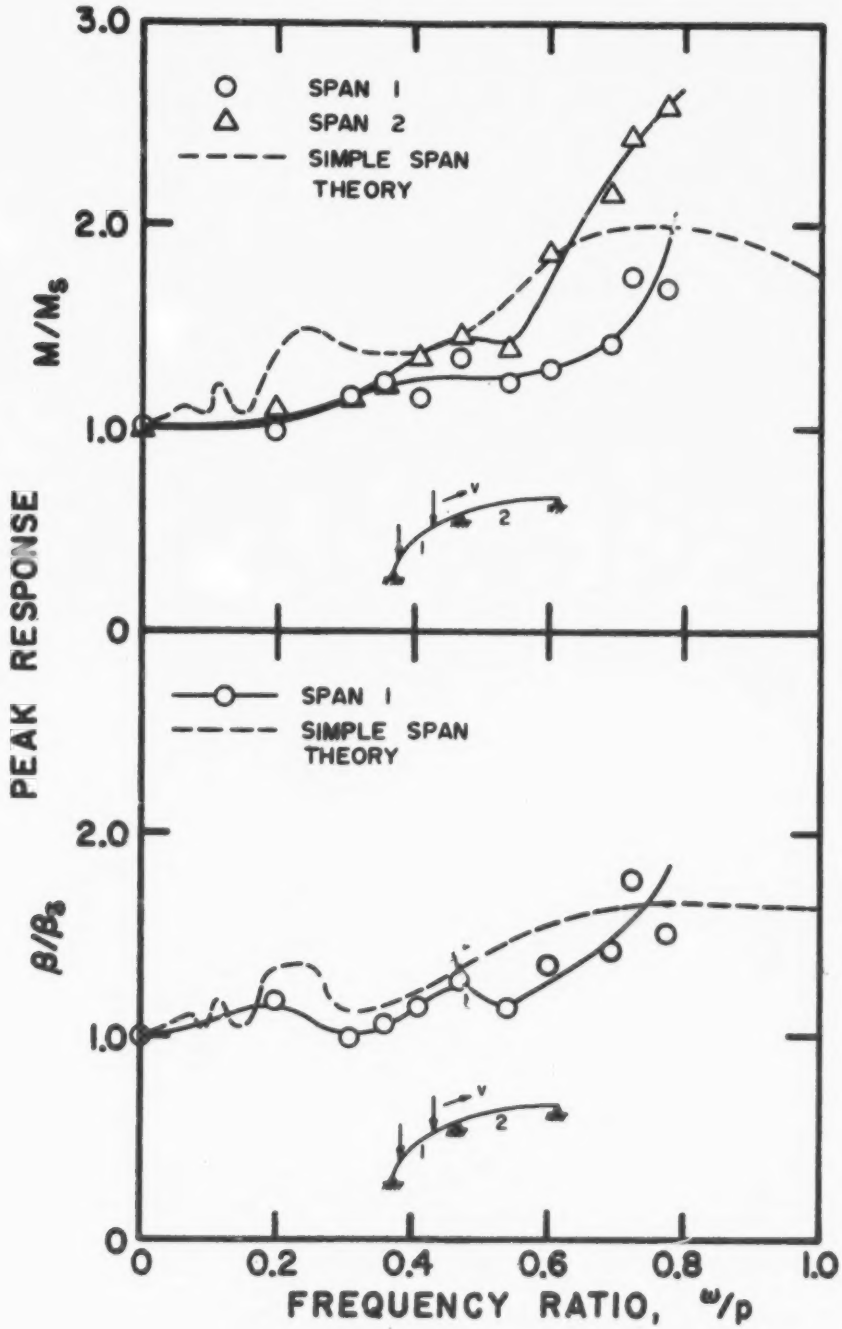


Figure 44. Response envelopes of a 45°-45° 2-span continuous curved guideway for 2 point loads spaced at ℓ/2.

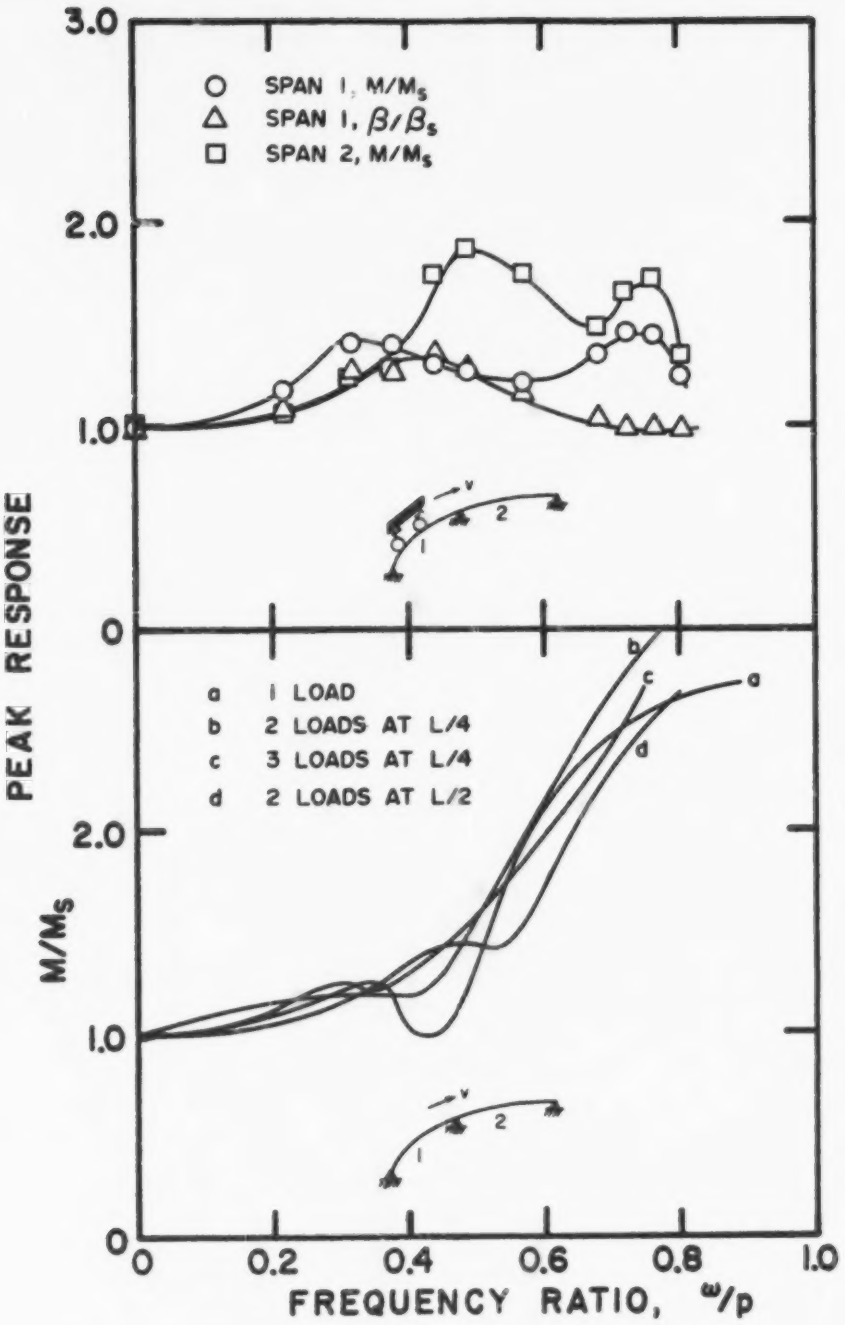


Figure 45. Response envelopes of a 45°-45° guideway for the AGT vehicle (top); response envelopes for span 2 of the same guideway for various point load configurations (bottom).

In Figs. 33 through 35, one sees that the response curves for the AGT vehicle on the 30°-30° guideway are consistently lower than those for 2 point loads at $\ell/4$. The AGT vehicle on the 45°-45° 2-span configuration gives rise to a maximum response amplification of only 1.9 at a frequency ratio of around 0.5 (see Fig. 45). Differences between the curves of Figs.33 through 35 and those of Fig. 45 are due primarily to differences in the dimensionless modeling parameters (see Eqs. 22). The "damping" effect of the AGT vehicle on the 45°-45° guideway with its corresponding parameters is more pronounced. Thus, the AGT vehicle on the 30°-30° guideway shows an approach to resonance at $\omega/p$ a little less than 1 while the AGT vehicle on the 45°-45° guideway shows no apparent resonance.

Resonance conditions for the point load configurations occur in a range of frequency ratios of about 0.75 to 0.90. One exception to this is 3 point loads at $\ell/2$ on the 30°-30° guideway where resonance occurs at $\omega/p$ slightly greater than 0.5 (see Fig. 39). These values could be more refined if it were possible to attain higher vehicle speeds with the propulsion system. Previous results [9] show that resonance for a point force on a 2-span straight guideway occurs at $\omega/p$ near unity, so that one effect of curvature appears to be a slight lowering of the frequency ratio at which resonance occurs.*

The dashed lines in the 2-span plots represent the theoretical response curves for a simple curve span with the same included angle as one of the two spans. Thus, one can identify the frequency ratio or crossover point at which the 2-span guideway continuous over the middle support is no longer as dynamically efficient as 2 simple spans placed end to end. From examining Figs. 32 through 44 it can be seen that crossover points for the 30°-30° guideway, in general, occur at lower frequency ratios than those for the 45°-45° guideway. In addition, crossover points for span 2, the exit span, are at lower

*This lower value of $\omega/p$ for resonance assumes that the load speed, length $\ell$, EI and mass per unit length remain the same between straight and curved configurations.

values of $\omega/p$ than those for span 1 for a given guideway configuration. The crossover points occur at frequency ratios between about 0.20 and 0.80. The former corresponds with the bending responses for 2 point loads at $\ell/4$ on the 30°-30° guideway (Figs. 33 and 34), while the latter represents the crossover point for the twist response of 1 point load on the same guideway (Fig. 32). Most of the crossover points occur at $\omega/p$ between 0.50 and 0.70. It should be mentioned that the simple span theory curves of Figs. 33 through 35 are for 2 point loads at $\ell/4$ and cannot be used to determine crossover points for the AGT vehicle whose response curves also appear in these figures. Finally, in this discussion of crossover points it should be noted that the midspan static responses for the simple and 2-span guideways are not the same. As shown in Table 2, $M_s$ and $\beta_s$ for the 2-span continuous guideway are less than they are for the simple span guideways. Thus, if the dynamic responses, M and $\beta$, for the 2-span and simple span configurations are both compared with the <u>same</u> static responses, $M_s$ and $\beta_s$ of the simple span configurations, the resulting 2-span response curve would be lower and the crossover points would be slightly higher. The crossover points obtained from Figs. 32 through 44 may be considered as absolute minimum points.

In Figures 40 and 45, the experimental moment response curves of the different point load configurations for span 2, the critical span, are reproduced. For both the 30°-30° and 45°-45° guideways the greatest moment magnification is given by 2 point loads at $\ell/4$. The point load configurations which give the least moment amplification are more difficult to determine but appear to be 3 point loads at $\ell/2$ and 1 point load for the 30°-30° and 45°-45° guideways respectively. In comparing this last result for the two guideway configurations it should be noted that it was not possible to test 3 point loads at $\ell/2$ on the 45°-45° guideway. Excluding this load arrangement from the

30°-30° guideway, the lowest moment response is then given by 1 point load, which is consistent with the 45°-45° guideway.

Three-Span Experiments - Results for the 30°-30°-30° 3-span continuous guideway are presented in Figs. 46 through 53. In comparing the moment responses for each span one sees that in most cases span 3, the exit span, gives the greatest moment magnification. As with the 2-span guideways, this is in agreement with previous results for multiple span straight guideways. This phenomenon can be attributed to a complex pattern of wave propagation in the bending modes whereby guideway vibrations build up ahead of the vehicle and dynamic response in the last span is increased.

For the sake of completeness the response curves for the AGT vehicle and 2 point loads at $\ell/4$ are compared (Figs. 47 through 49). Once again the AGT vehicle curves are lower than the point load curves, an indication of its "damping" effect on the guideway. Resonance appears to occur at frequency ratios between 0.80 and 0.95. As noted previously, exact values cannot be determined due to a lack of data at higher frequency ratios. This in turn is a result of the limitations of the propulsion system. For point loads on 3-span straight guideways resonance has been found to occur at $\omega/p$ near unity [9].

Once again the theoretical simple span response curves are plotted with the multiple span curves for the point load vehicle configurations. Crossover points for spans 2 and 3 are generally lower than those for span 1. For 1 point load the crossover point for the exit span (span 3) is 0.58 (Fig. 46). However, if the 3-span and simple span dynamic responses were compared with the same static responses, those of the simple span, it can be expected that this value (0.58) would increase slightly because of the reasons discussed previously. This crossover frequency ratio is close to that for 1 point load on a 3-span straight guideway which is 0.60 [9].

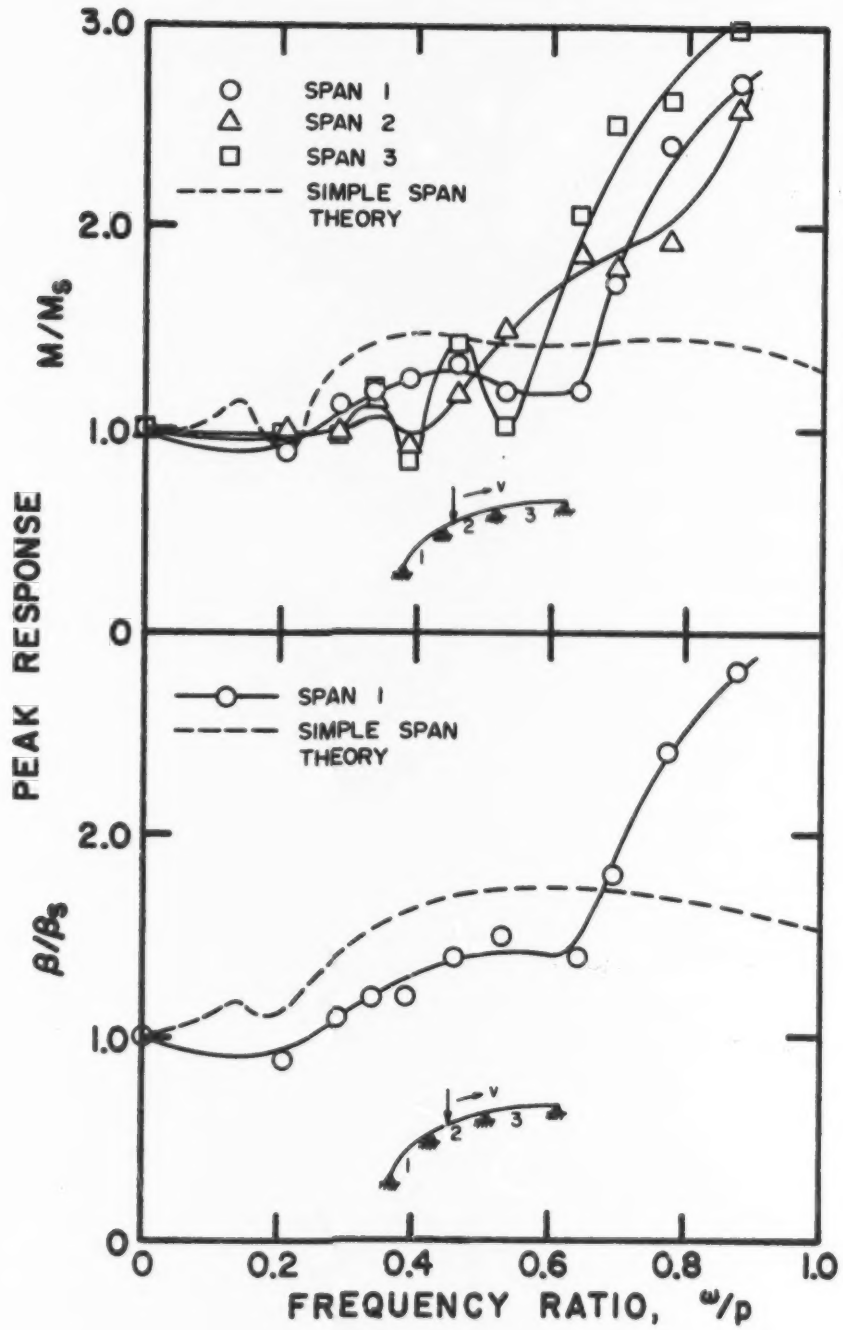


Figure 46. Response envelopes of a 30°-30°-30° 3-span continuous curved guideway for 1 point load.

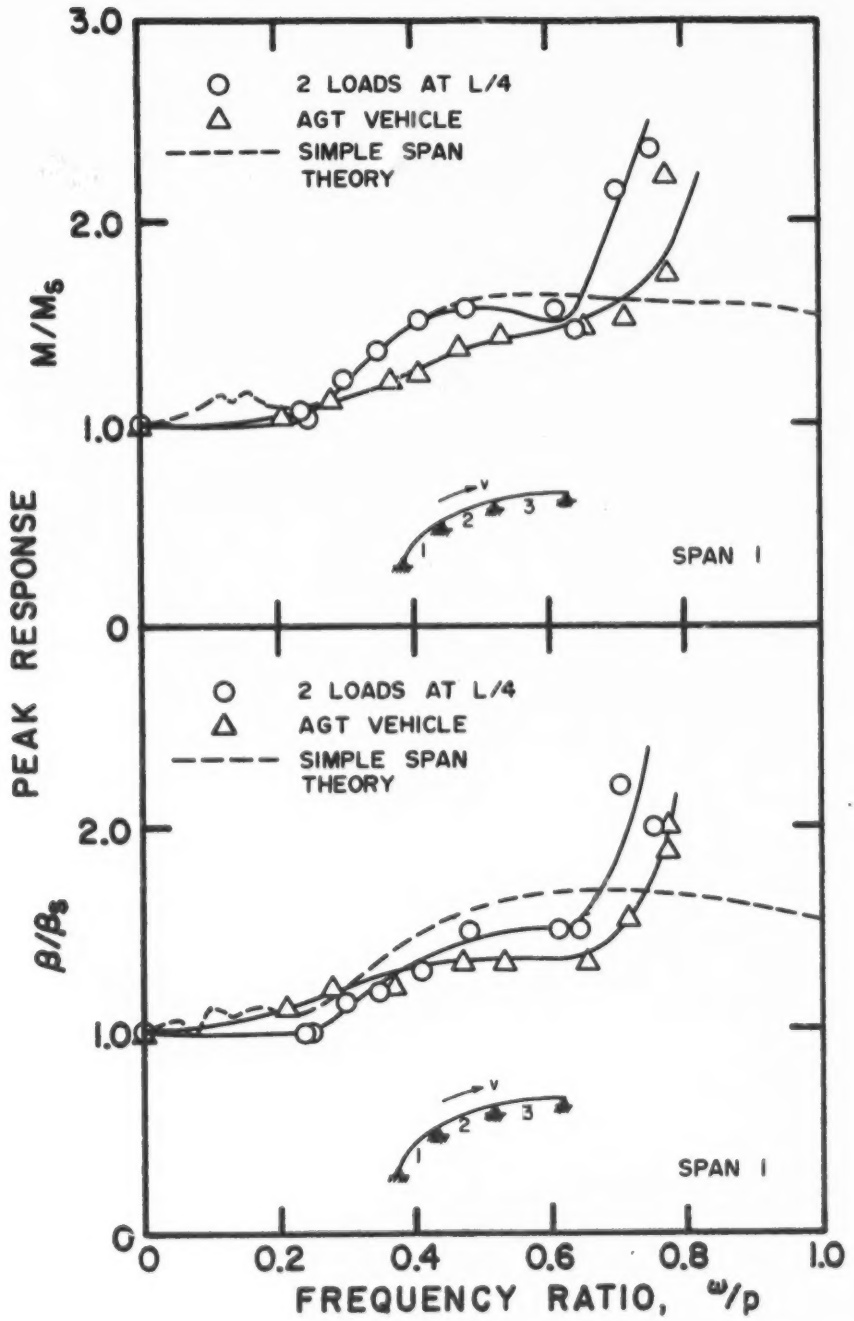


Figure 47. Response envelopes for span 1 of a 30°-30°-30° 3-span continuous curved guideway for 2 point loads spaced at ℓ/4 and the AGT vehicle

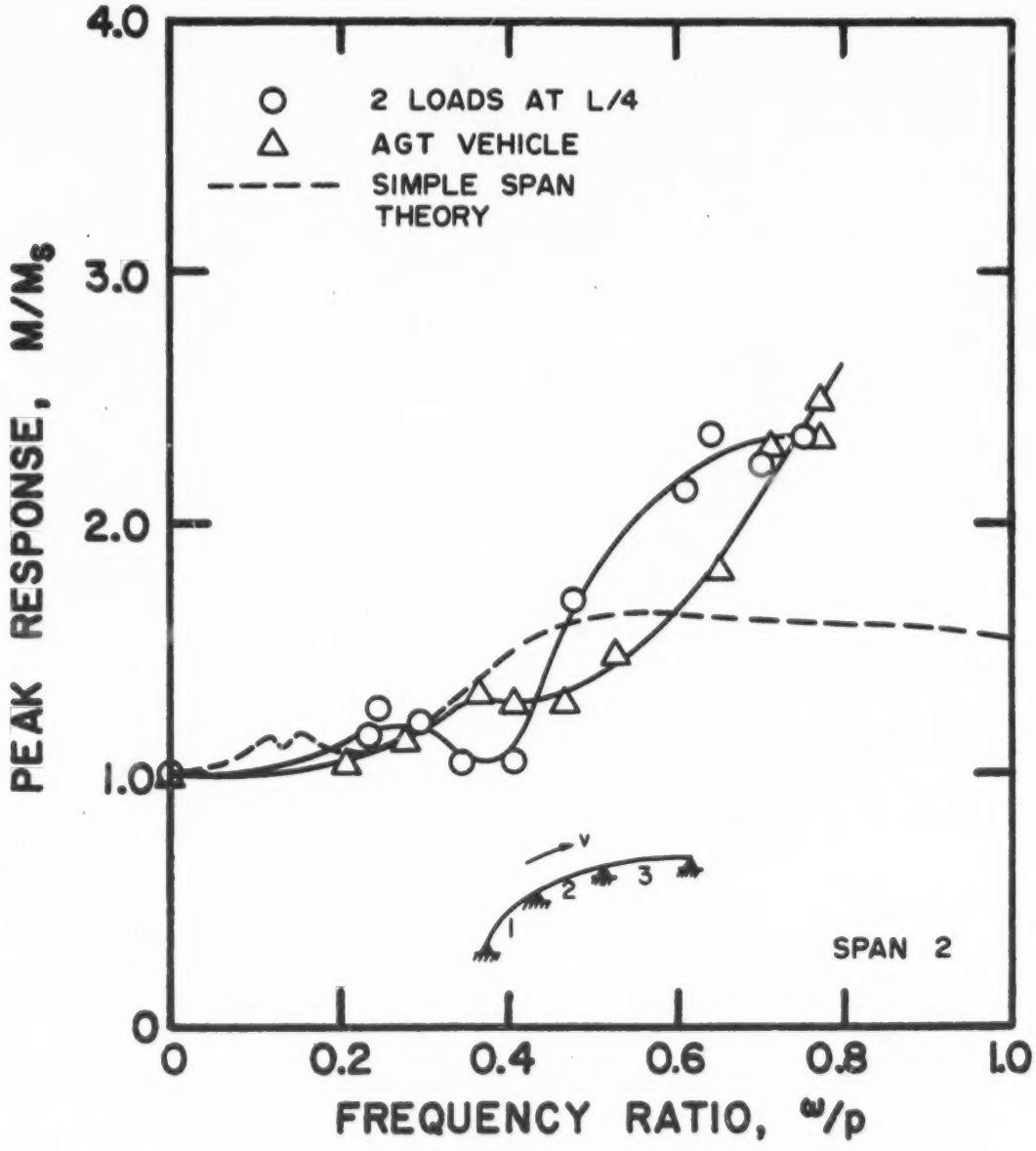


Figure 48. Response envelopes for span 2 of a 30°-30°-30° 3-span continuous curved guideway for 2 point loads spaced at ℓ/4 and the AGT vehicle.

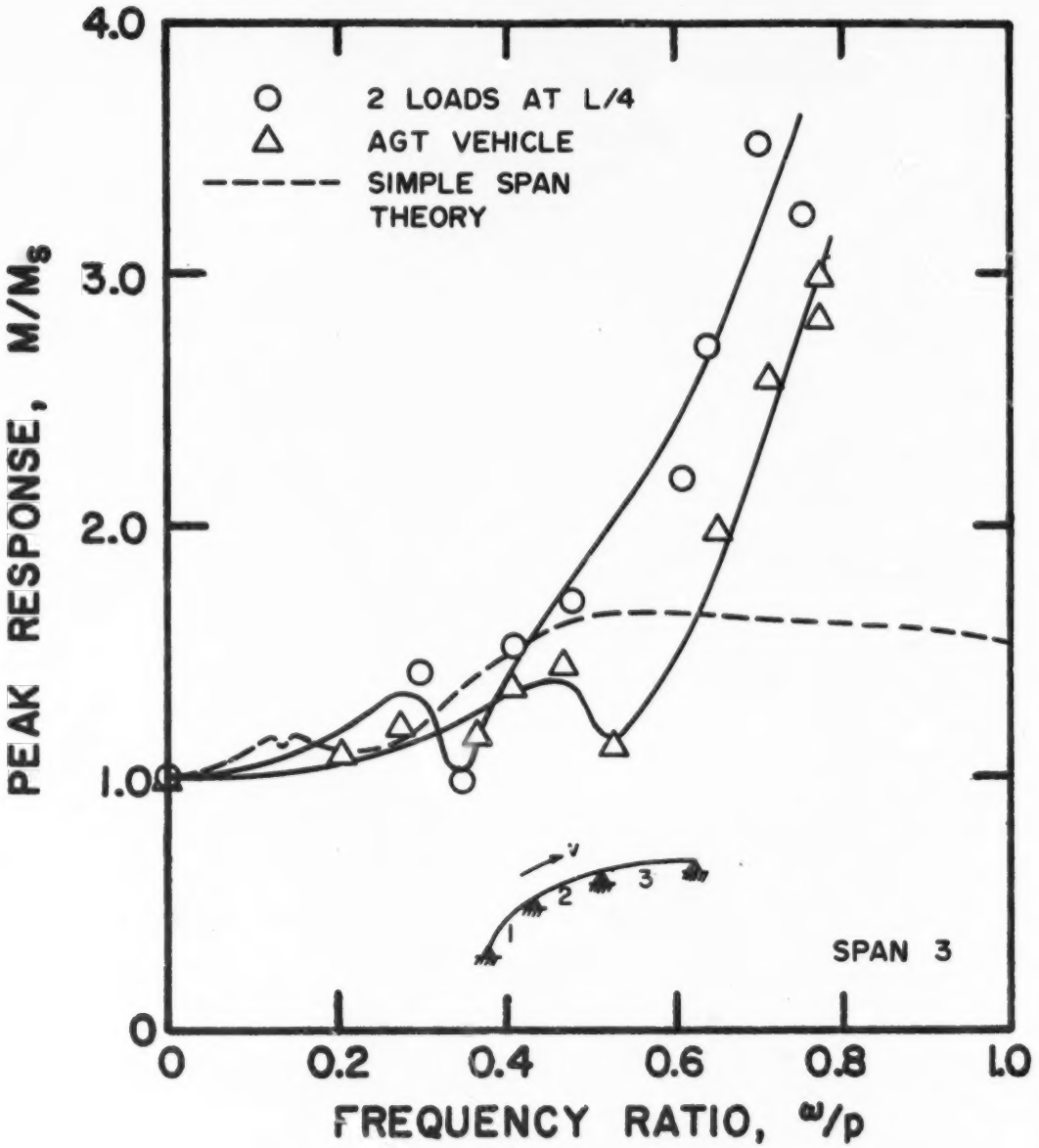


Figure 49. Response envelopes for span 3 of a 30°-30°-30° 3-span continuous curved guideway for 2 point loads spaced at ℓ/4 and the AGT vehicle.

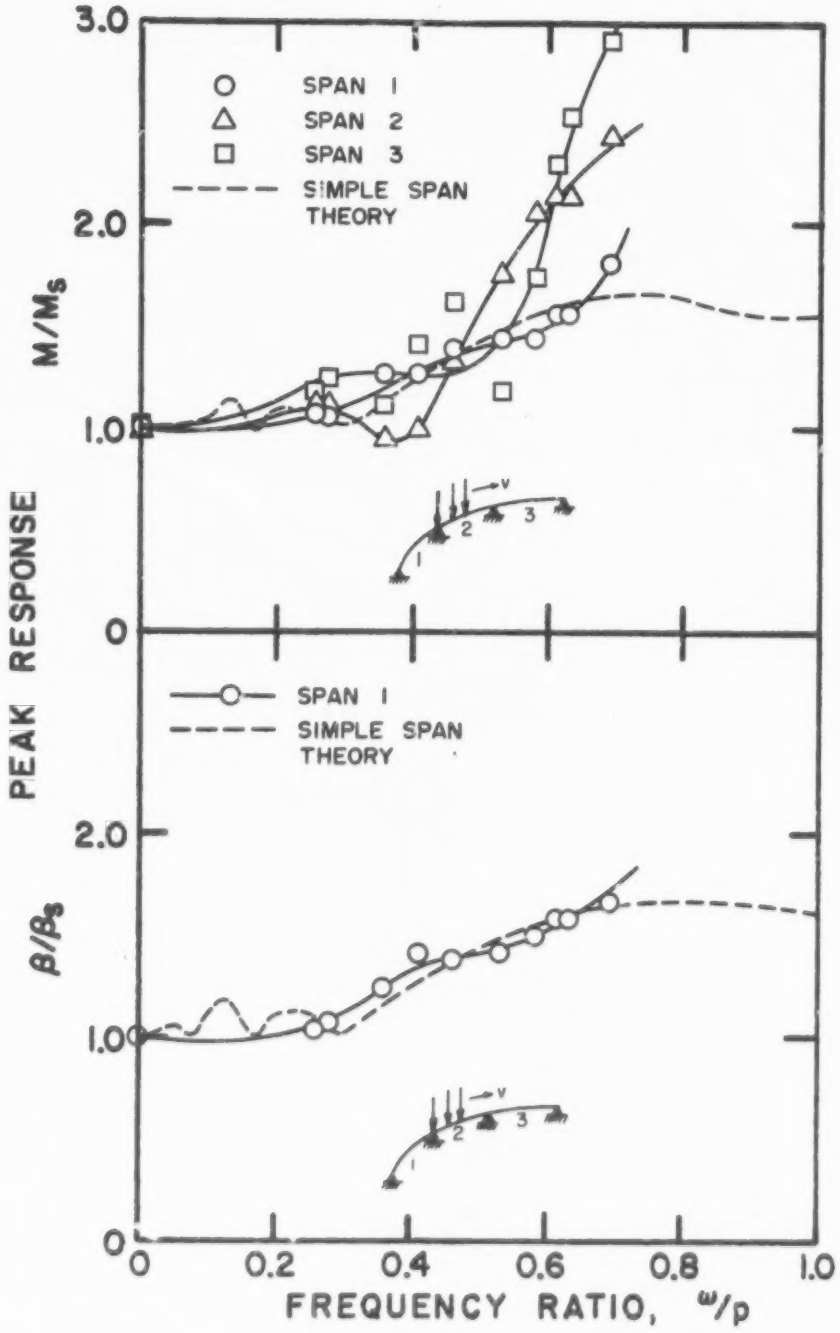


Figure 50. Response envelopes of a 30°-30°-30° 3-span continuous curved guideway for 3 point loads spaced at ℓ/4.

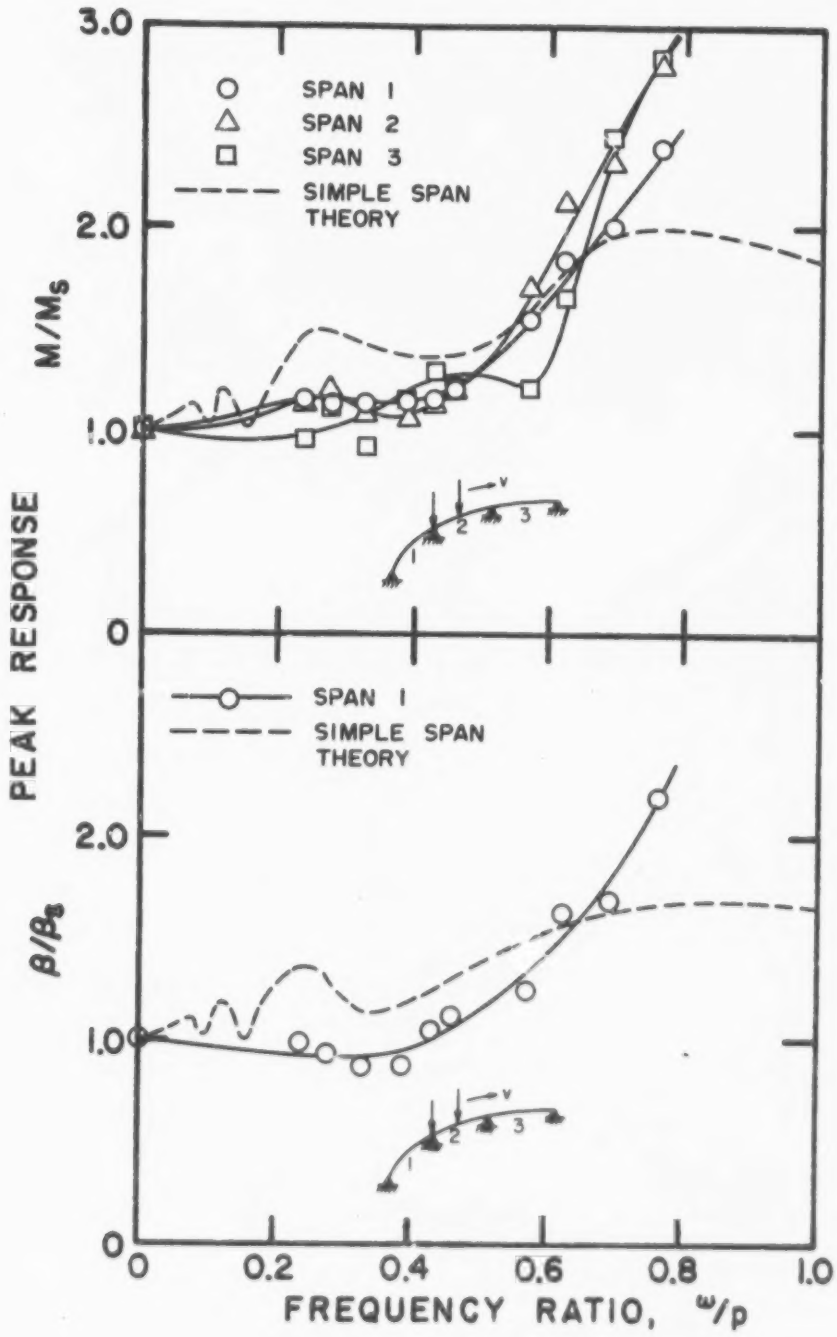


Figure 51. Response envelopes of a 30°-30°-30° 3-span continuous curved guideway for 2 point loads spaced at ℓ/2.

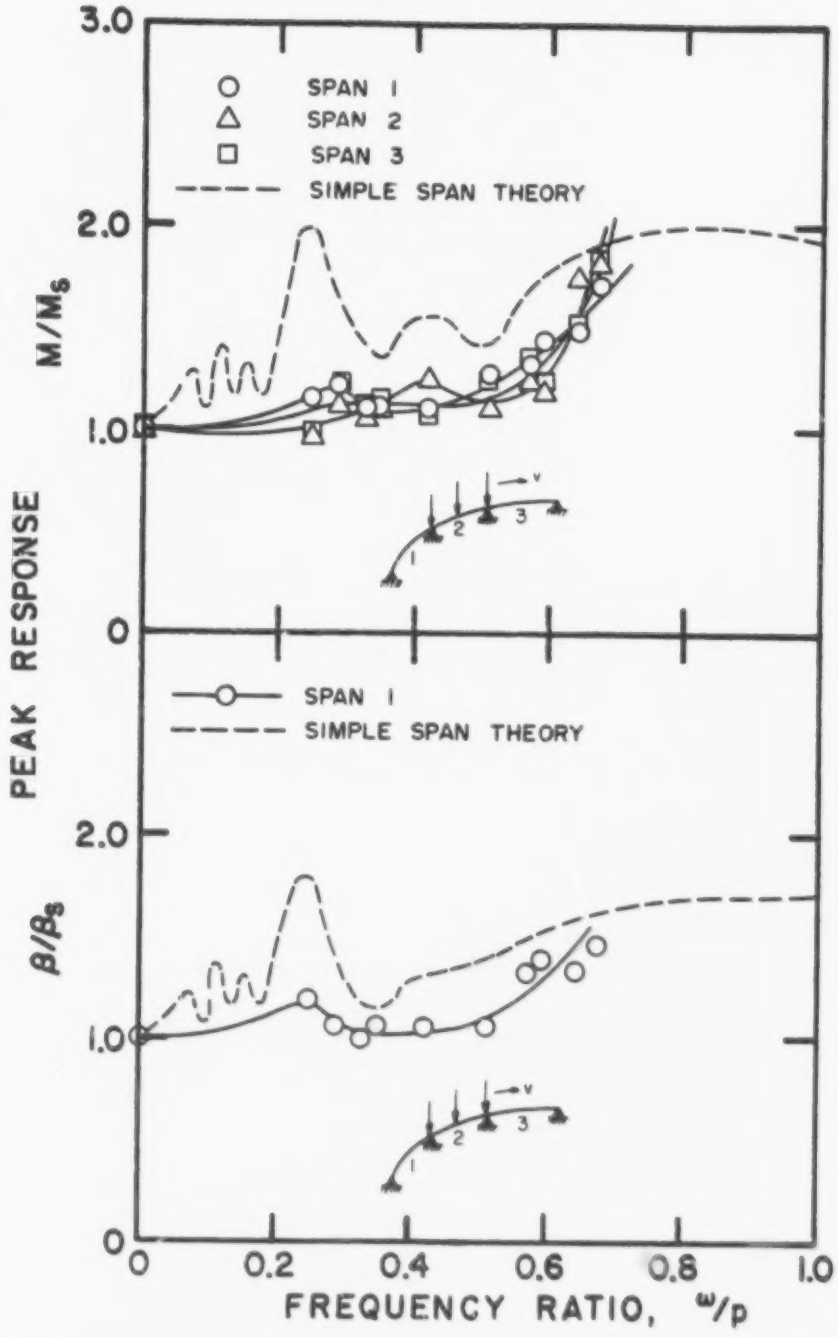


Figure 52. Response envelopes of a 30°-30°-30" 3-span continuous curved guideway for 3 point loads spaced at ℓ/2.

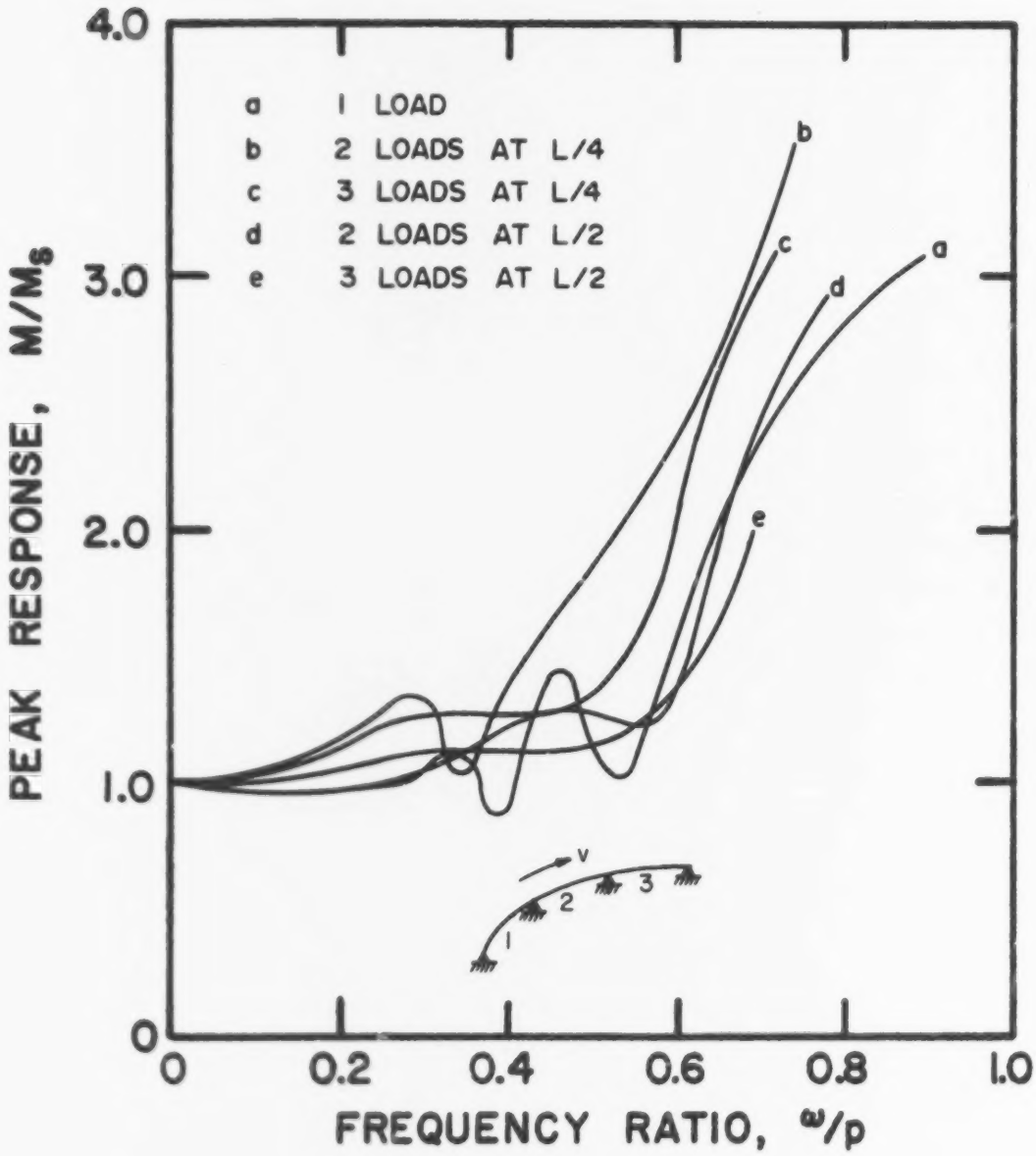


Figure 53. Response envelopes for span 3 of a 30°-30°-30° 3-span continuous curved guideway for various point load configurations.

From Fig. 53 one sees that as with the 2-span guideways the 2 point load vehicles at $\ell/4$ arrangement results in the greatest moment magnification for the exit span (span 3). The least amplification is given by 3 loads at $\ell/2$. Different dynamic responses for different load arrangements are due to the fact that at some spacings the guideway bending vibrations for each load tend to reinforce each other while at other spacings they tend to interfere.

Effects of End Constraints - Midspan bending moment response envelopes for a single point load and the AGT vehicle traveling on a 30°-30°-30° 3-span continuous curved guideway with various end constraints are shown in Figs. 54 through 56. For the point load vehicle, the guideway configuration which is least restrained, i.e., the extreme ends are simply supported, yields the highest bending moment amplification in all three spans. Clamping the entrance and exit spans at their extreme ends and for 1/3 their lengths results in lower moment magnifications. For span 1, the entrance span, the lowest response is given by the ends clamped configuration, while for span 2, the interior span, and span 3, the exit span, the lowest moment amplification is obtained from the 1/3 clamped arrangement.

As with the moving point load, the AGT vehicle with the extreme ends simply supported results in moment response envelopes for all of the spans which are higher than those with the ends restrained. For spans 1 and 2, the two constrained conditions yield the same moment amplifications while for span 3 the response with the ends clamped configuration may be slightly lower.

In summary, the effect of clamping the extreme ends and clamping 1/3 of the lengths of the entrance and exit spans is a reduction of the bending moment magnifications in all three spans as compared with simply supporting the ends for both the point load and AGT vehicles. For the AGT vehicle traveling on a 6-span

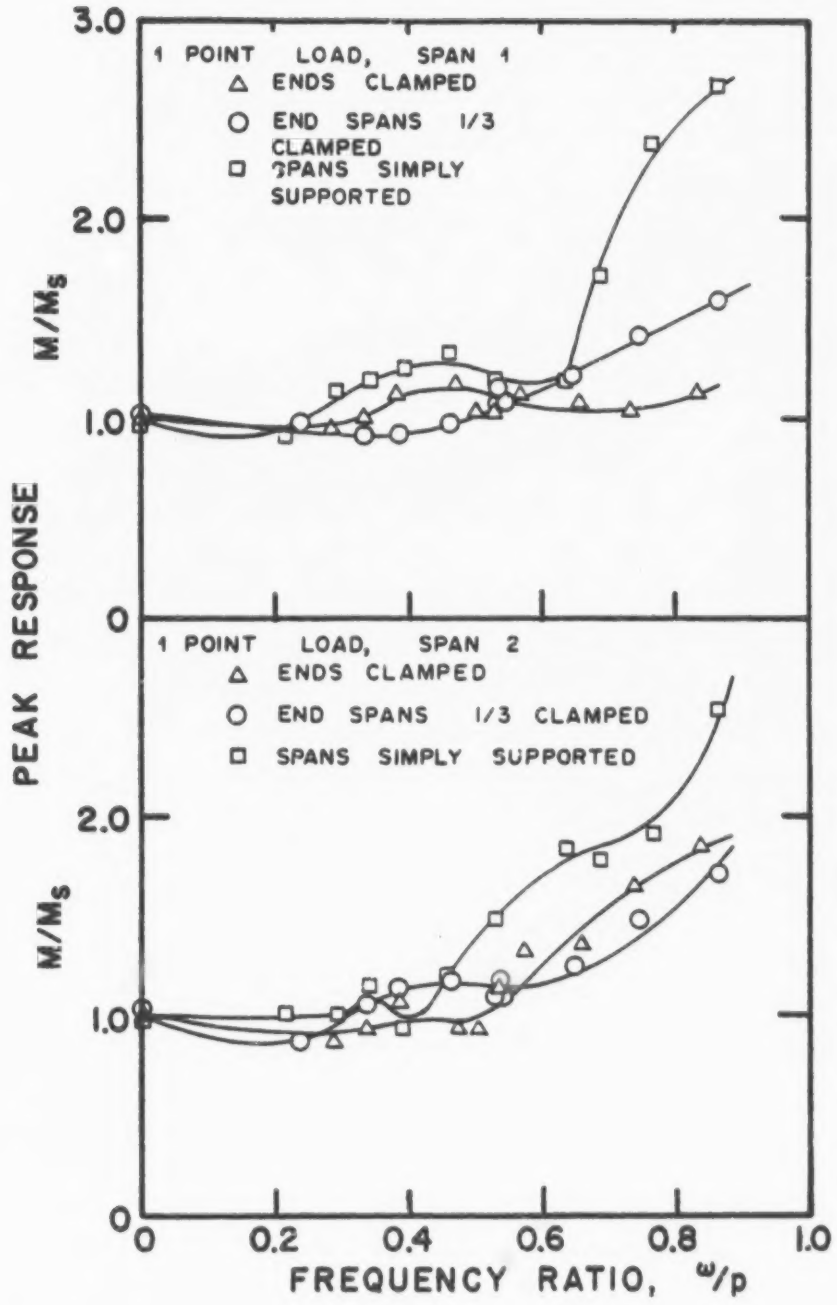


Figure 54. End constraint effects for a point-loaded, 30°-30°-30° curved guideway.

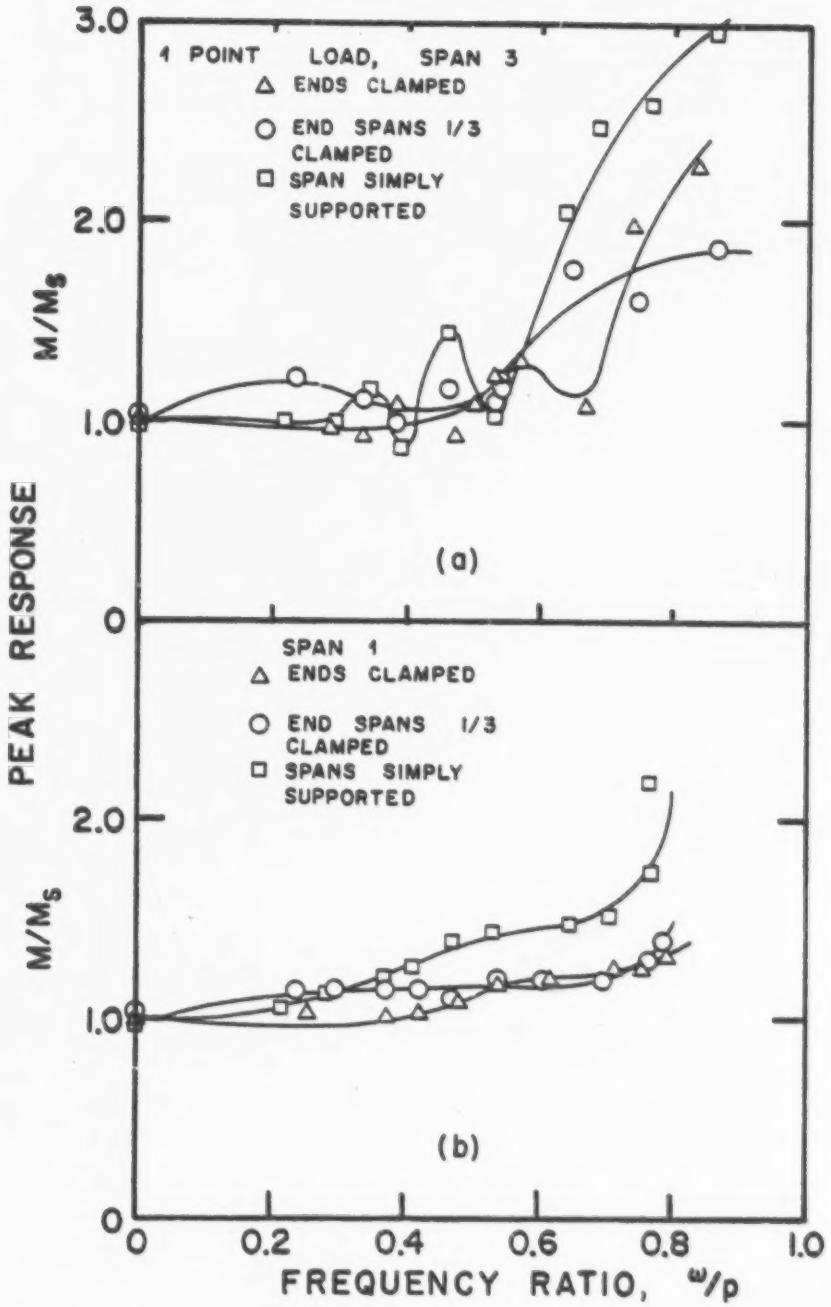


Figure 55. End constraint effects for a 30°-30°-30° guideway: (a) point load; (b) AGT vehicle.

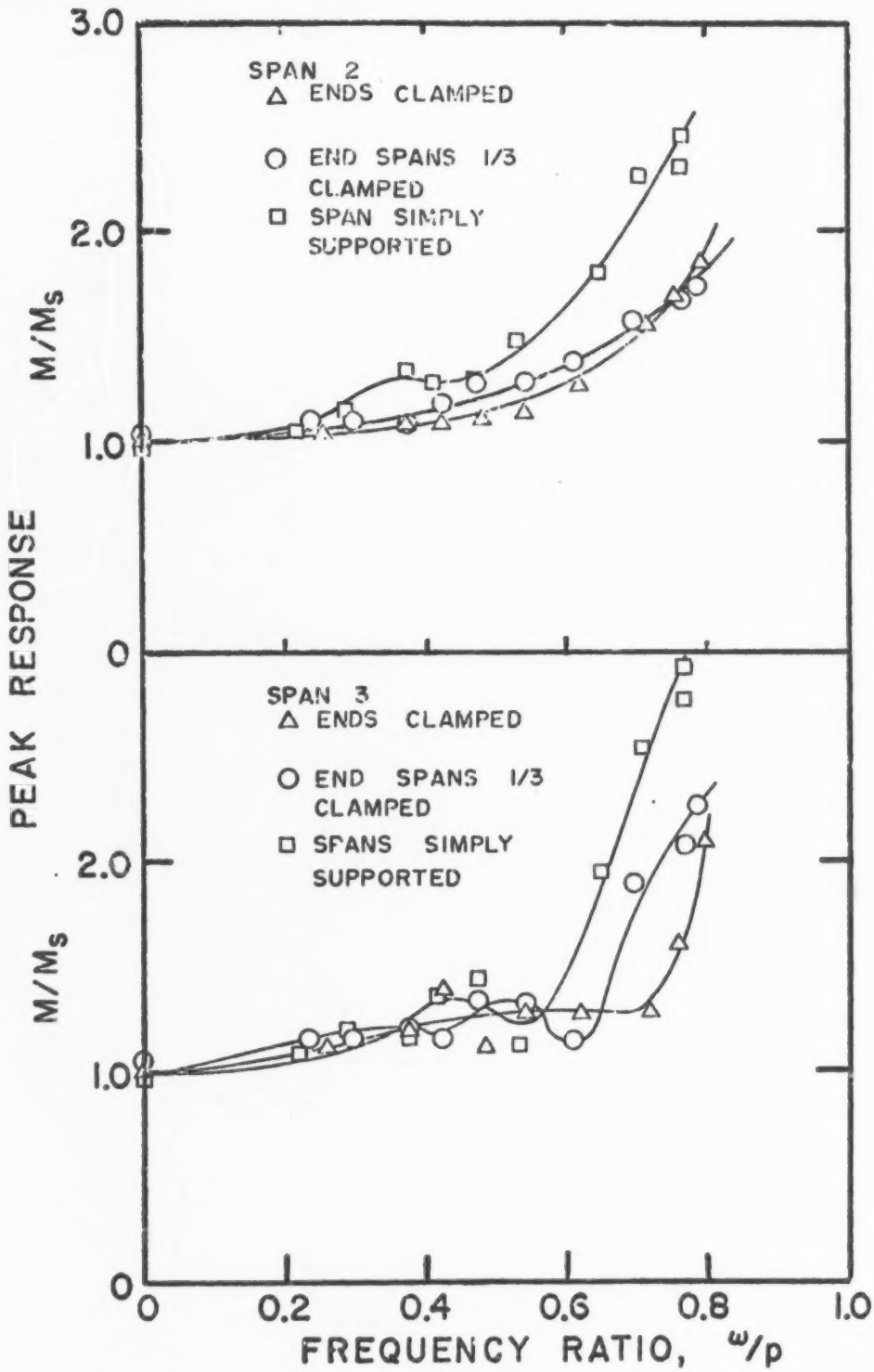


Figure 56. End constraint effects for a 30°-30°-30° guideway with AGT vehicle.

straight guideway increasing the end restraints also results in reduced moment responses. However, for the single point load on a 6-span straight guideway increasing end restraints sometimes yielded higher moment amplifications (9).

Summary and Conclusions - The experimental facility simulated two types of Automated Guideway Transit (AGT) vehicles traversing simple and multiple span curved guideways. The vehicle which is short and relatively light-weight is modeled as a moving point mass load; and the longer, relatively heavy vehicle is modeled as a spring mass load. The dimensionless parameters to be preserved between model and prototype curved guideways were identified as the included angle between supports $\theta_0$, the rigidity ratio A, the radius ratio $\xi$, and the loading parameter. $\theta_0$, A, and $\xi$ for the model are in ranges which encompass prototype values for these parameters. Preservation of the loading parameter for point vehicles involves preserving the vehicle mass to span mass ratio, $m_0/m_g$. For the spring vehicle, the parameters given by Eqs. (22) must be maintained. Finally, in order for the results obtained from the model to be directly applicable to prototype curved guideway transit systems, the experimental data is presented in dimensionless form.

Experiments were conducted with the two types of vehicles traversing simple-, 2-, and 3-span guideways. For the simple span curved guideways with the point load vehicle configurations, theoretical results obtained by assuming constant point forces were compared with the experimental results obtained by using mass loads applied through the point of contact between the vehicle and the guideway. In this study it was found that the theory and the experiment are in agreement for all point load configurations tested except 3 loads spaced at $\ell/2$, in which case the differences were attributed to inertial effects of the vehicle masses. Since in the full scale situation, the point vehicles are actually moving masses, there is a need to know under what conditions the inertial effects are important.

For the point load vehicles, inertial forces are directly related to the vehicle mass to span mass ratio. The problem, then, is to identify for a particular load configuration when $m_0/m_g$ is small enough that inertial effects can be neglected and the point force theory used to predict guideway responses. This can be done by varying the value of $m_0/m_g$ experimentally* and determining its value at which the point force theory and the mass load experiment deviate significantly. Apparently for all the load configurations tested in this study, except for 3 point loads at $\ell/2$, $m_0/m_g \approx 0.12$ is small enough to neglect inertial effects. Additional experimental work may be helpful in determining the value of $m_0/m_g$ for which inertial effects are negligible for 3 point loads at $\ell/2$ and may also show that the point force theory is valid for $m_0/m_g$ up to some value greater than 0.12 for the other load configurations.

The important conclusion of this first series of experiments is:

> If the vehicle mass to span mass ratio ($m_0/m_g$) is less than 0.12, dynamic responses of prototype simple span curved guideways may be accurately calculated using the constant point force theory for most point load configurations tested.

Theoretical results for the multiple span curved guideways are not available at this time. However, the second series of experiments gives some insight into their behaviour. The conclusions of these experiments are summarized.

1) The exit span of a multiple span curved guideway receives the greatest bending moment magnification. This behaviour is consistent with that of multiple span straight guideways.
2) Resonance conditions for multispan curved guideways for the load configurations tested occur at frequency ratios ($\omega/p$) between about 0.75 and 0.95. These are slightly lower than their straight guideway counterparts, which are near $\omega/p = 1$.

---

*This could be accomplished analytically also.

3) Crossover points obtained from the experimental data presented here can be useful in choosing between a multiple span continuous guideway and a series of simple span guideways. For example, for 1 point load traveling on the 30°-30° 2-span curved guideway, the crossover point for bending moment in the exit span is 0.52 (Fig. 32). In other words, for $\omega/p < 0.52$ the 30°-30° 2-span continuous guideway is dynamically more efficient than the two 30° simple spans placed end to end. The reverse is true for $\omega/p > 0.52$.

4) An implication of conclusion 3 is that for $\omega/p$ less than the crossover point, in the absence of dynamic theory for multiple span curved guideways, one may conservatively approximate their responses by applying the dynamic analysis of simple span curved beams as presented in Chapter 2. This can be useful in assessing the performance of existing curved guideway structures.

5) For both the 30° and 45° multispan guideways, the maximum bending response is given by 2 point loads spaced at $\ell/4$ as compared with the other point load configurations tested. This can be seen in the summary curves of Figs. 33, 38, and 46.

Finally, the following conclusion related to sprung vheicle experiments is appropriate.

The sprung mass AGT vehicle has the capacity to absorb some energy in its pitch motion and thus reduce dynamic responses in both simple and multiple span curved guideways.

This has design implications, for as observed in this study, different AGT vehicle parameters give rise to different guideway responses. It may be possible to select the parameters to optimize guideway "damping". However, one must also consider passenger ride comfort, in which case the need to know the AGT vehicle

responses (heave accelerations) as it traverses the guideways becomes important. Optimization of the AGT vehicle parameters then becomes a two-constraint problem.

With its validity established by the simple span curved guideway experiments, then, this facility has been shown to be an effective means of obtaining insight into the dynamic behaviour of various multiple span curved guideway-vehicle configurations for which analyses has yet to be done.

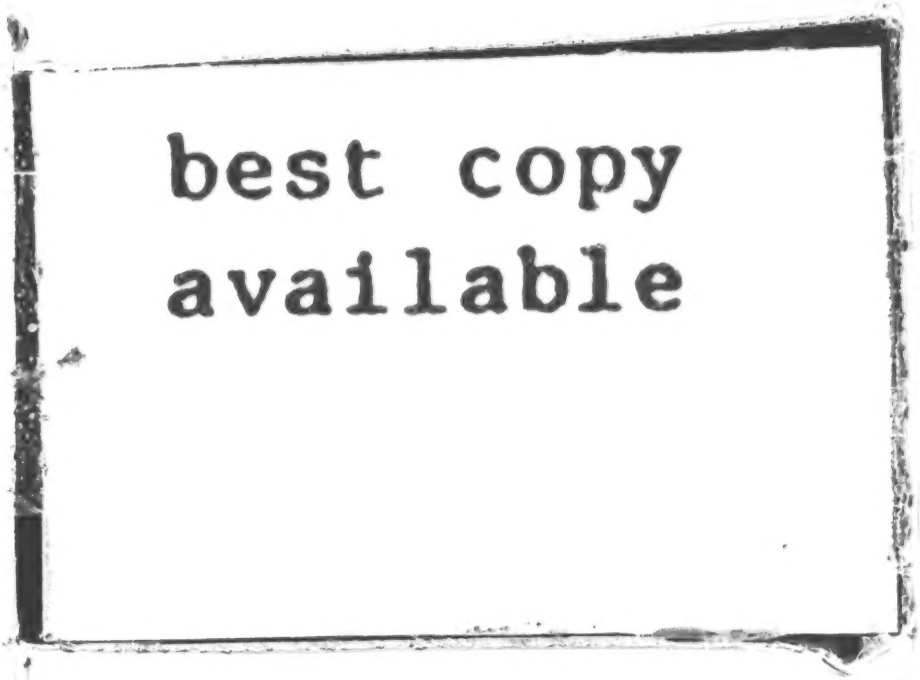

## 4. CABLE-STAYED GUIDEWAY STUDIES

Introduction - In applications where especially long clear guideway spans (100 to 1000 ft.) are required, a cable support system replacing rigid interior piers is a viable alternative. Such a three-span guideway is shown in Fig. 57, where the extreme ends are on simple supports. The cables are symmetrically placed with respect to the horizontal guideway in order to restrain dynamic bending from both upward and downward motion during vehicle passage. For mathematical modeling, such cable-stayed systems can be approximated by linear springs (constant $k_c$) at each suspension point, also shown in Fig. 57. This is justified [12] as long as the axial guideway loads have negligible effect on guideway frequencies and mode shapes. Also, by tuning the cable stiffness so that each "spring" support is effectively equal, a better degree of ride comfort is possible [13]. Previous studies [9,12] have also shown that an important dynamic design parameter for such guideways is cable stiffness relative to the guideway stiffness, or

$$K = \frac{k_c}{k_s} = \frac{k_c \ell^3}{48EI} \tag{23}$$

where an equal distance $\ell$ is assumed between supports, and the bending stiffness is EI. This ratio lies in the range $1<K<5$ in practical designs.

The purposes of this Chapter are two-fold. First, the dynamic response theory for cable-stayed bridges with a constant speed, constant intensity vertical point force is derived. Second, calculations such as time histories of span moment responses are then compared with typical model test measurements as a means of validating the theory.

Frequencies and Mode Shapes - Although the general theory for the free vibration frequencies and mode shapes was set forth by Lin [14], a few inconsistencies were found in this work. The theory [illegible] deficiencies. The following

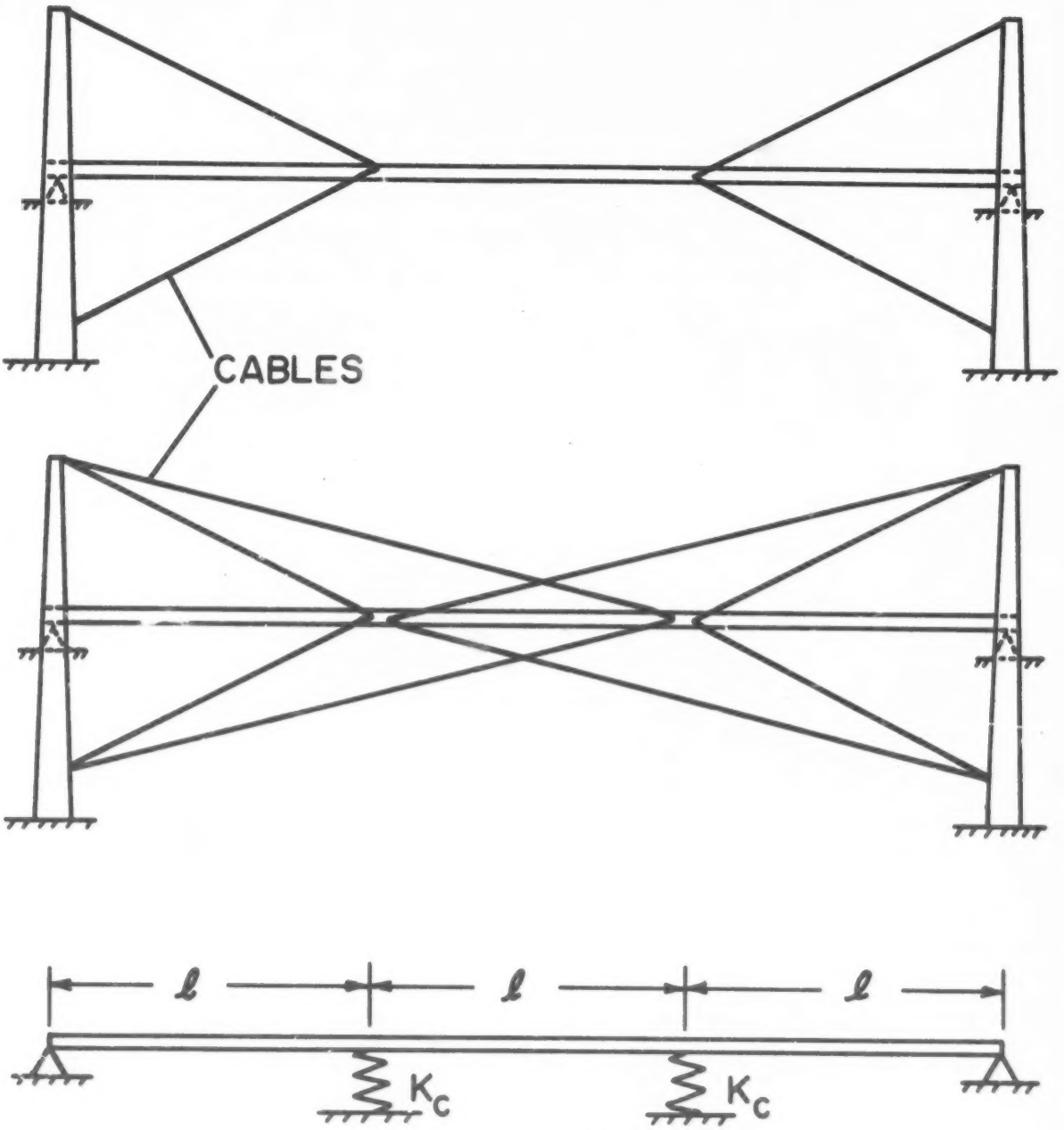


Figure 57. Two possible cable suspensions for a three-span guideway and the mathematical model.

Dynamic Theories and Experiments for
Alternative Guideway-Vehicle Systems: Part II

CONTENTS


| Chapter | | Page |
|---|---|---|
| 1 | EXECUTIVE SUMMARY | 1 1/A12 |
| 2 | THEORY FOR SIMPLE, CURVED GUIDEWAYS | 3 1/A14 |
| | Introduction, 3 | 1/A14 |
| | Dynamic Theory, 3 | 1/A14 |
| | Tandem Vehicle Simulations , 10 | 1/B7 |
| | Parametric Studies and Conclusions, 11 | 1/B8 |
| 3 | LABORATORY STUDIES OF CURVED GUIDEWAY-VEHICLE DYNAMICS | 27 1/C10 |
| | Introduction, 27 | 1/C10 |
| | Guideway Models and Response Measurements, 27 | 1/C10 |
| | Vehicle Models, 34 | 1/D3 |
| | Simple Span Experiments, 40 | 1/D9 |
| | Two-Span Experiments, 52 | 1/E7 |
| | Three-Span Experiments, 69 | 1/F10 |
| | End Constraint Effects, 78 | 1/G5 |
| | Summary and Conclusions, 82 | 1/G9 |
| 4 | CABLE-STAYED GUIDEWAY STUDIES | 86 1/G13 |
| | Introduction, 86 | 1/G13 |
| | Frequencies and Mode Shapes, 86 | 1/G13 |
| | Responses to Transit Loads, 97 | 2/A12 |
| | Theory and Experiment: Comparisons and Conclusions, 100 | 2/B1 |

| Chapter | | Page | |
|---|---|---|---|
| 5 | LATERAL RESPONSES OF VEHICLES ON CURVES | 118 | 2/C6 |
| | Introduction, 118 | | 2/C6 |
| | Equations of Motion, 120 | | 1/C8 |
| | System Equations and Parameters, 120 | | 2/C8 |
| | Response Statistics, 124 | | 2/C12 |
| | Solutions for Covariance, 126 | | 2/C14 |
| | Range of Parameters, 127 | | 2/D1 |
| | Numerical Results and Conclusions, 131 | | 2/D5 |
| | APPENDIX I | 136 | 2/D10 |
| | Cable-Stayed Guideway Response Program, 136 | | 2/D10 |
| | APPENDIX II | 150 | 2/E10 |
| | Equations of Vehicle Motion, 150 | | 2/E10 |
| | APPENDIX III | 156 | 2/F2 |
| | Vehicle Response Program, 156 | | 2/F2 |
| | REFERENCES | 176 | 2/G8 |

$A$ = cross sectional area of beam guideway

$A_{m,n}$; $B_{m,n}$; $C_{m,n}$; $D_{m,n}$ = mode shape coefficients

$D$ = finite difference operator

$EI$ = bending sitffness

$k_c$ = cable stiffness constant

$k_s$ = span stiffness constant

$K$ = cable-guideway stiffness parameter, Eq. (23)

$\ell$ = individual span length

$L$ = total guideway length

$m$ = mode number

$N$ = total number of spans

$n$ = span number

$P$ = point vertical force

$t$ = time

$v$ = speed of P

$x$ = horizontal coordinate, Fig. 58

$X_n$ = local coordinate along span n

$y(x,t)$ = guideway vertical deflection

$Y_{m,n}(x_n)$ = $m^{th}$ mode shape of span n

$Y_m(x)$ = sum of modes, Eq. (54)

$\beta_m, \gamma_n$ = coefficients, Eq. (36), (37)

$\lambda_m$ = frequency parameter, Eq. (29)

$\rho$ = guideway mass density

$\omega_m$ = guideway frequencies

$\Lambda_{m,1}$; $\Lambda_{m,2}$; $\Lambda_{m,3}$; $\Lambda_{m,4}$ = coefficients of Eq. (40) .

The differential equation governing the free vibrations of a uniform elastic guideway is, neglecting damping, the well-known Bernoulli-Euler equation,

$$EI \frac{\partial^4 y(x,t)}{\partial x^4} + \rho A \frac{\partial^2 y(x,t)}{\partial t^2} = 0 \qquad (24)$$

It is often convenient to rewrite Eq. (24) in terms of a local coordinate, $X_n$, as shown in Fig. 58, such that

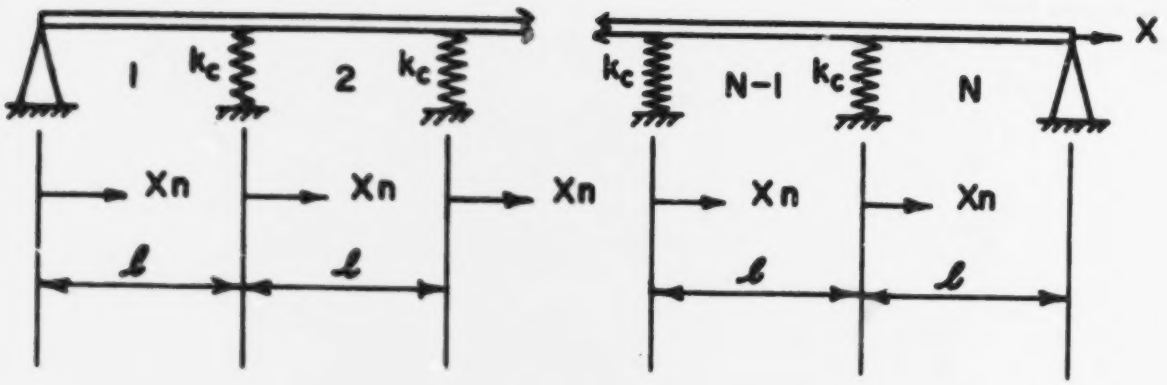


Figure 58. Model of the N-span cable-stayed guideway with extreme ends simply supported.

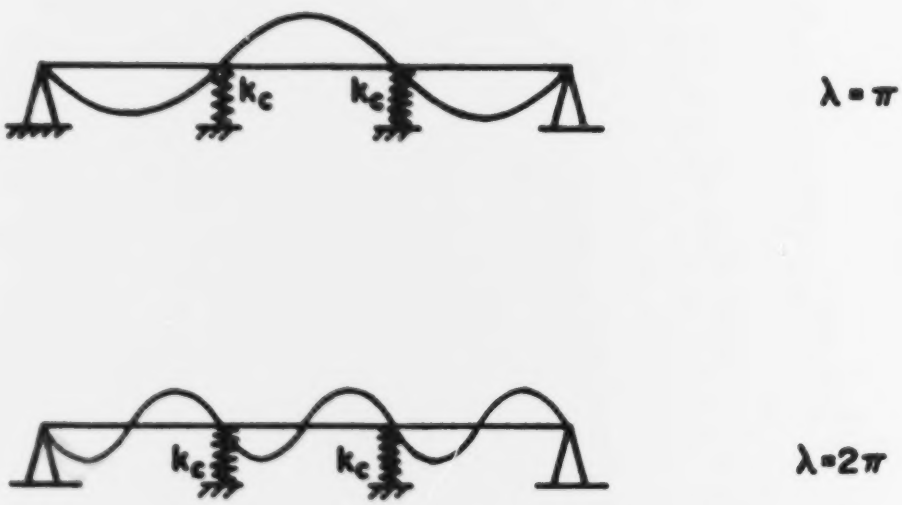


Figure 59. Two possible mode shapes for a three-span guideway, for $\lambda_m = \pi, 2\pi$.

$$X_n = x - (n-1)\ell \tag{25}$$

and

$$Y(x,t) = \sum_{m=1}^{\infty} Y_m(x)\cdot T(t) \tag{26}$$

where T(t) is a function of time and

$$Y_m(x) = \sum_{n=1}^{N} Y_{m,n}(X_n) \quad . \tag{27}$$

Assuming that the motion is harmonic (24) is reduced to

$$\ell^4 \frac{d^4 Y_{m,n}(X_n)}{dX_n^4} - \lambda_m^4 Y_{m,n}(X_n) = 0 \tag{28}$$

$$\text{for } n = 1,2,\ldots,N$$
$$m = 1,2,\ldots$$

and where the frequency parameter is given in terms of the guideway frequencies $\omega_m$ as

$$\lambda_m = \left(\frac{\rho A \omega_m^2 \ell^4}{EI}\right)^{1/4} \quad . \tag{29}$$

The constraints provided at each interior support are characterized by a displacement spring-constant $k_c$ while the two exterior supports are assumed to be non-yielding knife-edge supports (simply supported). Referring to Fig. 58, the boundary conditions at the interior supports are:

$$\left.\begin{aligned} Y_{m,n}(\ell) &= Y_{m,n+1}(0) \\ Y'_{m,n}(\ell) &= Y'_{m,n+1}(0) \\ \frac{k_c \ell^3}{EI} Y_{m,n}(\ell) &= Y'''_{m,n}(\ell) - Y'''_{m,n+1}(0) \\ Y''_{m,n}(\ell) &= Y''_{m,n+1}(0) \end{aligned}\right\} \quad n=1,2,\ldots,N-1 \tag{30}$$

The boundary conditions at the two exterior supports can be described as:

$$Y_{m,1}(0) = Y_{m,N}(\ell) = 0$$

$$Y''_{m,1}(0) = Y''_{m,N}(\ell) = 0 \qquad (31)$$

The most general solution to Eq. (28) may be written as follows.

$$\left.\begin{aligned} Y_{m,n}(X_n) = A_{m,n} \sin \lambda_m \frac{X_n}{\ell} + B_{m,n} \sinh \lambda_m \frac{X_n}{\ell} \\ + C_{m,n} \sin(\lambda_m - \frac{\lambda_m X_n}{\ell}) + D_{m,n} \sinh(\lambda_m - \frac{\lambda_m X_n}{\ell}) \end{aligned}\right\} \qquad (32)$$

for $0 \leq X_n \leq \ell$ and

$$Y_{m,n}(X_n) = 0 \text{ for } \ell < X_n < 0 \quad .$$

This solution is good for all modes for which $\lambda_m$ is <u>not</u> equal to $\pi$ or to a multiple of $\pi$. When $\lambda_m$ is equal to $\pi$ or to an integer multiple of $\pi$, there is no displacement at any of the supports since each support is a node point. This is illustrated in Fig. 59. For these modes, the mode shapes are described by:

$$Y_{m,n}(X_n) = (-1)^n \sin \frac{\lambda_m X_n}{\ell} \quad , \quad \lambda_m = \pi, 2\pi, 3\pi, \ldots$$

for $0 \leq X_n \leq \ell$

$$Y_{m,n}(X_n) = 0 \text{ for } \ell < X_n < 0 \quad . \qquad (33)$$

Substitution of (32) into the boundary conditions (30) results in the following set of simultaneous difference equations for the unknown constants $A_{m,n}$, $B_{m,n}$, $C_{m,n}$ and $D_{m,n}$.

$$A_{m,n} \sin \lambda_m + B_{m,n} \sinh \lambda_m - (D \sin\lambda_m)\, C_{m,n} - (D \sinh \lambda_m)\, D_{m,n} = 0 \qquad (34a)$$

$$(D-\cos \lambda_m)A_{m,n} + (D-\cosh \lambda_m)B_{m,n} + (-D \cos \lambda_m+1)C_{m,n} + (-D \cosh \lambda_m+1)\, D_{m,n} = 0 \qquad (34b)$$

$$\left(\frac{k_c \ell^3}{EI\lambda_m^3} \sin\lambda_m + \cos\lambda_m - D\right) A_{m,n} + \left(\frac{k_c \ell^3}{EI\lambda_m^3} \sinh\lambda_m - \cosh\lambda_m + D\right) B_{m,n} + (D \cos\lambda_m - 1)C_{m,n} + (-D \cosh\lambda_m - 1)D_{m,n} = 0 \qquad (34c)$$

$$A_{m,n} \sin\lambda_m + B_{m,n} \sinh \lambda_m + (D \sin\lambda_m)C_{m,n} - (D \sinh\lambda_m)D_{m,n} = 0 \qquad (34d)$$

where D's are the finite difference operators. Equations (34) are recognized to be homogeneous. It is well-known that the operators D in difference equations can be treated algebraically [14]. As in algebraic simultaneous equations that are homogeneous, a non-trivial solution to Eqs. (34) exists only if the determinant of the coefficients of the unknown constants is zero. Upon simplifying and expanding the determinant and equating it to zero one obtains:

$$(D^4 - 2\gamma_m D^3 + 2\beta_m D^2 - 2\gamma_m D + 1)\, C_{m,n-2} = 0 \qquad (35)$$

where

$$\gamma_m = -\frac{k_c \ell^3}{4EI\lambda_m^3} (\sinh\lambda_m - \sin\lambda_m) + \cosh\lambda_m + \cos\lambda_m \qquad (36)$$

$$\beta_m = -\frac{k_c \ell^3}{2EI\lambda_m^3} (\sinh\lambda_m \cos\lambda_m - \sin\lambda_m \cosh\lambda_m) + 2 \cosh\lambda_m \cos\lambda_m + 1 \qquad (37)$$

By eliminating any three unknowns such as $A_{m,n}$, $B_{m,n}$ and $C_{m,n}$ from Eqs. (34), the same difference equation can be obtained or

$$C_{m,n+2}-2\gamma_m C_{m,n+1}+2\beta_m C_{m,n}-2\gamma_m C_{m,n-1}+C_{m,n-2}=0 \tag{38}$$

or

$$(D^4-2\gamma_m D^3+2\beta_m D^2-2\gamma_m D+1)C_{m,n-2}=0 \tag{39}$$

Equation (38) has been written in a form that manifests the perfect symmetry in the coefficients. This type of difference equation occurs in problems of "repeated structures", where an overall structure is composed of a series of identical structural elements as in the case of long continuous bridges.

In the case where the two exterior supports allow rotation but restrict displacement (simple supports), the mode shapes of vibration, $Y_{m,n}$, conform to spatial periodicities and this fact should be reflected in the expression for constant $C_{m,n}$. $C_{m,n}$ is then expressible in terms of circular functions such as:

$$C_{m,n}=\Lambda_{m,1}\cos n\theta_{m,1}+\Lambda_{m,2}\sin n\theta_{m,1}$$
$$+\Lambda_{m,3}\cos n\theta_{m,2}+\Lambda_{m,4}\sin n\theta_{m,2} \tag{40}$$

where the parameters $\theta_{m,1}$ and $\theta_{m,2}$ are related to the coefficients in Eq. (38) as follows:

$$\cos\theta_{m,1}=\frac{\gamma_m}{2}+\left[\left(\frac{\gamma_m}{2}\right)^2-\frac{\beta_m-1}{2}\right]^{1/2} \tag{41}$$

and

$$\cos\theta_{m,2}=\frac{\gamma_m}{2}-\left[\left(\frac{\gamma_m}{2}\right)^2-\frac{\beta_m-1}{2}\right]^{1/2} \tag{42}$$

It must be remembered that Eq. (38) and its solution, Eq. (40), have been obtained for interior spans only using the boundary conditions (30) at the interior supports. One must now extend solutions to include n=0 and n=N so that Eq. (40) will be good for the

exterior spans as well. Thus,

$$
\begin{aligned}
&Y_{m,0}(\ell)=Y_{m,1}(0)=0\\
&Y'_{m,0}(\ell)=Y'_{m,1}(0)\\
&Y''_{m,0}(\ell)=Y''_{m,1}(0)=0\\
&Y_{m,N}(\ell)=Y_{m,N+1}(0)=0\\
&Y'_{m,N}(\ell)=Y'_{m,N+1}(0)\\
&Y''_{m,N}(\ell)=Y''_{m,N+1}(0)=0
\end{aligned}
\qquad (43)
$$

Equation (43) as used here gives the actual boundary conditions at the exterior supports when these supports are simple supports as shown in Fig. 58. These conditions can then be used to determine the values of $\Lambda_{m,1}$, $\Lambda_{m,2}$, $\Lambda_{m,3}$ and $\Lambda_{m,4}$ which are needed in the solution for $C_{m,n}$ in Eq. (40).

It can be shown that the four equations for $\Lambda_{m,1}$, $\Lambda_{m,2}$, $\Lambda_{m,3}$ and $\Lambda_{m,4}$ are again homogeneous and that the coefficients of the unknowns in these equations are functions of the frequency parameter $\lambda_m$. The equation for the frequency parameter $\lambda_m$ is then obtained by equating the determinant of the coefficients to zero, i.e.,

$$
\begin{vmatrix}
a_{11} & a_{12} & a_{13} & a_{14}\\
a_{21} & a_{22} & a_{23} & a_{24}\\
a_{31} & a_{32} & a_{33} & a_{34}\\
a_{41} & a_{42} & a_{43} & a_{44}
\end{vmatrix} = 0 \qquad (44)
$$

where:

$$
\begin{aligned}
a_{11} &= \cos\Theta_{m,1}\left[(\cos\Theta_{m,1}-\cos\lambda_m)\left(\frac{2\lambda_m^3 EI}{k_c\ell^3}\right)-\sin\lambda_m\right]\\
&= \cos\Theta_{m,1}\cdot\sigma_1(\Theta_{m,1})
\end{aligned}
$$

$$a_{12} = \sin \theta_{m,1} \cdot \sigma_1(\theta_{m,1})$$

$$a_{13} = \cos \theta_{m,2} \cdot \sigma_1(\theta_{m,2})$$

$$a_{14} = \sin \theta_{m,2} \cdot \sigma_1(\theta_{m,2})$$

$$a_{21} = \cos(N+1)\theta_{m,1} \cdot \sigma_1(\theta_{m,1})$$

$$a_{22} = \sin(N+1)\theta_{m,1} \cdot \sigma_1(\theta_{m,1})$$

$$a_{23} = \cos(N+1)\theta_{m,2} \cdot \sigma_1(\theta_{m,2})$$

$$a_{24} = \sin(N+1)\theta_{m,2} \cdot \sigma_1(\theta_{m,2})$$

$$a_{31} = \cos \theta_{m,1}\{\cos\theta_{m,1}[1+ \frac{\sin\lambda_m}{\sinh\lambda_m} + \frac{2\cos\lambda_m}{\sinh\lambda_m} (\frac{2\lambda_m^3 EI}{k_c \ell^3})]$$

$$- \frac{2}{\sinh\lambda_m} (\frac{2\lambda_m^3 EI}{k_c \ell^3})\cos^2 \theta_{m,1}$$

$$- (\cos\lambda_m + \frac{\cosh\lambda_m}{\sinh\lambda_m} \sin\lambda_m + \frac{2\cosh\lambda_m}{\sinh\lambda_m} \cos\lambda_m (\frac{2\lambda_m^3 EI}{k_c \ell^3}))$$

$$+ \frac{2\cosh\lambda_m}{\sinh\lambda_m} (\frac{2\lambda_m^3 EI}{k_c \ell^3})\cos \theta_{m,1}\}$$

$$= \cos \theta_{m,1} \cdot \sigma_2(\theta_{m,1})$$

$$a_{32} = \sin \theta_{m,1} \cdot \sigma_2(\theta_{m,1})$$

$$a_{33} = \cos \theta_{m,2} \cdot \sigma_2(\theta_{m,2})$$

$$a_{34} = \sin\theta_{m,2} \cdot \sigma_2(\theta_{m,2})$$

$$a_{41} = \cos(N+1)\theta_{m,1} \cdot \sigma_2(\theta_{m,1})$$

$$a_{42} = \sin(N+1)\theta_{m,1} \cdot \sigma_2(\theta_{m,1})$$

$$a_{43} = \cos(N+1)\theta_{m,2} \cdot \sigma_2(\theta_{m,2})$$

$$a_{44} = \sin(N+1)\theta_{m,2} \cdot \sigma_2(\theta_{m,2})$$

Since only real values for $\Theta_{m,1}$ and $\Theta_{m,2}$ are admitted to the solution, a root from the frequency equation is rejected if:

$$(\frac{\gamma_m}{2})^2 - \frac{\beta_m - 1}{2} < 0 \qquad (45)$$

or if both

$$\left| \frac{\gamma_m}{2} - [(\frac{\gamma_m}{2})^2 - \frac{\beta_m - 1}{2}]^{1/2} \right| > 1 \quad \text{and} \qquad (46)$$

$$\left| \frac{\gamma_m}{2} + [(\frac{\gamma_m}{2})^2 - \frac{\beta_m - 1}{2}]^{1/2} \right| > 1 \qquad (47)$$

If:

$$\left| \frac{\gamma_m}{2} - [(\frac{\gamma_m}{2})^2 - \frac{\beta_m - 1}{2}]^{1/2} \right| \leq 1 \quad \text{and} \qquad (48)$$

$$\left| \frac{\gamma_m}{2} + [(\frac{\gamma_m}{2})^2 - \frac{\beta_m - 1}{2}]^{1/2} \right| > 1 \qquad (49)$$

only the $\Theta_{m,2}$ terms in the solution (40) are retained and the frequency equation is reduced:

$$\sin(N\Theta_{m,2}) = 0 \qquad (50)$$

If:

$$\left| \frac{\gamma_m}{2} - \left[ (\frac{\gamma_m}{2})^2 - \frac{\beta_m - 1}{2} \right]^{1/2} \right| > 1 \geq \left| \frac{\gamma_m}{2} + \left[ (\frac{\gamma_m}{2})^2 - \frac{\beta_m - 1}{2} \right]^{1/2} \right| . \qquad (51)$$

only the $\Theta_{m,1}$ terms in the solution (40) are retained and the frequency equation is reduced to:

$$\sin(N\Theta_{m,1}) = 0 \quad . \qquad (52)$$

Thus equations (44), (50) and (52) are the frequency equations used to obtain the possible $\lambda_m$ values for the modes for which $\lambda_m$ is not equal to $\pi$ or a multiple of $\pi$. As mentioned earlier, for the modes for which $\lambda_m = \pi$ or a multiple of $\pi$, the mode shapes are described by Eq. (33).

Once the frequency parameters $\lambda_m$ and their corresponding $C_{m,n}$ values from Eq. (40) are obtained, the values of the other constants

i.e., $A_{m,n}$, $B_{m,n}$ and $C_{m,n}$ can be readily obtained by substituting Eq. (32) into any three of the boundary conditions (43). By doing so, one can show that the relationships among the four constants are as follows:

$$A_{m,n} = C_{m,n+1}$$

$$B_{m,n} = D_{m,n+1} \qquad (53)$$

$$D_{m,n} = \frac{1}{\sinh\lambda_m}\left[(C_{m,n+1} - 2C_{m,n}\cos\lambda_m + C_{m,n-1}) \cdot \left(\frac{2EI\lambda_m^3}{k_c \ell^3}\right) - C_{m,n}\sin\lambda_m\right]$$

Using these constants along with the frequency parameters $\lambda_m$ in Eqs. (32) and (33) enables one to obtain the desired mode shapes for every mode and every span along the continuous beam.

Table 4 shows some typical six-span values of $\lambda_m$ for different values of the dimensionless stiffness constant K. It is noted that for the relatively low value of K=1.39, there exist five values of $\lambda_m$ below $\pi$; but for the higher K values, the lowest $\lambda_m$ is equal to $\pi$. Values for the highest, K=208, represent hard pier supports, for practical purposes. The values of K shown here are those for which experimental guideway response data were measured. This topic will be discussed subsequent to the calculations for the forced responses which follow.

Responses to Transit Loads - In the last section, the methods for calculating the frequency parameters $\lambda_m$ and the corresponding mode shapes $Y_{m,n}(X_n)$ were outlined in detail. By combining Eqs. (32) and (33), one obtains a complete set $Y_m(x)$ of orthogonal mode shapes valid for every point on an N-span guideway, or

$$Y_m(x) = \sum_{n=1}^{N} Y_{m,n}(X_n) \qquad 0 \leq X_n \leq \ell \quad . \qquad (54)$$

For a transit point force of constant magnitude P, starting at x=0 at t=0 and traveling at constant horizontal speed v, Eq.

Table 4. Values of $\lambda_m$ for Typical Stiffness Parameters, for a Six-Span Cable-Stayed Guideway

| m | K = 1.39 | K = 3.48 | K = 4.17 | K = 208 |
|---|---|---|---|---|
| 1 | 2.7874 | 3.1416 | 3.1416 | 3.1416 |
| 2 | 2.7895 | 3.1643 | 3.1799 | 3.2589 |
| 3 | 2.8127 | 3.2205 | 3.2706 | 3.5506 |
| 4 | 2.8968 | 3.2872 | 3.3702 | 3.9144 |
| 5 | 3.0423 | 3.3457 | 3.4508 | 4.2761 |
| 6 | 3.1416 | 3.3849 | 3.5013 | 4.5681 |
| 7 | 4.0627 | 4.5903 | 4.7306 | 6.2832 |
| 8 | 4.4355 | 4.8084 | 4.9196 | 6.3979 |
| 9 | 4.8786 | 5.1326 | 5.2125 | 6.6691 |
| 10 | 5.3532 | 5.5255 | 5.5793 | 6.9952 |
| 11 | 5.8435 | 5.9532 | 5.9846 | 7.3117 |
| 12 | 6.2832 | 6.2832 | 6.2832 | 7.5582 |

(24) for guideway motion becomes

$$EI \frac{\partial^4 y}{\partial x^4} + \rho A \frac{\partial^2 y}{\partial t^2} = P\delta(x-vt) \tag{55}$$

where the total load on the beam is given by

$$\int_0^L P\delta(x-vt)dx = \begin{cases} P, & 0 \le vt \le L \\ 0, & \text{otherwise} \end{cases}$$

Based on the following transform pairs

$$\bar{Y}_m(t) = \int_0^L Y_m(x) Y(x,t) dx \tag{56}$$

$$y(x,t) = \sum_0^\infty \frac{1}{I_m} \bar{Y}_m(t)\, Y_m(x) \tag{57}$$

where the normalizing factor is

$$I_m = \int_0^L Y_m^2(x)dx = \sum_{n=1}^{N} \int_0^{\ell} [Y_{m,n}(X_n)]^2 dX_n \tag{58}$$

and where use is made of orthogonality,

$$\int_0^L Y_i(x) \cdot Y_j(x)\, dx = 0 \quad \text{for} \quad i \neq j \tag{59}$$

the ordinary differential equation is obtained [15,16].

$$\ddot{\bar{Y}}_m(t) + \omega_m^2 \bar{Y}_m(t) = P_m(t) \tag{60}$$

The right side of Eq. (60) is evaluated as

$$P_m(t) = \frac{1}{\rho A} \int_0^L P\delta(x-vt) Y_m(x) dx = \frac{P}{\rho A} Y_m(vt) \quad . \tag{61}$$

Equation (60) with Eq. (61) can be solved by numerical techniques to yield the value of $\bar{Y}_m(t)$ at any material point x on the guideway. From this, the deflection can be calculated from Eq. (57), and the bending moment from

$$M = EI \frac{\partial^2 y}{\partial x^2} = EI \sum_{m=1}^{\infty} \frac{1}{I_m} \bar{Y}_m(t) \cdot Y_m''(x) \quad . \tag{62}$$

For computations, the upper limit in Eqs. (57) and (62) must be replaced by a finite number, NM. For a six-span configuration with $1<K<500$, series truncation at NM=10 was found to give satisfactory convergences for midspan deflection histories; but suitable convergence for midspan moment histories required NM=60. For a three-span configuration over the same range of K, NM=6 and 40 were satisfactory for convergence of deflection and moment histories, respectively. These NM values were obtained by trial and error by comparing consecutive partial sums until the next higher value of NM did not affect the particular responses except beyond the third significant figure.

A Fortran IV computer program was written and all calculations described above were carried out on an IBM 370/175 digital computer. A printout of this program is in Appendix A. The sequence of calculations is as follows:

a. Calculate $\lambda_m$ values for all values of m=1,2,...,NM.
b. Calculate each mode shape.
c. Calculate normalized deflection and moment time histories at each midspan position; and then at other specified span points. Each deflection and moment history is normalized to the respective value for the simple span, or $y/y_{ss}$ and $M/M_{ss}$.
d. The solutions so obtained were also used to check all the boundary conditions at all support points.

Although the program as presently formulated is for calculating responses for any number of equal spans from N=2 to N=6, and only for a single transit point load, extensions for N>6 and for any number of point loads on unequal spans are planned for the future.

Theory and Experiment: Comparisons and Conclusions - Time histories of midspan bending moments were measured for both three and six-span guideways where five different stiffness parameters K were used (not including the hard-pier cases, $K\to\infty$). Table 5

Table 5. Cable-Stayed Span and Load Configurations, with Peak Midspan Values of $M_s/M_{ss}$

3-Span

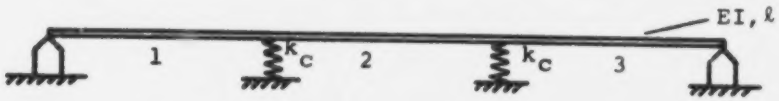


| K | Other Ref. | Load Type | Value of $M_s/M_{ss}$ for Span No.: 1 | 2 | 3 |
|---|---|---|---|---|---|
| 1.39 | 9 | Single Point Load | .872 | .741 | .872 |
| 2.09 | | | .851 | .727 | .851 |
| 2.78 | 9 | | .840 | .721 | .840 |
| 3.48 | | | .833 | .716 | .833 |
| 4.17 | 9 | | .828 | .714 | .828 |
| 1.39 | 9 | 2 Point Loads Spaced ℓ/4 | .859 | .703 | .859 |
| 2.09 | | | .836 | .686 | .836 |
| 2.78 | 9 | | .825 | .677 | .825 |
| 3.48 | | | .817 | .672 | .817 |
| 4.17 | 9 | | .812 | .668 | .812 |

6-Span

| K | Other Ref. | Load Type | Value of $M_s/M_{ss}$ for Span No.: 1 and 6 | 2 and 5 | 3 and 4 |
|---|---|---|---|---|---|
| 1.39 | 9 | Single Point Load | .872 | .743 | .745 |
| 2.09 | | | .851 | .727 | .727 |
| 2.78 | 9 | | .840 | .719 | .717 |
| 3.48 | | | .832 | .713 | .711 |
| 4.17 | 9 | | .827 | .710 | .706 |
| ∞ | 9 | | .799 | .691 | .692 |
| 1.39 | 9 | 2 Point Loads Spaced ℓ/4 | .859 | .694 | .709 |
| 2.07 | | | .836 | .686 | .686 |
| 2.78 | 9 | | .824 | .676 | .673 |
| 3.48 | | | .817 | .669 | .665 |
| 4.17 | 9 | | .812 | .664 | .660 |
| ∞ | 9 | | .801 | .689 | .683 |

lists the type of experiments performed, with their load configurations and references. Table 5 also lists the peak static (zero speed) midspan moments, $M_s$, relative to $M_{ss}$ for these guideway configurations, for the point load as well as for the AGT vehicle of Chapter 3. In presenting experimental data, each midspan moment was plotted as a function of each constant value of the frequency ratio, $\omega/p$. Each of these peak moments was normalized by $M_{ss}=P\ell/4$; and p is the simple span frequency, calculated from Eq. (1).

The first comparisons of theory and experiment are for the three-span guideway. Figure 60 shows a typical experimental time history of the midspan moment (strain) for the exit span, for the time that the load is on the span, and for about 1-1/2 cycles during free vibration. The results of theoretical calculations, shown as opaque circles, agree quite well with the measurements. The dynamic amplification of the moment is about 1.3, and occurs while the load is on this span. These results are all based on a stiffness parameter of K=3.48 and a transit frequency ratio of $\omega/p = 0.61$.

Comparisons of peak midspan moments, calculated and measured for three-span configurations, are shown in Figs. 61 through 64. In Fig. 61, for the lowest value of cable stiffness, or K=1.39, the peak response ratio just exceeds 2.0 for the critical span number three, at the highest range of $\omega/p$. Span three is also the critical one for K=3.48, as shown at the top of Fig. 64.

Comparisons for the six-span configurations are shown in Figs. 65 through 67 for K=1.39; and in Figs. 68 through 73 for K=3.48. Again, the theory and experiments are in good agreement. Also the exit span number six is the critical one, with the interesting fact that its peak responses (open and closed circles) are really quite close to those for the same span on rigid or hard piers (triangles).

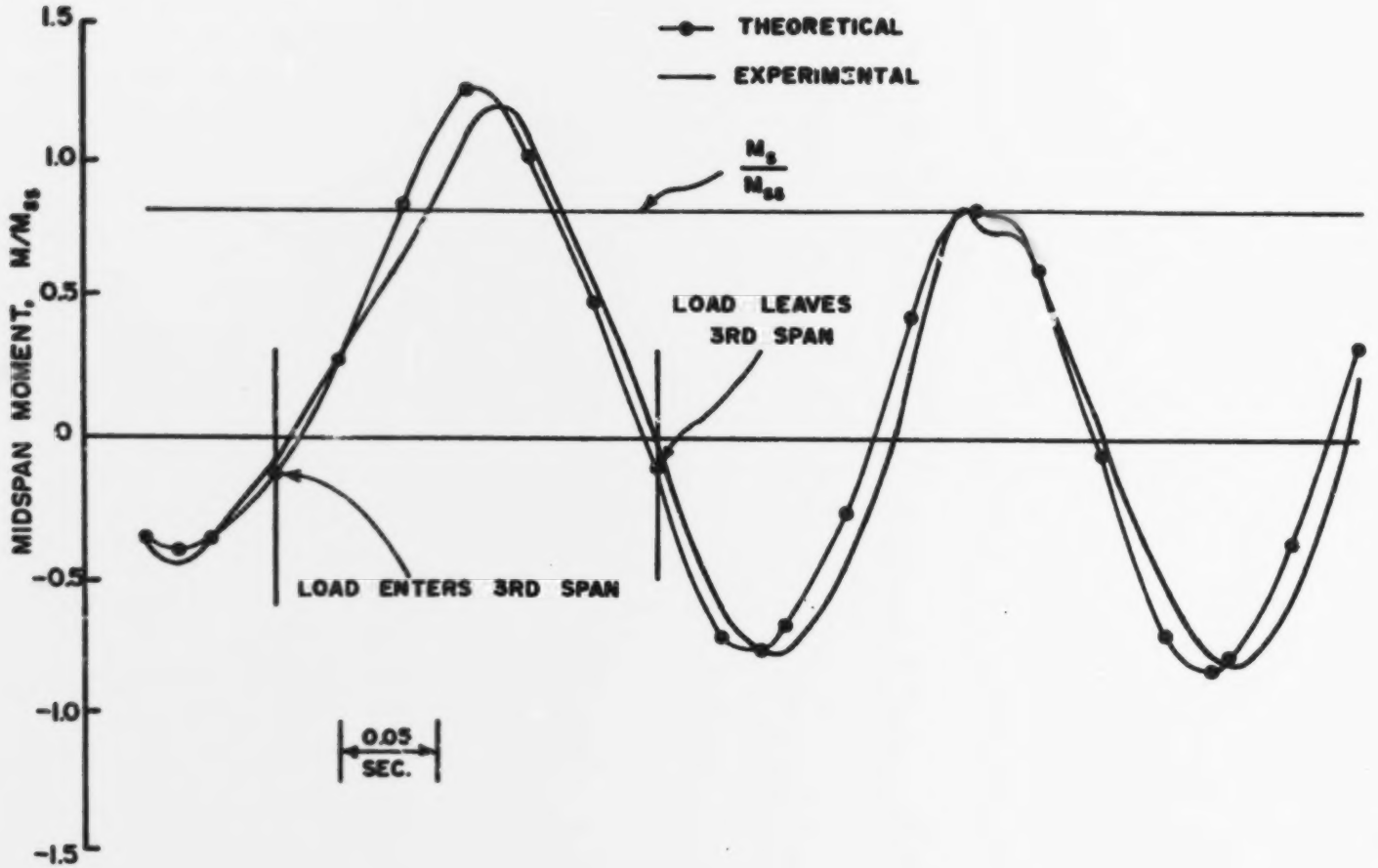


Figure 60. Time histories, predicted and measured, for midspan moment of the exit span: N = 3, K = 3.28, $\omega/p = 0.61$.

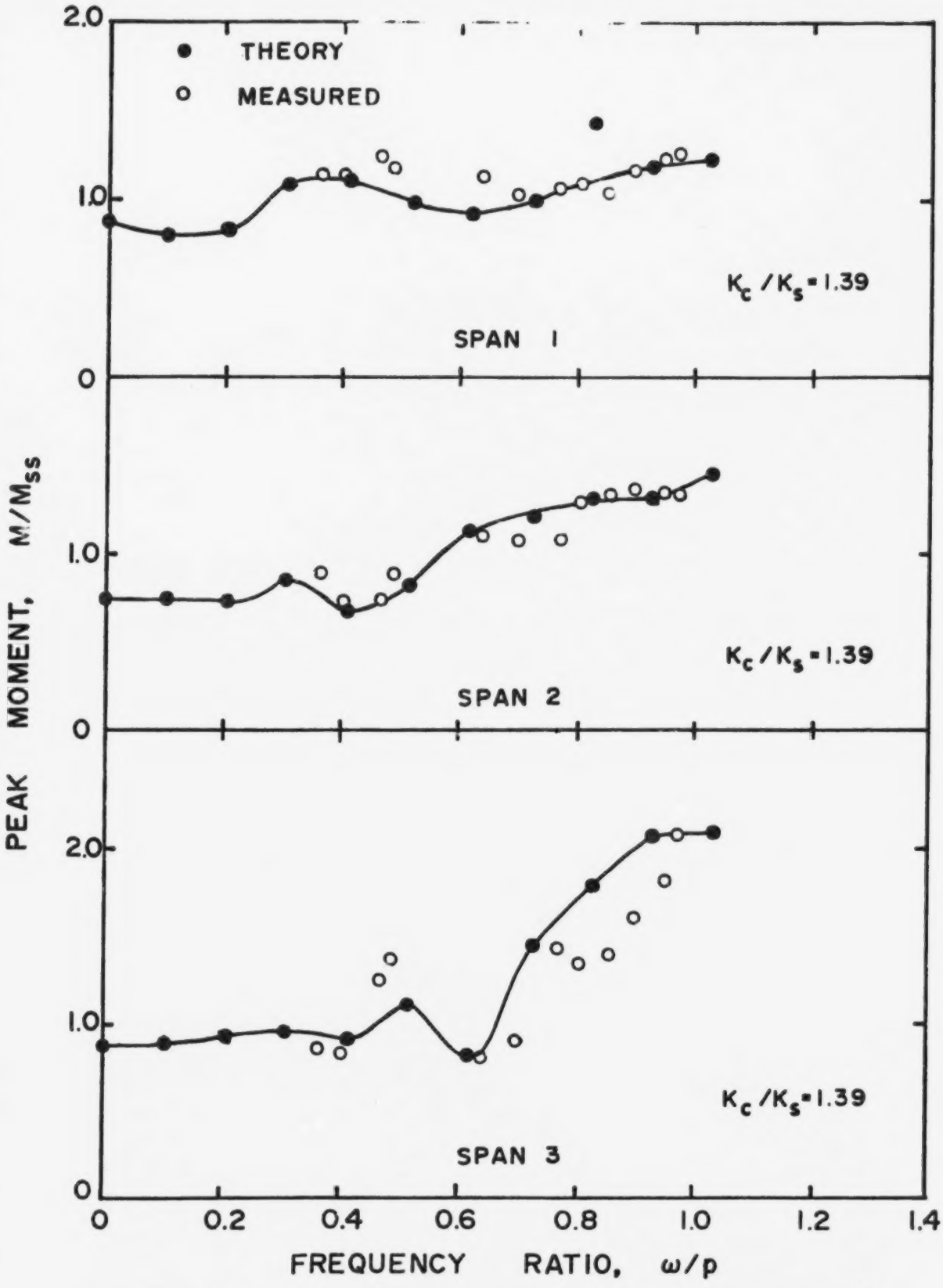


Figure 61. Peak midspan responses for a three-span cable-stayed guideway with a transit point load.

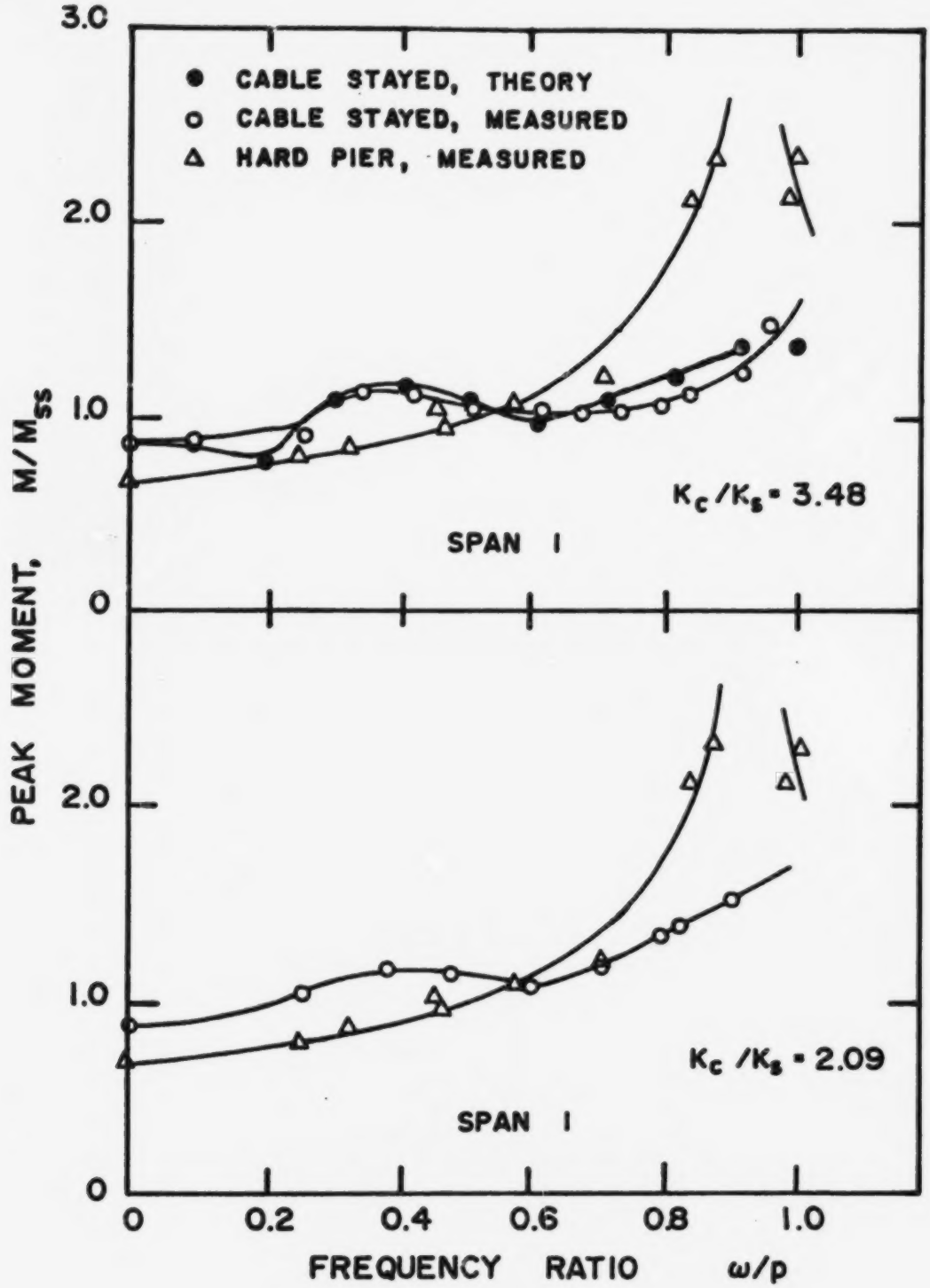


Figure 62. Peak midspan responses for a three-span, cable-stayed guideway with a transit point load: span one.

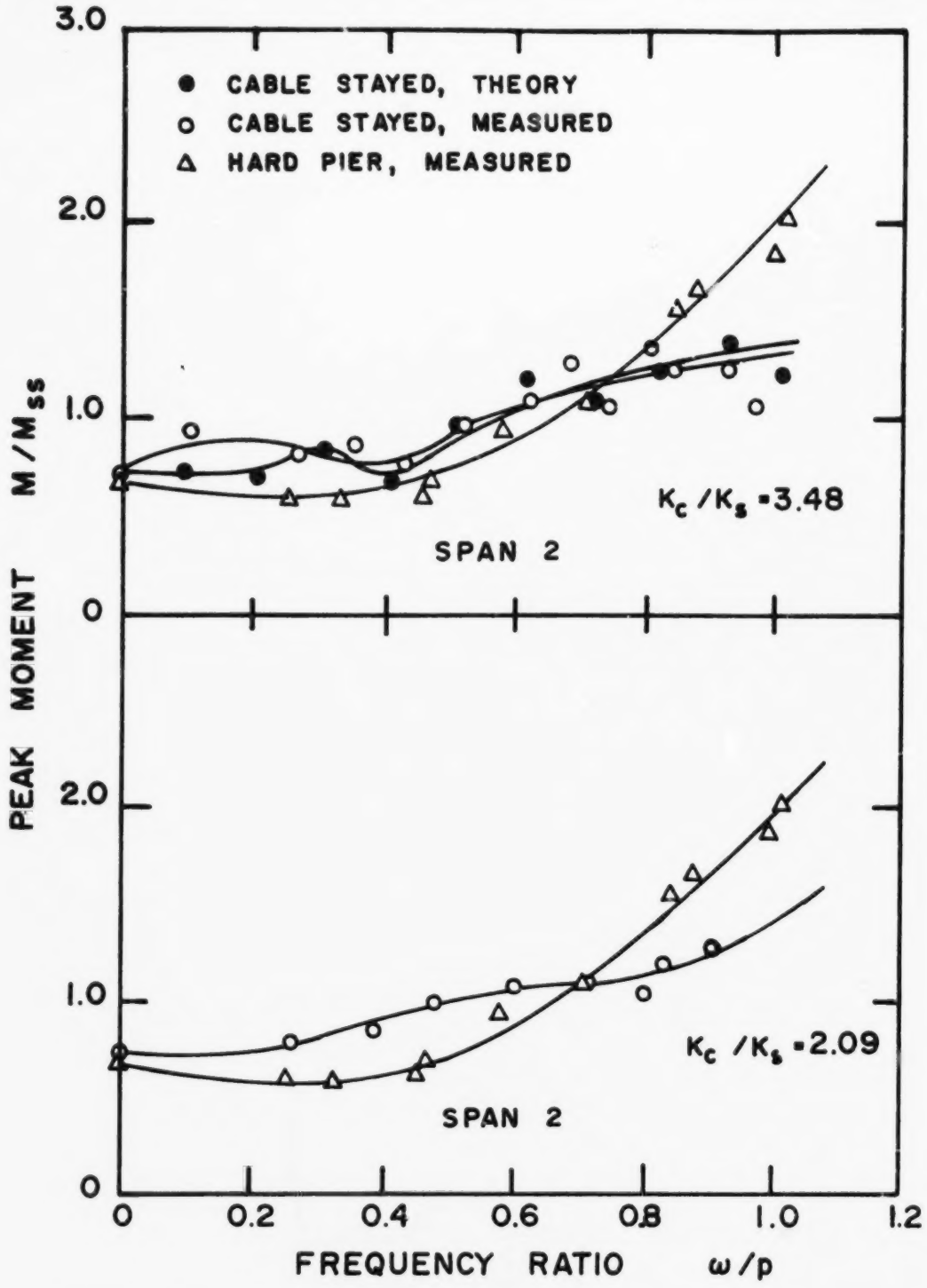


Figure 63. Peak midspan responses for a three-span, cable-stayed guideway with a transit point load: span two.

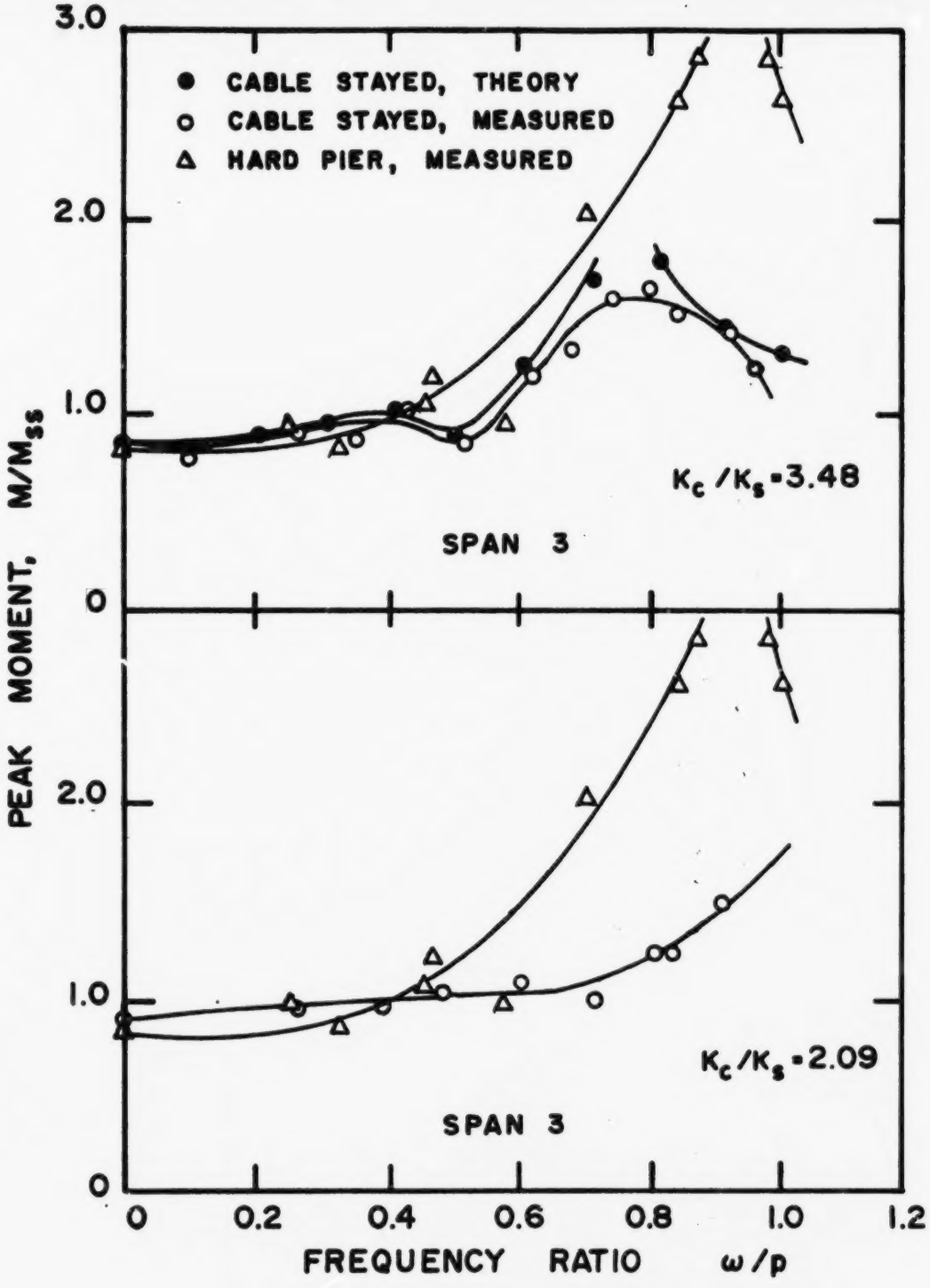


Figure 64. Peak midspan responses for a three-span, cable-stayed guideway with a transit point load: span three.

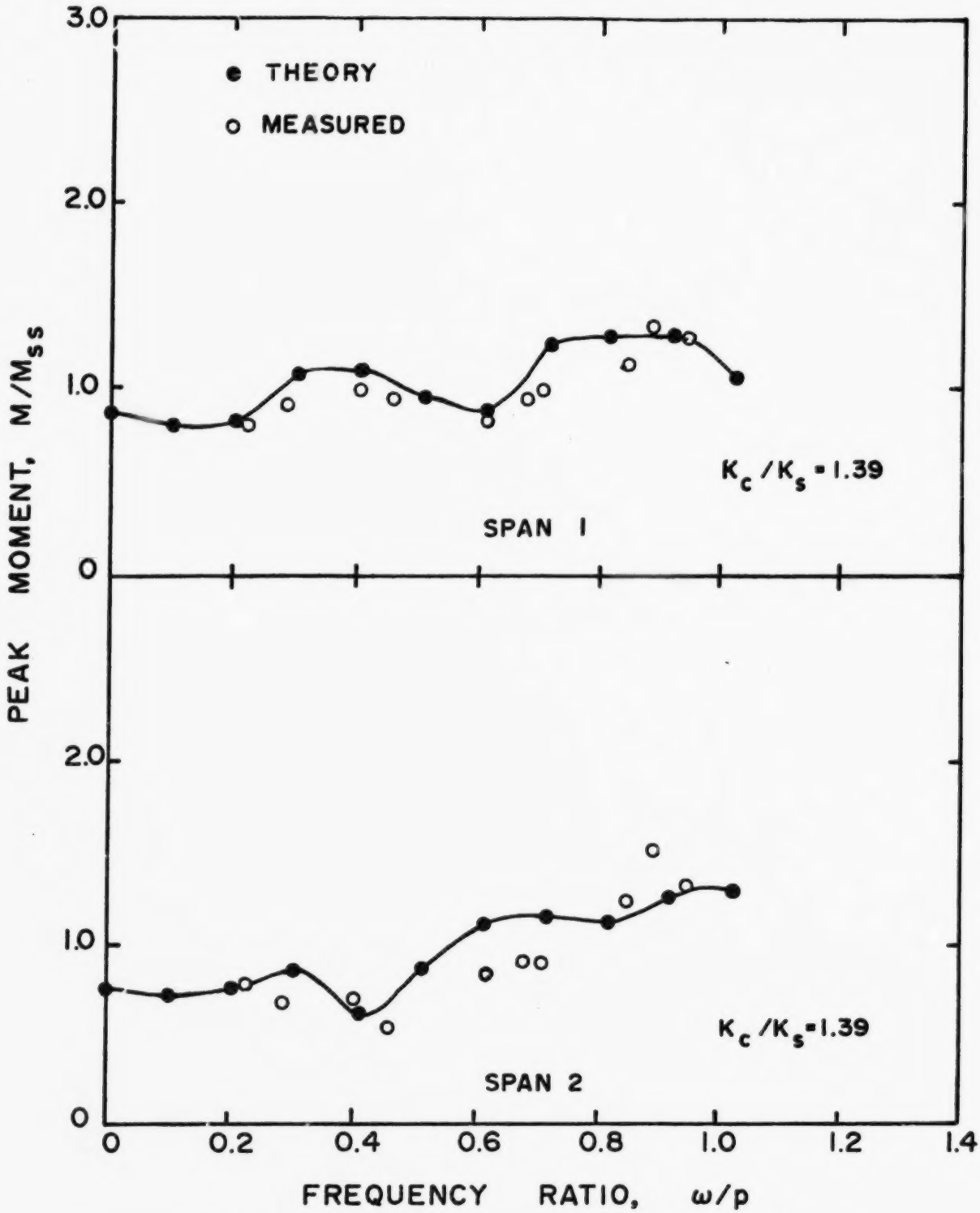


Figure 65. Peak midspan responses for a low stiffness, six-span, cable-stayed guideway with a transit point load: spans one and two.

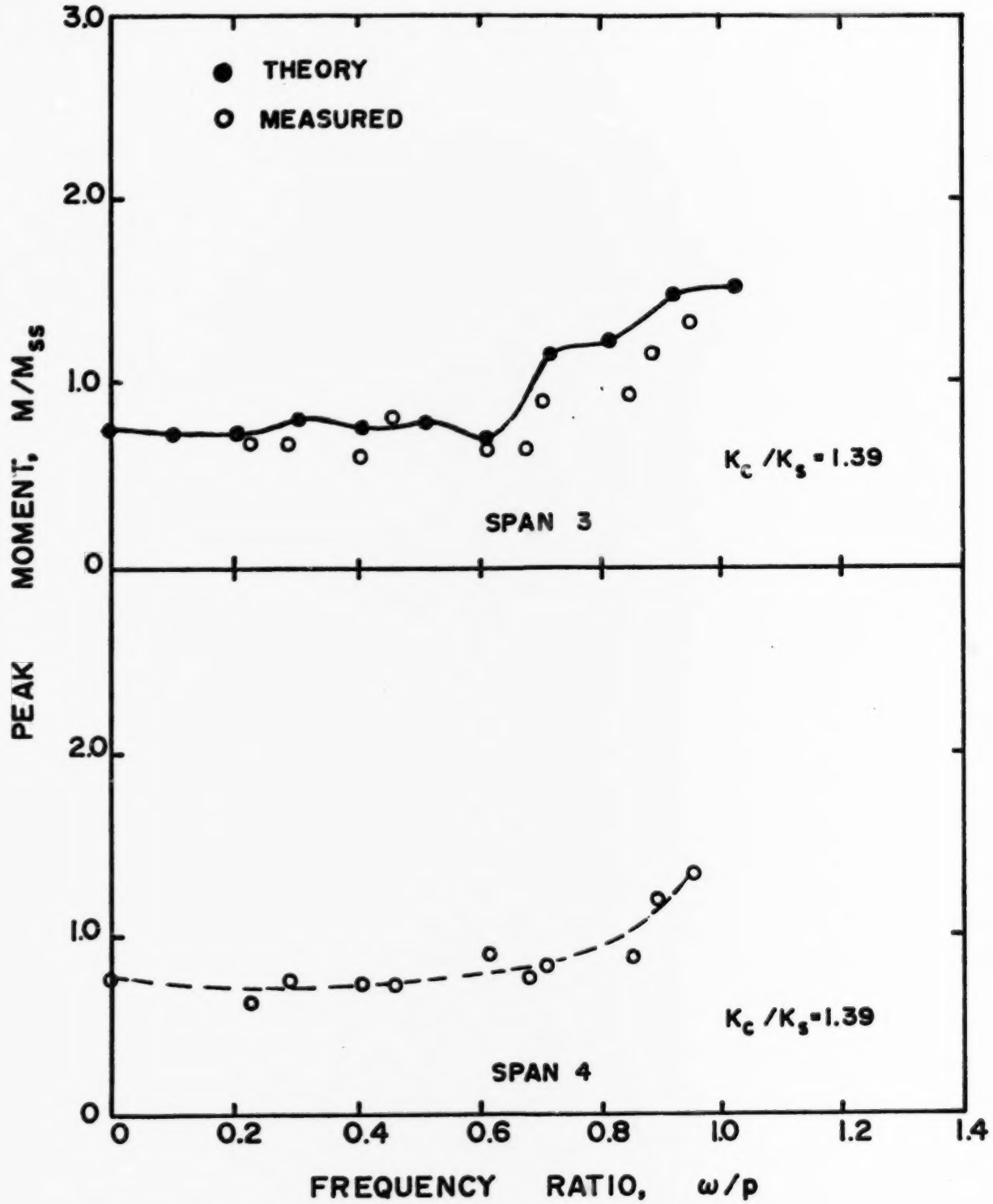


Figure 66. Peak midspan responses for a low stiffness, six-span, cable-stayed guideway with a transit point load: spans three and four.

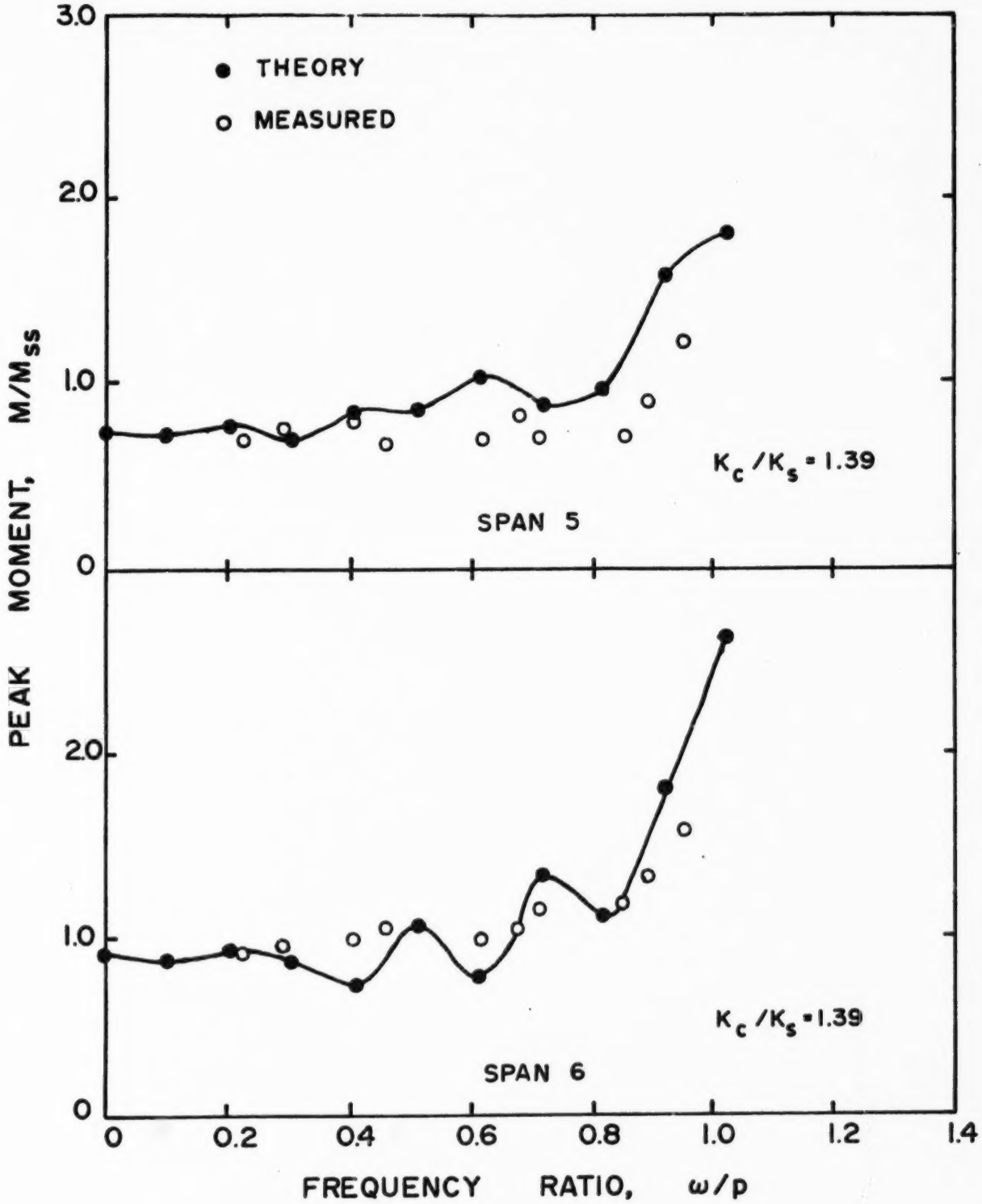


Figure 67. Peak midspan responses for a low stiffness, six-span, cable-stayed guideway with a transit point load: spans five and six.

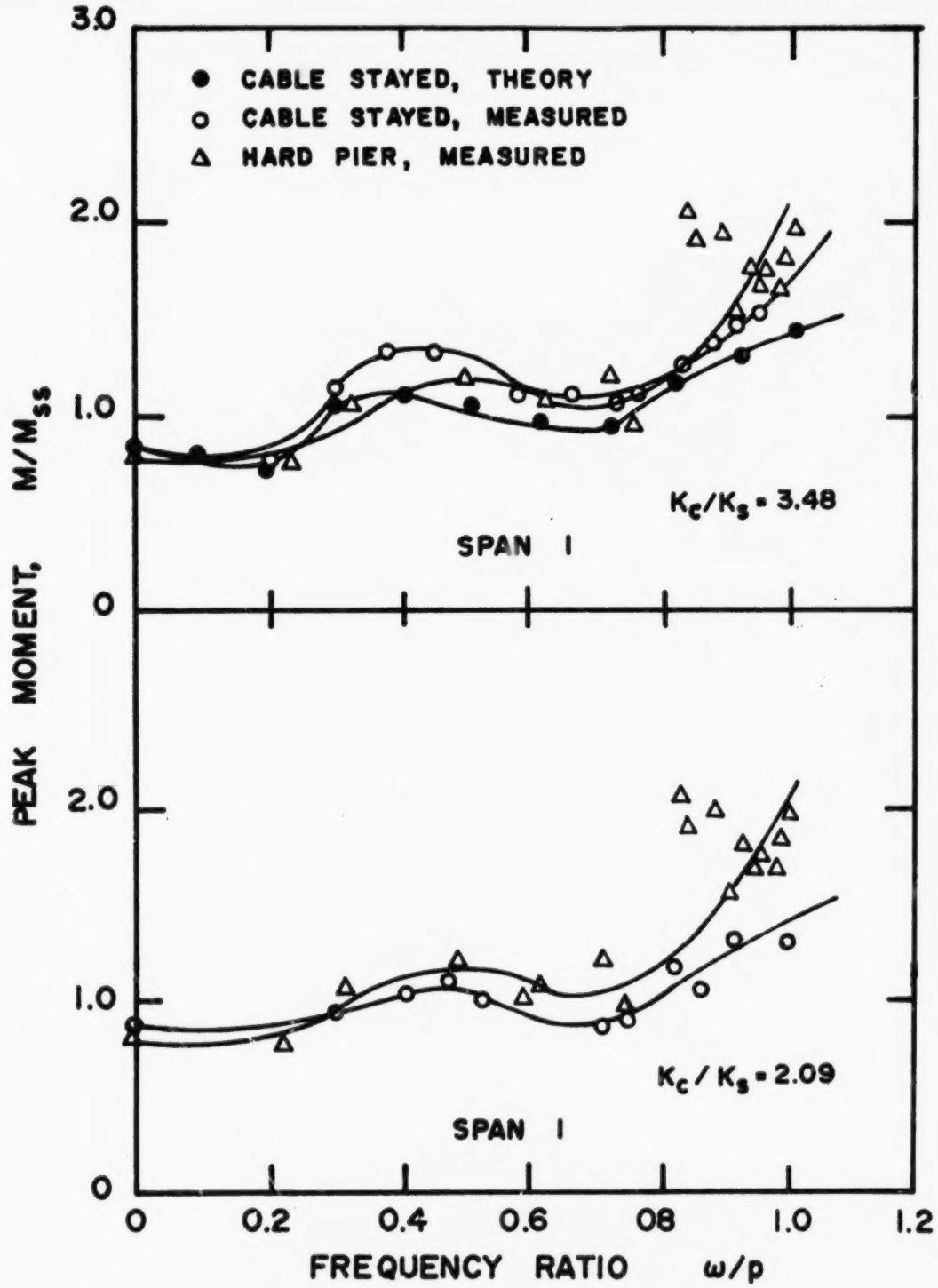


Figure 68. Peak midspan responses for medium stiffness, six-span, cable-stayed guideways with a transit load: span one.

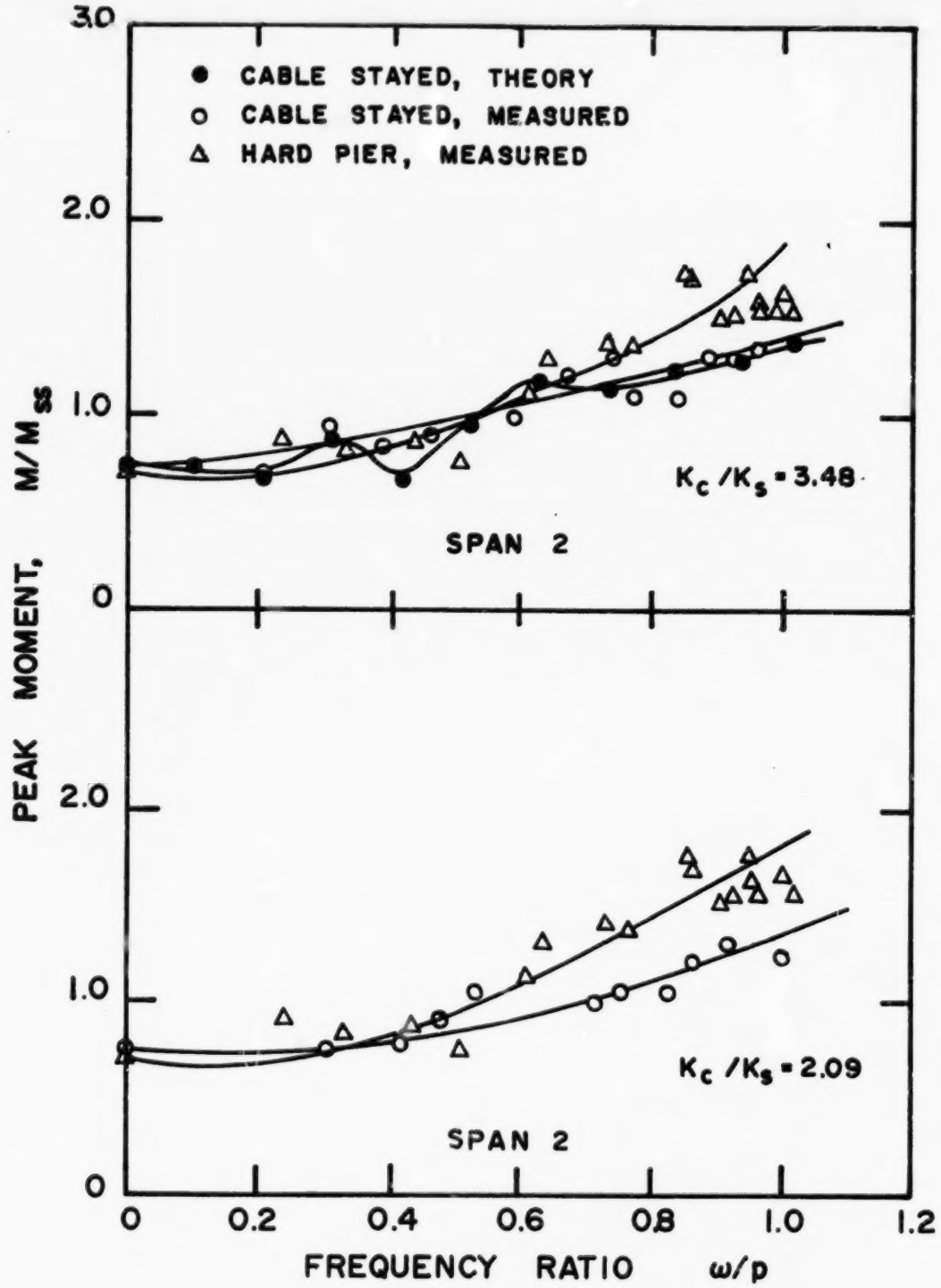


Figure 69. Peak midspan responses for medium stiffness, six-span, cable-stayed guideways with a transit load: span two.

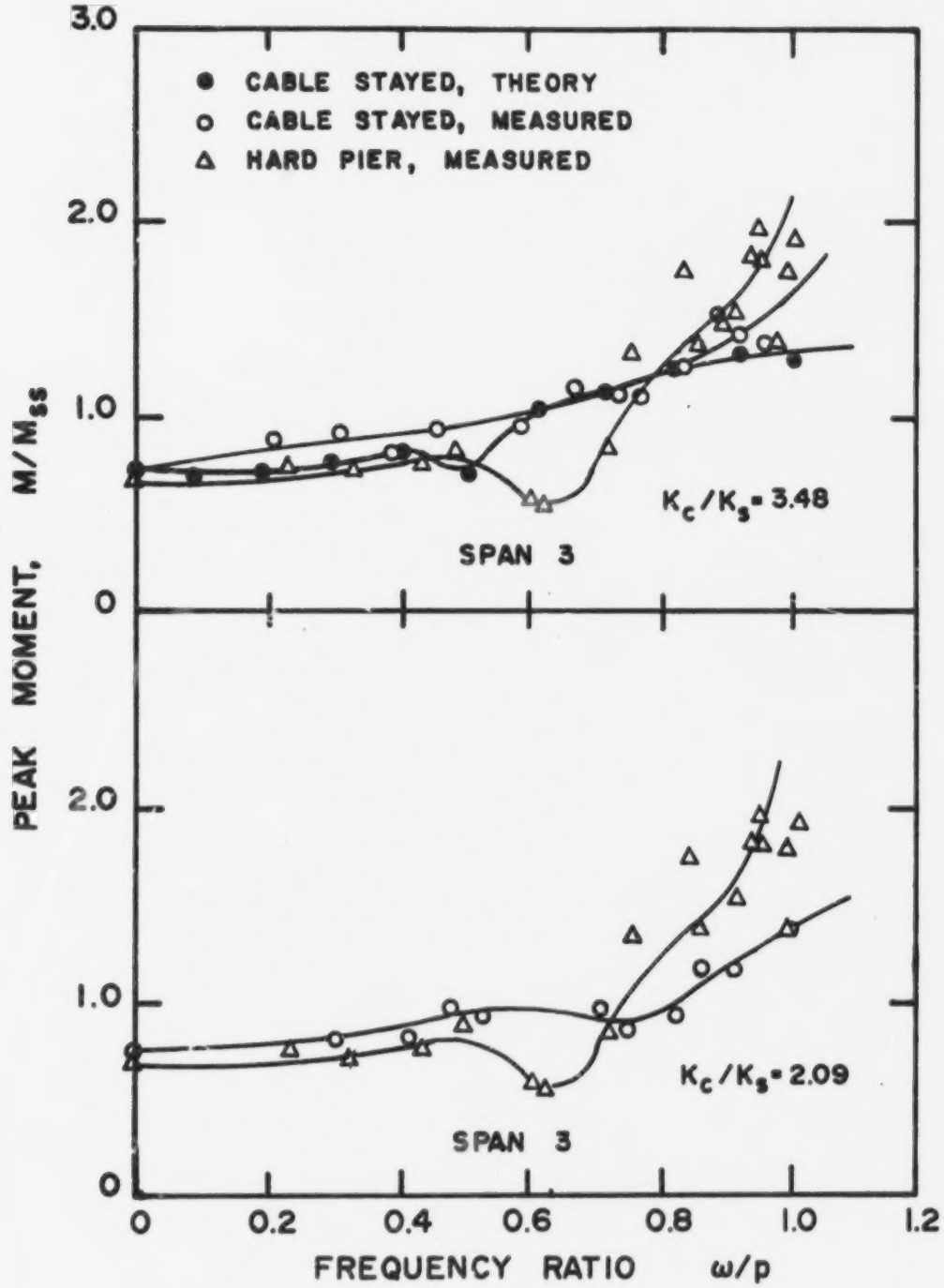


Figure 70. Peak midspan responses for medium stiffness, six-span, cable-stayed guideways with a transit load: span three.

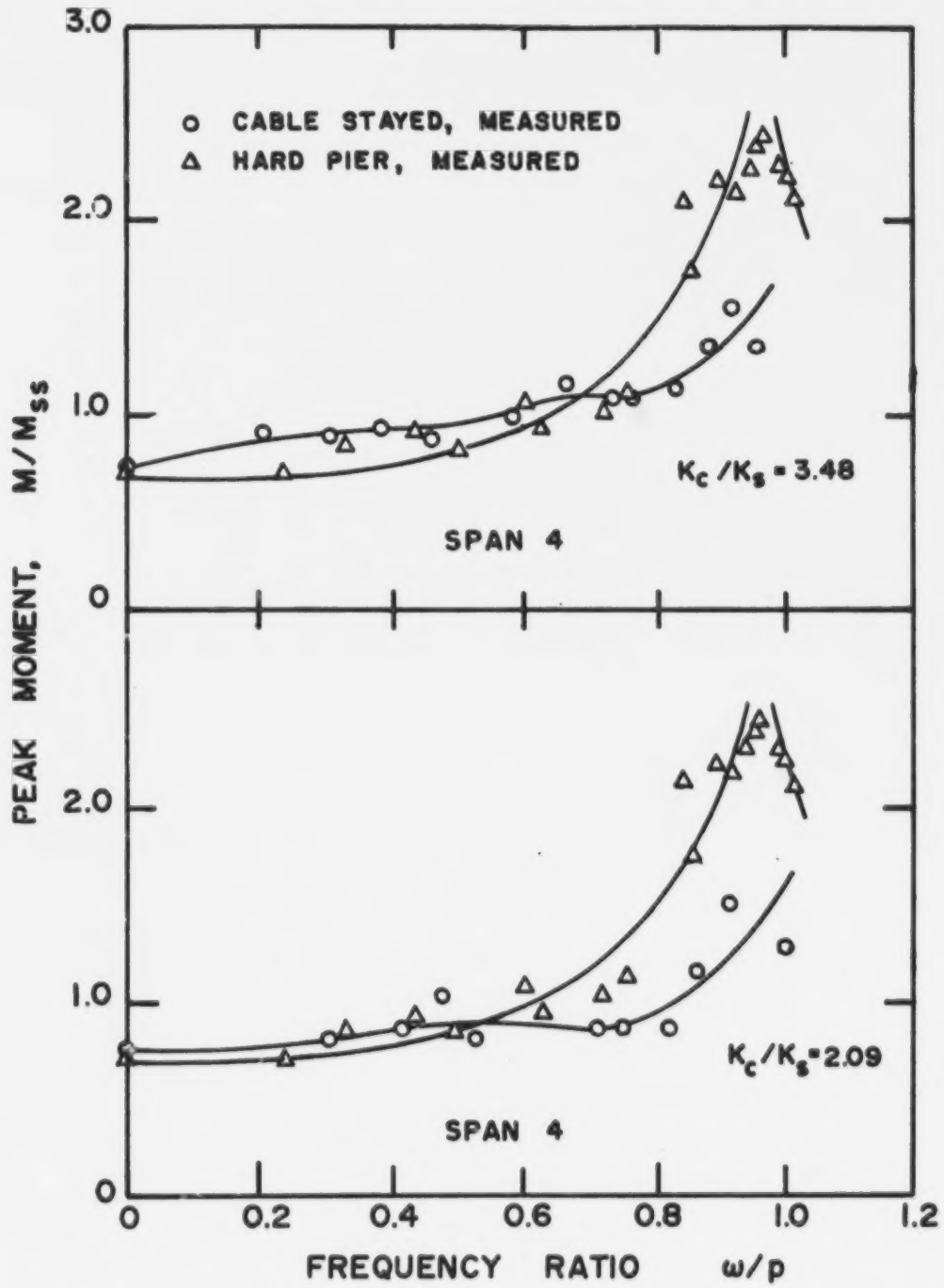


Figure 71. Peak midspan responses for medium stiffness, six-span, cable-stayed guideways with a transit load: span four.

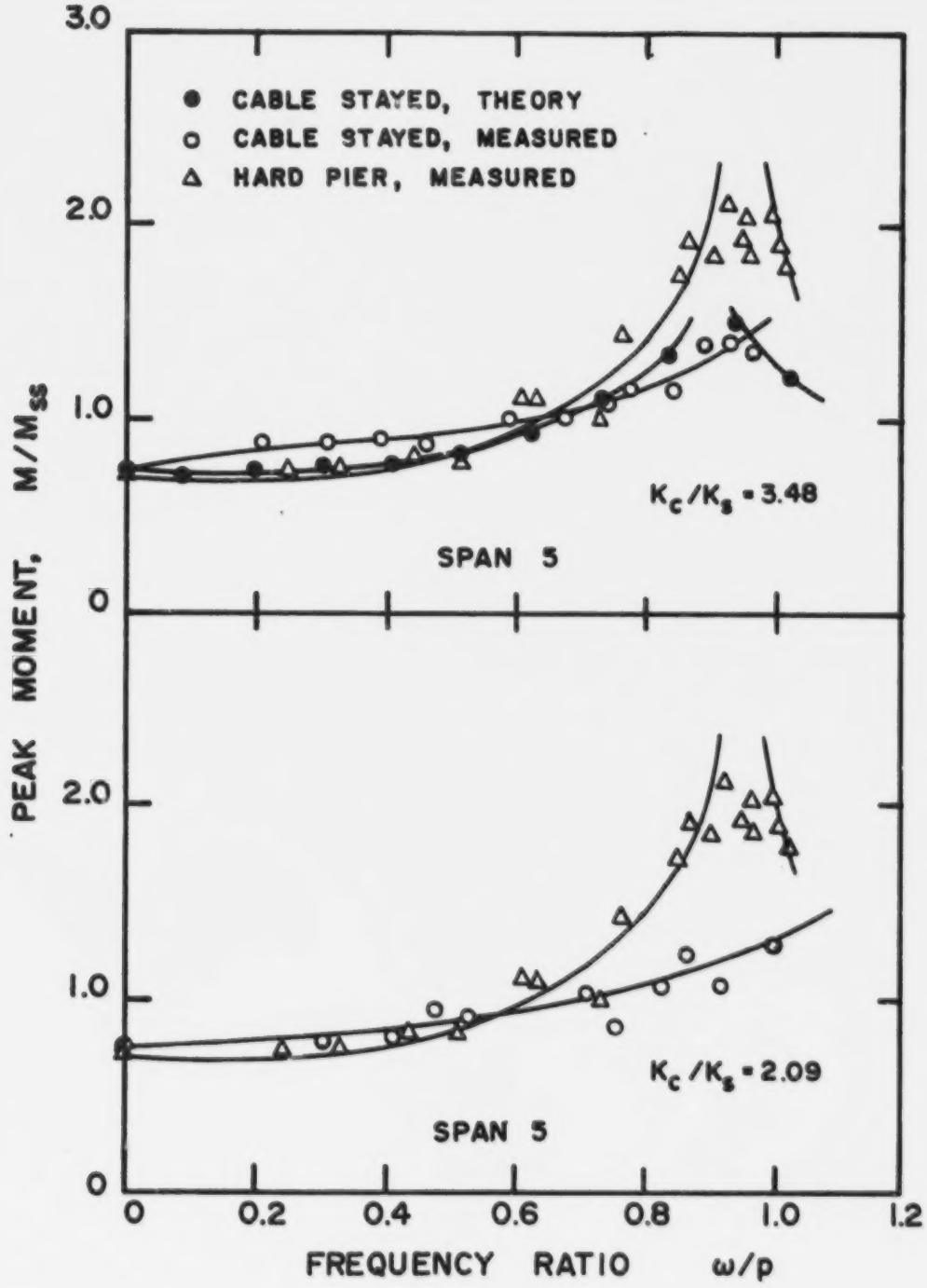


Figure 72. Peak midspan responses for medium stiffness, six-span, cable-stayed guideways with a transit load: span five.

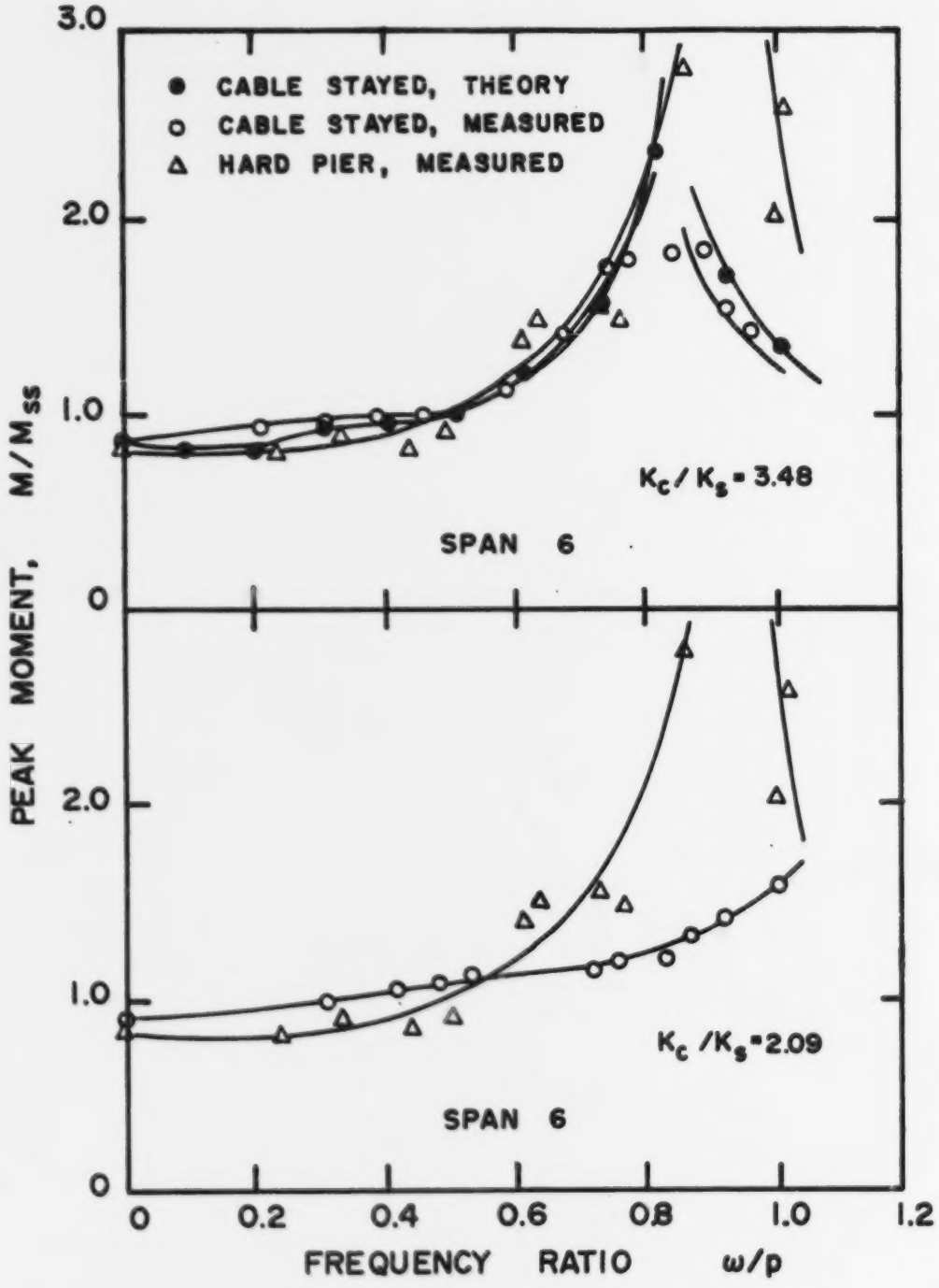


Figure 73. Peak midspan responses for medium stiffness, six-span, cable-stayed guideways with a transit load: span six.

The conclusion of these studies is that the analytical model can predict quite well the dynamic response of cable stayed guideways to transit loads, provided that the total mass of such loads is less than about one-seventh of a single span mass; and that the transit frequency ratio does not exceed 0.8. Further work is needed to optimize cable-stayed configurations, by, for instance, allowing for uneven span lengths and even for unequal cable stiffness, $k_c$. The described analytical procedures and the experimental facility can be employed for such future studies.

## 5. LATERAL RESPONSES OF VEHICLES ON CURVES*

Introduction - As an automated guideway transit (AGT) vehicle traverses a curve, the lateral vehicle motion becomes especially important. A prediction of lateral vehicle acceleration is needed to determine passenger ride quality [18-22]; and vehicle displacements are needed to estimate maintenance requirements for the suspension system [23]. An AGT vehicle model previously studied for its stability on a straight guideway [24], is now studied as it traverses a rigid, statistically rough guideway of constant mean radius R, at a constant forward speed u. Lateral wind loads are also included. The major assumptions for the vehicle-guideway model, shown in Fig. 74, are summarized.

(a) Lateral translation (y), roll ($\phi$) and yaw ($\theta$) comprise the essential vehicle motion during curve traverse. As in previous studies [25], heave and pitch vibrations are supressed or simply uncoupled from the lateral motion.

(b) The passenger compartment and chassis is a single rigid body of mass m, pivoting about point 0, the geometric center of the chassis.

(c) Inertia of the wheel assemblies are insignificant, but their stiffness and damping characteristics are lumped with those of the levitation support system (C, K) and of the lateral support system (c, k).

(d) Vehicle displacements with respect to the reference frame are assumed small so that linearization of all equations of motion is appropriate.

(e) All wheels are on free gimbals.

(f) Guideway roughness ($y_1$, $y_2$, $z_0$) and wind loading ($F_w$) are modelled as purely random Gaussian noise.

Based on the equations of vehicle motion, nondimensional system parameters are identified. Peak lateral accelerations and displacements are then predicted in the statistical sense: rms values of

---

*Statistical calculations were done by D. J. Fromnes [17].

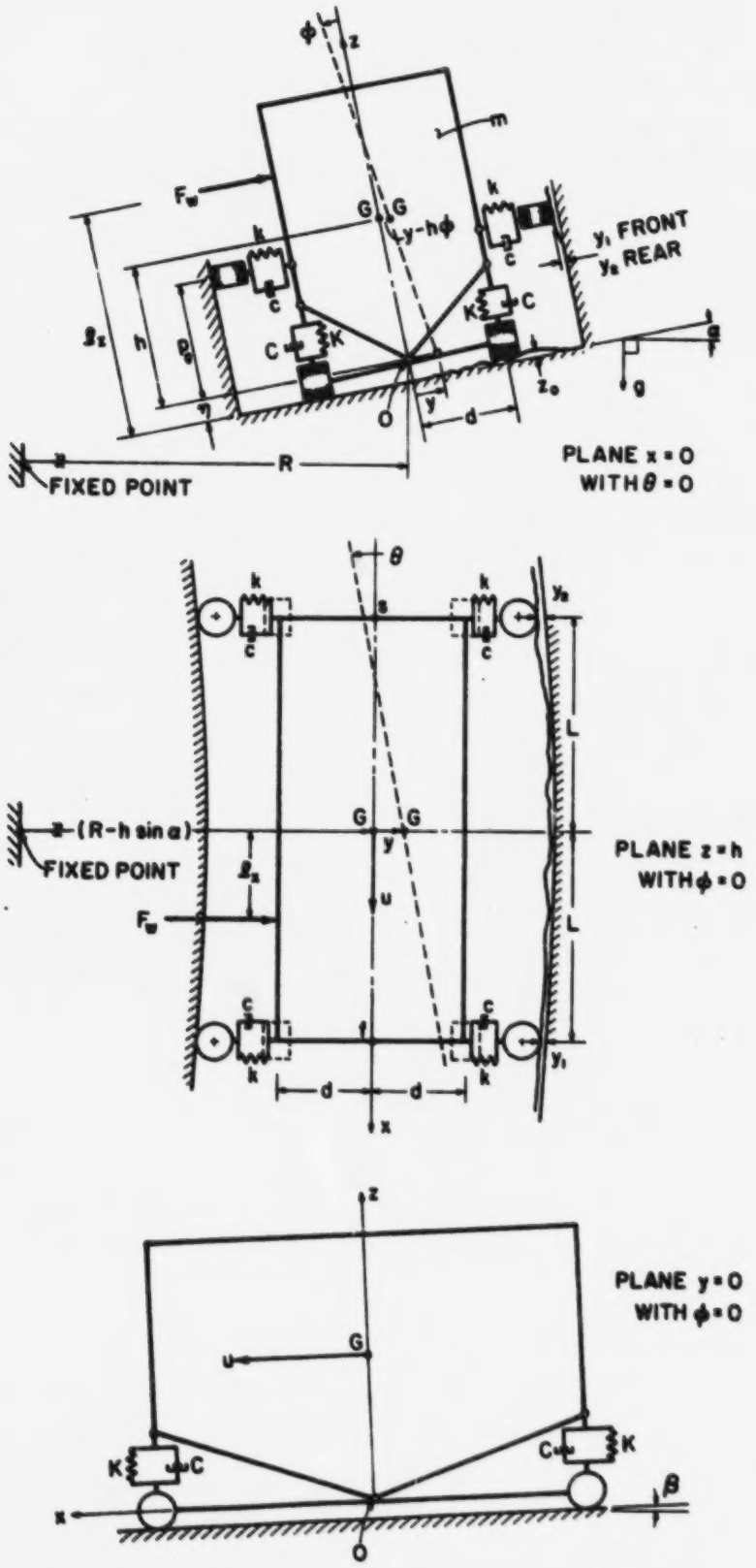


Figure 74. Vehicle model on a curved guideway

acceleration and mean displacements with $\pm 3\sigma$ bounds for the displacements. Results are presented for a base vehicle and for system parameter variations close to this base vehicle. These results, and the accompanying computer program developed to predict such responses, should greatly aid designers of future AGT vehicles.

Equations of Motion - Based on the vehicle-guideway model of Fig. 74, the equations of vehicle motion are derived in Appendix II. The absolute linear and angular velocities of the vehicle are first derived, as well as the absolute acceleration anywhere in the vehicle; then, with the kinetic energy and the generalized forces (conservative and nonconservative), Lagrange's equations are employed to obtain the three Appendix II Eqs. (19-22) in terms of the three generalized coordinates y, $\theta$ and $\phi$. In this derivation, the vehicle experiences instantaneous bank and elevation angles $\alpha = \alpha(t)$, $\beta = \beta(t)$ and possibly time derivatives $\dot{\alpha}$, $\dot{\beta}$, which are predetermined for a given traverse speed on a specified guideway contour. To help insure a comfortable ride, either no change or only gradual changes in the guideway contours at the vehicle design speed are allowed. Thus, $\alpha$, $\beta$, $\dot{\alpha}$ and $\dot{\beta}$ assume a mean, instantaneous value over the entire length of the vehicle, where $\dot{\alpha}$, $\dot{\beta}$ are taken as either zero or constant. Also, the guideway roughness dimensions, $y_1$, $y_2$ and $z_0$, as well as the wind load, $F_w$, act as vehicle input forcing functions. These will be characterized later. Finally, it is noted that Eqs. (19), (20) and (21) are identical to those in Ref. [24] for the special case of this vehicle on a straight, smooth guideway in which $y_1 = y_2 = \dot{y}_1 = \dot{y}_2 = 0$, where $\alpha = \beta = \dot{\alpha} = \dot{\beta} = 0$ and $R \to \infty$.

System Equations and Parameters - The nondimensional system parameters are derived by casting the final equations of Appendix II in nondimensional form. To do this, the following quantities are defined.

The characteristic frequency parameters are:

$$\Omega_1 = (4k/m)^{1/2}; \quad \Omega_3 = (4K/m)^{1/2}$$

$$\Omega_\theta = (4kL^2/I_z)^{1/2} = t_0/t \tag{64}$$

where the last frequency defines the nondimensional time $t_0$ in terms of time t. The vehicle lateral displacement, rotations and their derivatives in nondimensional form, where $(\,)' = d/dt_0$, are defined as

$$\begin{aligned} x_1 &= y/h; \quad & x_2 &= x_1' = \dot{y}/(h\Omega_\theta) \\ x_3 &= \phi \;; \quad & x_4 &= x_3' = \dot{\phi}/\Omega_\theta \\ x_5 &= \theta \;; \quad & x_6 &= x_5' = \dot{\theta}/\Omega_\theta \end{aligned} \tag{65}$$

The nondimensional vehicle input parameters are defined as

$$\begin{aligned} x_7 &= y_1/h; \quad & x_7' &= \dot{y}_1/(h\Omega_\theta) \\ x_8 &= y_2/h; \quad & x_8' &= \dot{y}_2/(h\Omega_\theta) \\ x_9 &= z_0/h; \quad & x_9' &= \dot{z}_0/(h\Omega_\theta) \\ x_{10} &= F_w/(mh\Omega_\theta^2) \end{aligned} \tag{66}$$

The vehicle geometry, wind load location and mass distribution parameters are

$$\begin{aligned} D_0 &= d/h; \quad L_0 = L/h; \quad P_0 = p/h \\ L_x &= \ell_x mh/I_z \;; \quad L_z = \ell_z/h \\ R_o &= R/h \;; \quad R_x = (I_x/m)^{1/2}/h \end{aligned} \tag{67}$$

The vehicle suspension parameters for frequency and damping are

$$\begin{aligned} \bar{\Omega}_1 &= \Omega_1/\Omega_\theta; \quad \bar{\Omega}_3 = \Omega_3/\Omega_\theta \\ \xi_1 &= 2c/(m\Omega_1); \quad \xi_3 = 2C/(m\Omega_3); \quad \xi_\theta = 2L^2c/(I_z\Omega_\theta) \end{aligned} \tag{68}$$

The vehicle speed and pendulum parameters are

$$U = u/(R\Omega_\theta); \quad V = (g \cos\alpha \cos\beta)/(h\Omega_\theta^2) \tag{69}$$

The guideway bank and grade change effects are characterized by

$$\alpha' = \dot{\alpha}/\Omega_\theta \;; \quad \beta' = \dot{\beta}/\Omega_\theta \tag{70}$$

Using the symbols of Eqs. (65-70), Eqs. (19-21) of Appendix II were rewritten and then combined to yield Eqs. (22-24), or the state variable form. That is

$$\underset{\sim}{x}' = \underset{\sim}{A}\,\underset{\sim}{x} + \underset{\sim}{B}\,\underset{\sim}{u} + \underset{\sim}{c} \tag{71}$$

where the state vector is

$$\underset{\sim}{x} = \{x_1\ x_2 \ldots x_{10}\}^T \tag{72}$$

whose elements are given by Eqs. (65) and (66). The matrices $\underset{\sim}{A}$ and $\underset{\sim}{B}$ are taken as constant coefficients where $\alpha' = \beta' = 0$. The input white noise disturbance vector $\underset{\sim}{u} = \underset{\sim}{u}(t_0)$ and the constant matrix $\underset{\sim}{c}$ are fully determined only when the inputs of Eqs. (66) are defined. This is done next.

In dimensional form, the spectral density for guideway roughness as well as for wind loading can be expressed in the general form

$$\phi_i(s) = \gamma_i/(\nu_i^2 - s^2) \tag{73}$$

where $(\gamma_i, \nu_i)$ is the set of empirical constants corresponding to spectra for $z_i = y_1$, $y_2$, $z_0$ and $F_w$, for each i = 7, 8, 9, 10, respectively; and s is the Laplace operator. A stationary Gaussian signal with the spectral density of Eq. (73) can be obtained by passing stationary white noise , w(t), with zero mean through a linear filter expressed by

$$\dot{z}_i(t) = -\nu_i z_i(t) + w_i(t) \tag{74}$$

where

$$E[w_i(t)w_i(\tau)] = \pi\gamma_i\delta(t - \tau) \tag{75}$$

the w(t) vector is expressed in nondimensional form using Eqs. (64-70). Thus

$$\underset{\sim}{u}(t_0) = \{0\ \ 0\ \ 0\ \ 0\ \ 0\ \ 0\ \ u_7\ \ u_8\ \ u_9\ \ u_{10}\}^T \tag{76}$$

where

$$u_i(t_0) = w_i(t)/(h\Omega_\theta) \qquad \text{for } i = 7, 8, 9$$

$$= w_i(t)/(mh\Omega_\theta^3) \qquad \text{for } i = 10$$

Likewise, the nondimensional forms of Eqs. (73) - (75) are, respectively

$$\phi_i(s_0) = \frac{\bar{\gamma}_i}{\bar{\nu}_i^2 - s_0^2} \tag{77}$$

$$x_i'(t_0) = -\bar{\nu}_i x_i(t_0) + u_i(t_0) \tag{78}$$

$$E[u_i(t_0)u_i(\tau_0)] = q_{ii}\delta(t_0 - \tau_0) \tag{79}$$

where $t_0 = t\Omega_\theta$, $\tau_0 = \tau\Omega_\theta$ and $s_0 = s/\Omega_\theta$ and

$$\begin{aligned} \bar{\gamma}_i &= \frac{2}{\pi}\left(\frac{A}{R}\right)U \quad ; \ \bar{\nu}_i = \omega_1/\Omega_\theta \quad \text{for } i = 7, 8, 9 \\ \bar{\gamma}_i &= \frac{\bar{\beta}\nu}{(mh)^2\Omega_\theta^5} \ ; \ \bar{\nu}_i = \nu/\Omega_\theta \quad \text{for } i = 10 \end{aligned} \tag{80}$$

The loading intensities are given by

$$\begin{aligned} q_{ii} &= 2\left(\frac{A}{R}\right)\left(\frac{R}{h}\right)^2 U \quad \text{for } i = 7, 8, 9 \\ q_{ii} &= 2\pi\bar{\gamma}_i \quad \text{for } i = 10 \end{aligned} \tag{81}$$

The spectral constants for guideway roughness, A and $\omega_1$, as well as those for wind loading, $\bar{\beta}$ and $\nu$, will be discussed presently. Further, the restriction that $y_1(t)$ and $y_2(t)$ are correlated by the time lag 2L/u (see Eq. (16) of Appendix II), then it follows that

$$u_7(t_0) = u_8[t_0 + 2L_0/(UR_0)] \tag{82}$$

It is seen that Eq. (78) provides the needed inputs $x_7'$, $x_8'$ and $x_9'$ for the state equations (22-24) of the Appendix II; and that the last state equation is given for wind loading by Eq. (78) where i = 10.

In summary, then, the ten first order linear differential equations for vehicle behavior are given explictly by Eqs. (65) for $x_1' = x_2$, $x_3' = x_4$ and $x_5' = x_6$; by Eqs. (22-24) of Appendix II for $x_2'$, $x_4'$ and $x_6'$; and by Eqs. (78) for $x_7'$ through $x_{10}'$. This leads to the coefficient matrices $\underset{\sim}{A}$, $\underset{\sim}{B}$ and $\underset{\sim}{C}$ of Eq. (71). Finally, forms for lateral acceleration, $a_y^*$, and lateral deflections at the guidewheels, $\rho_y^*$, are given by Eqs. (25) and (26) of Appendix II. By defining the system parameters of Eqs. (67-70) and the spectral

constants of Eqs. (80) and (81), the ten equations represented by Eq. (71) can be solved in a statistical sense to yield a measure of $a_y^*$ and $\rho_y^*$. The theoretical basis for calculating these responses is presented next.

Response Statistics - With the ten state variable equations established, the mean values of the variables, denoted by an overbar, and the covariance matrix, $\underset{\sim}{X}$ are calculated following established methods [26-28]. The development is limited to steady-state solutions in which the bank and grade angles are constant, or $\alpha' = \beta' = 0$; and $\underset{\sim}{X}' = 0$. The equation for the means of the states is

$$\bar{\underset{\sim}{x}}' = \underset{\sim}{A}\,\bar{\underset{\sim}{x}} + \underset{\sim}{B}\,\bar{\underset{\sim}{u}} + \underset{\sim}{c} \tag{83}$$

where, for steady-state and $\bar{\underset{\sim}{x}}(0) = 0$, the solution for the mean is [29]

$$\bar{\underset{\sim}{x}} = -\,(\underset{\sim}{A}^2)^{-1}\,\underset{\sim}{A}\,(\underset{\sim}{B}\,\bar{\underset{\sim}{u}} + \underset{\sim}{c}) \tag{84}$$

The steady-state covariance equation is given by [30]

$$\underset{\sim}{X}' = \underset{\sim}{A}\,\underset{\sim}{X} + \underset{\sim}{X}\,\underset{\sim}{A}^T + \underset{\sim}{R} = \underset{\sim}{0} \tag{85}$$

where

$$\underset{\sim}{R} = \underset{\sim}{B}\,\underset{\sim}{Q}\,\underset{\sim}{B}^T + q_{ii}[b_j\ b_i^T\ \underset{\sim}{\varphi}^T(d_{ij}) + \underset{\sim}{\varphi}(d_{ij})b_i\ b_j^T]$$

$\underset{\sim}{\varphi}(t_0) = \exp(\underset{\sim}{A}\ t_0)$ = state transition matrix

$b_i, b_j$ = the ith and jth columns of $\underset{\sim}{B}$

$\underset{\sim}{Q}$ = covariance matrix of inputs

$q_{ii}$ = variance of the ith input $u_i(t_0)$

Since time correlated inputs are included, Eq. (77) is generalized as

$$u_i = u_j(t_0 + d_{ij}) \tag{86}$$

where the only nonzero value of $d_{ij}$ is $d_{7,8} = 2L_0/(UR_0)$ from Eq. (82).

Solutions X of Eq. (85) are used to calculate the statistical responses corresponding to $a_y^*$ and $\rho_y^*$. It is observed that these responses can be expressed in the general forms

$$\underset{\sim}{a}^* = \{a_x^*\ a_y^*\ a_z^*\}^T = \underset{\sim}{A}_a\,\underset{\sim}{x}_e + \underset{\sim}{c}_a \tag{87}$$

$$\underset{\sim}{\rho}^* = \{\rho_x^*\ \rho_y^*\ \rho_z^*\}^T = \underset{\sim}{A}_\rho\,\underset{\sim}{x}_e \tag{88}$$

where $\underset{\sim}{A}_a$, $\underset{\sim}{A}_\rho$ and $\underset{\sim}{c}_a$ are matrices of constants derived from nondimensional forms of Eqs. (5) and (6), derived for these studies from Eqs. (25) and (26) of Appendix II. Here, the extended state vector is given by

$$\underset{\sim}{x}_e = \{x_1 \quad x_2 \quad x_2' \quad x_3 \quad x_4 \quad x_4' \quad x_5 \quad x_6 \quad x_6'\}^T \tag{89}$$

Since rms acceleration and mean guidewheel displacements (as measured from static equilibrium) are needed, variances and means of states are computed. The means are computed from Eq. (84), where

$$\bar{\underset{\sim}{x}}_e = \{\bar{x}_1 \quad \bar{x}_2 \quad \bar{x}_2' \quad \bar{x}_3 \quad \bar{x}_4 \quad \bar{x}_4' \quad \bar{x}_5 \quad \bar{x}_6 \quad \bar{x}_6'\}^T \tag{90}$$

The covariances X are solutions of Eq. (85), and the technique for obtaining such solutions will be outlined presently. The covariance of $x_e$ is defined by

$$\begin{aligned}\sigma^2_{x_e} = {} & [\underset{\sim}{C} \vdots \underset{\sim}{D}] \begin{bmatrix} \underset{\sim}{X} & \underset{\sim}{A}^{-1} \underset{\sim}{B} \underset{\sim}{Q} \\ (\underset{\sim}{A}^{-1} \underset{\sim}{B} \underset{\sim}{Q})^T & \underset{\sim}{Q} \end{bmatrix} [\underset{\sim}{C} \vdots \underset{\sim}{D}]^T + \underset{\sim}{c}_a \underset{\sim}{c}_a^T \\ & + [\underset{\sim}{C} \vdots \underset{\sim}{D}] \begin{bmatrix} \bar{\underset{\sim}{x}} \\ \hline \bar{\underset{\sim}{u}} \end{bmatrix} \underset{\sim}{c}_a^T + \underset{\sim}{c}_a \begin{bmatrix} \bar{\underset{\sim}{x}} \\ \hline \bar{\underset{\sim}{u}} \end{bmatrix} [\underset{\sim}{C} \vdots \underset{\sim}{D}]^T \end{aligned} \tag{91}$$

Here, the partitioned (9 x 14) array $[\underset{\sim}{C} \vdots \underset{\sim}{D}]$ and the (9 x 1) vector $\underset{\sim}{c}_a$ are given in Appendix II. The mean-square components of $\underset{\sim}{x}_e$ are given by

$$\bar{\sigma}^2_{x_{eij}} = \sigma^2_{x_{eij}} + \bar{x}_{e_i} \bar{x}_{e_j} \tag{92}$$

Then, with Eqs. (87) - (91), the covariances of acceleration and displacement become, respectively

$$\sigma^2_{a*} = \underset{\sim}{A}_a \bar{\underset{\sim}{\sigma}}^2_{x_e} \underset{\sim}{A}_a^T + \underset{\sim}{A}_a \bar{\underset{\sim}{x}}_e \underset{\sim}{c}_a^T + \underset{\sim}{c}_a \bar{\underset{\sim}{x}}_e^T \underset{\sim}{A}_a^T + \underset{\sim}{c}_a \underset{\sim}{c}_a^T \tag{93}$$

$$\underset{\sim}{\sigma}^2_{\rho*} = \underset{\sim}{A}_\rho \bar{\underset{\sim}{\sigma}}^2_{x_e} \underset{\sim}{A}_\rho^T \tag{94}$$

For stationary inputs, the rms values of acceleration are the square root of the diagonals of $\underset{\sim}{\sigma}^2_{a*}$, Eq. (93). The square of the standard

deviation of deflections are the diagonal elements of $\underset{\sim}{\sigma}^2_{\rho^*}$, Eq. (89). Finally, the mean deflections of the suspension system are given by

$$\bar{\underset{\sim}{\rho}}^* = \underset{\sim}{A}_\rho \bar{\underset{\sim}{x}}_e \tag{95}$$

This completes the theory for computing the response statistics. Of course, the covariance matrix, $\underset{\sim}{X}$, the solution to Eq. (85), is still needed. The method used to solve this equation is discussed next.

Solution for Covariance - There are several algorithms available for solving Eq. (85), the steady-state covariance propagation equation [31,32]. The algorithm used here produces a truncated infinite series approximation, where convergence criteria have been established [33]. However, a difference exists between a practical convergence criterion and the analytical prediction. While [33] gives the criterion with the provision that $\underset{\sim}{A}$ is Hurwitzian when $\underset{\sim}{R}$ is positive definite, experimentation with the procedure has shown that, to ensure convergence, the numerical value of the arbitrary scalar parameter q in the following recursion formula must be two and one-half times greater the largest real part of any eigenvalue.

The matrix series for $\underset{\sim}{X}$ is generated by the recursion formula

$$\underset{\sim}{X}_{n+1} = \underset{\sim}{x}_n + \underset{\sim}{V}^{2n} \underset{\sim}{X}_n (\underset{\sim}{V}^{2n})^T \tag{96}$$

where

$$\begin{aligned} \underset{\sim}{X}_1 &= \underset{\sim}{W} + \underset{\sim}{V}\,\underset{\sim}{W}\,\underset{\sim}{V}^T \\ \underset{\sim}{W} &= 2q\underset{\sim}{U}\,\underset{\sim}{R}\,\underset{\sim}{U}^T \\ \underset{\sim}{V} &= \underset{\sim}{U}(q\underset{\sim}{I} + \underset{\sim}{A}) \\ \underset{\sim}{U} &= (q\underset{\sim}{I} - \underset{\sim}{A})^{-1} \end{aligned} \tag{97}$$

Generation of successive terms in the series is aborted when the relative change of partial sums becomes sufficiently small. Accuracy of the final solution is checked by computing the residual, given by

$$\hat{\underset{\sim}{R}} = \underset{\sim}{X}_{n+1}\,\underset{\sim}{A}^T + \underset{\sim}{A}\,\underset{\sim}{X}_{n+1} + \underset{\sim}{R} \tag{98}$$

If each element of $\hat{\underset{\sim}{R}}$ has an absolute magnitude which implies a relative error of less than 5 percent, the result is considered satisfactory. Further improvements can be made [32], but were found to

be unnecessary since, for the appropriate q parameter, this series solves Eq. (85) to within one percent for systems of order up to 149.

The numerical procedure has been implemented in Fortran IV for execution in WATFIV or G-Level on an IBM 370 model 165. The source program consists of a main program and subroutines which perform the matrix operations. The package is completely self-contained. It includes subroutines for addition, subtraction and transposition as well as procedures to do a truncated power series estimate of state transition matrices, raise matrices to integer powers and matrix inversion. It takes approximately 52 seconds of computer time to execute the present tenth order vehicle system. The input structure, sample input data and program printout are in Appendix III .

Other vehicle-guideway models can be examined by altering the subroutine state which generates the matrices A, B and R. Also, the last part of the main program, dealing with kinematics, may need revision if a different coordinate system is used.

Range of Parameters - For this vehicle-guideway model, there are 27 nondimensional system input parameters which are needed to calculate the responses. The first 16 are identified by Eqs. (67)-(70); and the following 8 are the statistical parameters $\bar{\gamma}_i$ and $\bar{\nu}_i$, Eqs. (80), $i = 7,8,9,10$; the last three are the coordinates $\bar{\rho}_i = \rho_i/h$, Appendix II.

The range of vehicle characteristics were established through Refs. [35,36]. For instance, the physical properties of extant and future transit vehicles are listed in Tables 6 and 7, respectively. The uncoupled frequencies $\Omega_1$, $\Omega_3$ and $\Omega_\theta$ for these latter AGT vehicles are in the range of 1 to 2 hz and their damping ratios $\xi_1$, $\xi_3$ and $\xi_\theta$ are generally in the range of 0.2 to 0.3. Further vehicle characteristics (see Fig. 74) are: $2L$ = 6 to 20 ft; $2d$ = 4 to 6 ft; $h$ = 1 to 3 ft; $p_o$ = 1 to 3 ft; $m$ = 400 to 7000 lb-sec$^2$/ft; $u$ = 20 to 88 ft/sec. Also, the radius of gyration $(I_x/m)^{1/2}$ must be less than $d$, the longest dimension of the planar projection of the vehicle. In addition, the locations of the center of the wind load $(\ell_x, \ell_z)$, which depend to a great extent on the vehicle shape, are in the ranges $-L < \ell_x < L$ and $0 < \ell_z < 2h$. Finally, ranges of $\bar{\rho}_i$ are in Table 8.

For the guideway, the nonstatistical characteristics are the nominal values of the radius of curvature, the grade angle, the bank

Table 6

Extant PRT Systems [34]

| System | Capacity (Seats)/ wt.(lbs) | Length (ft) | Width (ft) | Height (ft) | Weight Empty (lbs) |
|---|---|---|---|---|---|
| CABTRACK (U.K.) | 4/640 | 9.84 | 4.92 | 5.58 | 1320 |
| AEROSPACE (USA) | 6/960 | 9.84 | 5.91 | 5.58 | 2400 |
| CABINTAXI (Germany) | 2/320 | 6.56 | 5.25 | 5.25 | 1540 |
| CONTROLLED VEHICLE SYSTEMS (Japan) | 4/640 | 10.83 | 5.25 | 5.25 | 2160 |
| ARAMIS (France) | 4/640 | 7.55 | 4.27 | 4.27 | 1430 |
| MORGANTOWN (USA) | 8/1280 | 15.42 | 5.91 | 5.91 | 8660 |

Table 7

AGT Vehicle Characteristics [35]

| | PRT | Small GRT | Large GRT |
|---|---|---|---|
| Number of Passengers | 4 | 6 | 12 |
| Wheel Base (ft) | 6 | 10 | 20 |
| Track Width (ft) | 3.6 | 5.4 | 6.7 |
| Empty Mass (lbs) | 2000 | 4750 | 8000 |
| Gross Mass (lbs.) | 2780 | 6000 | 10,700 |
| Speed (f/s) | 44-88 | 44-88 | 44-88 |
| (mph) | 30-60 | 30-60 | 30-60 |

angle and the time rate of change of these latter two at a given vehicle speed. Here, R = 2400 ft is chosen to give a lateral centrifugal acceleration of less than 0.1 g's for vehicle speeds less than 88 ft/sec. The bank angle is chosen as the slope at which side slipping impends for a vehicle proceeding at its design speed around a frictionless curve; typically $\alpha = 0.01$. A typical grade angle of $\beta = 0.03$ is reasonable. Finally, since steady-state statistical responses exclude time variations in $\alpha$ and $\beta$, the values of $\dot{\alpha}$ and $\dot{\beta}$ are chosen as zero.

While selected values of these characteristics are sufficient to determine particular sets of 16 parameters in Eqs. (67-70), there remain the eight parameters which characterize the stochastic guideway and wind inputs. The guideway roughness parameter A ranges from $3.7 \times 10^{-6}$ ft for smooth runways to $2.0 \times 10^{-5}$ ft for smooth highways [36]. Further, the guideway frequency parameter $\omega_1$ is given in terms of vehicle speed u, the guideway irregularity wavelength, $\lambda$, or

$$\omega_1 = 2\pi\, u/\lambda \tag{99}$$

where $50 \leq \lambda \leq 300$ ft. accounts for construction and settlement irregularities. Thus, for u between 20 and 60 mph, the extreme values are $0.61 \leq \omega_1 \leq 11.1$ rad/sec. These data are sufficient to estimate the ranges of $\bar{\gamma}_i$ and $\bar{\nu}_i$, i = 7,8,9, in Eqs. (80a). The two remaining statistical parameters for wind loading, $\bar{\gamma}_{10}$ and $\bar{\nu}_{10}$ can be estimated from Eqs. (80b) in which

$$\bar{\beta} = (\bar{F}_w)^2/\pi \tag{100}$$

where $\bar{F}_w$ is the rms value of the wind force [26] equal to a design value of 550 lbs for a vehicle 50 ft. long and 10 ft high. By scaling the loading area, for a vehicle 10 ft long and 5 ft high, $\bar{F}_w \simeq 55$ lbs, for which $\bar{\beta} \simeq 963$ $lb^2$. Finally, the wind correlation frequency constant $\nu$ lies between 0.4 and 3 rad/sec [37].

Table 8 summarizes a typical set of nondimensional system parameters which serves as a basic vehicle-guideway model for the numerical study which follows. The basic model parameters were calculated from nominal values of the data presented above, and vary within the range shown. This basic model represents a practical, 10 or 12 passenger AGT vehicle with a design speed of up to 60 mph on a 2400 ft. radius curve.

Table 8

Typical System Parameters

| PARAMETER | MEANING | BASIC CASE | TYPICAL RANGE |
|---|---|---|---|
| $D_o = d/h$ | width ratio | 1.67 | 0.7 to 3 |
| $L_o = L/h$ | length ratio | 3.33 | 1 to 10 |
| $L_x = \ell_x\ mh/I_z$ | wind center & mass distribution | 0.36 | -0.75 to 0.75 |
| $L_z = \ell_z/h$ | wind center | 2 | 0.67 to 4 |
| $P_o = p/h$ | guidewheel height | 1 | 0.08 to 4 |
| $R_o = R/h$ | guideway radius | 1600 | 90 to 2400 |
| $R_x = (I_x/m)^{1/2}/h$ | mass distribution | 1.66 | 0.7 to 2.9 |
| $U = u/(R\Omega_\theta)$ | vehicle speed | (0.006) | 0.001 to 0.01 |
| $V = (g \cos\alpha \cos\beta)/h\Omega_\theta^2$ | pendulum | 1.84 | 0.07 to 3.3 |
| $\alpha' = \dot{\alpha}/\Omega_\theta$ | bank variation | 0 | —— |
| $\beta' = \dot{\beta}/\Omega_\theta$ | grade variation | 0 | —— |
| $\bar{\gamma}_i = 2AU/(\pi R)$ (i = 7,8,9) | guideway roughness | $2.7 \times 10^{-9}$ U | $10^{-9}$ U to $5 \times 10^{-8}$ U |
| $\bar{\gamma}_{10} = \bar{\beta}\nu/(m^2h^2\Omega_\theta^5)$ | wind load | $1.2 \times 10^{-6}$ | $10^{-9}$ to $4 \times 10^{-3}$ |
| $\bar{\nu}_i = \omega_1/\Omega_\theta$ (i = 7,8,9) | guideway frequency | 0.5 | 0.05 to 0.9 |
| $\bar{\nu}_{10} = \nu/\Omega_\theta$ | wind frequency | 0.27 | 0.03 to 1 |
| $\xi_1 = 2c/(m\Omega_1)$ | heave damping | 0.3 | 0.2 to 0.3 |
| $\xi_3 = 2C/(m\Omega_3)$ | lateral damping | 0.3 | 0.2 to 0.3 |
| $\xi_\theta = 2L^2c/(I_z\Omega_\theta)$ | yaw damping | 0.3 | 0.2 to 0.3 |
| $\bar{\Omega}_1 = \Omega_1/\Omega_\theta$ | heave frequency | 1 | 0.5 to 4 |
| $\bar{\Omega}_3 = \Omega_3/\Omega_\theta$ | lateral frequency | 1 | 0.5 to 4 |
| $\bar{\rho}_1 = \rho_1/h$ | x coordinate | -3.3 to 3.3 | -10 to 10 |
| $\bar{\rho}_2 = \rho_2/h$ | y coordinate | -1.7 to 1.7 | -3 to 3 |
| $\bar{\rho}_3 = \rho_3/h$ | z coordinate, $a_y^*$ | 0.6 | 0.4 to 0.8 |

Numerical Results and Conclusions - The rms lateral acceleration responses $a_y^* = a_y/h\Omega_\theta^2$ were studied in a systematic way using the "basic case" parameters of Table 8, varying selected values one at a time. The peak rms acceleration for each U over its range was determined from calculated contour plots of $a_y^*$ for $\bar{\rho}_1$ and $\bar{\rho}_2$ ranging over the length and width of the base vehicle, at the floor level of $\bar{\rho}_3 = 0.6$.

The main results are shown in Figs 75 and 76, where the left ordinates are valid for any value of h and $\Omega_\theta$ ($=\Omega_1=\Omega_3$); but the right ordinates correspond to h=1.5 ft and $\Omega_\theta$ = 1 hz = $2\pi$ rad/sec. For this latter rather specific vehicle on 2400ft radius curve, at a speed of u=61 mph, the nondimensional speed is U=0.00597.

Of all the factors affecting lateral acceleration, the parameters for guidewheel height, $P_0 = p_0/h$, and velocity, $U=u/R\Omega_\theta$, dominate. Thus, $P_0$=1 yields a minimum for $a_y^*$ at fixed U, as shown in Fig 75. Vehicle speed values in parentheses are for $\Omega_\theta$ =1hz and R=2400 ft. It is noted that the lateral acceleration is especially sensitive to $P_0$ in the mid-speed range (u=49 mph).

Figure 76 shows the variation of lateral acceleration with U, with and without wind and guideway roughness. Curve a depicts the peak floor level values of $a_y^*$ (and of $a_y$ in g's for the specific case of h=1.5 ft, $\Omega_\theta$=1hz and R=2400 ft.). The nominal wind roughness of Table 8 has a negligible effect on $a_y^*$, especially for U>0.0024. Curve b is simply based on $u^2/R$, the centrifugal acceleration at the vehicle's mass center for the specific case referred to above, for a 2400 ft smooth radius curve. Thus

$$a_y = R\Omega_\theta^2 U^2 = 2942\, U^2, \text{ in g's} \qquad (101)$$

Figure 76 shows that the peak lateral rms acceleration predicted for the statistically rough guideway is consistently higher than $a_y$ as predicted from the elementary theory, Eq (101). For instance, guideway roughness with or without wind increases the lateral acceleration by about 13% at U = 0.006.

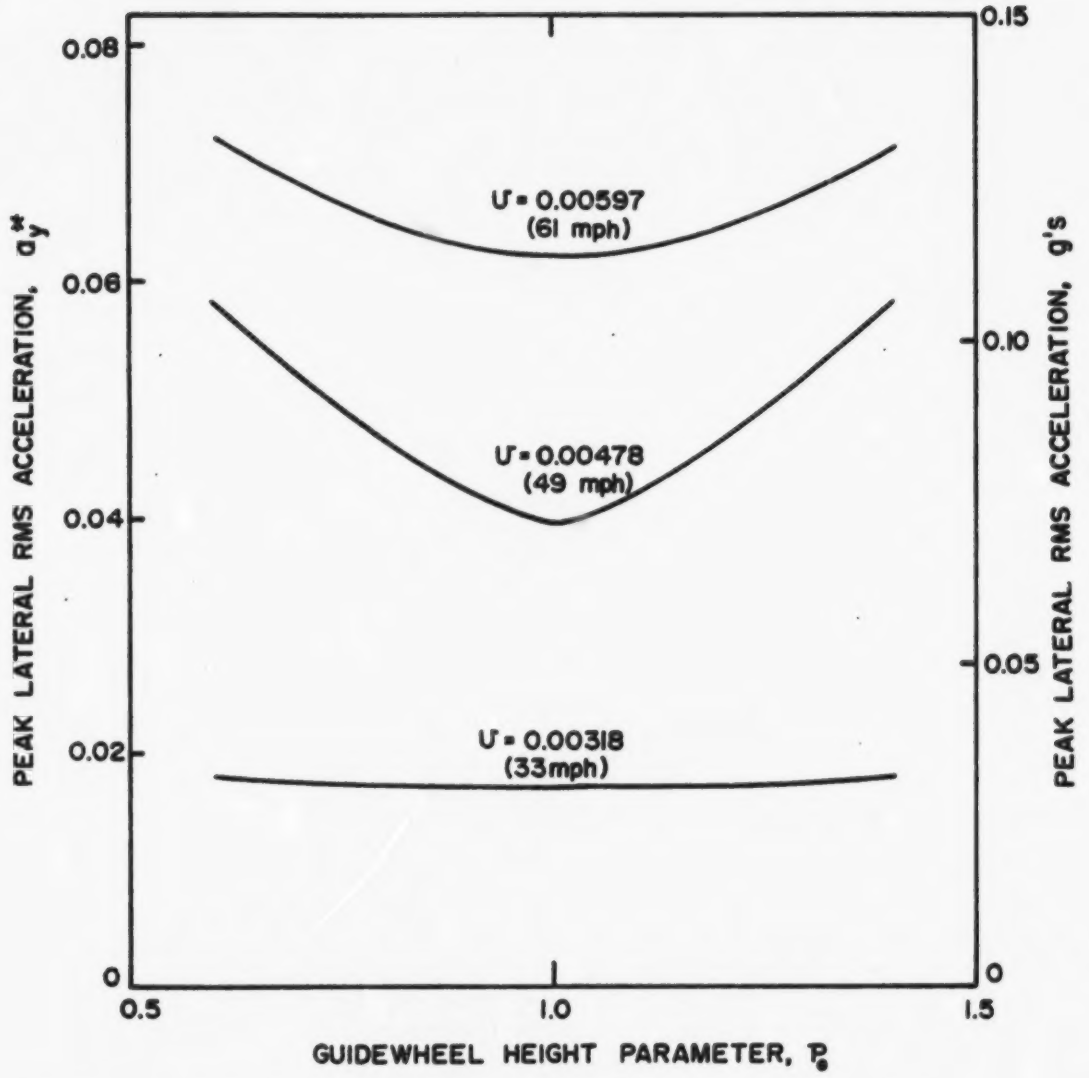


Figure 75. Variation in lateral vehicle acceleration response with guidewheel height, for a constant speed vehicle.

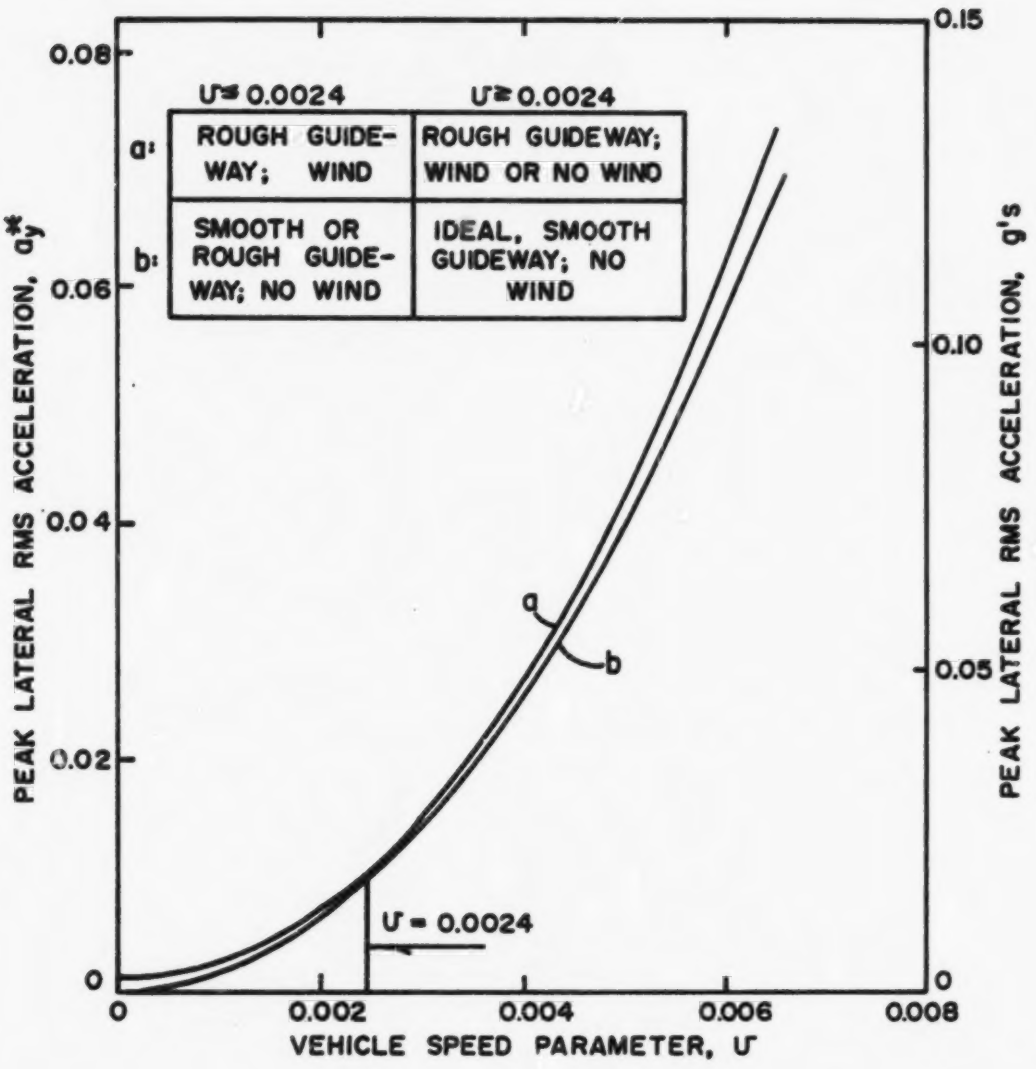


Figure 76. Effects of vehicle speed, guideway roughness and wind load on vehicle lateral rms acceleration response.

The results of varying other parameters from the "basic case" of Table 8, and the effects on $a_y^*$ in Fig 76 are summarized.

1. Excursions on both wind and guideway roughness and frequency parameters over the ranges of Table 8 leave $a_y^*$ virtually unchanged.
2. An increase in all damping factors $\xi_1$, $\xi_2$, and $\xi_3$ from 0.2 to 0.3 depresses $a_y^*$ by about 5 percent.
3. An increase in the suspension parameters, $\bar{\Omega}_3$ from 0.5 to 1.75 depresses $a_y^*$ by about 10 percent.
4. The parameters $P_0$, $R_0$ and V, when varied between their extreme values of Table 8, change $a_y^*$ by less than 6 percent.
5. An increase in the length parameter $L_0$ by a factor of two leaves $a_y^*$ virtually unchanged.

Finally, although the theoretical calculation of the rms value of lateral suspension system stroke, $\rho_y^*$, appears to be correct, reasonable numerical results have yet to be obtained from the computer algorithm. However, the following elementary estimate of $\rho_y^*$, based on the statistical response $a_y^*$ of curve a, Fig 76, may suffice in many design cases. On a smooth guideway without wind, for an average lateral displacement of $\rho_y$, the total force on all lateral spring suspensions is $4k\rho_y$. This force is balanced by the centrifugal force, $mu^2/R$. Since $\Omega_1^2 = 4k/m$ and $\rho_y^* = \rho_y/h$ it follows that

$$\rho_y^* = \frac{mu^2}{4kRh} = \frac{u^2}{\Omega_1^2 Rh} = \frac{U^2}{\bar{\Omega}_1^2} R_0 \qquad (102)$$

For a better estimate of stroke, when the vehicle is on a rough guideway (with or without wind), the value of $\rho_y^*$ in Eq (102) should be amplified by the increase of curve a over curve b, Fig 76. For instance, if $R_0 = 1600$, $\bar{\Omega}_1 = 1$ and $U = 0.006$, curve a is 13% higher than curve b, so

$$\rho_y^* \simeq 1.13 \frac{U^2}{\bar{\Omega}_1^2} R_0 = 0.065 \qquad (103)$$

If h = 1.5 ft, then a reasonable estimate of the average stroke would be $\rho_y \approx 0.1$ ft. The special virtue of the above calculation is its simplicity. Thus, the stroke is most strongly dependent on U and the suspension parameter, $\Omega_1$; but only linearly dependent on the guideway radius.

In conclusion, it is important to keep all of these calculations in perspective. They are meant as initial design guidelines only. It is recalled that all of these results are based on a rather simplified, three-degree-of-freedom vehicle model with steady-state responses. Some AGT vehicles may need further degrees of freedom for more precise transient descriptions of responses, especially during curve entrance and exit. Ultimately, of course, experimental response data from many prototype AGT vehicles should be compared with results obtained here. Just how many classes of AGT vehicles the above model accurately depicts is left to future research and development efforts.

# APPENDIX I

# CABLE-STAYED GUIDEWAY RESPONSE PROGRAM

```
      $JOB     DU.D06.AA3603/BARBAS,TIME=0180,PAGES=0020
     1        IMPLICIT REAL*8(A-H,O-Z)
     2         LOGICAL*4 DEBUG,SFLAG,SPECAL,PNCH
     3         REAL*4 OUT,DEL,TF,CPN6,CPN7,TT
     4        LOGICAL TRANS
     5        LOGICAL SWITCH
     6         DIMENSION XZ(61),XZD(61),Y(61,20),DIST(3),IBAY(3),NUMB(20)
     7        DIMENSION IA7(12),NOUT(20),DISTN(20),OUT(400,20),OUTDP(20),XU(61)
     8        DIMENSION U(61),U1(61),U2(61),V1(61),V2(61),VV(61),IPL(20)
     9        DIMENSION JL(61)
    10        DIMENSION B1(61),B2(61),OMEGA(61),ZET(61),AINV(61)
    11        DIMENSION W(61),B(61),S(61),A(61),A1(61),A2(61),X(61),X1(61),
              *     X2(61),P(61),P1(61),P2(61)
    12        DIMENSION Y7(61,6),YX(61,6),YY(61,6),Y3(61,6),Y4(61,6),FO(61,6)
    13        DIMENSION P2(61)
    14        DIMENSION APF(61,6),BPF(61,6),CPF(61,6),DPF(61,6)
    15        DIMENSION CN(15),DN(15)
    16        DIMENSION SNORM(61)
    17        DIMENSION H(4,4)
    18        DIMENSION QL(61)
    19        DIMENSION CC(61),GG(61),AA(61),AB(61),AC(61)
    20        EQUIVALENCE(A1,B1),(A2,B2)
    21        EQUIVALENCE (XZ,X1)
    22        DATA DEBUG/.FALSE./
    23        DATA NM/20/
    24        DATA Z/167.04D0/
    25        DATA NUMB/2*0,2*1,2*2,2*3,2*4,2*5,2*6,6*0/
    26        DATA INTVL,PNCH,IOUT/1,.FALSE.,1/
    27        DATA IBAY/0,0,0/
    28        DATA FINIS,DELT/1.4D0,0.00980/
    29        DATA EI,AREA,GAMMA/2.4414D4,0.625D0,.688D0/
    30        DATA F,DESTRT,DESTOP/2.7D0,100.D0,100.D0/
    31        DATA IPL/1,1,0,1,0,1,0,1,0,0,0,0,0,0,0,0,0,0,0,0/
    32        DATA BL,VEL,NBAY,ZET/42.00,18.D0,3,61*0.D0/
    33        DATA DIST/0.0,0.0,0.0/
    34        DATA IA8,IA7/0,2,3,4,5,1,6,7,8,9,10,11,12/
    35        DATA TRANS/.FALSE./
    36        DATA FIX1,FIX2,FIX3,FIX4,OSTORE,M/0.D0,0.D0,0.D0,0.D0,0.D0,0/
    37        DATA SWITCH/.FALSE./
    38        DATA 9.D0/3.D0,1.0005D0/
    39        NAMELIST/INPUT/NM,XZ,XZD,DELT,FINIS,DEBUG,IOUT,IPL,DESTRT,
              *     BL,VEL,NBAY,ZET,EI,F,GAMMA,AREA,IBAY,PNCH,DIST,DESTOP
    40        NAMELIST/DEBUG1/ T,ISTEP,Z,N,ZN,NSPAN,SFLAG,IC1,V1,V2
    41        NAMELIST/DEBUG2/X,X1,X2,P,P1,P2,T,U1,U2,XU
    42        NAMELIST/DEBUG3/CC,GG,W,B,S,A,A1,A2,DISTN,IPL,NUMB
    43      3 FORMAT(1H )
    44      4 FORMAT(11X,2HQX,14X,3HANF,14X,3HBNF,14X,3HCNF,14X,3HDNF)
    45      5 FORMAT(2X,F15.8,2X,F15.8,2X,F15.8,2X,F15.8,2X,F15.8)
    46      6 FORMAT(22X,5HLAMDA,18X,5HSNORM)
    47      7 FORMAT(18X,F12.8,7X,F15.4)
    48      8 FORMAT(1H1)
    49      9 FORMAT(9X,2HIX,15X,1HY,14X,2HY',13X,3HY'',13X,4HY''',13X,2HEQ)
    50     10 FORMAT(10X,I1,7X,F12.5,4X,F12.5,4X,F12.5,4X,F12.5)
    51     15 FORMAT(1H0,/1H0,T5,'STATIC MIDPT DEFL. OF SINGLE SPAN=',D14.6,
              *  'IN.',/1H0,
              *T5,'MAXIMUM BENDING MOMENT OF SINGLE SPAN=',D14.6,' IN.-LB.')
    52     16 FORMAT(1H0,T5,'TRANSIT FREQUENCY =',D14.6,' HZ.',/1H0,T5,
              *   'CROSSING RATIO =',D14.6)
    53     17 FORMAT(1H0,//,T10,'TIME=',F7.3,/)
    54     18 FORMAT(1H ,T10,I2,6D18.6)
```

MICROFILMED FROM
BEST AVAILABLE COPY

```
      19 FORMAT(I4,F6.3,5D13.5)
      20 FORMAT(1H1,T51,'DATA SUMMARY')
      21 FORMAT(T8,'TIME',5(14X,I2,4X),/1H )
      22 FORMAT(I4,F8.4,5D20.5)
         PI=3.1415926D0
         N=NBAY
         PIO=PI
         GO TO 26
      25 TRANS=.TRUE.
         QS=0
      26 QSTORE=Q
         Q=Q+DQ
         IF (Q .GE. PIO .AND. QSTORE .LT. PIO) GO TO 27
         GO TO 29
      27 Q=PIO
         QX=PIO
         SWITCH=.TRUE.
         PIO=PIO+PI
         GO TO 49
      29 G=-Z/(2.0D0*Q**3)*(DSINH(Q)*DCOS(Q)-DSIN(Q)*DCOSH(Q))
     1   +(2*DCOSH(Q)*DCOS(Q)+1)
         G=-Z/(4*Q**3)*(DSINH(Q)-DSIN(Q))+DCOSH(Q)+DCOS(Q)
         A4=(G/2)**2-((N-1)/2
         IF (A4 .LT. 0.D0) GO TO 25
         A5=DSQRT((G/2)**2-((N-1)/2)
         A6=G/2+A5
         A7=G/2-A5
         IF (DABS(A6) .GT. 1.D0 .AND. DABS(A7) .GT. 1.D0) GO TO 25
         IF (DABS(A7) .GT. 1.D0 .AND. DABS(A6) .LE. 1.D0) GO TO 33
         IF (DABS(A7) .LE. 1.D0 .AND. DABS(A6) .GT.1.D0)  GO TO 40
         R1=DABCOS(A7)
         R2=DABCOS(A7)
         S11=((DCOS(R1)-DCOS(Q))*(2*Q**3/Z)-DSIN(Q))
         S12=((DCOS(R2)-DCOS(Q))*(2*Q**3/Z)-DSIN(Q))
         H(1,1)=DCOS(R1)*S11
         H(1,2)=DSIN(R1)*S11
         H(1,3)=DCOS(R2)*S12
         H(1,4)=DSIN(R2)*S12
         H(2,1)=DCOS((N+1)*R1)*S11
         H(2,2)=DSIN((N+1)*R1)*S11
         H(2,3)=DCOS((N+1)*R2)*S12
         H(2,4)=DSIN((N+1)*R2)*S12
         S21= DCOS(R1)*(1+DSIN(Q)/DSINH(Q)
     1   +2*DCOS(Q)/DSINH(Q)*(2*Q**3/Z))
     2   -(2/DSINH(Q))*(2*Q**3/Z))*(DCOS(R1))**2
     3   -(DCOS(Q)+DCOSH(Q)*DSIN(Q)/DSINH(Q)
     4   +2*DCOSH(Q)*DCOS(Q)/DSINH(Q)*(2*Q**3/Z))
     5   +2*DCOSH(Q)/DSINH(Q)*(2*Q**3/Z)*DCOS(R1)
         S22= DCOS(R2)*(1+DSIN(Q)/DSINH(Q)
     1   +2*DCOS(Q)/DSINH(Q)*(2*Q**3/Z))
     2   -(2/DSINH(Q))*(2*Q**3/Z)*(DCOS(R2))**2
     3   -(DCOS(Q)+DCOSH(Q)*DSIN(Q)/DSINH(Q)
     4   +2*DCOSH(Q)*DCOS(Q)/DSINH(Q)*(2*Q**3/Z))
     5   +2*DCOSH(Q)/DSINH(Q)*(2*Q**3/Z)*DCOS(R2)
         H(3,1)=DCOS(R1)*S21
         H(3,2)=DSIN(R1)*S21
         H(3,3)=DCOS(R2)*S22
         H(3,4)=DSIN(R2)*S22
         H(4,1)=DCOS((N+1)*R1)*S21
         H(4,2)=DSIN((N+1)*R1)*S21
```

```
104           H(4,3)=DCOS((N+1)*R2)*S22
105           H(4,4)=DSIN((N+1)*R2)*S22
106           FF=H(1,1)*(H(2,2)*(H(3,3)*H(4,4)-H(4,3)*H(3,4))
             1   -H(2,3)*(H(3,2)*H(4,4)-H(4,2)*H(3,4))
             2   +H(2,4)*(H(3,2)*H(4,3)-H(4,2)*H(3,3)))
107           C=-H(1,2)*(H(2,1)*(H(3,3)*H(4,4)-H(4,3)*H(3,4))
             1   -H(2,3)*(H(3,1)*H(4,4)-H(4,1)*H(3,4))+
             2   H(2,4)*(H(3,1)*H(4,3)-H(4,1)*H(3,3)))
108           D=H(1,3)*(H(2,1)*(H(3,2)*H(4,4)-H(4,2)*H(3,4))
             1   -H(2,2)*(H(3,1)*H(4,4)-H(4,1)*H(3,4))+
             2   H(2,4)*(H(3,1)*H(4,2)-H(4,1)*H(3,2)))
109           E=-H(1,4)*(H(2,1)*(H(3,2)*H(4,3)-H(4,2)*H(3,3))-
             1   H(2,2)*(H(3,1)*H(4,3)-H(4,1)*H(3,3))+
             2   H(2,3)*(H(3,1)*H(4,2)-H(4,1)*H(3,2)))
110           DET=FF+C+D+E
111           IF (DET .EQ. 0.D0) GO TO 31
112           IF (FIX4 .LT. 0.D0 .AND. DET .GT. 0.D0) GO TO 30
113           IF (FIX4 .GT. 0.D0 .AND. DET .LT. 0.D0) GO TO 30
114           IF (FIX3 .GT. 0.D0 .AND. FIX4 .GT. 0.D0 .AND. DET .GT. 0.D0
             *   .AND. FIX3 .GT. FIX4 .AND. DET .GT. FIX4) GO TO 30
115           IF (FIX3 .LT. 0.D0 .AND. FIX4 .LT. 0.D0 .AND. DET .LT. 0.D0
             *   .AND. FIX3 .LT. FIX4 .AND. DET .LT. FIX4) GO TO 30
116           FIX3=FIX4
117           FIX4=DET
118           QSTORE=0
119           GO TO 26
120        30 QX=QSTORE+D0*DABS(FIX4)/(DABS(FIX4)+DABS(DET))
121           GO TO 32
122        31 QX=0
123        32 TRANS=.FALSE.
124           FIX3=FIX4
125           FIX4=DET
126           QSTORE=0
127           GO TO 48
128        33 R1=DARCOS(A6)
129           Y1=DSIN(N*R1)
130           FIX2=0.D0
131           FIX3=0.D0
132           FIX4=0.D0
133           IF (Y1 .EQ. 0.D0) GO TO 36
134           IF (TRANS .AND. DABS(Y1) .LT. 0.01D0) GO TO 36
135           IF (FIX1 .LT. 0.D0 .AND. Y1 .GT. 0.D0) GO TO 34
136           IF (FIX1 .GT. 0.D0 .AND. Y1 .LT. 0.D0) GO TO 34
137           FIX1=Y1
138           QSTORE=0
139           TRANS=.FALSE.
140           GO TO 26
141        34 QX=QSTORE+D0*DABS(FIX1)/(DABS(FIX1)+DABS(Y1))
142           GO TO 38
143        36 QX=0
144        38 FIX1=Y1
145           TRANS=.FALSE.
146           QSTORE=0
147           GO TO 48
148        40 R2=DARCOS(A7)
149           Y2=DSIN(N*R2)
150           FIX1=0.D0
151           FIX3=0.D0
152           FIX4=0.D0
153           IF (Y2 .EQ. 0.D0) GO TO 44
```

```
154         IF (TRANS .AND. DABS(Y2) .LT. 0.01D0) GO TO 44
155         IF (FIX2 .LT. 0.D0 .AND. Y2 .GT.0.D0) GO TO 42
156         IF (FIX2 .GT. 0.D0 .AND. Y2 .LT. 0.D0) GO TO 42
157         FIX2=Y2
158         QSTORE=Q
159         TRANS=.FALSE.
160         GO TO 26
161      42 QX=QSTORE+D0*DABS(FIX2)/(DABS(FIX2)+DABS(Y2))
162         GO TO 46
163      44 QX=Q
164      46 FIX2=Y2
165         TRANS=.FALSE.
166         QSTORE=0
167         GO TO 48
168      48 M=M+1
169         QL(M)=QX
170         JL(M)=0
171         IF (SWITCH) JL(M)=M
172         SWITCH=.FALSE.
173      49 IF  (M .EQ.  NM) GO TO 50
174         GO TO 26
175      50 IF (.NOT. DEBUG) GO TO 60
176         WRITE (3,4)
177         WRITE(3,3)
178      60 M=0
179         DO 99 I=1,NM
180         QX=QL(I)
181         IF (I .EQ. JL(I)) GO TO 98
182         GG(I)=(-Z/(2*QX**3))*(DSINH(QX)*DCOS(QX)-DSIN(QX)*DCOSH(QX))
          1   +(2*DCOSH(QX)*DCOS(QX)+1)
183         GG(I)=(-Z/(4*QX**3))*(DSINH(QX)-DSIN(QX))+DCOSH(QX)+DCOS(QX)
184         AA(I)=DSQRT((GG(I)/2)**2-(F(I)-1)/2.D0)
185         AB(I)=GG(I)/2.D0+AA(I)
186         AC(I)=GG(I)/2.D0-AA(I)
187         IF (DABS(AB(I)) .LE. 1.D0 .AND. DABS(AC(I)) .LE. 1.D0) GO TO 66
188         IF (DABS(AB(I)) .LE. 1.D0 .AND. DABS(AC(I)) .GT. 1.D0) GO TO 70
189         IF (DABS(AC(I)) .LE. 1.D0 .AND. DABS(AB(I)) .GT. 1.D0) GO TO 80
190      66 R1=DARCOS(AB(I))
191         R2=DARCOS(AC(I))
192         S11=((DCOS(R1)-DCOS(QX))*(2*QX**3/Z)-DSIN(QX))
193         S12=((DCOS(R2)-DCOS(QX))*(2*QX**3/Z)-DSIN(QX))
194         S21= DCOS(R1)*(1+DSIN(QX)/DSINH(QX)
          1   + 2*DCOS(QX)/DSINH(QX)*(2*QX**3/Z))
          2   -2/DSINH(QX)*(2*QX**3/Z)*(DCOS(R1))**2
          3   -(DCOS(QX)+DCOSH(QX)*DSIN(QX)/DSINH(QX)
          4   + 2*DCOSH(QX)*DCOS(QX)/DSINH(QX)*2*QX**3/Z)
          5   +2*DCOSH(QX)/DSINH(QX)*(2*QX**3/Z)*DCOS(R1)
195         S22= DCOS(R2)*(1+DSIN(QX)/DSINH(QX)
          1   + 2*DCOS(QX)/DSINH(QX)*(2*QX**3/Z))
          2   -2/DSINH(QX)*(2*QX**3/Z)*(DCOS(R2))**2
          3   -(DCOS(QX)+DCOSH(QX)*DSIN(QX)/DSINH(QX)
          4   + 2*DCOSH(QX)*DCOS(QX)/DSINH(QX)*2*QX**2/Z)
          5   +2*DCOSH(QX)/DSINH(QX)*(2*QX**3/Z)*DCOS(R2)
196         H(1,1)=DCOS(R1)*S11
197         H(1,2)=DSIN(R1)*S11
198         H(1,3)=DCOS(R2)*S12
199         H(1,4)=DSIN(R2)*S12
200         H(2,1)=DCOS((N+1)*R1)*S11
201         H(2,2)=DSIN((N+1)*R1)*S11
202         H(2,3)=DCOS((N+1)*R2)*S12
```

```
203         H(2,4)=DSIN((N+1)*R2)*S12
204         H(3,1)=DCOS(R1)*S21
205         H(3,2)=DSIN(R1)*S21
206         H(3,3)=DCOS(R2)*S22
207         H(3,4)=DSIN(R2)*S22
208         C1=(H(1,1)*H(2,4)-H(1,4)*H(2,1))
209         C2=(H(1,2)*H(2,4)-H(1,4)*H(2,2))
210         C3=(H(1,3)*H(2,4)-H(1,4)*H(2,3))
211         C4=(H(3,4)*H(2,1)-H(2,4)*H(3,1))
212         C5=(H(3,4)*H(2,2)-H(2,4)*H(3,2))
213         C6=(H(3,4)*H(2,3)-H(2,4)*H(3,3))
214         EL2=-(C1*C6-C3*C4)/(C2*C6-C3*C5)
215         EL3=-(C1*C6+(C2*C6*EL2))/(C3*C6)
216         EL4=-(H(1,1)+H(1,2)*EL2+H(1,3)*EL3)/H(1,4)
217         L=NBAY+5
218         DO 68 J=1,L
219         CN(J)=DCOS((J-2)*R1)+EL2*DSIN((J-2)*R1)+EL3*DCOS((J-2)*R2)
          *   +EL4*DSIN((J-2)*R2)
220      68 CONTINUE
221         L=NBAY+3
222         DO 69 J=1,L
223      69 DN(J)=(1/DSINH(QX))*((CN(J+2)-2*CN(J+1)*DCOS(QX)+CN(J))
          1   *2*QX**3/Z-CN(J+1)*DSIN(QX))
224         GO TO 90
225      70 R1=DARCOS(AB(I))
226         S11=((DCOS(R1)-DCOS(QX))*(2*QX**3/Z)-DSIN(QX))
227         H(1,1)=DCOS(R1)*S11
228         H(1,2)=DSIN(R1)*S11
229         EL2=-(H(1,1)/H(1,2))
230         L=N+5
231         DO 78 J=1,L
232         CN(J)=DCOS((J-2)*R1)+EL2*DSIN((J-2)*R1)
233      78 CONTINUE
234         L=N+3
235         DO 79 J=1,L
236      79 DN(J)=(1/DSINH(QX))*((CN(J+2)-2*CN(J+1)*DCOS(QX)+CN(J))
          1   *2*QX**3/Z-CN(J+1)*DSIN(QX))
237         GO TO 90
238      80 R2=DARCOS(AC(I))
239         S22=  DCOS(R2)*(1+DSIN(QX)/DSINH(QX)
          1   +  2*DCOS(QX)/DSINH(QX)*(2*QX**3/Z))
          2   -2/DSINH(QX)*(2*QX**3/Z)*(DCOS(R2))**2
          3   -(DCOS(QX)+DCOSH(QX)*DSIN(QX)/DSINH(QX)
          4   +  2*DCOSH(QX)*DCOS(QX)/DSINH(QX)*2*QX**3/Z)
          5   +2*DCOSH(QX)/DSINH(QX)*(2*QX**3/Z)*DCOS(R2)
240         H(3,3)=DCOS(R2)*S22
241         H(3,4)=DSIN(R2)*S22
242         EL4=-(H(3,3)/H(3,4))
243         L=N+5
244         DO 88 J=1,L
245         CN(J)=DCOS((J-2)*R2)+EL4*DSIN((J-2)*R2)
246      88 CONTINUE
247         L=N+3
248         DO 89 J=1,L
249      89 DN(J)=(1/DSINH(QX))*((CN(J+2)-2*CN(J+1)*DCOS(QX)+CN(J))
          1   *2*QX**3/Z-CN(J+1)*DSIN(QX))
250         GO TO 90
251      90 M=M+1
252         DO 91 L=1,NBAY
253         ANF(M,L)=CN(L+3)
```

MICROFILMED FROM
BEST AVAILABLE COPY

```
234           BNF(M,L)=DN(L+2)
255           CNF(M,L)=CN(L+2)
256           DNF(M,L)=DN(L+1)
257        91 CONTINUE
258           IF (.NOT. DEBUG) GO TO 99
259           WRITE (3,3)
260           DO 96 J=1,NRAY
261        96 WRITE (3,5) QL(I),ANF(I,J),BNF(I,J),CNF(I,J),DNF(I,J)
262           GO TO 99
263        98 M=M+1
264        99 CONTINUE
265           DO 105 M=1,NM
266           IF (M .EQ. JL(M)) GO TO 104
267           TEM=0.00
268           DO 100 I=1,NRAY
269           IF (DABS(ANF(M,I)) .LT. 0.000000001D0) ANF(M,I)=0.00
270           IF (DABS(BNF(M,I)) .LT. 0.000000001D0) BNF(M,I)=0.00
271           IF (DABS(CNF(M,I)) .LT. 0.000000001D0) CNF(M,I)=0.00
272           IF (DABS(DNF(M,I)) .LT. 0.000000001D0) DNF(M,I)=0.00
273           T1=ANF(M,I)**2*(0.500-DSIN(2*QL(M))/(4*QL(M)))
274           T2= ANF(M,I)*BNF(M,I)*DSIN(QL(M))*DCOSH(QL(M))/QL(M)
          *     -ANF(M,I)*BNF(M,I)*DCOS(QL(M))*DSINH(QL(M))/QL(M)
275           T3=2*ANF(M,I)*CNF(M,I)*(DSIN(QL(M))/(2*QL(M))-0.500*DCOS(QL(M)))
276           T4= ANF(M,I)*DNF(M,I)*(DSINH(QL(M))-DSIN(QL(M)))/QL(M)
277           T5=BNF(M,I)**2*(DSINH(2*QL(M))/(4*QL(M))-0.500)
278           T6= BNF(M,I)*CNF(M,I)*(DSINH(QL(M))-DSIN(QL(M)))/QL(M)
279           T7= BNF(M,I)*DNF(M,I)*(DCOSH(QL(M))-DSINH(QL(M))/QL(M))
280           T8=CNF(M,I)**2*(0.500-DSIN(2*QL(M))/(4*QL(M)))
281           T9=2*CNF(M,I)*DNF(M,I)*DSIN(QL(M))*DCOSH(QL(M))/(2*QL(M))
          *     -2*CNF(M,I)*DNF(M,I)*DCOS(QL(M))*DSINH(QL(M))/(2*QL(M))
282           T10=DNF(M,I)**2*(-0.500+DSINH(2*QL(M))/(4*QL(M)))
283           TEM= T1+T2+T3+T4+T5+T6+T7+T8+T9+T10+TEM
284        100 CONTINUE
285           SNORM(M)=TEM*BL
286           GO TO 105
287        104 SNORM(M)=NRAY*BL/2.00
288        105 CONTINUE
289           WRITE(3,8)
290           WRITE(3,6)
291           WRITE(3,3)
292           DO 110 M=1,NM
293        110 WRITE (3,7) QL(M),SNORM(M)
294           IF (.NOT. DEBUG) GO TO 121
295           IX=0
296           WRITE (3,8)
297           WRITE (3,9)
298           WRITE(3,3)
299        111 DO 120 M=1,NM
300           WRITE (3,3)
301           IF (M .EQ. JL(M)) GO TO 116
302           DO 115 I=1,NRAY
303           YZ(M,I)=ANF(M,I)*DSIN(QL(M)*IX)+BNF(M,I)*DSINH(QL(M)*IX)
          1   +CNF(M,I)*DSIN(QL(M)*(1-IX))+DNF(M,I)*DSINH(QL(M)*(1-IX))
304           YX(M,I)=QL(M)*ANF(M,I)*DCOS(QL(M)*IX)
          *      +QL(M)*BNF(M,I)*DCOSH(QL(M)*IX)
          1   -QL(M)*CNF(M,I)*DCOS(QL(M)*(1-IX))
          *   -QL(M)*DNF(M,I)*DCOSH(QL(M)*(1-IX))
305           YY(M,I)=-(QL(M)**2*ANF(M,I)*DSIN(QL(M)*IX))
          1   +QL(M)**2*BNF(M,I)*DSINH(QL(M)*IX)
          2   -(QL(M)**2*CNF(M,I)*DSIN(QL(M)*(1-IX)))
```

```
     3   +QL(M)**2*DNF(M,I)*DSINH(QL(M)*(1-IX))
306       Y3(M,I)=-(QL(M)**3*ANF(M,I)*DCOS(QL(M)*IX)
     1   +QL(M)**3*BNF(M,I)*DCOSH(QL(M)*IX)
     2   +QL(M)**3*CNF(M,I)*DCOS(QL(M)*(1-IX))
     3   -(QL(M)**3*DNF(M,I)*DCOSH(QL(M)*(1-IX)))
307       Y4(M,I)=QL(M)**4*ANF(M,I)*DSIN(QL(M)*IX)
     1    +QL(M)**4*BNF(M,I)*DSINH(QL(M)*IX)
     2   +QL(M)**4*CNF(M,I)*DSIN(QL(M)*(1-IX))
     3   +QL(M)**4*DNF(M,I)*DSINH(QL(M)*(1-IX))
308       EQ(M,I)=Y4(M,I)-QL(M)**4*YZ(M,I)
309   115 WRITE (3,10) IX,YZ(M,I),YX(M,I),YY(M,I),Y3(M,I),EQ(M,I)
310       GO TO 120
311   116 DO 117 I=1,NBAY
312       IT1=(-1)**I
313       YZ(M,I)=IT1*DSIN(QL(M)*IX)
314       YX(M,I)=IT1*QL(M)*DCOS(QL(M)*IX)
315       YY(M,I)=-IT1*(QL(M))**2*DSIN(QL(M)*IX)
316       Y3(M,I)=-IT1*(QL(M))**3*DCOS(QL(M)*IX)
317       Y4(M,I)=IT1*(QL(M))**4*DSIN(QL(M)*IX)
318       EQ(M,I)=Y4(M,I)-QL(M)**4*YZ(M,I)
319   117 WRITE (3,10) IX,YZ(M,I),YX(M,I),YY(M,I),Y3(M,I),EQ(M,I)
320   120 CONTINUE
321       IX=IX+1
322       IF (IX .GT. 1) GO TO 121
323       WRITE(3,8)
324       WRITE(3,9)
325       WRITE (3,3)
326       GO TO 111
C         INITIALIZE SIMULATION
327   121 DO 123 I=1,NM
328       XZ(I) = 0.D0
329   123 XZD(I) = 0.D0
330       WRITE(3,8)
331       NSPAN = 1
332       PHO=GAMMA/386.4DO
333       T = 0.D0
334       SPECAL= .FALSE.
335       ICT = 1
336       SFLAG = .FALSE.
337       ISTEP = 0
338       N = 1
339       CON1 = 1.D0/3.D0
340       CON2 = 1.D0/(2.D0*DELT)
341       CON3 = 1.D0/DELT**2
342       CON4 = F/(PHO*AREA)
343       CON5 = 1.D0/DELT
344       AN = NBAY
345       SL = BL*NBAY
346       V = VEL*12.D0
347       DO 131 I=1,20
348       OUT(1,I) = 0.
349   131 OUTDP(I)=0.D0
350       DO 132 I= 3,14
351   132 DISTN(I) = .5D0*BL
352       DO 134 I=1,6,2
353       J=(I+1)/2
354       DISTN(I+14) =DIST(J)*BL
355       DISTN(I+15) = DIST(J)*BL
356       NUMB(I+14) = IBAY(J)
357       NUMB(I+15) = IBAY(J)
```

```
      134 CONTINUE
          WRITE(3,INPUT)
C         CALCULATE OMEGAS
          T1 = BL**4
          T2 = RHO*AREA
          DO 180 M=1,NM
      180 OMEGA(M)=DSQRT(E*QL(M)**4/(T1*T2))
C         CALCULATE SIMPLE SPAN MIDPOINT STATIC DEFL. AND BENDING MOMENT
      189 DEFS= F*(BL**3)/(48.D0*EI)
          DEFM= F*BL/4.D0
          WRITE (3,15) DEFS,DEFM
C         CALCULATE TRANSIT FREQUENCY&CROSSING FREQUENCY RATIO
          TRATIO = V/BL
          CRATIO =      PI*TRATIO/OMEGA(1)
          WRITE(3,16) TRATIO,CRATIO
C         CALCULATE MODE SHAPES FOR DESIRED TIME HISTORY OUTPUTS
          DO 192 I=3,20
          IF(IPL(I).EQ.0) GO TO 192
          CALL SHAPE(NM,NUMB(I),DISTN(I),BL,ANF,BNF,
     *  CNF,DNF,Y(1,I),NDAY,DL,JL)
      192 CONTINUE
C          DIFFERENTIAL EQUATION HAS THE FORM
C         W*XDDOT + B*XDOT + S*X =P
C         FORM W,B,S, MATRICES
          DO 198 I=1,NM
          W(I) = 1.D0
          B(I) = 2.*ZET(I)*OMEGA(I)
      198 S(I) =  OMEGA(I)*OMEGA(I)
C         SET UP THE "NASTRAN" ALGORITHM
C         ALGORITHM USES THE FOLLOWING DIFFERENCE EQUATION
C         X= AINV*(PP + A1*X1 +A2*X2)
C         WHERE
C         A = W/DELT**2 + B/(2.*DELT) +S/3.
C         AINV = INVERSE(A)
C         A1 = 2.*W/DELT**2 -S/3.
C         A2 = -W/DELT**2+B/(2.*DELT)-S/3.
C         PP= (P+P1+P2)/3
C         FORM A,A1,A2
          DO 200 I=1,NM
          A(I) = W(I)*CON3 +B(I)*CON2 + S(I)*CON1
          IF (DABS(A(I)) .LT. 1.D-33) A(I)=0.D0
          A1(I) = 2.D0*W(I)*CON3-S(I)*CON1
          IF (DABS(A1(I)) .LT. 1.D-33) A1(I)=0.D0
          A2(I) = -W(I)*CON3 + B(I)*CON2 -S(I)*CON1
          IF (DABS(A2(I)) .LT. 1.D-33) A2(I)=0.D0
          AINV(I) = 1.D0/A(I)
          IF (DABS(AINV(I)) .LT. 1.D-33) AINV(I)=0.D0
          B1(I) = A1(I)*AINV(I)
          IF (DABS(B1(I)) .LT. 1.D-33) B1(I)=0.D0
          B2(I) = A2(I)*AINV(I)
          IF (DABS(B2(I)) .LT. 1.D-33) B2(I)=0.D0
      200 CONTINUE
          IF(DEBUG) WRITE(3,DEBUG3)
C         SET INITIAL CONDITIONS
C         ASSUMPTION: XDD=0.,T<0,R=0.
          DO 210 I=1,NM
          X2(I) = XZ(I) - XZD(I)*DELT
          IF (DABS(X2(I)) .LT. 1.D-33) X2(I)=0.D0
          P2(I)= S(I)*X2(I)+B(I)*XZD(I)
      210 P1(I)= S(I)*XZ(I)+B(I)*XZD(I)
```

```
398           IF(.NOT. DEBUG) GO TO 400
399           WRITE(3,17) T
400           DO 240 I=1,NM
401       240 WRITE(3,18) I,P1(I),XZ(I),XZD(I)
402       400 T =T +DELT
403           ISTEP = ISTEP + 1
404           DEBUG = .FALSE.
405           IF(T.LT.DESTOP .AND.T.GT.DESTPT) DEBUG=.TRUE.
406           Z =V*T
      C       DETERMINE SPAN(BEAM) NUMBER
407           NSP= NSPAN
408           NSPAN = Z/SL + 1.D0
409           IF((NSPAN-NSP).GT.0) SFLAG= .TRUE.
      C       DETERMINE BAY(SPAN) NUMBER
410           N=(Z-(NSPAN-1)*SL)/BL+1.D0
      C       CALCULATE LOCALIZED COORDINATE
411           ZN = Z- (NSPAN-1)*SL-(N-1)*BL
412           IF(ZN .LT. 0.D0) GO TO 3000
413           IF (ZN.GT.BL) GO TO 3000
414           IF(DEBUG) WRITE(3,DEBUG1)
      C       FORM P
415           CALL SHAPI(NM,N,ZN,BL,ANF,BNF,CNF,DNF,Y(1,1),NBAY,QL,JL)
416           DO 560 I=1,NM
417       560 P(I) = Y(I,1)*CON4
418           IF(.NOT. SFLAG) GO TO 590
419           SFLAG = .FALSE.
420           IF(SPECAL) GO TO 575
421           SPECAL= .TRUE.
422           DO 570 I=1,NM
423           U2(I) = X2(I)
424           U1 (I) = X1(I)
425           V2(I) = P2(I)
426       570 V1(I) = P1(I)
427       575 DO 580 I=1,NM
428           P2(I) = 0.D0
429           P1(I) = 0.D0
430           X2(I) = 0.D0
431       580 X1(I) = 0.D0
      C       FORM PP
432       590 DO 600 I=1,NM
433           IF(SPECAL) VV(I) = (V1(I) + V2(I))*CON1
434           IF (.NOT. SPECAL) GO TO 600
435           IF (SPECAL .AND. DABS(VV(I)) .LT. 1.D-33) VV(I)=0.D0
436       600 PP(I)=(P(I)+P1(I)+P2(I))*CON1
      C       CALCULATE NEW X
437           DO 700 I=1,NM
438           IF(SPECAL) U(I) = VV(I)*AINV(I) +B1(I)*U1(I) + B2(I)*U2(I)
439           X(I) = PP(I)*AINV(I) + B1(I)*X1(I) + B2(I)*X2(I)
440           IF (DABS(X(I)) .LT. 1.D-33) X(I)=0.D0
441       700 CONTINUE
442           IF(.NOT. DEBUG) GO TO 935
443           WRITE(3,17) T
444           DO 900 I=1,NM
445       900 WRITE(3,18) I,P(I),X(I),Y(I,1),SIGRN(I),VV(I),U(I)
446           WRITE(3,DEBUG1)
447           WRITE(3,DEBUG2)
      C       SET PLOT AND 'PUNCH' OUTPUT
448       935 IF(MOD(ISTEP,IOUT) .NE. 0) GO TO 945
449           ICT = ICT+1
450           IF(IPL(1) .EQ.0) GO TO 936
```

MICROFILMED FROM
BEST AVAILABLE COPY

```
451          CALL DEFL1(NM,X,Y(1,1),SNORM,OUTDP(1))
452       936 IF(IPL(2).EQ.0) GO TO 937
453          CALL MOM1(NM,N,ZN,BL,ANF,BNF,CNF,DNF,QL,SNORM,
                *  F1,X,OUTDP(2),JL)
454       937 IF(.NOT. SPECAL) GO TO 939
455          DO 938 I=1,NM
456          XU(I) = U(I)
457          IF (DABS(XU(I)) .LT. 1.D-33) XU(I)=0.D0
458       938 CONTINUE
459          GO TO 941
460       939 DO 940 I=1,NM
461       940 XU(I) = X(I)
462       941 DO 942 I=3,20,2
463          IF(IPL(I) .EQ.0) GO TO 942
464          CALL DEFL1(NM,XU,Y(1,I),SNORM,OUTDP(I))
465       942 CONTINUE
466          DO 943 I=4,20,2
467          IF(IPL(I) .EQ.0) GO TO 943
468          CALL MOM1(NM,NUMB(I),DIST(I),BL,ANF,BNF,CNF,DNF,QL,
                *  SNORM,F1,XU,OUTDP(I),JL)
469       943 CONTINUE
470          DO 944 I=1,20
471       944 OUT(ICT,I) = OUTDP(I)
          C      ROTATE BACK VALUES
472       945 DO 950 I=1,NM
473          IF(.NOT.SPECAL) GO TO 948
474          U2(I) = U1(I)
475          IF (DABS(U2(I)) .LT. 1.D-33) U2(I)=0.D0
476          U1(I)= U(I)
477          IF (DABS(U1(I)) .LT. 1.D-33) U1(I)=0.D0
478          V2(I) = V1(I)
479          IF (DABS(V2(I)) .LT. 1.D-33) V2(I)=0.D0
480          V1(I) = 0.D0
481       948 P2(I) = P1(I)
482          IF (DABS(P2(I)) .LT. 1.D-33) P2(I)=0.D0
483          P1(I) = P(I)
484          IF (DABS(P1(I)) .LT. 1.D-33) P1(I)=0.D0
485          X2(I)= X1(I)
486          IF (DABS(X2(I)) .LT. 1.D-33) X2(I)=0.D0
487          X1(I)=X(I)
488          IF (DABS(X1(I)) .LT. 1.D-33) X1(I)=0.D0
489       950 CONTINUE
490          IF(T.LE.FINIS) GO TO 400
          C      PREPARE OUTPUT
491          DEL = DELT*ICUT
492          TF = FINIS
493          CON6 = 1.D0/DEFS
494          CON7 = 1.D0/DEFM
495          DO 1100 I=1,20,2
496          IF(IPL(I).EQ.0) GO TO 1050
497          DO 1030 J=1,ICT
498       1030 OUT(J,I)= -OUT(J,I)*CON6
499       1050 IF(IPL(I+1).EQ.0) GO TO 1100
500          DO 1080 J=1,ICT
501       1080 OUT(J,I+1)= -OUT(J,I+1)*CON7
502       1100 CONTINUE
          C      SET UP 'PUNCHED' OUTPUT
503          J=0
504          DO 1200 I=1,20
505          IF(IPL(I) .EQ.0) GO TO 1200
```

```
506           J= J+1
507           NOUT(J) = I
508     1200  CONTINUE
509           DO 1280 I= 1,J,5
510           WRITE(3,20)
511           TT= -DEL
512           L1= NOUT(I)
513           L2 = NOUT(I+1)
514           L3 = NOUT(I+2)
515           L4 = NOUT(I+3)
516           L5 = NOUT(I+4)
517           WRITE(3,21) L1,L2,L3,L4,L5
518           DO 1270 L=1,IGT
519           TT = TT +DEL
520           WRITE(3,22) L,TT,OUT(L,L1), OUT(L,L2), OUT(L,L3),
             * OUT(L,L4), OUT(L,L5)
521     1270  IF(PNCH) WRITE(2,19) L,TT,OUT(L,L1),OUT(L,L2),OUT(L,L3),
             * OUT(L,L4),OUT(L,L5)
522           IF(PNCH) WRITE(2,19)
523     1280  CONTINUE
524     2000  STOP
525     3000  WRITE(3,DEBUG1)
526           STOP
527           END

528           SUBROUTINE DEFL1(NM,X1,Y,SNORM,DEF)
      C       THIS SUBROUTINE CALCULATES THE BEAM DEFLECTION
529           IMPLICIT REAL*8(A-H,O-Z)
530           DIMENSION X1(NM), Y(NM), SNORM(NM)
531           DEF = 0.D0
532           DO 950 I=1,NM
533      950  DEF= DEF+X1(I)*Y(I)/SNORM(I)
534           RETURN
535           END

536           SUBROUTINE SHAP1(NM,N,ZN,BL,ANF,BNF,CNF,DNF,Y,NBAY,QL,JL)
      C       THIS SUBROUTINE CALCULATES 'NM' MODE SHAPES AT LOCATION'ZN'
      C       OF SPAN'N'
537           IMPLICIT REAL*8(A-H,O-Z)
538           LOGICAL SET
539           DIMENSION ANF(61,6),BNF(61,6),CNF(61,6),DNF(61,6)
540           DIMENSION Y(NM),QL(NM),JL(NM)
541           IT1=(-1)**N
542           DO 530 M=1,NM
543           SET=.FALSE.
544           IF (M .EQ. JL(M)) SET=.TRUE.
545           IF (.NOT. SET) GO TO 520
546           ZNP=QL(M)*ZN/BL
547           Y(M)=IT1*DSIN(ZNP)
548           IF (DABS(Y(M)) .LT. 1.D-33) Y(M)=0.D0
549           GO TO 530
550      520  Y(M)=ANF(M,N)*DSIN(QL(M)*ZN/BL)
             *   +BNF(M,N)*DSINH(QL(M)*ZN/BL)
             *   +CNF(M,N)*DSIN(QL(M)-QL(M)*ZN/BL)
             *   +DNF(M,N)*DSINH(QL(M)-QL(M)*ZN/BL)
551           IF (DABS(Y(M)) .LT. 1.D-33) Y(M)=0.D0
552      530  CONTINUE
553           RETURN
554           END
```

```
555           SUBROUTINE MOM1(NM,N,ZN,BL,ANE,BNE,CNE,DNE,OL,
     *     SNORM,FI,X,WMOMT,JL)
556           IMPLICIT REAL*8(A-H,O-Z)
557           LOGICAL SET
558           DIMENSION ANE(61,6),BNE(61,6),CNE(61,6),DNE(61,6)
559           DIMENSION SNORM(NM),X(NM),WMOM(61),CON(61),Y(61),OL(NM),JL(NM)
560           DATA INIT/0/
561           IF(INIT.NE.0) GO TO 200
562           INIT = 1
563           DO 150 I=1,NM
564       150 CON(I)=(OL(I)/BL)**2
565       200 IT1=(-1)**(N+1)
566           DO 400 M=1,NM
567           SET=.FALSE.
568           IF (M .EQ. JL(M)) SET=.TRUE.
569           IF (.NOT. SET) GO TO 300
570           ZNP=OL(M)*ZN/BL
571           WMOM(M)=IT1*CON(M)*DSIN(ZNP)
572           IF (DABS(WMOM(M)) .LT. 1.D-33) WMOM(M)=0.D0
573           GO TO 400
574       300 Y(M)=-ANE(M,N)*DSIN(OL(M)*ZN/BL)
     *       +BNE(M,N)*DSINH(OL(M)*ZN/BL)
     *       -CNE(M,N)*DSIN(OL(M)-OL(M)*ZN/BL)
     *       +DNE(M,N)*DSINH(OL(M)-OL(M)*ZN/BL)
575           IF (DABS(Y(M)) .LT. 1.D-33) Y(M)=0.D0
576           WMOM(M)=CON(M)*Y(M)
577           IF (DABS(WMOM(M)) .LT. 1.D-33) WMOM(M)=0.D0
578       400 CONTINUE
579           WMOMT = 0.D0
580           DO 600 I= 1,NM
581       600 WMOMT = WMOMT +WMOM(I)*X(I)/SNORM(I)
582           WMOMT = FI*WMOMT
583           RETURN
584           END

      $DATA
```

| LAMDA | SNORM |
|---|---|
| 3.14159265 | 63.0000 |
| 3.22053845 | 56.6971 |
| 3.34574589 | 278.9047 |
| 4.80841682 | 137.3204 |
| 5.52545593 | 62.9516 |
| 6.28318530 | 63.0000 |
| 7.44607325 | 70.9104 |
| 8.45020831 | 62.0470 |
| 9.42477795 | 63.0000 |
| 9.52627795 | 64.0587 |
| 10.50967644 | 65.1116 |
| 11.54682308 | 62.4563 |
| 12.56637060 | 63.0000 |
| 13.63041471 | 63.8567 |
| 14.67410632 | 62.5733 |
| 15.70796325 | 63.0000 |
| 15.72996325 | 62.9922 |
| 16.76412669 | 63.3609 |
| 17.80978965 | 62.7564 |
| 18.84955590 | 63.0000 |

## APPENDIX II
## EQUATIONS OF VEHICLE MOTION

The origin 0 of the (x, y, z) reference frame is located at the mean axle elevation $\eta$ above the guideway centerline contour, moving with the same trajectory speed u in the same circular arc of radius R as the vehicle, as shown in Fig. 74). However, the reference axes for the respective principal moments of inertia of the vehicle ($I_x$, $I_y$, $I_z$) are parallel to x, y, z, but through the mass center G. The velocity and acceleration of the origin 0 are

$$\dot{\underset{\sim}{R}} = u\underset{\sim}{i} \tag{1}$$

$$\ddot{\underset{\sim}{R}} = -(u^2/R)\underset{\sim}{j} \tag{2}$$

The angular velocity of these axes, with unit vectors ($\underset{\sim}{i}$,$\underset{\sim}{j}$,$\underset{\sim}{k}$), is

$$\underset{\sim}{\omega} = \dot{\alpha}\,\underset{\sim}{i} + \dot{\beta}\,\underset{\sim}{j} - (u/R)\underset{\sim}{k} \tag{3}$$

which maintains the plane z=0 as always coincident with the vehicle axles and parallel with the guideway surface. By previous assumptions, it follows that $\dot{\omega}=0$.

The absolute velocity $\underset{\sim}{v}$ and acceleration $\underset{\sim}{a}$ of any point on the vehicle body at a distance $\underset{\sim}{\rho}$ from the origin 0 are expressed as

$$\underset{\sim}{v} = \dot{\underset{\sim}{R}} + \dot{\underset{\sim}{\rho}} + \underset{\sim}{\omega}\times\underset{\sim}{\rho} \tag{4}$$

$$\underset{\sim}{a} = \ddot{\underset{\sim}{R}} + \ddot{\underset{\sim}{\rho}} + \underset{\sim}{\omega}\times(\underset{\sim}{\omega}\times\underset{\sim}{\rho}) + 2\underset{\sim}{\omega}\times\dot{\underset{\sim}{\rho}} \tag{5}$$

where

$$\underset{\sim}{\rho} = \rho_1\,\underset{\sim}{i} + (y + \rho_1\theta + \rho_2 - \rho_3\phi)\,\underset{\sim}{j} + \rho_3\,\underset{\sim}{k} \tag{6}$$

The coordinates ($\rho_1$, $\rho_2$, $\rho_3$) locate the desired material point referenced at vehicle equilibrium (at $y=\theta=\phi=0$). The velocity and acceleration of this material point relative to origin 0 are obtained by differentiation of Eq. (6), or

$$\dot{\underset{\sim}{\rho}} = (\dot{y} + \rho_1\dot{\theta} - \rho_3\dot{\phi})\,\underset{\sim}{j} \tag{7}$$

$$\ddot{\underset{\sim}{\rho}} = (\ddot{y} + \rho_1\ddot{\theta} - \rho_3\ddot{\phi})\,\underset{\sim}{j} \tag{8}$$

Thus, with Eqs. (1) - (3) and (6) - (8), Eqs. (4) and (5) give the absolute velocity and acceleration at ($\rho_1$, $\rho_2$, $\rho_3$). In the alternative matrix notation, these are $\underset{\sim}{v} = \{v_x\ v_y\ v_z\}^T$ and $\underset{\sim}{a} = \{a_x\ a_y\ a_z\}^T$

where $\{\ \}^T$ denotes the transpose. The components of v and the lateral acceleration $a_y$ are

$$v_x = u + \dot{\beta}\rho_3 + \rho_0 u/R \tag{9a}$$

$$v_y = \dot{\rho} - \dot{\alpha}\rho_3 - \rho_1 u/R \tag{9b}$$

$$v_z = \dot{\alpha}\rho_0 - \dot{\beta}\rho_1 \tag{9c}$$

$$a_y = -u^2/R + \ddot{y} + \rho_1\ddot{\theta} - \rho_3\ddot{\phi} - \dot{\alpha}(\dot{\alpha}\rho_0 - \dot{\beta}\rho_1) - (u/R)(\dot{\beta}\rho_3 + \rho_0 u/r) \tag{10a}$$

where

$$\rho_0 = y + \rho_1\theta + \rho_2 - \rho_3\phi \tag{10b}$$

To obtain the rotational energy of the vehicle, its absolute angular velocity, $\underset{\sim}{\Omega}$, is needed. Since the angular velocity $\underset{\sim}{\omega}_r$ of the vehicle relative to the (x, y, z) reference axes is

$$\underset{\sim}{\omega}_r = \dot{\phi}\,\underset{\sim}{i} + \dot{\theta}\,\underset{\sim}{k} \tag{11}$$

and the angular velocity $\omega$ of this reference frame is given by Eq. (3), then $\underset{\sim}{\Omega}$ is the sum of these, of

$$\underset{\sim}{\Omega} = \{(\dot{\phi} + \dot{\alpha})\ \dot{\beta}\ (\dot{\theta} - u/R)\}^T = \{\Omega_x\ \Omega_y\ \Omega_z\}^T \tag{12}$$

The total kinetic energy T of the vehicle is the sum of the translational and rotational energies, or

$$T = \frac{1}{2} m\, \underset{\sim}{v}_G^T\, \underset{\sim}{v}_G + \frac{1}{2}\, \underset{\sim}{\Omega}^T\, \underset{\sim}{I}\, \underset{\sim}{\Omega} \tag{13}$$

where $v_G$ is the column vector whose three components are the absolute velocity at the mass center G, given by from Eqs. (9) at $\rho_1 = \rho_2 = 0$ and $\rho_3 = h$; $\underset{\sim}{I}$ is the inertia matrix whose only nonzero terms are the diagonal elements $I_x$, $I_y$, $I_z$; and $\underset{\sim}{\Omega}$ is the column vector whose elements are given by Eq. (12). Thus, Eq. (13) becomes

$$\begin{aligned} 2T = {} & m[u + \dot{\beta}h + (y - \phi h)(u/R)]^2 \\ & + m(\dot{y} - \dot{\phi}h - \dot{\alpha}h)^2 + m\,\dot{\alpha}^2(y - \phi h)^2 \\ & + I_x(\dot{\phi} + \dot{\alpha})^2 + I_y\,\dot{\beta}^2 + I_z(\dot{\theta} - u/R)^2 \end{aligned} \tag{14}$$

The virtual work $\delta W$ done by the generalized conservative and nonconservative forces $Q_y$, $Q_\phi$, $Q_\theta$ acting through respective virtual

displacements $\delta y$, $\delta\phi$ and $\delta\theta$, is expressed as

$$\delta W = Q_y\,\delta y + Q_\phi\,\delta\phi + Q_\theta\,\delta\theta \tag{15}$$

Consider the composition the generalized forces. Linear spring and coulomb damping forces and their moments are accounted for in a straightforward manner, as is the wind force $F_w$, acting as shown in Fig. 74. As a component of $Q_\phi$, there is an unbalanced "pendulum" moment contributing to roll motion, which is approximated by $mgh\phi\cos\alpha\cos\beta$. Perturbation forces arise because of guideway roughness and construction tolerances. Let $y_1 = y_1(t)$ characterize these wall tolerances, being the deviation from the mean sidewall separation dimension, between the front lateral suspension points on the moving vehicle. The counterpart tolerance dimension $y_2 = y_2(t)$ between the back lateral suspension points thus has a time lag of $2L/u$, so that

$$y_2(t) = y_1(t - 2L/u) \tag{16}$$

Let $z_0 = z_0(t)$ represent the dimensional tolerance and roughness deviations from the plane $z = \eta$ on the levitation surface, across its width only. The supression of the length variation in $z_0$, forward to rear of the vehicle at a given instant, is consistent with the supression of vehicle heave and pitch vibrations in this study. Thus, $z_0$ contributes to the roll force only.

With these assumptions, the generalized force components of Eq. (15) become

$$\begin{aligned}
Q_y &= F_w - 4ky + 4pk\phi - k(y_1 + y_2) \\
&\quad - 4c\dot{y} + 4pc\dot{\phi} - c(\dot{y}_1 + \dot{y}_2) \\
Q_\phi &= -\ell_z F_w - 4(p^2k + d^2K)\phi + 4pky + 2dKz_0 + pk(y_1 + y_2) \\
&\quad + mgh\phi\cos\alpha\cos\beta - 4(p^2c + d^2C)\dot{\phi} + 4pc\dot{y} + 2dC\dot{z}_0 + pc(\dot{y}_1 + \dot{y}_2) \\
Q_\theta &= \ell_x F_w - 4kL^2\theta - kL(y_1 - y_2) - 4c\,L^2\,\dot{\theta} \\
&\quad - cL(\dot{y}_1 - \dot{y}_2)
\end{aligned} \tag{17}$$

When Lagrange's equations, or

$$\frac{d}{dt}\left(\frac{\partial T}{\partial \dot{g}_i}\right) - \frac{\partial T}{\partial g_i} = Q_i; \quad (g_i = y, \ \phi, \ \theta) \tag{18}$$

are employed with Eqs. (14) and (17), the following equations of vehicle motion are obtained.

$$\begin{aligned} &m\ddot{y} + 4c\dot{y} + (4k - m\dot{\alpha}^2 - mu^2/R^2)y \\ &- mh\ddot{\phi} - 4pc\dot{\phi} - (4pk - mh\dot{\alpha}^2 - mhu^2/R^2)\phi \\ &= -k(y_1 + y_2) - c(\dot{y}_1 + \dot{y}_2) + F_w + mu(u + \dot{\beta}h)/R \end{aligned} \tag{19}$$

$$\begin{aligned} &(I_x + mh^2)\ddot{\phi} + 4(p^2c + d^2C)\dot{} + [4(p^2k + d^2K) \\ &- mh^2\dot{\alpha}^2 - mu^2h^2/R^2 - mghcos\alpha cos\beta]\phi \\ &- mh\ddot{y} - 4pc\dot{y} - (4pk - mh\dot{\alpha}^2 - mhu^2/R^2)y \\ &= pk(y_1 + y_2) + pc(\dot{y}_1 + \dot{y}_2) + 2dKz_0 + 2dC\dot{z}_0 \\ &- \ell_z F_w - muh(u + \dot{\beta}h)/R \end{aligned} \tag{20}$$

$$I_z\ddot{\theta} + 4cL^2\dot{\theta} + 4kL^2\theta = -kL(y_1 - y_2) - cL(\dot{y}_1 - \dot{y}_2) + \ell_x F_w \tag{21}$$

In nondimensional form, in terms of the system parameters defined by Eqs. (64-70), the above equations are reduced to state variable form, where $x_7'$, $x_8'$ and $x_9'$ are defined by Eq. (74) of Chapter 5.

$$\begin{aligned} x_2' = &- (1 - (R_x^2 + 1)^{-1}P_0)\xi_1\bar{\Omega}_1 x_2 \\ &+ [(1 - (R_x^2 + 1)^{-1}P_0)\bar{\Omega}_1^2 - (1 - (R_x^2 + 1)^{-1}) \cdot \\ &\quad (\alpha'^2 + U^2)]x_1 \\ &+ [2P_0(1 - (R_x^2 + 1)^{-1}P_0)\xi_1\bar{\Omega}_1 + D_o^2\xi_3\bar{\Omega}_3 \cdot \\ &\quad (R_x^2 + 1)^{-1}]x_4 \\ &+ [P_0(1 - (R_x^2 + 1)^{-1}P_0)\bar{\Omega}_1^2 - (1 - (R_x^2 + 1)^{-1}) \cdot \\ &\quad \cdot(\alpha'^2 + U^2) - (R_x^2 + 1)^{-1}D_o\bar{\Omega}_3^2 \\ &+ (R_x^2 + 1)^{-1}V]x_3 \end{aligned}$$

$$- \tfrac{1}{4}(1 - (R_x^2 + 1)^{-1})P_0\bar{\Omega}_1^2(x_7 + x_8)$$

$$- \tfrac{1}{2}(1 - P_0(R_x^2 + 1)^{-1})\xi_1\bar{\Omega}_1(x_7' + x_8')$$

$$+ \tfrac{1}{2} D_0(1 + R_x^2)^{-1}\bar{\Omega}_3^2 x_9$$

$$+ D_o(1 + R_x^2)^{-1}\xi_3\bar{\Omega}_3 x_9'$$

$$+ (1 - L_z)(R_x^2 + 1)^{-1}x_{10}$$

$$+ (1 - (R_x^2 + 1)^{-1})(U^2R_0 + U\beta') \qquad (22)$$

$$x_4' = [- 2 R_x^{-2}((P_0 - 1)P_0\xi_1\bar{\Omega}_1 + D_0^2\xi_3\bar{\Omega}_3)]x_4$$

$$- R_x^{-2}[(P_0 - 1)P_0\bar{\Omega}_1^2 + D_0\bar{\Omega}_3^2 - V]x_3$$

$$+ 2R_x^{-2}(P_0 - 1)\xi_1\bar{\Omega}_1 x_2 + R_x^{-2}(P_0 - 1)\bar{\Omega}_1^2 x_1$$

$$+ \tfrac{1}{4} R_x^{-2}(P_0 - 1)\bar{\Omega}_1^2(x_7 + x_8)$$

$$+ \tfrac{1}{2} R_x^{-2}(P_0 - 1)\xi_1\bar{\Omega}_1(x_7' + x_8')$$

$$+ R_x^{-2}(1 - L_z)x_{10} + R_x^{-2}D_0\bar{\Omega}_3^2 x_9$$

$$+ R_x^{-2}D_0\xi_3\bar{\Omega}_3 x_9' \qquad (23)$$

$$x_6' = -2\xi_\theta x_6 - x_5 - (x_8 - x_7)/4L_0$$

$$+ \xi_\theta(x_8' - x_7') + L_x x_{10} \qquad (24)$$

From Eq. (10a) above and the nondimensional parameters in Chapter 5, Eqs. (65-70), the nondimensional form of lateral acceleration is

$$
\begin{aligned}
a_y^* &= a_y/h\Omega_\theta^2 \\
&= x_2' + [-\alpha'^2 - (U/R_0)^2]x_1 - x_6'\rho_3/h \\
&\quad - 2\alpha x_4\rho_2/h + [\alpha'^2\rho_3/h - U\beta'\rho_2/(hR_0) \\
&\quad + (U/R_0)^2\rho_3/h]x_3 + x_6'\rho_1/h + 2Ux_4\rho_2/(hR_0) \\
&\quad - [\alpha'^2\rho_1/h + \alpha'\beta'\rho_2/h + (U/\bar{R})^2\rho_1/h]x_3
\end{aligned} \tag{25}
$$

From Eq. (6) above and from the parameters of Chapter 5, the nondimensional lateral deflection at the guidewheels has the form

$$
\rho_y^* = \rho_y/h = x_1 - x_3\rho_3/h + x_5\rho_1/h \tag{26}
$$

where $\rho_2 = d$ has been deleted to give the suspension displacements relative to static equilibrium.

The (9 x 14) partitional array $[\underset{\sim}{C} \vdots \underset{\sim}{D}]$ of Eq. (91) is given by

$$
\left[\begin{array}{cccccccccccccc}
1 & 0 & 0 & 0 & 0 & 0 & 0 & 0 & 0 & 0 & 0 & 0 & 0 & 0 \\
0 & 1 & 0 & & & & & & 0 & & & & & 0 \\
 & \multicolumn{5}{c}{\text{row 2 of } \underset{\sim}{A}} & & & \vdots & \multicolumn{5}{c}{\text{row 2 of } \underset{\sim}{B}} & \\
0 & 0 & 1 & 0 & & & & & 0 & & & & & 0 \\
0 & 0 & 0 & 1 & 0 & & & & 0 & & & & & 0 \\
 & \multicolumn{5}{c}{\text{row 4 of } \underset{\sim}{A}} & & & \vdots & \multicolumn{5}{c}{\text{row 4 of } \underset{\sim}{B}} & \\
0 & 0 & 0 & 0 & 1 & 0 & & & 0 & & & & & 0 \\
0 & 0 & 0 & 0 & 0 & 1 & 0 & & 0 & & & & & 0 \\
 & \multicolumn{5}{c}{\text{row 6 of } \underset{\sim}{A}} & & & \vdots & \multicolumn{5}{c}{\text{row 6 of } \underset{\sim}{B}} &
\end{array}\right] \tag{27}
$$

The only nonzero component of the column vector $\underset{\sim}{c}$ of Eq. (71) is its second element, given by

$$
c_2 = [1 - (R_x^2 + 1)^{-1}](U^2R_0 + U\beta') \tag{28}
$$

The only nonzero component of the (9 x 1) vector $c_a$ of Eq. (87) is its third element, given by $c_{a3} = c_2$, the above element.

# APPENDIX III

# VEHICLE RESPONSE PROGRAM

```
      DIMENSION P(31)
      DIMENSION A(10,10),C(10,10)
      DIMENSION A1(10,10),A2(10,10),A3(10,10)
      DIMENSION AB(10),ORD(10)
      DIMENSION B(20,4),VECC(10),XBAR(10),XEBAR(9)
      DIMENSION Q(4,4),COV(14,14),CD(9,14),CA(9),CD2(9,14)
      DIMENSION CD3(14,9),AA(9),SIGRHO(10)
      DIMENSION RHOBAR(10),APHO(10),SIGRO(10)
      DIMENSION AB1(10),YMEAN(10)
      DIMENSION XU(14)
      DIMENSION DXBAR(10)
C
C     PROGRAM PACKAGE FOR COMPUTING RMS LATERAL ACCELERATIONS
C
C     INPUT STRUCTURE:
C
C     CARD(S)                                   CONTENT
C     1          NUMBER OF PARAMETERS AND SYSTEM ORDER IN 2I2  (LP,N)
C     2 THROUGH (LP+1)    PARAMETERS  P(1) THROUGH P(LP), ONE PER CARDIN F10.0
C     LP+2    POSITION NUMBER OF PARAMETER TO BE SWEPT (NPVAR) IN I5
C     LP+3    SIZE OF PARAMETER VARIATION (PVAR) IN F10.0
C     LP+4    LIMITS OF PARAMETER RANGE IN 2F10.0
C     LP+5 THROUGH LP+7          THREE POINTS AT EXTREMA OF PLANE SWEPT FOR MAX
C                     RMS ACCELERATIONS.  X,Y,Z COORDINATES IN 3F10.0
C     LP+8    MESH SIZE (XVAR,YVAR,ZVAR) IN X,Y AND Z DIRECTIONS IN 3F10.0
C
C     NRC IS ROW DIMENSION OF ARRAYS IN CALLING PROGRAM
      NRC=10
C     IN IS THE INPUT UNIT NUMBER
C     IOUT IS THE OUTPUT UNIT NUMBER
      IN=1
      IOUT=3
C     LP IS NUMBER OF PARAMETERS IN P VECTOR
C     N IS SYSTEM ORDER
    1 READ(IN,2,END=9999)LP,N
    2 FORMAT(2I2)
      CALL READER(P,LP,NPVAR,XMIN,YMIN,ZMIN,XVAR,YVAR,ZVAR,PVAR,
     $ITERX,ITERY,ITERZ,ITERP,PMIN)
C
C     PRINT OF PARAMETER AND MESH RANGES
C
      WRITE(IOUT,5)(P(I),I=1,LP)
    5 FORMAT(1H1,'INITIAL PARAMETER LIST'/15(/1X,F12.4))
      WRITE(IOUT,10)XMIN,YMIN,ZMIN
   10 FORMAT(1X,'THE MESH STARTS AT',3F12.4)
      NODES=ITERX*ITERY*ITERZ
      WRITE(IOUT,15)NODES,ITERX,ITERY,ITERZ
   15 FORMAT(1X,'SCANS',I7,'NODES BY TAKING',3I7,'STEPS IN X,Y,Z DIRECTI
     $ONS RESPECTIVELY')
```

```
      WRITE(IOUT,20)XVAR,YVAR,ZVAR
   20 FORMAT(1X,'THIS IS STEPS OF',3F12.4,'UNITS IN X,Y,Z DIRECTIONS')
      WRITE(IOUT,25)NPVAR,PVAR,PMIN
   25 FORMAT(1X,//' THE',I5,'TH PARAMETER IS VARIANT, WITH VARIATIONS OF'
     $,F12.4,'BEGINNING AT',F12.4)
C
CC    BEGINNING OF PARAMETER SWEEP
C
         DO 500 IP=1,ITERP
           P(NPVAR)=PMIN+(IP-1)*PVAR
C
CC    ESTABLISHMENT OF A AND C FROM PARAMETERS
C
      CALL STATE(P,A,B,C,LP,NPO,N,1.0)
         WRITE(IOUT,27)
   27    FORMAT(1H1)
         WRITE(IOUT,28)
   28    FORMAT(1X,'COEFFICIENT MATRIX'//)
         DO 30 I=1,N
            WRITE(IOUT,29)(A(I,J),J=1,N)
   29       FORMAT(1X,10E12.3)
   30    CONTINUE
         WRITE(IOUT,31)
   31    FORMAT(1X,//' CORRELATION MATRIX'//)
         DO 35 I=1,N
            WRITE(IOUT,29)(C(I,J),J=1,N)
   35    CONTINUE
      WRITE(IOUT,36)
   36 FORMAT(1X,//'INPUT COEFFICIENT ARRAY'//)
      DO 37 I=1,N
         WRITE(IOUT,29)(B(I,J),J=1,4)
   37 CONTINUE
C     SOLVE STEADY STATE COVARIANCE EQUATION
         CALL SERIES(A,C,N,NRO,A1,A2,A3)
C     COMPUTE RESIDUAL FROM SOLN. OF STATE COVARIANCE EQUATION
      CALL EQUATE(C,A1,NRO,N,N)
      CALL STATE(P,A,B,C,LP,NRO,N,1.)
         CALL RESID(A,C,A1,A2,A3,N,NPO)
C     COMPUTE MEANS OS STATES
      DO 40 I=1,10
      VECC(I)=0.0
   40 CONTINUE
      R=P(8)
      RX=P(9)
      U1=P(5)/(P(8)*P(1))
      RXINV=((RX**2)+1)**(-1)
      VECC(2)=(1-RXINV)*((U1**2)*R+U1*P(7))
      CALL STATE(P,A,B,C,LP,NRO,N,0.0)
         CALL EQUATE(A1,C,NRO,N,N)
      CALL PROD(A,A,A2,N,N,N,NRO,NRO,NPO)
```

```
      CALL CINV(A2,A1,N,NRO,IFLAG)
      CALL EQUATE(A1,A2,NRO,N,N)
      CALL SUM(A2,A2,A2,0.0,-1.0,N,N,NRO,NRO,NRO)
      CALL PROD(A2,A,A1,N,N,N,NRO,NRO,NRO)
      DO 42  I=1,N
      XBAR(I)=0.0
      DO 41  J=1,N
      XBAR(I)=A1(I,J)*VECC(J)+XBAR(I)
   41 CONTINUE
   42 CONTINUE
      DO 44  I=1,10
      DXBAR(I)=0.0
      DO 43  J=1,10
      DXBAR(I)=A(I,J)*XBAR(J)+DXBAR(I)
   43 CONTINUE
      DXBAR(I)=DXBAR(I)+VECC(I)
   44 CONTINUE
      XBAR(1)=XBAR(1)
      XBAR(2)=XBAR(2)
      XBAR(3)=DXBAR(2)
      XBAR(4)=XBAR(3)
      XBAR(5)=XBAR(4)
      XBAR(6)=DXBAR(4)
      XBAR(7)=XBAR(5)
      XBAR(8)=XBAR(6)
      XBAR(9)=DXBAR(6)
      DO 52  I=1,4
      DO 51  J=1,4
      C(I,J)=0.0
   51 CONTINUE
   52 CONTINUE
      C(1,1)=P(22)*U1
      C(2,2)=P(23)*U1
      C(3,3)=P(24)*U1
      C(4,4)=P(25)
      CALL CINV(A,A1,N,NRO,IFLAG)
      CALL PROD(A1,B,A2,N,4,N,10,20,10)
      CALL PROD(A2,Q,A3,N,4,4,10,4,10)
      CALL SUM(A3,A3,A3,0.0,-1.0,N,N,NRO,NRO,NRO)
      DO 60  I=1,10
      DO 55  J=1,10
      COV(I,J)=C(I,J)
   55 CONTINUE
   60 CONTINUE
      DO 70  I=11,14
      DO 65  J=11,14
      I2=I-10
      J2=J-10
      COV(I,J)=Q(I2,J2)
   65 CONTINUE
```

```
 70 CONTINUE
    DO 80 I=1,10
    DO 75 J=11,14
    J2=J-10
    COV(I,J)=A3(I,J2)
 75 CONTINUE
 80 CONTINUE
    DO 90 I=11,14
    DO 85 J=1,10
    I2=I-10
    COV(I,J)=A3(J,I2)
 85 CONTINUE
 90 CONTINUE
    DO 100 I=1,9
    DO 95 J=1,14
    CD(I,J)=0.0
 95 CONTINUE
100 CONTINUE
    CD(1,1)=1.0
    CD(2,2)=1.0
    DO 105 I=1,10
    CD(3,I)=A(2,I)
105 CONTINUE
    DO 110 I=11,14
    I2=I-10
    CD(3,I)=B(2,I2)
110 CONTINUE
    CD(4,3)=1.0
    CD(5,4)=1.0
    DO 115 I=1,10
    CD(6,I)=A(4,I)
115 CONTINUE
    DO 120 I=11,14
    I2=I-10
    CD(6,I)=B(4,I2)
120 CONTINUE
    CD(7,5)=1.0
    CD(8,6)=1.0
    DO 125 I=1,10
    CD(9,I)=A(6,I)
125 CONTINUE
    DO 130 I=11,14
    I2=I-10
    CD(9,I)=B(6,I2)
130 CONTINUE
    DO 135 I=1,9
    CA(I)=0.0
135 CONTINUE
    CA(3)=VECC(2)
    CALL PROD(CD,COV,CD2,9,14,14,9,14,9)
```

```
      CALL TRANSP(CD,CD3,9,14,9,14)
      CALL PICD(CD2,CD3,A2,9,9,14,9,14,10)
      DO 137 I=1,10
      XU(I)=XBAR(I)
  137 CONTINUE
      DO 139 I=11,14
      XU(I)=0.0
  139 CONTINUE
      DO 143 I=1,9
      COV(1,I)=0.0
      DO 141 J=1,14
      COV(1,I)=CD(I,J)*XU(J)+COV(1,I)
  141 CONTINUE
  143 CONTINUE
      DO 147 I=1,9
      DO 145 J=1,9
      A3(I,J)=COV(1,I)*CA(J)
  145 CONTINUE
  147 CONTINUE
      CALL SUM(A2,A3,A3,1.0,1.0,9,9,10,10,10)
      DO 153 I=1,9
      DO 151 J=1,14
      COV(I,J)=CA(I)*XU(J)
  151 CONTINUE
  153 CONTINUE
      CALL PICD(COV,CD3,A2,9,9,14,14,14,10)
      CALL SUM(A2,A3,A3,1.0,1.0,9,9,10,10,10)
      DO 175 I=1,9
      DO 170 J=1,9
      A2(I,J)=CA(I)*CA(J)
  170 CONTINUE
  175 CONTINUE
      DO 1752 I=1,9
      DO 1751 J=1,9
      A3(I,J)=A3(I,J)+XEBAR(I)*XEBAR(J)
 1751 CONTINUE
 1752 CONTINUE
      CALL SUM(A2,A3,A3,1.0,1.0,9,9,10,10,10)
      BHO1=P(13)
      BHO2=P(12)
      BHO3=P(11)
      BHOBAR(IP)=XEBAR(1)-BHO3*XEBAR(4)+BHO1*XEBAR(7)
      ABHO(1)=1
      ABHO(2)=0
      ABHO(3)=0
      ABHO(4)=-BHO3
      ABHO(5)=0
      ABHO(6)=0
      ABHO(7)=BHO1
      ABHO(8)=0
```

```
      ARHO(9)=0
      DO 177 I=1,9
      XBAR(I)=0
      DO 176 J=1,9
      XBAR(I)=ARHO(I)*A3(I,J)+XBAR(I)
  176 CONTINUE
  177 CONTINUE
      SIGRO(IP)=0.0
      DO 178 I=1,9
      SIGRO(IP)=XBAR(I)*ARHO(I)+SIGRO(IP)
  178 CONTINUE
      YMEAN(IP)=0.0
      DO 179 I=1,9
      YMEAN(IP)=ARHO(I)*XEBAR(I)+YMEAN(IP)
  179 CONTINUE
C
C
         AXMAX=0.0
      AYMAX=0.0
         AZMAX=0.0
         DO 400 IX=1,ITERX
            DO 300 IY=1,ITERY
               DO 200 IZ=1,ITERZ
                  RHO1=XMIN+XVAR*(IX-1)
                  RHO2=YMIN+YVAR*(IY-1)
                  RHO3=ZMIN+ZVAR*(IZ-1)
C     MATRIX FORM OF THE KINEMATICS
      AA(1)=-(P(6)**2)-((P(5)/P(8))**2)
      AA(2)=0.0
      AA(3)=1.0
      AA(4)=-(P(6)**2)*RHO3+(P(5)/P(8))*P(7)*RHO2+((P(5)/P(8))**2)*RHO3
      AA(5)=-2*P(6)*RHO2
      AA(6)=-RHO3
      AA(7)=-(P(6)**2)*RHO1-P(6)*P(7)*RHO2-((P(5)/P(8))**2)*RHO1
      AA(8)=2*(P(5)/P(8))*RHO2
      AA(9)=RHO1
      SEEA=-(P(5)**2)/P(8)-(P(6)**2)*RHO2+P(6)*P(7)*RHO1
     $-(P(5)/P(8))*P(7)*RHO3-((P(5)/P(8))**2)*RHO2
      DO 185 I=1,9
      XEAE(I)=0
      DO 180 J=1,9
      XEAE(I)=AA(J)*A3(J,I)+XBAR(I)
  180 CONTINUE
  185 CONTINUE
      SIGXE=0
      DO 190 I=1,9
      SIGXE=XEAR(I)*AA(I)+SIGXE
  190 CONTINUE
      SCALAR=0
      DO 220 I=1,9
```

```
      SCALAR=AA(I)*XEBAR(I)+SCALAR
  220 CONTINUE
      SIGXE=SIGXE+SCALAR*SEEA
      DO 225 I=1,9
      XEAR(I)=SEEA*XEBAR(I)
  225 CONTINUE
      SCALAR=0.0
      DO 230 I=1,9
      SCALAR=XBAR(I)*AA(I)+SCALAR
  230 CONTINUE
      SIGXE=SIGXE+SCALAR+SCALAR+SEEA**2
      IF(ABS(SIGXE).GT.AYMAX)AYMAX=ABS(SIGXE)
      SAYMAX=SQRT(ABS(AYMAX))
  200          CONTINUE
  300        CONTINUE
  400     CONTINUE
          AB(IP)=P(NPVAR)
      AE1(IP)=P(NPVAR)
      CRD(IP)=SAYMAX*1.5/32.2
  500 CONTINUE
      WRITE(IOUT,600)(AB(I),ORD(I),YMEAN(I),SIGRO(I),I=1,ITERP)
  600 FORMAT(1X,4E10.3)
      GO TO 1
 9999 STOP
      END
      SUBROUTINE STATE(PR,A,B,Q,LP,NRO,N,OREQ)
      DIMENSION PR(LP),A(NRO,NRO),Q(NRO,NRO),
     $SAVE(20)
      DIMENSION A1(20,20),A2(20,20),SAVE1(20,20),SAVE2(20,20),
      DIMENSION SAVE3(20,20)
      DIMENSION B(20,4)
C  IF CRIO=1.0 THEN BQBT IS GENERATED
      ICUT=3
      M=4
C
C     ZERO THROUGH A AND C, THEN ESTABLISH NONZERO ELEMENTS
C
      DO 10 I=1,N
         DO 5 J=1,N
            A(I,J)=0.0
    5    CONTINUE
         DO 7 J=1,M
            B(I,J)=0.0
    7    CONTINUE
   10 CONTINUE
C
C     ESTABLISHMENT OF VARIABLE NOMENCLATURE
      OMEGA=PR(1)
      OMEGA3=PR(2)
```

```
      ZETA1A=PR(3)
      ZETA3=PR(4)
      U1=PR(5)/(PR(8)*PR(1))
      DALPHA=PR(6)
      DBETA=PR(7)
      D=PR(8)
      RX=PR(9)
      RZ=PR(10)
      P=PR(11)
      L=PR(12)
      EI=PR(13)
      V=PR(14)
      GNU1=PR(15)
      GNU2=PR(16)
      GNU3=PR(17)
      GNU4=PR(18)
      ECAP=PR(19)
      ELX=PR(20)
      ELZ=PR(21)
      C1=PR(22)*U1
      C2=PR(23)*U1
      C3=PR(24)*U1
      C4=PR(25)
      OMEGA1=PR(26)
      ZETA1=PR(27)
      DELAY=2*EL/(U1*R)
C
C     SET NONZERO ELEMENTS OF COEFFICIENT ARRAY
C
      RRX=((1/RX)**2+1)
      RXINV=(RX**2+1)**(-1)
      ARX=RX**(-2)
      OM1RAT=OMEGA1/OMEGA
      OM3RAT=OMEGA3/OMEGA
      A(1,2)=1.0
      A(2,1)=(1-RXINV*P)*OM1RAT**2-(1-RXINV)*(DALPHA**2+U1**2)
      A(2,1)=(-A(2,1))
      A(2,2)=-(1-RXINV*P)*ZETA1*OM1RAT)
      A(2,3)=P*(1-RXINV*P)*OM1RAT**2-(1-RXINV)*(DALPHA**2+U1**2)-RXINV
     $*D*OM3RAT**2+RXINV*V
      A(2,4)=2*P*(1-RXINV*P)*ZETA1*OM1RAT+D**2*ZETA3*OM3RAT*RXINV
      A(3,4)=1.0
      A(4,1)=ARX*(P-1)*OM1RAT**2
      A(4,2)=2*ARX*(P-1)*ZETA1*OM1RAT
      A(4,3)=-(ARX)*((P-1)*P*OM1RAT**2+D*OM3RAT**2-V)
      A(4,4)=(-2)*ARX*((P-1)*P*ZETA1*OM1RAT
     $+D**2*ZETA3*OM3RAT)
      A(5,6)=1.0
      A(6,5)=(-1.0)
      A(6,6)=(-2.0)*ZETA
```

```
      A(7,7)=-GNU1
      A(6,7)=(-0.25)/EL-A(7,7)*ZETA
      A(8,8)=-GNU2
      A(9,9)=-GNU3
      A(10,10)=-BCAP*GNU4
      E(7,1)=-A(7,7)
      E(8,2)=-A(8,8)
      E(9,3)=-A(9,9)
      E(10,4)=GNU4/OMEGA
      A(2,7)=(-0.25)*(1-RXINV)*P*OM1RAT**2-A(7,7)*0.5*P*RXINV*ZETA1*
     $OM1RAT
      A(2,8)=A(2,7)
      A(2,9)=(-0.5)*(1-RXINV)*D*OM3RAT)+A(9,9)*D*RXINV*ZETA3*OM3RAT
      A(2,10)=(1-ELZ)*RXINV
      A(4,7)=0.25*(P-1)*ARX*OM1RAT**2+
     $A(7,7)*0.25*(P-1)*(ARX)*ZETA1*OM1RAT
      A(4,8)=A(4,7)
      A(4,9)=D*OM3RAT**2*ARX+
     $A(9,9)*D*ZETA3*OM3RAT*ARX
      A(4,10)=(1-ELZ)*ARX
      A(6,8)=0.25/EL+A(8,8)*ZETA
      A(6,10)=ELX
      E(2,3)=D*RXINV*ZETA3*OM3RAT*GNU3
      E(2,2)=(-0.5)*(1-P*RXINV)*ZETA1*OM1RAT*GNU2
      E(2,1)=(-0.5)*(1-P*RXINV)*ZETA1*OM1RAT*GNU1
      E(4,3)=D*ZETA3*OM3RAT*ARX*GNU3
      E(4,2)=0.5*(P-1)*ZETA1*OM1RAT*ARX*GNU2
      E(4,1)=0.5*(P-1)*ZETA1*OM1RAT*ARX*GNU1
      E(6,2)=ZETA*GNU2
      E(6,1)=(-ZETA)*GNU1
C
CC    IF C MATRIX IS NOT REQUIRED, RETURN
C
      IF(OREC.NE.1)RETURN
      DO 40 I=1,N
         DO 30 J=1,N
            A1(I,J)=0.0
30       CONTINUE
         A1(I,I)=1.0
40    CONTINUE
      CALL SUM(A,A1,A1,DELAY,1.0,N,N,NRO,20,20)
      DO 70 I=2,5
      IFACT=1
         IEXP=I
         IFACT=IFACT*I
      COEF=(DELAY**IEXP)/IFACT
      CALL SUM(A,A,SAVE3,COEF,0.,N,N,NRC,NRO,20)
      CALL POWER(SAVE3,A2,SAVE1,SAVE2,IEXP,20,N)
         CALL SUM(A2,A1,A2,1.00,1.0,N,N,20,20,20)
         AMAX=0.0
```

```
      DO 60 INNERI=1,N
         DO 50 INNERJ=1,N
            IF(ABS(A2(INNERI,INNERJ)).LT.1.0E-5)GO TO 50
            REL=ABS((A2(INNERI,INNERJ)-A1(INNERI,INNERJ))/A2(INNERI,
     $      INNERJ))
            IF(REL.GT.AMAX)AMAX=REL
   50    CONTINUE
   60    CONTINUE
         CALL ECUATE(A2,A1,20,N,N)
         IF(AMAX.LT.0.100)GO TO  90
   70 CONTINUE
      WRITE(IOUT,80)AMAX
   80 FORMAT(1X,' 5 STEPS TO APPROX. STATE TRANS. MATRIX. AMAX IS',
     $E12.5)
   90 DO 110 I=1,N
         DO 100 J=1,N
         SAVE(I)=A1(I,J)*B(J,1)
  100    CONTINUE
  110 CONTINUE
      DO 130 I=1,N
         DO 120 J=1,N
         SAVE1(I,J)=SAVE(I)*B(J,2)
  120    CONTINUE
  130 CONTINUE
C     TRANSPOSE OF STATE TRANSITION MATRIX IS ACCOMPLISHED BY INTERPOSING
C     INDICES
      DO 150 I=1,N
         DO 140 J=1,N
         SAVE(I)=A1(I,J)*B(J,1)
  140    CONTINUE
  150 CONTINUE
      DO 170 I=1,N
         DO 160 J=1,N
         SAVE2(I,J)=SAVE(J)*B(I,2)
  160    CONTINUE
  170 CONTINUE
      CALL SUM(SAVE1,SAVE2,A2,1.0,1.0,N,N,20,20,20)
      DO 190 I=1,M
         DO 180 J=1,M
         C(I,J)=0.0
  180    CONTINUE
  190 CONTINUE
      C(1,1)=Q1
      C(2,2)=Q2
      C(3,3)=Q3
      C(4,4)=Q4
      CALL PRCD(B,Q,A1,N,M,M,20,NRO,20)
      CALL TRANSP(B,SAVE1,N,M,20,20)
      CALL PRCD(A1,SAVE1,Q,N,N,M,20,20,NRO)
      CALL SUM(Q,A2,C,1.0,Q1,N,N,NRO,20,NRO)
```

```
  200 FORMAT(1H ,10(4E12.5/))
      RETURN
      END
      SUBROUTINE READER(P,LP,NPVAR,XMIN,YMIN,ZMIN,XVAR,YVAR,ZVAR,PVAR,
     $ITERX,ITERY,ITERZ,ITERP,PMIN)
      DIMENSION P(LP),PLANE(9)
C     READER ESTABLISHES INITIALIZATION DATA FROM DATA CARDS, AND PROCESSES IT
C
C        INPUT-- READ FROM CARDS
C
C        P- PARAMETER VECTOR
C        NPVAR- SUBSCRIPT OF VARIANT PARAMETER
C        PVAR- SIZE OF VARIATION IN VARIANT PARAMETER
C        PMIN,PMAX- BOUNDS OF PARAMETER VARIATION
C        PLANE- X,Y,Z COORDINATES, IN VEHICLE COORDINATE SYSTEM, OF LIMITS
C             OF THE PLANE IN WHICH MAXIMUM ACCELERATION IS FOUND
C              READ IN AS: X1,Y1,Z1;X2,Y2,Z2;X3,Y3,Z3.
C
C     OUTPUT- IN ARGUMENT LIST
C
C        ALL READ DATA PLUS:
C        XMIN,YMIN,ZMIN- LOWER BOUNDS FOR PLANAR SWEEP
C        XVAR,YVAR,ZVAR- MESH SIZE FOR PLANAR SWEEP
C        ITERX,ITERY,ITERZ- NUMBER OF STEPS IN EACH COORDINATE DIRECTION
C
      IN=1
      IOUT=3
      READ(IN,3)(P(I),I=1,LP)
    3 FORMAT(F20.0)
      READ(IN,4)NPVAR
    4 FORMAT(I5)
      READ(IN,3)PVAR
      ITERP=1
      READ(IN,5)PMIN,PMAX
    5 FORMAT(3F10.0)
      ITERP=(PMAX-PMIN)/PVAR
      ITERP=ITERP+1
   20 READ(IN,5)(PLANE(I),I=1,9)
      READ(IN,5)XVAR,YVAR,ZVAR
      XMIN=AMIN1(PLANE(1),PLANE(4),PLANE(7))
      XMAX=AMAX1(PLANE(1),PLANE(4),PLANE(7))
      ITERX=(XMAX-XMIN)/XVAR
      ITERX=ITERX+1
      YMIN=AMIN1(PLANE(2),PLANE(5),PLANE(8))
      YMAX=AMAX1(PLANE(2),PLANE(5),PLANE(8))
      ITERY=(YMAX-YMIN)/YVAR
      ITERY=ITERY+1
      ZMIN=AMIN1(PLANE(3),PLANE(6),PLANE(9))
      ZMAX=AMAX1(PLANE(3),PLANE(6),PLANE(9))
      ITERZ=(ZMAX-ZMIN)/ZVAR
```

```
      ITER2=ITER2+1
   50 RETURN
      END
      SUBROUTINE POWER(A,BOUNCR,SAVER,WORKER,NEXP,NRODIM,NORDER)
      DIMENSION A(NRODIM,1),BOUNCR(NRODIM,1),SAVER(NRODIM,1),
     $WORKER(NRODIM,1)
C     MAKES SAVER INITIALLY AN IDENTITY MATRIX
      DO 20 I=1,NORDER
         DO 10 J=1,NORDER
            SAVER(I,J)=0.0
   10    CONTINUE
         SAVER(I,I)=1.0
   20 CONTINUE
      CALL EQUATE(A,BOUNCR,NRODIM,NORDER,NORDER)
      IF(NEXP.EQ.0)RETURN
   25 KN=NEXP/2+NEXP/2
C     TRUNCATION USED FOR TEST IF EVEN
      IF(KN.EQ.NEXP) GO TO 30
      CALL EQUATE(SAVER,WORKER,NRODIM,NORDER,NORDER)
      CALL PROD(BOUNCR,WORKER,SAVER,NORDER,NORDER,NORDER,
     $NRODIM,NRODIM,NRODIM)
      IF (NEXP.EQ.1)RETURN
   30 CALL EQUATE(BOUNCR,WORKER,NRODIM,NORDER,NORDER)
      CALL PROD(WORKER,WORKER,BOUNCR,NORDER,NORDER,NORDER,
     $NRODIM,NRODIM,NRODIM)
      NEXP=NEXP/2
      GO TO 25
      END
      SUBROUTINE SUM(A,B,C,X,Y,N,M,MAXRA,MAXRB,MAXRC)
      DIMENSION A(MAXRA,M),B(MAXRB,M),C(MAXRC,M)
      DO 2 I=1,N
         DO 1 J=1,M
            C(I,J)=X*A(I,J)+Y*B(I,J)
    1    CONTINUE
    2 CONTINUE
      RETURN
      END
      SUBROUTINE PROD(A,B,C,L,M,N,MAXRA,MAXRB,MAXRC)
      DIMENSION A(MAXRA,N),B(MAXRB,M),C(MAXRC,M)
      DO 6 I=1,L
         DO 5 J=1,N
            IF(ABS(A(I,J)).LT.1.0E-20) A(I,J)=0.0
    5    CONTINUE
    6 CONTINUE
      DO 8 I=1,N
         DO 7 J=1,M
            IF(ABS(B(I,J)).LT.1.0E-20) B(I,J)=0.0
    7    CONTINUE
    8 CONTINUE
      DO 3 I=1,L
```

```
      DO  2 J=1,M
          C(I,J)=0.0
          DO  1 K=1,N
            C(I,J)=A(I,K)*B(K,J)+C(I,J)
    1     CONTINUE
    2   CONTINUE
    3 CONTINUE
      RETURN
      END
      SUBROUTINE TRANSP(A,AT,N,M,MAXRA,MAXRAT)
      DIMENSION A(MAXRA,M),AT(MAXRAT,N)
      DO 2 I=1,N
         DO  1 J=1,M
      AT(J,I)=A(I,J)
    1    CONTINUE
    2 CONTINUE
      RETURN
      END
      SUBROUTINE EQUATE(A,B,NRODIM,NROW,NCOL)
      DIMENSION A(NRODIM,1),B(NRODIM,1)
      DO 2 I=1,NROW
         DO  1 J=1,NCOL
           B(I,J)=A(I,J)
    1    CONTINUE
    2 CONTINUE
      RETURN
      END
      SUBROUTINE CINV(A,D,NPO,MXPO,IFLAG)
      DIMENSION A(MXPO,MXPO),D(MXPO,MXPO)
      DIMENSION WK(10,10),WK2(10,10)
      CALL MINV(A,D,NPO,MXPO,IFLAG)
      IF(IFLAG.EQ.1) RETURN
      CALL ITER(A,D,WK,WK2,MXPO,NPO)
      RETURN
      END
      SUBROUTINE MINV(A,P,N,KP,IFLAG)
C                                                                       00000020
      DIMENSION A(1), P(1), IX(150), B(150), G(150), DETR(150)          00000030
C                                                                       00000040
C   DIRECT MATRIX INVERSION -- BORDERING METHOD.                        00000050
C   THE DETERMINANT RATIO DET%I61< / DET%I< IS PRINTED. DET%I< IS THE   00000060
C   DETERMINANT OF THE FIRST I BY I SUB-MATRIX OF A.                    00000070
C   THE INVERSION CHECK P*A IS CALCULATED AND PRINTED.                  00000080
C                                                                       00000090
C                                                                       00000100
C     SUBROUTINE ARGUMENTS                                              00000110
C   A  # INPUT  MATRIX TO BE INVERTED. SIZE%N,N<.                       00000120
C   P  # OUTPUT RESULT MATRIX. SIZE%N,N<.                               00000130
C   N  # INPUT  SIZE OF MATRIX A AND P. %MAX # 150<                     00000140
C   KP # INPUT  ROW DIMENSION OF A AND P IN CALLING PROGRAM.            00000150
```

```
C                                                                               00000160
C  THE MAXIMUM SIZES ARE                                                        C0000170
C      N = 150                                                                  00000180
C                                                                               C0000190
 1001 FORMAT(26H1N EXCEEDS MINV ALLOWABLE./ 17HOPROGRAM STOPPED.)               00000200
 1002 FORMAT(1H1,10X,18HMATRIX IS SINGULAR/11X,17HPROGRAM HAS ENDED)            00000210
 1004 FORMAT(//10X,45HSUBROUTINE MINV HAS CALCULATED THE DATA BELOW             00000220
     *      //10X,44HTHE DETERMIANT RATIOS DET(I+1) / DET(I) ARE               00000230
     *       //(8X,7E16.8))                                                    00000240
 1005 FORMAT(//10X,40HTHE DIAGONALS OF INVERSION CHECK P*A ARE                  0000025C
     *       //(8X,7E16.8))                                                    00000260
 1006 FORMAT(//10X,42HTHE MAXIMUM OFF-DIAGONAL ELEMENT OF P*A IS,               00000270
     *       E17.8, 2X, 4HAT (,I3, 1H,,I3, 1H) )                             00000280
C                                                                               00000290
      IFLAG=C                                                                   00000300
      IF (N .LE. 150) GO TO 150                                                 00000310
      WRITE(3,1001)                                                             00000320
      STOP                                                                      00000330
C                                                                               00000340
  150 DO 160 I=2,N                                                              00000350
  160 IX(I)=I                                                                   00000360
C     INVERT FIRST NON-ZERO ELEMENT IN FIRST COLUMN                             00000370
      DO 190 I=1,N                                                              00000380
      IF (A(I) .NE. C.) GO TO 220                                               00000390
  190 CONTINUE                                                                  00000400
      WRITE(3,1002)                                                             00000410
      IFLAG=1                                                                   00000420
      RETURN                                                                    00000430
C                                                                               00000440
C     START INVERSION WITH ROW I.                                               00000450
  220 IX(I)=1                                                                   00000460
      IX(1)=I                                                                   00000470
      DETR(1)=A(I)                                                              00000480
      I1=1+KP*(I-1)                                                             00000490
      P(I1)=1./A(I)                                                             00000500
      IF (N .EQ. 1) GO TO 999                                                   00000510
C                                                                               00000520
C     REORDERING LOOP                                                           00000530
      DO 630 I=2,N                                                              00000540
         K=I                                                                    00000550
         I1=I-1                                                                 00000560
  250 S=C.                                                                      00000570
         MIXL=KP*(L-1)                                                          00000580
         IL=IX(L)+MIXL                                                          00000590
      DO 450 L=1,I1                                                             00000600
      P(I)=0.                                                                   00000610
      Q(I)=C.                                                                   00000620
      DO 440 J=1,I1                                                             00000630
      IJ=I+KP*(IX(J)-1)                                                         00000640
      JI=IX(J)+KP*(L-1)                                                         00000650
```

```
      B(I)=B(I)-B(IJ)*A(JL)                                          00000650
      JI=J+KB*(IX(I)-1)                                              00000660
      IJ=IX(I)+KB*(J-1)                                              00000670
  440 G(I)=G(I)-A(LJ)*B(JI)                                          00000680
      II=IX(I)+KB*(I-1)                                              00000690
  450 S =S+A(LI)*B(I)                                                00000700
      AI=A(LI)+S                                                     00000710
      IF (A(LL) .EQ. 0.) GO TO 480                                   00000720
      ALEAR=ABS(AL/A(LL))                                            00000730
      GO TO 490                                                      00000740
  480 ALEAR=ABS(AL)                                                  00000750
  490 IF (ALEAR .GE. .1E-6) GO TO 550                                00000760
C                                                                    00000770
C     INTERCHANGE ROWS AND COLUMNS                                   00000780
      K=K+1                                                          00000790
      IF (K .GT. N) GO TO 540                                        00000800
      IX(L1)= IX(L)                                                  00000810
      IX(L)=IX(K)                                                    00000820
      IX(K)=IX(L1)                                                   00000830
      GO TO 250                                                      00000840
  540 IF (ALEAR .GE. .1E-8) GO TO 550                                00000850
  545 WRITE(3,1002)                                                  00000860
      IFIAG=1                                                        00000870
      RETURN                                                         00000880
C                                                                    00000890
  550 II=L+KB*(IX(L)-1)                                              00000900
      B(LL)=1./AL                                                    00000910
      DET(I)=AL                                                      00000920
      DO 570 I=1,L1                                                  00000930
      IL=I+KB*(IX(L)-1)                                              00000940
      LI=L+KB*(IX(I)-1)                                              00000950
      B(IL)=B(I)*B(LL)                                               00000960
      B(LI)=G(I)*B(LL)                                               00000970
      DO 570 J=1,L1                                                  00000980
      IJ=I+KB*(IX(J)-1)                                              00000990
  570 B(IJ)=B(IJ)+G(J)*B(IL)                                         00001000
  630 CONTINUE                                                       00001010
C                                                                    00001020
C     COMPUTE INVERSION CHECK B*A                                    00001030
      XOFF=0.0                                                       00001040
      DO 720 I=1,N                                                   00001050
      DO 710 J=1,N                                                   00001060
      X=0.0                                                          00001070
      KJA=KB*(J-1)                                                   00001080
      DO 703 K=1,N                                                   00001090
      IK=I+KB*(K-1)                                                  00001100
      KJ=K+KJA                                                       00001110
  703 X=X+B(IK)*A(KJ)                                                00001120
      IF (I .NE. J) GO TO 705                                        00001130
```

```
      G(I)=X                                                                    00001140
      GO TO 710                                                                 00001150
  705 IF (ABS(X) .LT. ABS(XOFF)) GO TO 710                                      00001160
      XOFF=X                                                                    00001170
      IOFF=I                                                                    00001180
      JOFF=J                                                                    00001190
  710 CONTINUE                                                                  00001200
  720 CONTINUE                                                                  00001210
C                                                                               00001220
C     PRINT THE DETERMINANT RATIO AND INVERSION CHECK                           00001230
C                                                                               00001240
  999 RETURN                                                                    00001290
      END                                                                       00001300
      SUBROUTINE RESID(A,C,X,WK,WK1,N,MXRO)
      DIMENSION A(MXPO,MXPO),C(MXPO,MXPO),X(MXPO,MXPO),WK(MXPO,MXPO),
     $WK1(MXPO,MXPO)
      CALL PROD(A,X,WK,N,N,N,MXRO,MXPO,MXRO)
      CALL TRANSP(A,WK1,N,N,MXRO,MXPO)
      CALL PROD(X,WK1,A,N,N,N,MXPO,MXPO,MXPO)
      CALL SUM(WK,A,A,1.0,1.0,N,N,MXRO,MXRO,MXRO)
      CALL SUM(A,C,A,1.0,1.0,N,N,MXPO,MXPO,MXPO)
      IOUT=3
      WRITE(IOUT,5)
    5 FORMAT(1X,'RESIDUAL,P FOR  AY+XA+C=P')
      DO 10 I=1,N
         WRITE(IOUT,8)(A(I,J),J=1,N)
    8    FORMAT(1X,10E12.3)
   10 CONTINUE
      RETURN
      END
      SUBROUTINE SERIES(A,C,N,NROMX,AYE,WORK,U)
      DIMENSION A(NROMX,NROMX),C(NROMX,NROMX),AYE(NPOMX,NPOMX),
     $WORK(NPOMX,NROMX),U(NROMX,NROMX)
      C=1.2
C
C     FORM IDENTITY MATRIX IN AYE
C
      DO 2 I=1,N
         DO 1 J=1,N
            AYE(I,J)=0.0
    1    CONTINUE
         AYE(I,I)=1.0
    2 CONTINUE
C
C     DEFINITION OF SERIES PARAMETER ARRAYS
C
      CALL SUB(AYE,A,U,0,-1.0,N,N,NPOMX,NPOMX,NPOMX)
      CALL CINV(U,WORK,N,NROMX,IFLAG)
      CALL SUM(AYE,A,U,0,1.0,N,N,NROMX,NPOMX,NPOMX)
      CALL PROD(WORK,U,X,N,N,N,NROMX,NPOMX,NPOMX)
```

```
      CALL TRANSP(WORK,U,N,N,NROWX,NROWX)
      CALL PROD(C,U,AYE,N,N,N,NROWX,NROWX,NPOWX)
      CALL PROD(WORK,AYE,C,N,N,N,NROWX,NROWX,NROWX)
      Q2=Q*2
      CALL SUM(C,AYE,C,Q2,0.0,N,N,NPOWX,NROWX,NROWX)
C
CCC   INITIALIZATION
C
      CALL TRANSP(A,U,N,N,NROWX,NPOWX)
      CALL PROD(C,U,AYE,N,N,N,NROWX,NROWX,NPOWX)
      CALL PROD(A,AYE,U,N,N,N,NROWX,NROWX,NPOWX)
      CALL SUM(C,U,C,1.0,1.0,N,N,NROWX,NPOWX,NROWX)
      NU=1
C
CCC   ITERATIVE PROCEDURE
C
    3 NU2=NU*2
      CALL POWER(A,AYE,U,WORK,NU2,NPOWX,N)
      CALL PROD(U,C,AYE,N,N,N,NROWX,NROWX,NPOWX)
      CALL TRANSP(U,WORK,N,N,NROWX,NROWX)
      CALL PROD(AYE,WORK,U,N,N,N,NROWX,NROWX,NROWX)
      CALL SUM(C,U,C,1.0,1.0,N,N,NROWX,NPOWX,NROWX)
      NU=NU+1
C
CCC   RELATIVE CHANGE IN SOLUTION MATRIX
C
      RELDEL=0.0
      DO 5 I=1,N
         DO 4 J=1,N
            IF(ABS(C(I,J)).LT.1.0E-20)C(I,J)=0
            IF(C(I,J).EQ.0) GO TO 4
            DEL=U(I,J)/C(I,J)
            IF (ABS(RELDEL).LT.ABS(DEL))RELDEL=DEL
    4    CONTINUE
    5 CONTINUE
C
CCC   STOPPING CRITERIA
C
      NUMAX=25
      IF(ABS(RELDEL).GE.0.00001)GO TO 6
      PRINT,'CONVERGENCE TENTATIVELY ACHIEVED'
      PRINT,NU,'ITERATIONS'
      CALL EQUATE(U,C,NPOWX,N,N)
      RETURN
    6 IF(NU.LT.NUMAX) GO TO 3
      PRINT,'CONVERGENCE TOO SLOW'
      PRINT,NUMAX,'ITERATIONS EXCEEDED'
      PRINT,'LAST RELATIVE CHANGE',RELDEL
      RETURN
      END
```

```
      SUBROUTINE ITER(A,D,WK,WK2,MXRO,NRO)
      DIMENSION A(MXRO,MXRO),D(MXRO,MXRO),WK(MXRO,MXRO),WK2(MXRO,MXRO)
      DO 15  I=1,10
      CALL PECI(A,D,WK,NRO,NRO,NRO,MXRO,MXRO,MXRO)
      CALL PECD(D,WK,WK2,NRO,NRO,NRO,MXRO,MXRO,MXRO)
         CALL SUM(D,WK2,D,2.,-1.,NRO,NRO,MXRO,MXRO,MXRO)
         CHANGE=0.0
         DO  12 J=1,NRO
            DO  10 K=1,NRO
               IF(J.EQ.K) GO TO 10
               IF(ABS(WK2(J,K)).GT.CHANGE)CHANGE=ABS(WK2(J,K))
10          CONTINUE
12       CONTINUE
         IF(CHANGE.LT.0.5 E-05)  GO TO 20
15    CONTINUE
20    CALL PECI(A,D,WK,NRO,NRO,NRO,MXRO,MXRO,MXRO)
      OFFDIA=0.0
      DO 25  I=1,NRO
         DO  23 J=1,NRO
            IF(I.EQ.J)  GO TO 23
            IF(ABS(WK(I,J)).GT.OFFDIA)OFFDIA=WK(I,J)
23       CONTINUE
25    CONTINUE
      RETURN
      END
```

```
2710
1.0
1.0
0.3
0.3
40.0
0.0
0.0
1600.
1.17
0.57
1.0
1.67
3.33
0.144
0.01
0.01
0.01
3.33
0.6
3.75
2.0
0.0000444
0.0000444
0.0000444
0.018
1.0
0.2
      8
100.
1500.          2200.
2.0            1.0             0.6
2.0            1.0             0.6
2.0            1.0             0.6
1.0            1.0             1.0
```

## REFERENCES


1. Richardson, H. H. and Wormley, D. U., "Transportation Vehicle/Beam-Elevated Guideway Dynamic Interactions: A State-of-the-Art Review," Trans. ASME, J. Dynamic Systems, Measurement and Control, Vol. 96, June 1974, pp. 169-179.

2. Wilson, J. F. and Biggers, S. B., "Dynamic Interactions of High Speed Tracked Air Cushion Vehicles with their Guideways," Trans. ASME, J. Dynamic Systems, Measurement and Control, Vol. 95, March 1973, pp. 76-85.

3. Tan, C. P. and Shore, S., "Dynamic Response of a Horizontally Curved Bridge," Proc. ASCE, J. Structural Div., Vol. 95, 1968, pp. 761-781.

4. Olusola, O.B., "Dynamic Interactions of Personal Rapid Transit Vehicles and Elevated Guideways," Ph.D. dissertation, UCLA School of Engineering and Applied Science, Report 7483, Dec. 1974.

5. Wilson, J. F. and Garg, D. P., "Frequencies of Annular Plate and Curved Beam Elements," AIAA Journal, Vol. 16, No. 3, March 1978, pp. 270-272.

6. Wilson, J. F., "Transient Dynamics of Curved Guideway Structures for Urban Vehicles," Modeling and Simulation, Vol. 8, Proc. 7th Annual Pittsburgh Conf., April 1977, pp. 159-164.

7. Private communication with Peter Likins, School of Engineering and Applied Science, Columbia University, August 1976.

8. Touma, A., and Wilson, J. F., "Design Optimization of Prestressed Concrete Spans for High Speed Ground Transportation," Computers and Structures, Vol. 3, 1973, pp. 265-279.

9. Wilson, J. F., "Dynamic Experiments of Alternative Guideway-Vehicle Systems," U.S. Dept. of Transportation Report, Contract No. DOT-OS-60130, June 1978.

10. Joseph, T. P., "Experimental Studies of Curved Guideway Responses to Moving Urban Transit Vehicles," M.S. Thesis, Duke University, School of Engineering, 1977.

11. Wilson, J. F. and Joseph, T. P., "Dynamics of Curved Guideway Spans for AGT Vehicles," Proc. of Conf. on AGT Technology Dev., U.S.-DOT, March 1978.

12. Wilson, J. F., "Experiments in Guideway-Levitation Vehicle Interaction Dynamics," U.S. Dept. of Transportation Report, PB 257941, July 1976.

13. Meisenholder, S. G., and Weidlinger, P., "Dynamic Interaction Aspects of Cable-Stayed Guideways for High Speed Ground Transportation," J. Dynamic Systems, Measurement and Control, Vol. 96, June 1974, pp. 180-192.

14. Lin, Y. K., "Free Vibrations of a Continuous Beam on Elastic Supports," International Journal of Mechanical Sciences, Vol. 4, pp. 409-423, 1962.

15. Ravera, R. J. and Anderes, J., "A Semi-Continuous Multi-Span Guideway Model for Vehicle-Guideway Dynamics Interaction," WP 10503, MITRE Corp., 1974.

16. Kolousek, V., "Dynamics in Engineering Structures," Chapter 5, Halsted Press, New York, N.Y., 1973.

17. Fromnes, D.J., "Modeling and Statistics in the Estimation of Vehicle Ride Quality", Ph.D. Dissertation, School of Engineering, Duke University, June, 1979.

18. "A Guide to Evaluation of Human Exposure to Whole Body Vibration", ISO/DIS 2631, International Organization for Standardization, New York, 1972.

19. Lee, R.A. and Predko, F., "Analytical Analysis of Human Vibration," S.A.E. Transactions 680091, 1968, pp. 346-370.

20. "Design Specifications for Urban Tracked Air Cushion Vehicles," U.S. Department of Transportation, Washington D.C., 1972.

21. Janeway, R.N., "Vehicle Vibration Limits to Fit the Passenger," S.A.E. Journal, Aug. 1948, pp. 48-49.

22. Smith, C.C., McGehee, D.Y., and Healy, A.J., "The Prediction of Passenger Riding Comfort From Acceleration Data".

23. Healey, A.J., "Performance of Mechanically Steered AGT Vehicles; Ride and Maintainability Implications", Proc. of Conf. on AGT Vehicle Technology, U.S. Dept. of Transportation, Cambridge, Mass., March, 1978.

24. Olusola, O.B. and Likins, P.W., "Stability Analysis of Constant Speed Transit Vehicles on Straight, Fixed Guideways," International Journal of Vehicle System Dynamics, 1975.

25. Cooperrider, N.K., Cox, J.J., and Hedrick, J.K., "Lateral Dynamics Optimization of a Conventional Railcar," Trans. ASME, J. Dynamics Systems, Measurement and Control, Vol. 97, Sept. 1975, pp. 293-299.

26. Hedrick, J. K., Billington, G.F., and Dreesback, D.A., "Analysis, Design, and Optimization of High Speed Vehicle Suspensions Using State Variable Techniques" Trans. ASME, J. Dynamic Systems, Measurement and Control, Vol. 96, June 1974, pp. 193-203.

27. Hedrick, J.K., "Some Optimal Control Techniques Applicable to Suspension System Design", ASME Paper No. 73-ICT-55, 1973.

28. Bryson, A.E. and Ho, Yu-Chi, Applied Optimal Control Optimization, Estimation, and Control, John Wiley & Sons, 1975, pp. 328-332.

29. Kwak, Y.K. "Investigation of Rubber-Tired Automated Guideway Transit Vehicles for Ride Quality Assessment", Ph.D. dissertation, Univ. of Texas, Austin, May 1978, p. 68.

30. Hedrick, J.K. and Firouztash, H., "The Covariance Propagation Equation with Time-Delayed Inputs", Technical Note, IEEE Trans. on Automatic Control, pp. 587-589, October, 1974.

31. Davison, E.J., and Man, F.T., "The Numerical Solutions of $A^TQ + QA = -C$", IEEE Trans. on Automatic Control, Aug. 1968, pp. 448-449.

32. Smith, P.G., "Numerical Solution of the Matrix Equation $AX + XA^T + B = 0$", IEEE Trans. on Automatic Control, June 1971, pp. 278-279.

33. Smith, R., "Matrix Equation XA + BX = C", SIAM Journal of Applied Math., vol. 16, no. 1, 1968, pp. 198-201.

34. MacKinnon, D., "High Capacity Personal Rapid Transit Systems Development", IEEE Trans. on Vehicle Technology, Vol. IV-24, no. 1, Feb. 1975, pp. 8-14.

35. "Automated Guideway Transit Systems Vehicle-Elevated Guideway Dynamics: Multiple-Vehicle Single Span Systems", UMTA Report No. MA-11-0023-75-1, p. 16.

36. Hullender, D.A., "Minimum Vehicle-Guideway Clearances Based on a Contact Frequency Criterion", ASME Trans., J. Dynamic Systems, Measurement and Control, Vol. 96, June 1974, pp. 213-217.

37. Young, J.W. and Wormley, D.N., "Optimization of Linear Vehicle Suspensions Subjected to Simultaneous Guideway and External Force Disturbances", Trans. ASME, J. Dynamic Systems, Measurement and Control, Vol. 95, June 1973, pp. 213-219.

# REQUEST FOR FEEDBACK TO
# The DOT Program Of University Research

DOT/RSPA/DPB-50/79/4 - "Dynamic Theories and Experiments of Alternative Guideway-Vehicle Systems"- PART II

| YES | NO | |
|---|---|---|
| ☐ | ☐ | Did you find the report useful for your particular needs? If so, how? |
| ☐ | ☐ | Did you find the research to be of high quality? |
| ☐ | ☐ | Were the results of the research communicated effectively by this report? |
| ☐ | ☐ | Do you think this report will be valuable to workers in the field of transportation represented by the subject area of the research? |
| ☐ | ☐ | Are there one or more areas of the report which need strengthening? Which areas? |
| ☐ | ☐ | Would you be interested in receiving further reports in this area of research? If so, fill out form on other side. |

Please furnish in the space below any comments you may have concerning the report. We are particularly interested in further elaboration of the above questions.

Cut Out Along This Line

**COMMENTS**

**Thank you for your cooperation. No postage necessary if mailed in the U.S.A.**

# RESEARCH FEEDBACK

**Your comments, please . . .**

This booklet was published by the DOT Program of University Research and is intended to serve as a reference source for transportation analysts, planners, and operators. Your comments on the other side of this form will be reviewed by the persons responsible for writing and publishing this material. Feedback is extremely important in improving the quality of research results, the transfer of research information, and the communication link between the researcher and the user.

**FOLD ON TWO LINES, STAPLE AND MAIL.**

Fold Fold

DEPARTMENT OF TRANSPORTATION
RESEARCH AND SPECIAL PROGRAMS Administration
WASHINGTON D.C. 20590

Official Business

PENALTY FOR PRIVATE USE, $300

POSTAGE AND FEES PAID
DEPARTMENT OF
TRANSPORTATION
DOT 513

OFFICE OF UNIVERSITY RESEARCH (DPB-50)
Research and Special Programs Administration
U.S. Department of Transportation
400 Seventh Street, S.W.
Washington, D.C. 20590

Fold Fold

**REQUEST FOR INFORMATION FROM THE UNIVERSITY RESEARCH PROGRAM**

☐ Check here if you would like to be placed on the mail list for the University Research Program Solicitation Booklet (DT-63C)

**IF YOU WISH TO BE ADDED TO THE MAIL LIST FOR FUTURE REPORTS, PLEASE FILL OUT THIS FORM.**

Name _____ Title _____
Use Block Letters or Type

Department/Office/Room _____

Organization _____

Street Address _____

City _____ State _____ Zip _____